DIPARTIMENTO DI SCIENZE CHIMICHE E FARMACEUTICHE

UNIVERSITA' DEGLI STUDI DI TRIESTE

TRIESTE, ITALY

FACULTE DES SCIENCES DEPARTEMENT DE CHIMIE

FACULTES UNIVERSITAIRES NOTRE-DAME DE LA PAIX

NAMUR, BELGIUM

Synthetic Approaches Towards Modified Peptide Nucleic Acids (PNAs) for Biomimetical Nanostructured Surfaces

A cotutelle dissertation submitted to the

Universita' Degli Studi di Trieste
& Facultés Universitaires Notre-Dame de la Paix

For the degree of

Dottorato di Ricerca in Scienze e Tecnologie Chimiche e Farmaceutiche
& Docteur en Sciences

Presented by

STEFAN MOHNANI

Financed by

EU Marie Curie Research Training Network (FP6) Grant

Scientific discipline sector

Scienze e Tecnologie Chimiche e Farmaceutiche
(CHIM/06 – Ciclo XXII – Anno Accademico 2009/2010)

Doctoral commission	*Head of Doctoral School*	*Signature:*
Prof. Stephane Vincent Prof. Maurizio Prato Prof. Davide Bonifazi Prof. Marcella Bonchio Prof. Annemieke Madder Prof. Carmela Aprile	Prof. Enzo Alessio	
	Promoter Prof. Davide Bonifazi	*Signature:*
	Co-promoter Prof. Maurizio Prato	*Signature:*

Acknowledgements

First and foremost, I would like to thank Professor Davide Bonifazi for providing me with a unique opportunity to pursue my doctoral studies in an international environment as part of the PRAIRIES EU Marie Curie consortium. Not only did I learn about organic chemistry, but also I was exposed to the multidisciplinary scientific discipline of nanotechnology alongside a world-class group of collaborative researchers at the forefront of their respective fields. I would also like to thank Davide personally for believing in me, supporting my ideas and guiding me throughout my doctoral research.

I am also very grateful to Professor Maurizio Prato, who as my co-promoter, has always offered valuable advice and support throughout this doctorate. He was also kind enough to allow me to invade his lab for an entire year! I would like to extend the thanks to Dr. Tatiana Da Ros who helped organize my stay in Trieste. Furthermore, I would like to thank Viviana Zigante for helping me with all the administrative issues I encountered during the PhD.

Many thanks go to Professor Alain Krief for sharing his enthusiasm for science, his entertaining anecdotes about the research world, and of course, those challenging questions that we all suffered at the blackboard during group meetings.

Thank you to Professor Francois Diederich and Professor Paolo Samori for accepting to host me for part of my doctoral studies in their research groups. The experiences of working at the ETH in Zurich and ISIS in Strasbourg were truly enriching.

Furthermore, I would like to thank all the people (Jens, Tobias, Davide (Guisto), Leslie, Michael, Petra, Jesse, Carlo, Sophie, Carlos, Joceline, Andrea, Halim, Yoosaf, Massimo, Thomas, Corinna, Nicola, Matthew, Mats, Jonas, Felix, Eva, Katalin, Zsolt, Tomas, Mihaela, Meike, Serpil, Mairena, Jose Luis....) who formed part of the PRAIRIES research training network for all the fruitful discussions and collaborations. I really enjoyed all our meetings at all those great locations around Europe. The after parties were always something to look forward to. I wish you all the best in your future careers.

I would like to thank all the staff working at the chemistry department at FUNDP and also the staff at the pharmaceutical department at the University of Trieste for all the services and assistance they kindly provided. In particular, a special mention is well deserved for Alain Burlet, Giuseppe Barbera and Andrea Ruggeri…thank you to all of you for the technical support you provided throughout my research.

To all the researchers on the third floor at the Chemistry department at FUNDP, past and present. Thanks for creating a great atmosphere to work in. The floor changed a lot over

the years, we moved furniture from left to right, up and down, and then all back again, but whether you were there in the beginning or towards the end of my time at FUNDP, I am grateful to all of you for welcoming me and helping me feel at home (because of course that's what the third floor became during the PhD!!).

The same thanks go to all the members of Prof. Prato's lab during my time there (Ana, Coke, Alejandro, Niksa, Valeria, Checco, Mildred, Laura, Noelia, Alessia, William, Marek, Alan, Longtian, Sara, Antonio, Chiara, Francesca, Luigi, Tomas…). You made me feel at home right away and it was really tough to move away after my year was up. I miss the Aperitivi! Ale, of course you deserve a special mention…thanks for taking in your homeless friend. It's a month of July in my life, which will never be forgotten…your 'allegria' was always a great motivation during tough moments!

Many thanks to all the COMS members, past and present (Vincent, Emerance, Simone, Claudia, Laura, Simon, Laure-Elie, Valentina, Rosaria, Ganesh, Hassan, Federica, Daphne, Adrian, Silvia, Arnaud, Riccardo, Benoît, Julie…). Working with you was always fun, sometimes challenging and is most definitely something I will miss. I can honestly say I had a great time during my PhD thanks to all of you!

Special thanks go to Guillaume and Simon, my patient housemates who survived me at work and at home for over a year. Simon…I still miss those daily breakfast discussions. Lorella, I appreciate all the work you did to help me during your master project (despite the difficult saponifications!), and for helping me with the printing of my thesis. Good luck for your PhD. Claudia and Laura, my sisters, I'm sure you miss my complaints…thank you for always being there for me. Vincenzo, I learnt a lot from you right in the beginning, your experience and opinion about organic chemistry was true and valuable to know! Finally, Simone and Maxime, we started together, we finished together…I couldn't have asked for better friends to share my PhD with. I'm sure you agree that our PhDs were way more than just organic synthesis! (need I say more…)

I would also like to thank the people closest to me, my family back home and also a special person in my life, Lele. Mum and dad, thanks for always being there for me; for sharing your opinions, which always seem to introduce a new perspective to every situation; for providing me with all the opportunities in the world and for all your love. Timo, you always set the benchmark that I have to challenge. Even though we banter back and forth, I know I can always depend on you. Thanks for your support. Lele, since we met I have valued your opinion, support and never ending patience and love. You helped me and supported me throughout the writing of this thesis in Belgium, Malta, Italy and Croatia. You were there through it all and always believed in me. Hvala!

This doctoral dissertation is dedicated to Mummu.

Table of Contents

List of Abbreviations ***IV***

Abstract ***VIII***

Résumé ***XIV***

Riassunto ***XXI***

CHAPTER 1 - INTRODUCTION **1**

1.1. POROUS NETWORKS **2**

1.1.1. Non-Covalent Interactions 2

1.1.1.1. Hydrogen Bonding 2

1.1.1.2. Dipole-Dipole interactions and Van der Waals contacts 11

1.1.1.3. Metal-ligand Coordination 14

1.1.2. Porous Networks Formed By Surface-Confined Covalent Reactions 16

1.1.3. Preorganised Cavities: The Macrocycle Approach 19

1.1.4. Single Pore Assemblies: An Enhanced Level of Control in Surface Self-assembly 22

1.2. EXPLOITING THE CAVITIES OF POROUS NETWORKS **26**

1.2.1. Cavity-Confined Host-Guest Recognition 27

1.2.2. Guest-Controlled Non-Covalent Confinement 31

1.2.3. Towards Biomolecular Hosting 36

1.2.4. Pore-templated Surface Functionalisation 38

1.3. TOWARDS THE THIRD DIMENSION: FROM STRUCTURES TO FUNCTIONALITY **40**

1.4. THE BIOMIMETIC APPROACH **47**

1.4.1. DNA 47

1.4.2. Peptide Nucleic Acids (PNAs) 58

1.5. PROJECT OBJECTIVES **60**

1.5.1. PRAIRIES Objectives 60
1.5.2. Design of the Angular and Linear Units 62
1.5.3. Target Supramolecular Assemblies 63

CHAPTER 2 - RESULTS AND DISCUSSION **66**

2.1 PNA SYNTHESIS **67**
2.1.1 Introduction to PNA synthesis strategies 67
2.1.2 Orthogonality and the protecting group strategy 75
2.1.3 Synthesis of PNA monomers 77
2.1.3.1 Synthesis of the thymine monomer 77
2.1.3.2 Synthesis of the adenine monomer 79
2.1.3.2.1 Synthesis of the Fmoc/Mmt protected adenine monomer 79
2.1.3.2.2 Synthesis of the Fmoc/Cbz protected adenine monomer 81
2.1.4 Solid phase synthesis of PNA oligomers 83
2.1.4.1 Solid phase PNA synthesis using the Fmoc/Mmt strategy 83
2.1.4.2 Microwave-assisted PNA synthesis using the Fmoc/Cbz strategy 87
2.1.4.2.1 Oligomerisation using the Biotage microwave system 87
2.1.4.2.2 Oligomerisation using the CEM Discovery SPS microwave system 94
2.1.4.2.3 Oligomerisation using the CEM Liberty microwave system 98
2.1.4.3 Isolation of the target oligomer via manual solid phase synthesis of PNA using the Fmoc/Cbz strategy 99
2.1.4.4 Deprotection of the PNA dodecamer 107

2.2 SYNTHESIS OF PNA-CHROMOPHORE ADDUCTS **110**
2.2.1 Attempts to synthesize PNA-porphyrin adducts via amide bond formation 111
2.2.2 Attempts to synthesize PNA-porphyrin adducts via Cu(I)-catalysed 1,3-dipolar cycloaddition 113
2.2.3 Development of a Cu(I)-free 1,3-dipolar cycloaddition reaction to prepare PNA-chromophore adducts 117
2.2.3.1 Introduction to the nitrile oxide-acetylene 1,3-dipolar cycloaddition reaction 118
2.2.3.2Evaluation of the nitrile oxide-acetylene 1,3-dipolar cycloaddition reaction using anthracene derivatives 119
2.2.3.3Preparation of PNA-anthracene adducts via nitrile oxide- acetylene 1,3-dipolar cycloaddition reactions 122
2.2.3.4 Development of a porphyrin nitrile oxide precursor 127
2.2.3.5 Preparation of PNA-chromophore adducts using via Cu(I)- free nitrile oxide-acetylene 1,3-dipolar cycloaddition reactions 134

2.3 PRELIMINARY AFM INVESTIGATION OF THE DEPOSITION OF PNA ONTO MICA SURFACES **140**

CHAPTER 3 – CONCLUSIONS **144**

CHAPTER 4 – PERSPECTIVES **150**

CHAPTER 5 – EXPERIMENTAL PART **152**

3.1. INSTRUMENTATION **152**

3.2. MATERIAL AND GENERAL METHODS **154**

3.3. EXPERIMENTAL PROCEDURES **155**

3.3.1 PNA monomers 155

3.3.2 Synthesis of chromophores and linkers 165

3.3.3 Solid phase PNA synthesis 187

3.3.3.1 Initial trials utilising Tentagel resin 187

3.3.3.2 Microwave solid phase PNA synthesis procedures (Biotage microwave) 189

3.3.3.3 Microwave solid phase PNA synthesis procedures (CEM Discover microwave) 191

3.3.3.4 Microwave solid phase PNA synthesis procedures (CEM Liberty microwave) 192

3.3.3.5 Manual solid phase PNA synthesis procedures 194

3.3.4. Isolated PNA oligomers **199**

3.3.5. Procedures for AFM experiments **213**

BIBLIOGRAPHY **215**

Curriculum Vitae **229**

List of Publications **230**

List of Abbreviations

A	adenine monomer (PNA)
ADA	acceptor-donor-acceptor
AEG	*N*-(2-minoethyl)glycine
AFM	atomic force microscopy
Alloc	allyloxycarbonyl
APCI	atmospheric pressure chemical ionization
aq	aqueous
Azoc	azidomethyloxycarbonyl
Boc	*tert*-butyloxycarbonyl
BPEPP	5,15-bis-[4-(phenylethynyl)phenyl]porphyrin
Bts	benzothiazole-2-sulfony
^{t}BuOCl	*tert*-butyl hypochlorite
ºC	degrees celsius
Cbz	benzyloxycarbonyl
Cl-Bhoc	chloro-benzhydryloxycarbonyl
CH_2Cl_2	dichloromethane
$CHCl_3$	chloroform
CH_3CN	acetonitrile
CV	cyclic voltammetry
δ	chemical hift
d	doublet
dd	doublet of doublets
DABCO	1,4-diazabicylco[2.2.2]octane
DAD	donor-acceptor-donor
DBA	dehydrobenzo[12]annulene
DCC	dicyclohexylcarbodiimide
Dde	*N*-[1-(4,4-dimethyl-2,6-dioxocyclohex-1-ylidene)ethyl]
DFT	density functional theory
DIEA	*N*,*N*-diisopropylethylamine
DNA	deoxyribonucleic acid
DMAP	4-dimethylaminopyridine
DMSO	dimethylsulfoxide
DMF	*N*,*N*-dimethylformamide
Dmt	dimethoxytrityl
dt	doublet of triplets
Dts	dithiasuccinoyl
DPDI	4,9-diaminoperylene-quinone-3,10-diimine
DPP	bis-2,9-diphenyl-1,10-phenanthroline
ε	extintion coefficient
EDC	1-ethyl-3-(3-dimethylaminopropyl) carbodiimide)
EDTA	ethylenediaminetetraacetic acid

ESI	electrospray ionization
EtOAc	ethyl acetate
Et_2O	diethylether
Et_3N	triethylenamine
FBhoc	fluoro-benzhydryloxycarbonyl
FHT	fixed hold time
Fmoc	9-fluorenylmethyl carbamate
Fmoc-OSu	*N*-(9-fluorenylmethoxycarbonyloxy) succinimide
FRET	fluorescence resonance energy transfer
Gly	glycine
h	hours
HBC	hexa-*peri*-hexabenzocoronene
H-bonds	hydrogen bonds
HBTU	*O*-benzotriazole-*N*,*N*,*N*',*N*'-tetramethyl-uronium-hexafluoro-phosphate
HOBT	1-hydroxybenzotriazole
HOPG	highly oriented pyrolitic graphite
HPLC	high performance liquid chromatography
HRMS	High resolution mass spectrometry
iPr_2NH	isopropylamine
IR	infrared
J	coupling constant
K	kelvin
LC-MS	liquid chromatography mass spectrometry
m	multiplet
M	molar
MALDI	matrix-assisted laser desorption/ionization
MBHA	4-methylbenzhydrylamine
MeCN	acetonitrile
MHz	megahertz
min	minutes
ML	monolayer
MM	molecular mechanics
Mmt	monomethoxytrityl
Mmt-Cl	monomethoxytrityl chloride
MOCNs	metal organic coordination networks
m.p.	melting point
MPc	metallophthalocyanines
MS	mass spectrometry
MW	microwave
4-N_3Cbz	4-azidobenzyloxycarbonyl
NCS	*N*-chlorosuccinimde
NEM	*N*-ethylmorpholine
NEt_3	triethylamine
nm	nanometer
NMP	*N*-methyl-2-pyrrolidone

NMR	nuclear magnetic resonance
OPE	oligophenylene-ethynylene
OTBDPS	*O-tert*-butyldiphenylsilyl
4-OMeCbz	4-methoxybenzyloxycarbonyl
4-OTBSCbz	*4-tert*-butyldimethylsilyloxybenzyloxycarbonyl
π bonds	pi bonds
Pc	phthalocyanine
PCR	polymerase chain reaction
PDMS	polydimethylsiloxane
Phe	phenylaniline
PEG	polyethylene glycol
PNA	peptide nucleic acid
PPh_3	triphenylposphine
ppm	parts per million
PS	polystyrene
PTCDI	3,4,9,10-perylenetetracarboxylic diimide
PyBOP	benzotriazol-1-yl-oxytripyrrolidinophosphonium hexafluorophosphate
Py	pyridine
q	quartet
RHE	reversible hydrogen electrode
r.t.	room temperature
Rf	retention factor
s	singlet
SAMs	self-assembled monolayers
Sat.	saturated
SCOFs	surface covalent organic frameworks
S_N2	bimolecular nucleophilic substitution
SPM	scanning probe microscopies
SPPS	solid phase peptide synthesis
SPS	solid phase synthesis
STM	scanning tunneling microscopy
t	triplet
T	thymine monomer (PNA)
t-BuOH	*tert*-butyl alcohol
TBAF	tetrabutylammonium fluoride
TBTA	tris-(benzyltriazolylmethyl)amine
TBTU	*O*-(Benzotriazol-1-yl)-*N*,*N*,*N*',*N*'-tetramethyluronium tetrafluoroborate
TCB	1,2,4-trichlorobenzene
Teoc	2-(trimethylsilyl)ethoxycarbonyl
Tf_2O	trifluoromethanesulfonic anhydride
TFA	trifluoroacetic acid
TFMSA	trifluoromethanesulfonic acid
THF	tetrahydrofuran
TLC	thin layer chromatography
TMEDA	tetramethylethylendiamine

TMS	trimethylsilyl
TMSBr	trimethylsilyl bromide
TMSI	trimethylsilyl iodide
TOF	time of flight
TOTU	*O*-(cyano(ethoxycarbonyl)methylenamino)-1,1,3,3-tetramethyluronium tetrafluoroborate
TPPs	tetra(phenyl)porphyrins
Tyr	tyrosine
UHV	ultra-high vacuum
UV	ultraviolet
UV-Vis	ultraviolet-visible
V	volts
ZnOEP	zinc octaethylporphyrin

Abstract

"There is plenty of room at the bottom". These were the famous words of Richard P. Feynman in 1959 that led to the birth of nanotechnology and nanoscience. Electronic devices based on inorganic semiconductors have been part of our daily lives for the last 60 years. Their miniaturisation has occurred gradually over the years, however, according to Moore's law the contemporary microelectronic industry's "top-down" manufacturing technique will soon reach its limits. Therefore, the recent development and increased knowledge of organic semiconductors has led to a tendency to explore alternative avenues with a focus on the creation of electronic devices based on organic molecules. The invention of techniques such STM (1981) and AFM (1986) have facilitated this research, allowing the imaging and manipulation of surfaces and molecules at the nanometre scale (0.1-100 nm). The next step is therefore the development of methods for the controlled fabrication of molecular assemblies and their integration into usable macroscopic systems. In this respect, the "bottom-up" approach offers considerable advantages over any other methodology (*i.e.* "top-down") for the construction of nanoscale functional materials and devices. This approach generally exploits the hierarchical self-assembly of functional molecules through multiple non-covalent interactions to prepare long range ordered and defect-free assemblies barely accessible through conventional covalent synthesis. However, an intrinsic drawback of investigating such systems in solution or in a crystal is that molecular components cannot be directly addressed on a nanometric scale. As a consequence, the best engineering methodology involves modifying the surfaces of bulk materials such as metals or semiconductors by deposition of functional organic materials. The modified surfaces are then characterised using scanning probe microscopies (*e.g.* STM, AFM). To this end, surface-confined, supramolecularly constructed, bi-dimensional (2D) networks, featuring regular porous domains (controllable both in shape and size) are of particular significance in this research domain because their cavities can be used as receptors for the confinement of other remotely controlled functional molecules (*e.g.* molecular switches, luminescent chromophores). Since these complex nanostructures could ultimately find applications as optoelectronic devices, research efforts in this domain have been gathering momentum in recent years.

In Chapter 1, the reader is introduced to the methods employed to construct porous networks on surfaces via supramolecular interactions. The second part of the chapter deals with recent examples of recognition, selection and immobilisation of guest molecules within the cavities of the networks, which is followed in the third part with a discussion about surface assemblies that display structural features or functionality in the third dimension. The

last section of the chapter is devoted to the construction of porous networks on surfaces via the interactions of biomimetic molecules (*e.g.* DNA), which leads to the objectives of the present doctoral project.

Inspired by the self-assembly of DNA into nanoporous arrays, it was postulated that the Watson-Crick base pairing of oligonucleotide's nucleobases would be ideal in preparing 2D porous networks with large receptor cavities. The idea was to covalently attach complementary single stranded oligonucleotides to rigid angular and linear unit core modules respectively, and then allow the two units to self-assemble on surfaces. However, instead of using DNA oligonucleotides, the use of peptide nucleic acid (PNA) oligonucleotides was proposed since more robust architectures would be obtained due to the higher duplex stability displayed by this class of biomimetic molecules. This doctoral dissertation describes the synthetic steps taken towards achieving this goal.

The design of the angular and linear units bearing complementary PNA oligomers, required for the preparation of self-assembled nanoporous arrays are shown in Figure i. However, prior to synthesizing these complex molecules, a simpler proof of principle was required to confirm that PNA duplexes could be formed on surfaces and also, whether the presence of chromophoric moieties (*e.g.* porphyrin) appended to the PNA strands had any effect on duplex formation and duplex stability. The molecule designed for this proof of principle was a self-complementary PNA dodecamer bearing a porphyrin adduct (Figure ii).

Angular units:

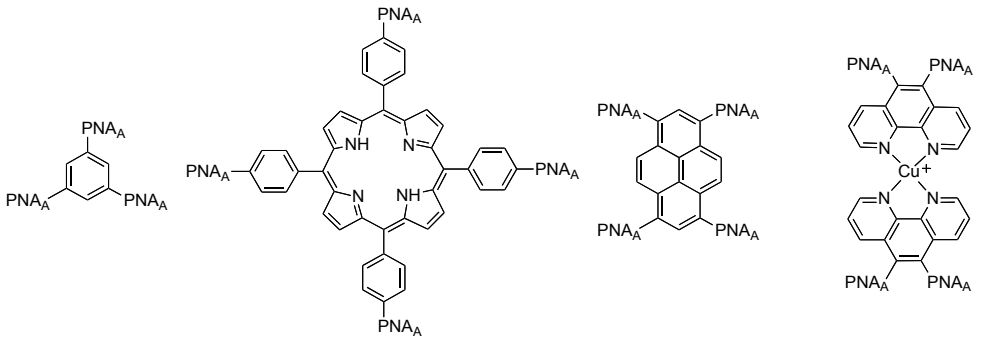

86 **87** **88** **89**

Linear units:

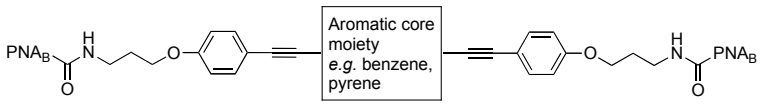

90

Figure i. The design of the angular and linear units.

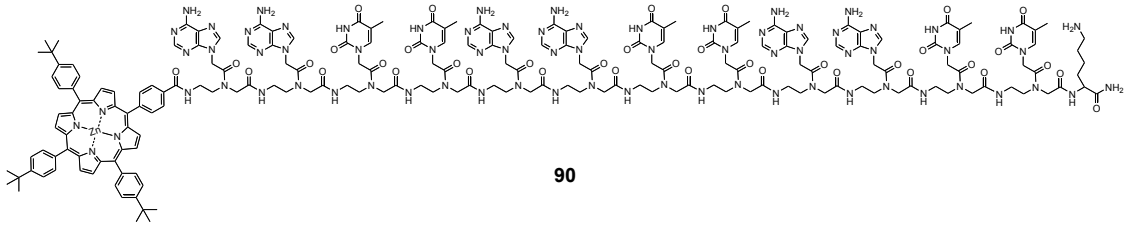

90

Figure ii. The self-complementary PNA-porphyrin adduct designed to serve as the proof of principle.

The synthesis of the self-complementary PNA oligomer required for the preparation of the PNA-porphyrin adduct is described in the first part of Chapter 2. The main synthetic routes and protecting-group strategies used to prepare PNA monomers and oligomers are described first. This is followed by a discussion of the orthogonal protecting group strategies chosen for our project that would allow the isolation of PNA oligomers bearing protected nucleobases following resin-cleavage. This is contrary to the general norm in existing strategies wherein resin-cleavage and nucleobase deprotection is carried out *in situ*, however, it was required in our synthetic strategy since the terminal amino group of the PNA oligomers was required for further solution phase reactions. To this end, two protecting group strategies were proposed, a Fmoc/Mmt and Fmoc/Cbz-protecting group strategies. The solid support chosen for the Fmoc/Mmt strategy was Tentagel featuring a base-cleavable linker. Due to the failure to hydrolyse the linker during the resin-cleavage step, the Fmoc/Mmt strategy was abandoned. In the second strategy, an acid-cleavable Rink amide resin was chosen as the solid support, therefore a Fmoc/Cbz-protecting group strategy was chosen since it would allow the TFA-mediated cleavage of the oligomer from the resin, without the deprotection of the Cbz groups from the nucleobases.

The preparation of the target PNA oligomer (sequence: TTAATTAATTAA) using the Fmoc/Cbz strategy is described in the next section. First, the required monomers for the oligomer synthesis were prepared using established procedures. Then, following reports of the advances in microwave assisted solid phase peptide synthesis claiming improved purity of oligomer products using short coupling times, the solid phase PNA oligomerisation was attempted using microwave irradiation. Three attempts were performed. The first, using a standard laboratory microwave, resulted in a complex mixture of products at the dodecamer stage. An improvement was observed in the results using the CEM discover SPS microwave which was specifically designed for solid phase synthesis, however, the crude dodecamer obtained was still inseparable from the by-products. Similar results were obtained with the CEM liberty microwave, which was an automated solid phase synthesis setup. Finally, utilising manual solid phase synthesis, the target PNA dodecamer was obtained. The HPLC chromatogram of crude PNA dodecamer obtained following resin cleavage displayed a single major product, which was subsequently purified. The oligomer was then deprotected by

treatment with TMSI, and was analysed by mass spectrometry, which confirmed that the target dodecamer had been isolated.

Section 2.2 described our efforts to prepare PNA-chromophore adducts. Following the isolation of the PNA dodecamer, attempts to covalently attach a porphyrin moiety to the resin-bound oligomer via an amide linkage failed, possibly due to steric hindrance. Subsequently, an azide linker was appended to the oligomer, and attempts to attach an acetylene functionalised porphyrin using a Cu(I)-catalysed 1,3-dipolar cycloaddition were performed. Unfortunately, this approach also did not yield the target adduct. These unsuccessful results paved the way to the development of a Cu(I)-free 1,3-dipolar cycloaddition that enabled the attachment of chromophores to the PNA oligomer.

Recently published reports of Cu(I)-free 1,3-dipolar cycloaddition reactions applied on DNA oligomers offered inspiration towards this goal. The reported strategies involved the generation of a nitrile oxide species, which then reacted with either an alkene or an alkyne to form an isoxazoline or an isoxazole. Two methods of generating the nitrile oxide species were evaluated using anthracene derivatives. The first method involved the base-mediated dehydrochlorination of anthracene hydroximoyl chloride to yield the nitrile oxide, which then reacted with a dipolarophile that was introduced into the reaction mixture. The second approach to generating a nitrile oxide species involved treating an *O*-silylated hydroxamic acid derivative of anthracene with trifluoromethanesulfonic anhydride in the presence of a base (Carreira's method). Following successful trapping of the nitrile oxides generated by both methods using trimethylsilyl ethylene as the dipolarophile, the reactions were applied on a resin-bound, acetylene-functionalised PNA dodecamer. Both methods yielded the target PNA-anthracene adduct (Figure iii).

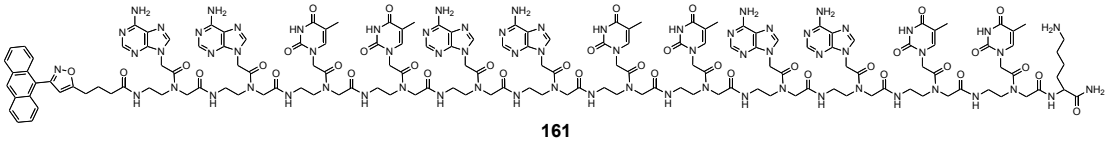

161

Figure iii. Molecular structure of the PNA-anthracene adduct.

Since the nitrile oxide-acetylene 1,3-dipolar cycloaddition reaction had never been applied on porphyrins, a method had to be developed. Attempts to prepare a hydroximoyl chloride derivative of a porphyrin resulted in the decomposition of the macrocycle upon treatment with chlorinating agents (NCS, *tert*-BuOCl, and 1-chlorobenzotriazole), therefore, the hydroximoyl chloride method was abandoned in favour of the Carreira method. An *O*-silylated hydroxamic acid derivative of porphyrin was synthesized, and upon exposure to trifluoromethanesulfonic anhydride and Et_3N, the nitrile oxide was generated and was trapped

with a large excess (200 eq.) of trimethylsilyl ethylene yielding the target tetra-isoxazole porphyrin (Figure iv) derivative in 62% yield, which corresponded to a yield of 89% per 1,3-dipolar cycloaddition. Optimisation of the reaction conditions using phenyl acetylene as the dipolarophile allowed similar yields to be obtained with only a 10 eq. excess of the acetylene.

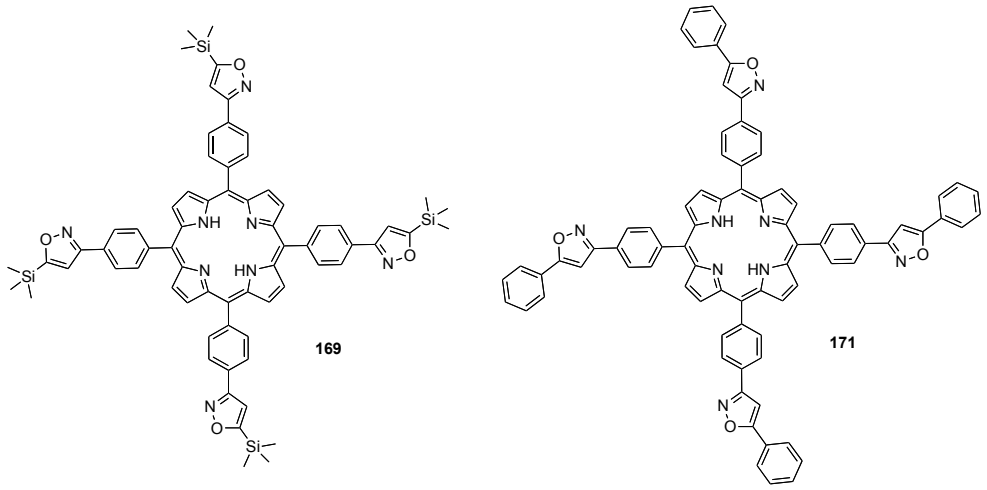

Figure iv. Molecular structures of the tetra-isoxazole porphyrins isolated using a Cu(I)-free nitrile oxide-acetylene 1,3-dipolar cycloaddition reaction. The nitrile oxide was generated using the Carreira method.

Having developed a protocol that was compatible with both PNA and porphyrin, the utility of the method to prepare a variety of PNA-chromophore adducts was tested. Hydroxamate derivatives of pyrene, porphyrin, phenanthroline and fluorescein chromophores were prepared. Subsequently, the corresponding nitrile oxide species were generated and were reacted with the resin-bound, acetylene-functionalised PNA dodecamer. The PNA-pyrene adduct was successfully isolated (Figure v), however, the other target PNA-chromophore products were not isolated. The porphyrin nitrile oxide derivative was insoluble in the reaction medium, thus preventing the cycloaddition reaction from proceeding. In the case of the fluorescein hydroxamate, the presence of nucleophilic functional groups in the starting material were probably reactive towards the trifluoromethanesulfonic anhydride reagent, therefore it was unlikely that the nitrile oxide species was formed, and thus the cycloaddition reaction could not proceed. Finally, the reaction with the phenanthroline derivative yielded a new product, however mass spectrometry analysis indicated that it did not correspond the target PNA-phenanthroline adduct. Further work is currently underway to re-evaluate these reactions.

In parallel to the synthetic work, a preliminary study into the deposition of PNA onto mica surfaces was investigated using AFM imaging. Deposition of drops of an aqueous

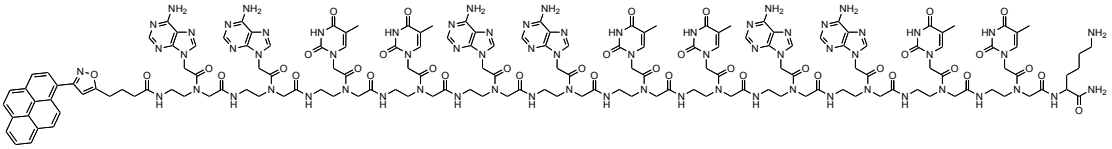

184

Figure v. Molecular structure of the PNA-pyrene adduct.

solution of deprotected self-complementary PNA dodecamer onto clean mica surfaces using spin coating resulted in aggregates of PNA on the surface (Figure vi [left]). Following annealing of the solution, a repeated deposition of a single drop of the solution resulted in a completely different surface assembly. The surface was saturated by what was thought to be PNA duplexes. This was confirmed by the deposition of drop of a solution that was diluted ten-fold which resulted in an AFM image where bright spot were intermitted by clean mica surface (Figure vi [right]). Topographical analysis of the surface indicated that the bright spots were an average in 1 nm in height, which closely corresponds to the expected height of PNA duplexes, thus confirming that PNA duplexes could be deposited onto surfaces.

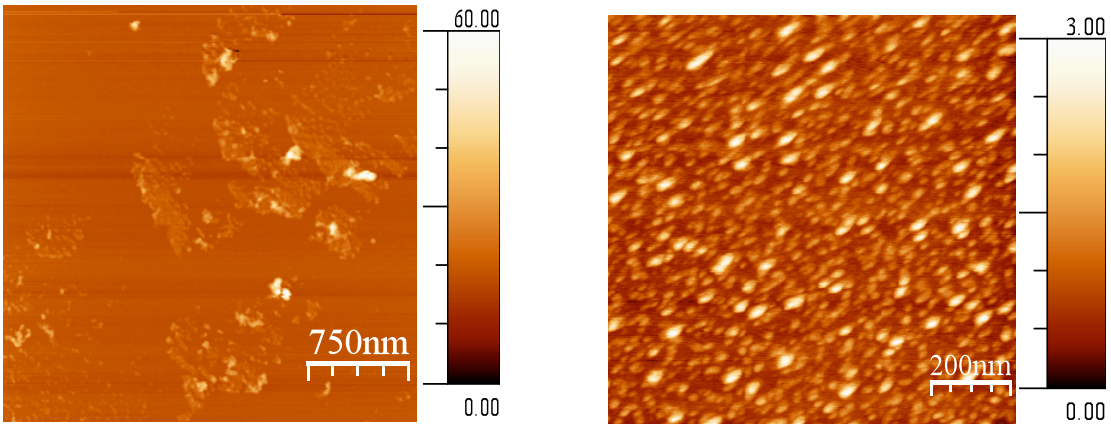

Figure vi. Tapping mode AFM images displaying (left) aggregates and (right) duplexes of PNA oligomers on mica surfaces following spin coating of a drop of a pre-annealing (left) and post-annealing (right) PNA solution. The height scales of the AFM image are 60 nm (left) and 3 nm (right).

Résumé

"There is plenty of room at the bottom". Ces célèbres mots, prononcés par Richard P. Feynman en 1959, conduisirent à la naissance de la nanotechnologie et de la nanoscience. Les appareils électroniques à base de semi-conducteurs font partie de notre quotidien depuis ces dernières six décennies. Leur miniaturisation a pris place graduellement au cours des années, cependant, d'après la loi de Moore, la technique de production *"top-down"* de l'industrie microélectronique contemporaine atteindra bientôt ses limites. Dès lors, les développements récents et la connaissance accrue des semi-conducteurs organiques ont mené à l'exploration de voies alternatives se concentrant sur la création d'appareils électroniques à base de molécules organiques. L'invention de techniques telles que la *STM* (1981) et *l'AFM* (1986) ont facilité cette recherche, permettant l'imagerie et la manipulation de surfaces et de molécules à l'échelle nanométrique (0.1-100 nm). L'étape suivante est alors le développement de méthodes permettant le contrôle de la fabrication d'assemblages moléculaires et leur intégration dans des systèmes macroscopiques fonctionnels. À cet égard, l'approche *"bottom-up"* offre des avantages considérables par rapport aux autres méthodologies (*i.e."top-down"*) pour la construction à l'échelle nanométrique de matériaux et appareils fonctionnels. Cette approche exploite généralement l'auto-assemblage hiérarchique de molécules fonctionnelles *via* de multiples interactions non-covalentes afin de préparer des assemblages ordonnés à longue-distance et sans défauts inhérents, à peine accessibles par de la synthèse covalente conventionnelle. Cependant, investiguer de tels systèmes en solution ou dans un cristal présente un inconvénient intrinsèque. En effet à l'échelle nanométrique, tous les composés moléculaires ne peuvent être atteints. Dès lors, la modification des surfaces de matériaux tels que les métaux ou semi-conducteurs, par déposition de matériaux organiques fonctionnels, semble être la méthodologie d'ingénierie la plus prometteuse. Les surfaces modifiées sont alors caractérisées *via* des microscopies à sonde locales (tel que la *STM, AFM*). À cette fin, des réseaux bidimensionnels (2D) construits d'une manière supramoléculaire que présentant une surface confinée et des domaines poreux réguliers (contrôlables à la fois en forme et en taille) sont d'une importance particulière dans ce domaine de recherche, étant donné que leurs cavités peuvent être utilisées comme récepteurs pour le confinement d'autres molécules fonctionnelles (comme par exemple des interrupteurs moléculaires ou des chromophores luminescents). Puisque ces nanostructures complexes pourraient ultimement trouver des applications comme appareils optoélectroniques, des efforts de recherche dans ce domaine ont provoqué beaucoup d'enthousiasme au cours des dernières années.

Dans le Chapitre 1, les méthodes employées pour construire des domaines poreux sur surfaces *via* des interactions supramoléculaires sont introduites au lecteur. La deuxième partie de ce chapitre traite des exemples récents de reconnaissance, sélection et immobilisation de molécules *guest* dans les cavités du réseau. Celle-ci est suivie d'une troisième partie présentant une discussion sur les assemblages sur surface exposant des caractéristiques structurelles ou des fonctionnalités dans la troisième dimension. La dernière section de ce chapitre est dévouée à la construction de réseaux poreux sur surfaces *via* les interactions de molécules biomimétiques (tel que l'ADN), ce qui mène ainsi aux objectifs de ce présent projet de thèse.

Sur base de l'auto-assemblage de l'ADN en réseaux nanoporeux, il a été postulé que l'appariement de Watson-Crick des nucléobases de l'oligonucléotide serait idéal pour la préparation de domaines 2D poreux présentant de larges cavités réceptrices. Notre idée fut d'attacher covalement des oligonucléotides complémentaires à simples brins à des modules rigides angulaires et linéaires, respectivement, et ainsi permettre aux deux modules de s'auto-assembler sur surface. Cependant, nous avons proposé l'utilisation d'oligonucléotides d'acides nucléiques peptidiques (ANP) en lieu et place d'oligonucléotides d'ADN afin d'obtenir des architectures plus robustes grâce à la stabilité plus élevée des duplex formés par cette classe de molécules biomimétiques. Cette dissertation doctorale décrit les étapes synthétiques réalisées afin d'accomplir cet objectif.

La conception des unités angulaires et linéaires portant des oligomères d'ANP complémentaires nécessaires à la préparation des réseaux nanoporeux auto-assemblés est décrite à la Figure i. Toutefois, avant de synthétiser ces molécules complexes, une preuve de principe plus simple était nécessaire pour confirmer que les duplex d'ANP pouvaient être formés sur surface, et également observer si la présence d'entités chromophoriques (comme la porphyrine) attachés aux brins d'ANP avait des effets sur la formation du duplex et sa stabilité. La molécule élaborée à cet égard fut un adduit formé par un dodécamère auto-complémentaire d'ANP portant une porphyrine (Figure ii).

La synthèse de l'oligomère auto-complémentaire d'ANP requis pour la préparation de l'adduit ANP-porphyrine est décrite dans la première partie du Chapitre 2. Les voies de synthèse principales et les stratégies de protection utilisées pour préparer les monomères et oligomères d'ANP sont décrites en premier lieu. Ensuite, une discussion sur les stratégies de protections orthogonales choisies pour notre projet est introduite au lecteur. Celles-ci permettraient l'isolation d'oligomères d'ANP portant des nucléobases protégées après clivage de la résine. Une telle stratégie est contraire aux normes rencontrées dans les méthodologies existantes, dans lesquelles le clivage de la résine et la déprotection des nucléobases sont réalisés *in situ*. Cela dit, procéder autrement était indispensable pour notre stratégie de

Unités angulaires:

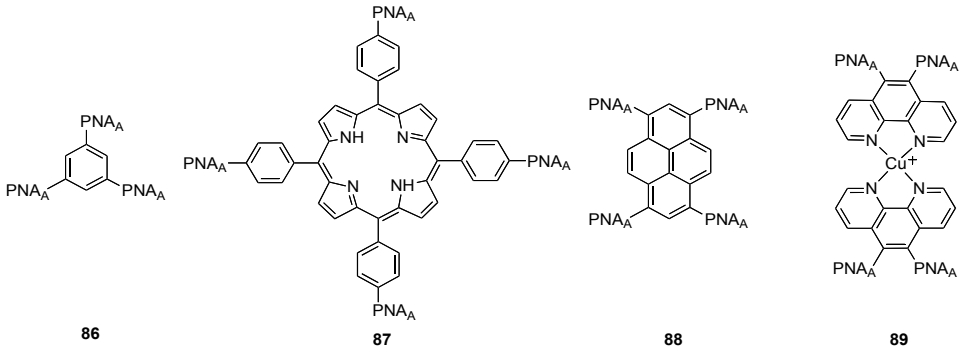

86 **87** **88** **89**

Unités linéaires:

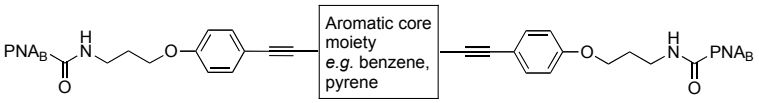

90

Figure i. La conception des unités angulaires et linéaires.

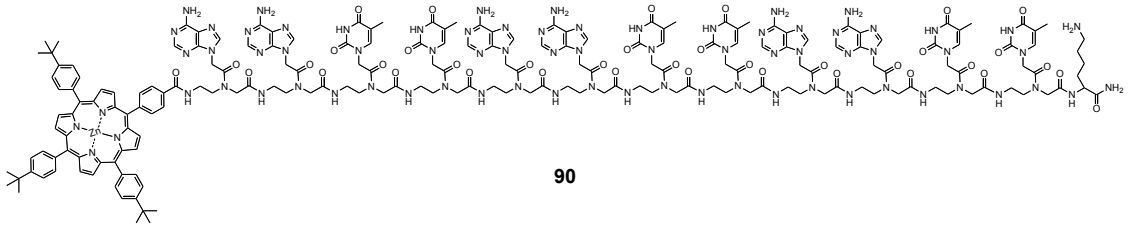

90

Figure ii. L'adduit ANP auto-complémentaire–porphyrine élaboré pour servir de preuve de principe.

synthèse puisque le groupement aminé terminal des oligomères d'ANP est nécessaire pour des réactions ultérieures en solution. A cette fin, nous avons proposé deux stratégies de protection, l'une impliquant des groupements protecteurs Fmoc/Mmt, et l'autre des groupements protecteurs Fmoc/Cbz. Le support solide choisi pour la stratégie Fmoc/Mmt fut le Tentagel, présentant un lien clivable dans des conditions basiques. À cause de l'hydrolyse non concluante de ce lien pendant l'étape de clivage de la résine, nous avons abandonné la stratégie Fmoc/Mmt. Dans la seconde stratégie, nous avons choisi comme support solide une résine amide de *Rink* clivable dans des conditions acides. Dès lors nous avons choisi une stratégie exploitant les groupements protecteurs Fmoc/Cbz puisque celle-ci permettrait le clivage de l'oligomère de la résine par du TFA, sans déprotéger les groupements protecteurs Cbz des nucléobases.

La préparation de l'oligomère d'ANP cible (séquence: TTAATTAATTAA) utilisant la stratégie Fmoc/Cbz est décrite dans la section suivante. Tout d'abord, les monomères

requis pour la synthèse de l'oligomère ont été préparés à partir de procédures déjà établies. Ensuite, sur base de rapports décrivant les avancées réalisées en synthèse peptidique sur phase solide assistée par micro-onde et clamant une pureté accrue des produits d'oligomérisation, tout en utilisant des temps de couplage courts, nous avons tenté de réaliser l'oligomérisation de l'ANP sur phase solide en utilisant des irradiations micro-ondes. Trois tentatives ont été effectuées. La première impliquait l'utilisation d'un micro-onde standard de laboratoire. Cet essai a résulté en un mélange complexe de produits au niveau du dodécamère. Une amélioration des résultats a été observée en utilisant le micro-onde *CEM discover SPS*, conçu spécifiquement pour la synthèse sur phase solide. Cependant, le dodécamère désiré était toujours inséparable des sous-produits. Des résultats similaires ont été observés avec le micro-onde *CEM liberty*, un système automatisé pour la synthèse sur phase solide. Finalement, en réalisant une synthèse manuelle sur phase solide, le dodécamère d'ANP cible a été obtenu. Le chromatogramme HPLC du brut du dodécamère d'ANP obtenu après clivage de la résine montre un seul produit majoritaire, qui a été purifié par la suite. L'oligomère a alors été déprotégé par traitement avec du TMSI et a été analysé par spectrométrie de masse, qui a confirmé que le dodécamère cible avait bien été isolé.

La section 2.2 décrit nos efforts pour préparer les adduits ANP-chromophore. Après avoir isolé le dodécamère d'ANP, des tentatives pour attacher covalement *via* un lien amide l'entité porphyrine à l'oligomère lié à la résine ne furent guère concluantes, certainement dû à un encombrement stérique. Subséquemment, un linker azoture a été greffé à l'oligomère, et des essais pour attacher une porphyrine fonctionnalisée par un groupement acétylène, *via* une cycloaddition 1,3-dipolaire catalysée par du Cu(I) ont été réalisés. Malheureusement, cette approche n'a pas non plus fourni l'adduit cible. Ces résultats non fructueux ont ouvert la voie au développement d'une cycloaddition 1,3-dipolaire sans Cu(I), qui a elle permis la liaison des chromophores aux oligomères d'ANP.

De récents rapports publiés sur les réactions de cycloaddition 1,3-dipolaire sans Cu(I) appliquées sur des oligomères d'ADN nous ont inspiré et aidé à atteindre ce but. Les stratégies rapportées impliquaient la génération d'un oxyde de nitrile, qui était alors mis en réaction avec soit un alcène ou un alcyne, pour former une isoxazoline ou un isoxazole respectivement. Deux méthodes permettant la génération des espèces d'oxyde de nitrile ont été évaluées en utilisant des dérivés anthracène. La première méthode impliquait une déhydrochlorination en présence d'une base, du chlorure d'hydroximoyle de l'anthracène, pour fournir l'oxyde de nitrile. Celui-ci était alors mis en réaction avec un dipolarophile introduit par la suite dans le mélange réactionnel. La seconde approche menant à la génération de l'oxyde de nitrile impliquait le traitement d'un dérivé acide hydroxamique *O*-silylé d'anthracène avec de l'anhydride trifluorométhanesulfonique en présence d'une base

(méthode de Carreira). Après piégeage concluant des oxydes de nitrile générés par chacune des méthodes, en utilisant de l'éthylène triméthylsilyle comme dipolarophile, les réactions ont été appliquées sur un dodécamère d'ANP lié à la résine et fonctionnalisé par un groupement acétylène. Chacune des deux méthodes a généré l'adduit cible ANP-anthracène (Figure iii).

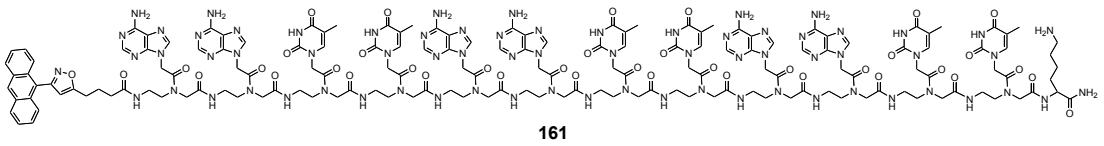

161

Figure iii. Structure moléculaire de l'adduit ANP-anthracène.

La réaction de cycloaddition 1,3-dipolaire entre un oxyde de nitrile et un acétylène n'ayant jamais été réalisée sur des porphyrines, nous avons dû développer une méthode. Des tentatives pour préparer le dérivé chlorure d'hydroximoyle de la porphyrine ont toutes résulté en la décomposition du macrocycle dès traitement avec des agents de chlorination (NCS, *tert*-BuOCl, et 1-chlorobenzotriazole). En conséquence, la méthode du chlorure d'hydroximoyle a été abandonnée pour la méthode de Carreira. Un dérivé d'acide hydroxamique *O*-silylé de porphyrine fut alors synthétisé, et lors de l'addition d'anhydride trifluorométhanesulfonique et de Et_3N, l'oxyde de nitrile fut généré et trappé avec un grand excès (200 eq.) d'éthylène triméthylsilyle, formant la porphyrine tetra-isoxazole désirée (Figure iv) avec un rendement de 62 %, ce qui correspond à un rendement de 89 % par cycloaddition 1,3-dipolaire. L'optimisation des conditions de réaction en utilisant un phénylacétylène comme dipolarophile a permis l'obtention de rendements similaires avec seulement 10 eq. d'excès en acétylène.

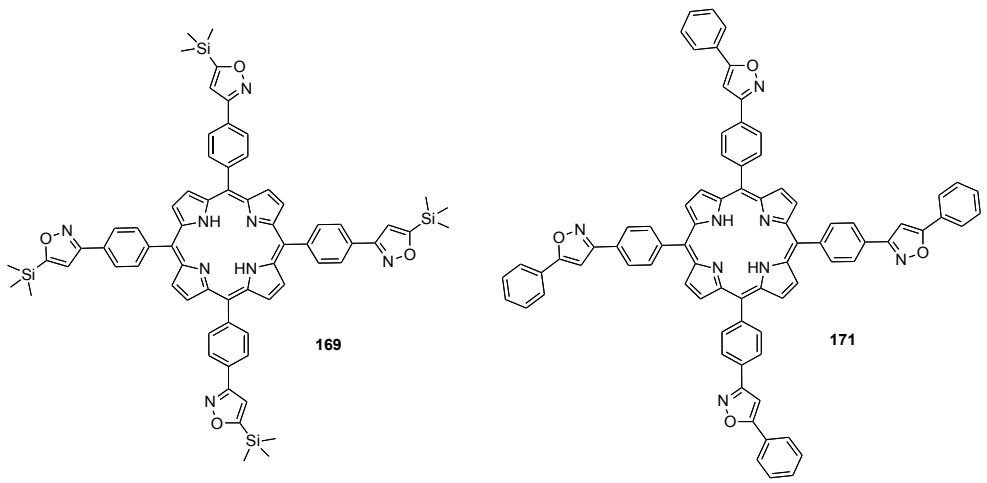

169 **171**

Figure iv. Structures moléculaires des porphyrines tetra-isoxazole isolées en utilisant une réaction de cycloaddition 1,3-dipolaire sans Cu(I) entre de l'oxyde de nitrile et de l'acétylène. L'oxyde de nitrile a été généré en utilisant la méthode de Carreira.

Ayant développé un protocole compatible à la fois avec l'ANP et la porphyrine, l'utilité de la méthode pour préparer une variété d'adduits ANP-chromophore a été testée. Des dérivés hydroxamates de chromophores pyrène, porphyrine, phénanthroline et fluorescéine ont été préparés. Ensuite, les espèces oxyde de nitrile correspondantes ont été générées et mises en réactions avec le dodécamère d'ANP lié sur la résine et fonctionnalisé par un groupement acétylène. L'adduit ANP-pyrène a été isolé avec succès (Figure v), tandis que les autres produits cibles ANP-chromophore n'ont pas été isolés. Le dérivé oxyde de nitrile de la porphyrine était insoluble dans le milieu réactionnel, empêchant ainsi la réaction de cycloaddition de se réaliser. Dans le cas de l'hydroxamate de fluorescéine, les groupements fonctionnels nucléophiles présents dans le produit de départ ont probablement réagit avec le réactif anhydride trifluorométhanesulfonique, empêchant probablement ainsi la formation des espèces d'oxyde de nitrile, et donc la réaction de cycloaddition d'avoir lieu. Finalement, la réaction avec le dérivé phénanthroline a fourni un nouveau produit. Cependant les analyses de spectrométrie de masses ont indiqué que ce dernier ne correspondait pas à l'adduit ANP-phénanthroline désiré. Des recherches supplémentaires sont en cours afin de réévaluer ces réactions.

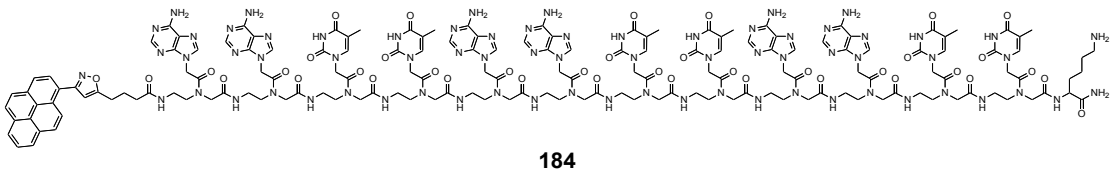

184

Figure v. Stucture moléculaire de l'adduit ANP-pyrène.

Parallèlement au travail synthétique, une étude préliminaire sur la déposition d'ANP sur des surfaces de mica a été examinée en utilisant de l'imagerie *AFM*. La déposition par *spin coating* de gouttes d'une solution aqueuse du dodécamère auto-complémentaire d'ANP déprotégé sur une surface de mica propre a résulté en des agrégats d'ANP sur la surface (Figure vi [gauche]). Après *annealing* de la solution, une nouvelle déposition d'une seule goutte de solution a résulté en un assemblage sur la surface tout à fait différent. La surface était saturée par ce que nous croyions être des duplex d'ANP. Ceci fut confirmé par la déposition d'une goutte de solution diluée dix fois, qui a résulté en une image *AFM* où des spots lumineux étaient séparés les uns des autres par la surface de mica propre (Figure vi [droite]). Une analyse topographique de la surface a indiqué que les spots lumineux avaient une hauteur moyenne de 1 nm, ce qui correspond très fortement à la hauteur attendue des duplex d'ANP, confirmant ainsi que les duplex d'ANP pouvaient être déposés sur surface.

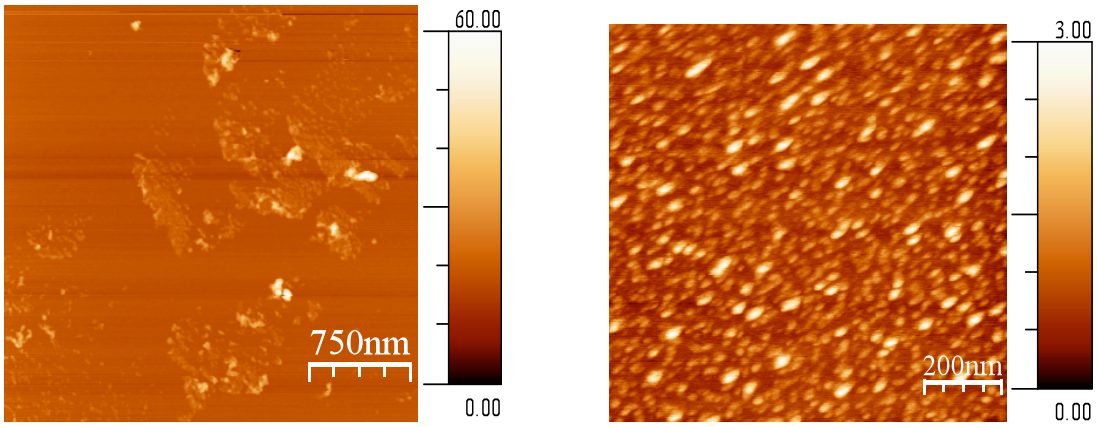

Figure vi. Images AFM en mode *tapping* montrant des agrégats (gauche) et des duplex (droite) d'oligomères d'ANP sur des surfaces de mica, après *spin coating* d'une goutte d'une solution d'ANP avant *annealing* (gauche) et après *annealing* (droite). L'échelle de hauteur des images *AFM* est de 60 nm (gauche) et 3 nm (droite).

Riassunto

"There is plenty of room at the bottom" - C'è spazio in abbondanza in fondo-. Queste le famose parole con cui Richard P. Feyman nel 1959 inaugurò i concetti di nanotecnologia e di nanoscienza. Le apparecchiature elettroniche basate su semiconduttori inorganici sono stati parte integrante della nostra vita quotidiana negli ultimi 60 anni. La loro miniaturizzazione è avvenuta gradualmente negli anni, ma d'altra parte, secondo la legge di Moore, la tecnica di produzione "*top-down*" dell'industria microelettronica contemporanea raggiungerà presto i suoi limiti. Pertanto, il recente sviluppo e la maggiore conoscenza dei semiconduttori organici hanno portato ad esplorare vie alternative, ponendo particolare attenzione alla creazione di dispositivi elettronici basati su molecole organiche. L'invenzione delle tecniche microscopiche di scansione ("scanning probe microscopies") quali STM (1981) e AFM (1986) ha facilitato questa ricerca, permettendo sia l'acquisizione di immagini che la manipolazione di superfici e molecole su scala nanometrica (0.1-100 nm). Il prossimo passo riguarderà perciò lo sviluppo di nuovi metodi per la produzione controllata di set molecolari e la loro implementazione in *devices* elettronici macroscopici. In questo senso, l'approccio sintetico "bottom-up" offre considerevoli vantaggi rispetto alle altre tecniche di miniaturizzazione (per es. "top-down") impiegate per la costruzione di materiali e dispositivi funzionalizzati su scala nanometrica. Questo approccio sfrutta generalmente il *self-assembly* gerarchizzato di molecole funzionali, in grado di interagire attraverso multiple interazioni non covalenti, formando sistemi multimolecolari ordinati su lungo raggio e privi di difetti, difficilmente accessibili attraverso i metodi classici di sintesi covalente. Uno svantaggio intrinseco dello studio di tali sistemi in soluzione o in cristalli è che le molecole non possono essere direttamente assemblate su scala nanometrica. Di conseguenza, la migliore tecnica di ingegnerizzazione consiste nella deposizione di materiali organici funzionali su superfici metalliche e semiconduttrici. Le superfici modificate così ottenute, sono quindi caratterizzate usando tecniche microscopiche di scansione (per es. STM, AFM). I reticoli supramolecolari bidimensionali (2D) depositati su superficie, caratterizzati da domini porosi (controllabili sia in forma che in dimensione), sono di particolare rilievo in questo ambito di ricerca, poiché le loro cavità possono fungere da recettori per il confinamento di altre molecole funzionali controllandole a distanza (per es. interruttori molecolari, cromofori luminescenti). Dal momento che queste complesse nano-strutture potrebbero trovare applicazione come dispositivi optoelettronici, gli sforzi della scienziati in questo ambito si sono notevolmente intensificati negli ultimi anni.

Nel Capitolo 1, il lettore viene introdotto ai diversi metodi impiegati per la costruzione di reticoli porosi su superficie attraverso interazioni supramolecolari. La seconda parte del capitolo riguarda esempi recenti di ricognizione, selezione e immobilizzazione di molecole ospiti all'interno delle cavità dei reticoli, ed a seguire nella terza parte verranno discussi *assembly* molecolari che mostrano caratteristiche o funzionalità strutturali anche nella terza dimensione. Infine, l'ultima sezione del capitolo è dedicata alla costruzione di reticoli porosi su superficie, attraverso le interazioni tra molecole biomimetiche (per es. DNA), introducendo dunque il lettore all'obbiettivo finale del presente progetto di dottorato.

Inspirati dall'auto-assemblaggio del DNA in matrici nano porose, è stato postulato che l'accoppiamento delle nucleobasi di oligonucleotidi secondo il modello Watson-Crick sarebbe ideale per la creazione di reticoli porosi 2D dotati di grandi cavità come recettori. L'idea è quella di funzionalizzare covalentemente singoli filamenti di oligonucleotidi complementari con unità rigide angolari e lineari, e lasciare che le due unità si auto-assemblino sulla superficie. Invece di usare oligonucleotidi di DNA, è stato proposto l'uso di oligonucleotidi di acidi peptidonucleici (PNA), dal momento che si possono ottenere strutture più robuste, grazie alla maggiore stabilità mostrata da questa classe di molecole biomimetiche. Questa dissertazione dottorale descrive i passaggi sintetici adottati per raggiungere questo obbiettivo.

Le strutture delle unità angolari e lineari funzionalizzate con oligomeri di PNA complementari, necessarie per la preparazione di matrici nanoporose auto-assemblanti, sono mostrate in Figura i. Tuttavia, prima di sintetizzare queste molecole complesse, è stato

Unità angolari:

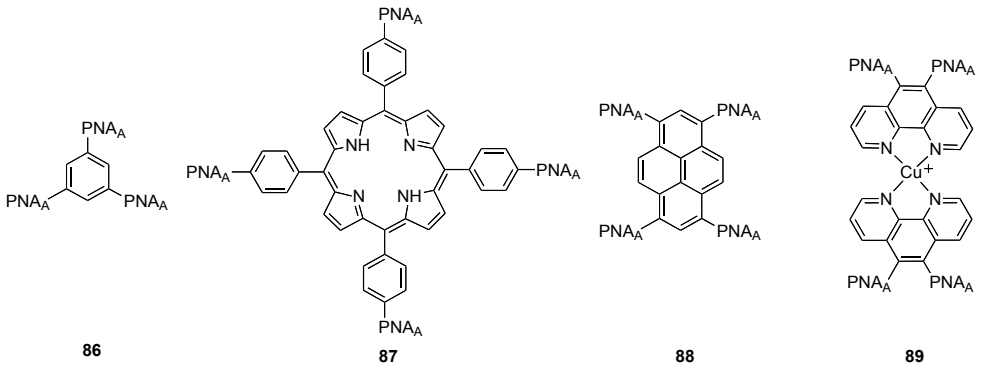

86 **87** **88** **89**

Unità lineari:

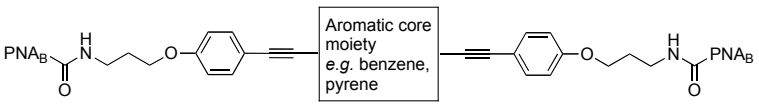

90

Figura i. Struttura della unità angolari e lineari

necessario dimostrare la validità del principio con un sistema più semplice, per confermare che la doppia elica di PNA potesse formarsi su superfici e verificare se la presenza di cromofori (per es. porfirine), legate alle catene di PNA, avesse qualche effetto sulla formazione della doppia elica e la stabilità della stessa.

La molecola progettata per questo test di prova è stata il dodecamero di PNA auto-complementare funzionalizzato con un addotto porfirinico (Figura ii).

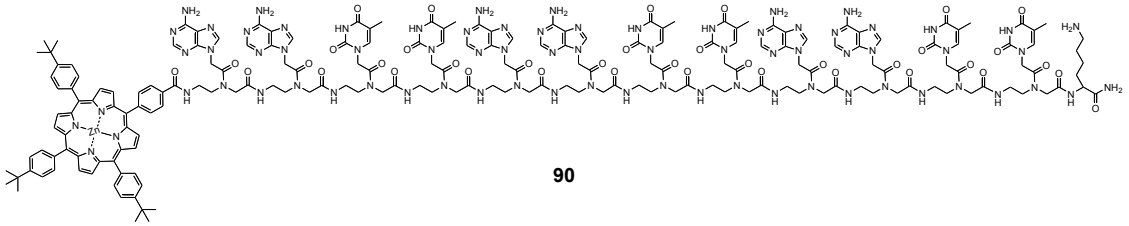

90

Figure ii. Addotto PNA-porfirina auto-complementare progettato per il test di prova

La sintesi dell'oligomero di PNA auto-complementare richiesta per la preparazione dell'addotto PNA-porfirina è descritta nella prima parte del Capitolo 2. Inizialmente sono illustrate le principali vie sintetiche e le strategie dei gruppi protettori usate per la preparazione di monomeri e oligomeri di PNA. A questa parte segue una discussione sulle strategie di gruppi protettori ortogonali scelti per il nostro progetto, che permettono l'isolamento degli oligomeri di PNA con le nucleobasi protette in seguito al lavaggio della resina. Ciò è contrario alle strategie comunemente utilizzate dove il lavaggio della resina e la deprotezione delle nucleobasi avviene *in situ*, tuttavia questo approccio è necessario nella nostra via sintetica, dal momento che il gruppo amminico terminale degli oligomeri di PNA servirà per ulteriori reazioni in soluzione. A questo fine, sono state proposte due diverse strategie di gruppi protettori, una strategia con Fmoc/Mmt e una con Fmoc/Cbz. Per la strategia Fmoc/Mmt è stato scelto il supporto solido Tentagel, caratterizzato da un linker rimovibile tramite lavaggio basico. A causa del fallimento dell'idrolisi del linker durante lo step di lavaggio della resina, la strategia Fmoc/Mmt è stata abbandonata. Nella seconda strategia è stata scelta una resina ammidica Rink a lavaggio acido come supporto solido, quindi una strategia con gruppi protettivi Fmoc/Cbz è stata adottata, in modo da permettere un lavaggio dell'oligomero dalla resina mediato da TFA, senza la deprotezione dei gruppi Cbz sulle nucleobasi.

La preparazione dell'oligomero target di PNA (sequenza: TTAATTAATTAA) usando la strategia Fmoc/Cbz è descritta nella sezione successiva. In primo luogo sono stati preparati i monomeri richiesti per la sintesi degli oligomeri, usando le procedure note in letteratura. In seguito, seguendo i dati recenti riguardanti la sintesi peptidica su fase solida mediata da microonde, ove si dichiara di ottenere una maggiore purezza degli oligomeri

prodotti in brevi tempi di reazione, è stata tentata l'oligomerizzazione di PNA su fase solida sfruttando le radiazioni del microonde. Sono stati fatti tre tentativi. Il primo, usando un normale microonde da laboratorio, ha portato a una complessa miscela di prodotti allo stadio di formazione del dodecamero. Un miglioramento è stato osservato usando il microonde "CEM discover SPS" che è stato specificamente progettato per la sintesi in fase solida, tuttavia, il grezzo del dodecamero ottenuto era ancora inseparabile dai sottoprodotti. Risultati simili si sono ottenuti con il microonde "CEM liberty", programmato per la sintesi automatizzata su fase solida. Infine, utilizzando la sintesi su fase solida manuale, si è ottenuto il dodecamero di PNA desiderato. Il cromatogramma registrato con analisi HPLC del grezzo del dodecamero di PNA, ottenuto in seguito al lavaggio dalla resina, ha mostrato un singolo picco maggioritario, che è stato successivamente purificato. L'oligomero è stato quindi deprotetto mediante trattamento con TMSI, ed è stato analizzato attraverso la spettroscopia di massa, che ha confermato l'effettivo isolamento del dodecamero desiderato.

Nella sessione 2.2 vengono descritti i nostri tentativi di sintesi degli addotti PNA-cromoforo. Dopo aver isolato il dodecamero di PNA, i tentativi di funzionalizzare covalentemente l'oligomero legato alla resina con un porfirina attraverso un legame ammidico non hanno avuto successo, probabilmente a causa dell'ingombro sterico. Di conseguenza un linker azidico è stato attaccato all'oligomero, e sono stati fatti diversi tentativi per legare la porfirina funzionalizzata con un acetilene attraverso la cicloaddizione 1,3-dipolare catalizzata da Cu(I). Anche questo approccio purtroppo non ha condotto al prodotto desiderato. Questi risultati negativi hanno spianato la strada allo sviluppo della cicloaddizione 1,3-dipolare in assenza di Cu(I) che dovrebbe permettere la formazione del legame tra i cromofori e l'oligomero di PNA.

Recenti pubblicazioni, che riportano l'applicazione di reazioni di cicloaddizione 1,3-dipolare in assenza di Cu(I) a oligomeri di DNA, hanno inspirato la scelta di questo obiettivo. Le strategie descritte implicavano la formazione di un ossido di nitrile che reagiva in seguito con un alchene o un alchino per generare un isossazolina o un isossazolo. Sono stati presi in considerazione due metodi per generare l'ossido di nitrile utilizzando derivati dell'antracene. Il primo metodo riguarda la deidroclorurazione base-catalizzata dell'idrossimoil cloruro dell'antracene per formare l'ossido di nitrile corrispondente, il quale reagisce con un dipolarofilo, precedentemente introdotto nella miscela di reazione. Il secondo approccio per generare un ossido di nitrile implica il trattamento di un acido idrossamico *o*-sililato derivato dell'antracene con anidride trifluorometansolfonica in presenza di una base (metodo di Carreira). In seguito all'isolamento dell'ossido di nitrile, prodotto con entrambi i metodi utilizzando il trimetilsilil etilene come dipolarofilo, le reazioni sono state applicate su un

dodecamero di PNA legato alla resina e funzionalizzato con un acetilene. Con entrambi i metodi è stato ottenuto l'addotto desiderato PNA-antracene (Figura iii).

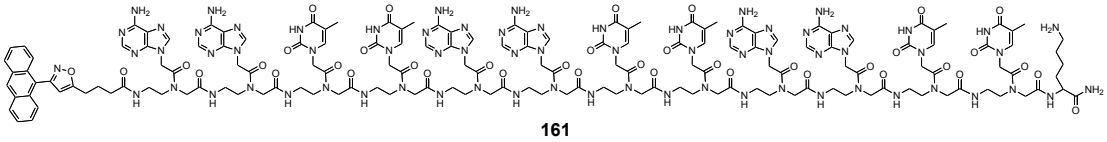

161

Figura iii. Struttura molecolare dell'addotto PNA-antracene.

Dal momento che non esistono esempi di reazione di ciclo addizione 1,3-dipolare tra ossido di nitrile e acetilene applicata alle porfirine, è stato necessario sviluppare un nuovo metodo di sintesi. I tentativi di sintetizzare un idrossimoil cloruro derivato della porfirina hanno portato alla decomposizione del macrociclo, a seguito di trattamento con agenti cloruranti (NCS, *tert*-BuOCl e 1-clorobenzotriazolo), per cui il metodo che prevede la formazione dell'intermedio idrossimoil cloruro è stato abbandonato, in favore del metodo di Carreira. L'acido idrossamico *o*-sililato derivato della porfirina è stato quindi sintetizzato e, in seguito al trattamento con anidride trifluorometansolfonica e trietilammina, è stato generato l'ossido di nitrile corrispondente. La conversione di quest'ultimo nel derivato porfirinico tetra-isossazolico (Figura iv) è stata ottenuto, impiegando un largo eccesso (200 equivalenti) di trimetilsilil etilene, con una resa del 62%, che corrisponde ad una resa dell'82% per ciclo addizione 1,3-dipolare. L'ottimizzazione delle condizioni di reazione, utilizzando il fenilacetilene come dipolarofilo, ha fornito risultati analoghi, lavorando con solo 10 equivalenti di acetilene in eccesso.

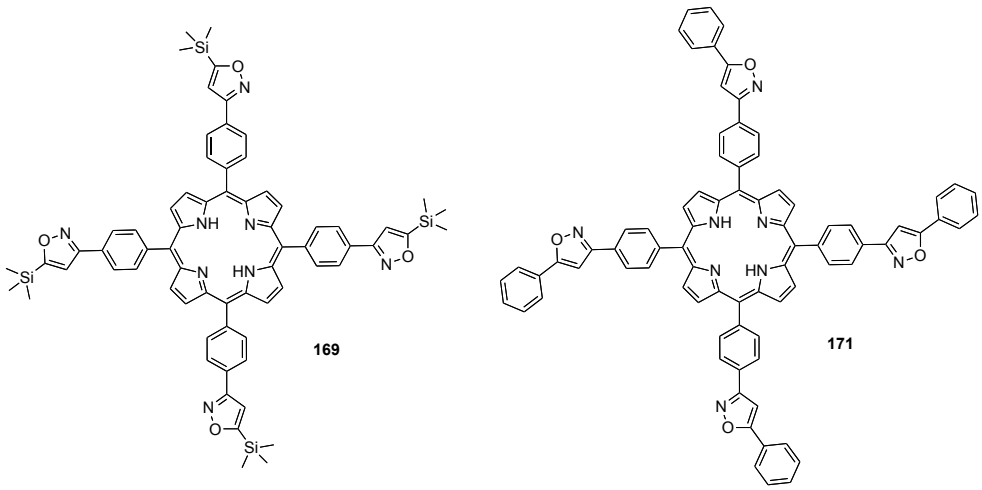

169 **171**

Figura iv. Strutture molecolari dei derivati tetra-isossazolici delle porfirine sintetizzati mediante reazione di cicloaddizione 1,3-dipolare, in assenza di Cu(I), tra ossido di nitrile e acetilene. L'ossido di nitrile è stato prodotto con il metodo di Carreira.

La procedura sviluppata, compatibile sia con il PNA che con le porfirine, è stata testata per verificarne l'applicabilità nella sintesi di una serie di addotti PNA-cromoforo. I corrispondenti derivati nitrilossidi dei cromofori sono stati sintetizzati e fatti reagire con il derivato acetilenico del dodecamero di PNA ancorato alla resina. Unicamente il complesso PNA-pirene è stato isolato (Figura v), al contrario degli altri target PNA-cromoforo. Il nitrilossido derivato della porfirina non era solubile nelle condizioni di reazione impiegate, impedendo la formazione dei prodotti di cicloaddizione. Nel caso del derivato fluoresceina idrossamato, la presenza del gruppo funzionale nucleofilo può aver dato luogo a una reazione collaterale con l'anidride trifluorometansolfonica, impedendo la formazione dell' ossido di nitrile corrispondente e, di conseguenza, impedendo la reazione di cicloaddizione. Infine, dalla reazione con il derivato della fenantrolina, è stato isolato un nuovo prodotto, che però non corrisponde all'addotto desiderato PNA-fenantrolina, come indicato dall'analisi di spettroscopia di massa. Sono in corso ulteriori studi per ottimizzare queste reazioni.

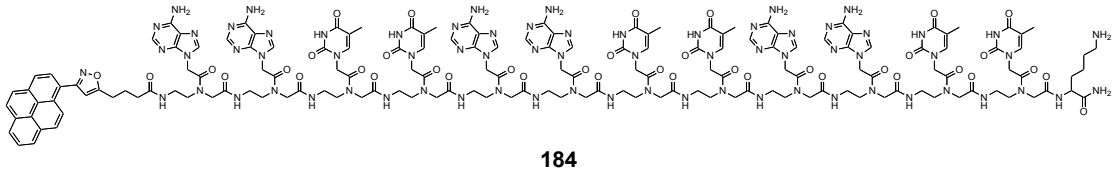

184

Figura v. Struttura molecolare del complesso PNA-pirene.

In parallelo alla sintesi dei composti suddetti, sono stati fatti studi sulla deposizione di PNA su superfici di mica, usando la tecnica di analisi AFM. Depositando la soluzione acquosa del dodecamero di PNA deprotetto e auto-complementare, con la tecnica *spin-coating*, si è osservata la formazione di aggregati di PNA sulla superficie (Figura vi [sinistra]). Dopo *annealing* della soluzione, ripetute deposizioni di singole gocce hanno permesso di ottenere una diversa funzionalizzazione della superficie. La mica risulta essere ricoperta da doppie eliche di PNA. Questo risultato è stato confermato depositando una goccia di soluzione di PNA diluita di dieci volte, le immagini AFM mostrano la presenza di punti luminosi alternati a tratti puliti di superficie (Figura vi [destra]). L'analisi topografica della superficie indica che i punti luminosi si trovano in media ad 1 nm di altezza, che corrisponde all'altezza attesa della doppia elica di PNA, confermando quindi che doppie eliche di PNA possono essere depositate sulla superficie.

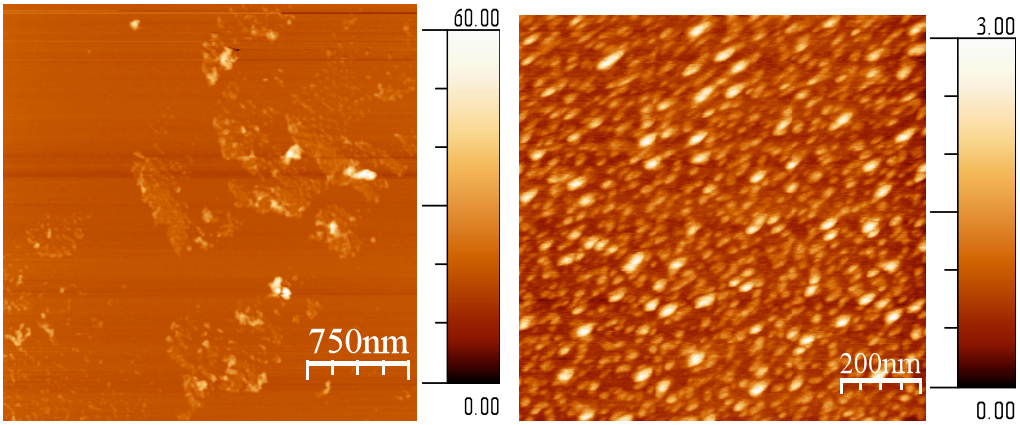

Figura vi. Immagini *tapping mode* AFM mostrano (a sinistra) aggregati e (a destra) doppie eliche di oligomeri di PNA su superfici di mica ottenute via *spin coating* di una goccia di soluzione di PNA *pre-annealing* (a sinistra) e *post-annealing* (a destra). L'altezza della scala delle immagini AFM è 60 nm (a sinistra) e 3 nm (a destra).

Introduction

The central challenge in the construction of molecular based devices is the necessity to develop methods for the controlled fabrication of well-defined organic systems, which meet the structural requirements for their nanotechnological applications. In this regard, the "bottom-up" approach based on non-covalent interactions offers considerable advantages over any other methodologies for the construction of ordered structures with nanometre precision over an extended large scale. The equilibrium between the constituents and the final product, along with the reversibility of the systems towards multistable nanostructured materials, contribute to the self-rearrangement of the components within the assembled structure and thus to the formation of long-range ordered and defect-free systems barely accessible through conventional covalent synthesis.[1-6] However, an intrinsic drawback of investigating such systems in solution or in a crystal is that molecular components cannot be directly addressed on a nanometric scale. As a consequence, the best engineering methodology involves modifying the surfaces of bulk materials such as metals or semiconductors by deposition of functional organic materials. In this regard, Scanning Probe Microscopies (SPM) and in particular Scanning Tunneling Microscopy techniques (STM)[7, 8] enable the nanoscale characterisation of these 2D molecule-based architectures in direct space. Although extensive work has been published on the study of the organisation of molecules on metallic surfaces,[9-23] strong hope is now put on the development of hybrid functional devices in which surfaces are modified with single molecules or molecular assemblies.[12, 24-26] The latter are believed to hold great promise to bring ultimate solutions in many applications ranging from electronics,[27-37] to medicine.[38, 39] Bi-dimensional (2D) networks, featuring regular porous domains (controllable both in shape and size) are of particular significance because their cavities can be used as receptors for the confinement of other remotely controlled functional molecules. For example the surface-confinement of luminescent chromophores could enhance their emissive properties in electroluminescent devices as a severe limitation with organic and metal-complexes luminophores is their susceptibility to the structural organization at the molecular level (e.g., their tendency to aggregate in solution) which induces multichromophoric interactions and dramatically alters the colour quality and the intensity of the emission signal. Moreover, porous networks may, not only serve as templates for the precise localisation of species through chemical interactions, but also, if properly equipped, as nanoreactors for the chemical transformation of encapsulated molecular reagents exploiting the spatial confinement as a strategy to achieve control over the chemical reactivity, stabilise

reactive species by isolating guests from the bulk environment or catalyse reactions effectively due to guest discrimination.[40]

Through the illustration of key examples that have recently appeared in the literature, the intention of this chapter is to provide a perspective of the current advances on molecular recognition at surfaces. In the first section (1.1) of the chapter, the main strategies that can be utilised to create extended 2D nano-porous patterned surfaces are illustrated. In the second section (1.2), the confinement of functional molecules within the cavities is discussed, emphasising on the selectivity and dynamicity of key supramolecular systems towards the hosting of molecular guests, with a particular focus on the biomolecular recognition and post-assembly covalent functionalisation. The third section (1.3), demonstrates that the third dimension can also be exploited. Surface confined molecules displaying structural features perpendicular to the surface will be described, as well as molecules displaying functionality in the third dimension. Moving from small molecules to oligomers, section 1.4 discusses the biomimetic approach *i.e.* examples where the porous networks are formed using DNA. This section leads on to the final section (1.5) in which, the objectives of the work described in this doctoral dissertation are presented.

1.1 POROUS NETWORKS

This section deals with the main strategies for the preparation of well-defined self-assembled architectures featuring pores on surfaces, which are directed by supramolecular interactions which join the molecular components via: *i*) H-bonding interactions (section 1.1.1.1), *ii*) dipole-dipole interactions and van der Waals contacts (section 1.1.1.2) and *iii*) metal-ligand coordination (section 1.1.1.3). Some examples that clearly illustrate the formation of mono- and bi-component networks on surfaces will be described. Thereafter, recent advances in the construction of porous networks on surface using surface-confined covalent reactions will be described (section 1.1.2), as well as the formation of porous networks using preformed covalent macrocycles (section 1.1.3). A sub-section (1.1.4) will also describe single pore assemblies, which demonstrate an enhanced level of control in the self-assembly process.

1.1.1 NON-COVALENT INTERACTIONS

1.1.1.1 Hydrogen Bonding

A substantial number of systems describing the formation monocomponent[41-46] and bicomponent[47-50] 2D porous networks in which the components are held together by H-bonding interactions have been published in the last decade. One of the first examples of

bicomponent networks featuring empty hexagonal domains able host molecular guests, such as fullerenes, was reported in 2003 by the groups of *Beton*, *Champness* and co-workers.[48] They described the formation of hexagonal arrays by the co-deposition of 3,4,9,10-perylenetetracarboxylic diimide (PTCDI) **1** and 2,4,6-triamino-1,3,5-triazine (melamine) **2** on a Ag-terminated silicon surface under Ultra-High Vacuum (UHV) conditions. As shown by detailed STM images, the two molecular modules organise in such way that hexagonal domains are formed. The melamine and PTCDI modules constitute the vertices and the straight edges of the hexagonal domains, respectively (Figure 1). The self-assembly is driven by intermolecular triple hydrogen-bonding interactions that are established between the complementary units of the molecular components.

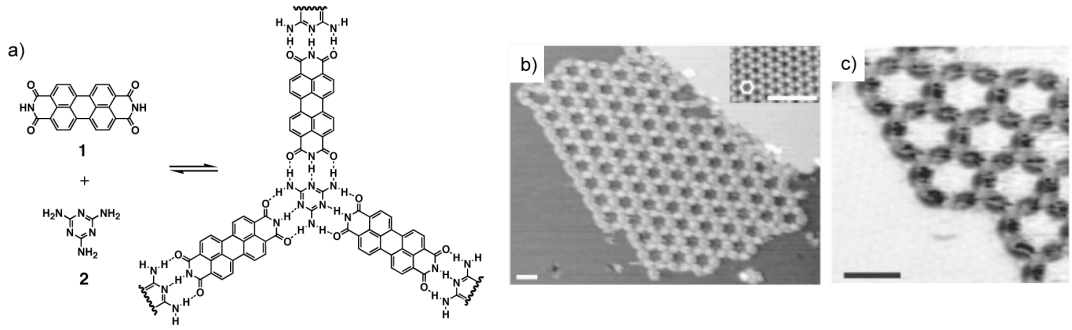

Figure 1. Self-assembly of a PTCDI–melamine supramolecular network; a) chemical structure of PTCDI **1** and melamine **2**; b) STM image of a PTCDI–melamine network. Inset, high-resolution view of the Ag/Si(111)–$\sqrt{3}\times\sqrt{3}$R30º substrate surface; c) inverted contrast image of the network. Scale bar, 3 nm.[48]

Usually, the molecules involved in the formation of the bi-dimensional arrays have defined recognition sites and their deposition on the surfaces leads to molecular confinement and auto-organisation. Yet in some cases, the molecular recognition sites can be activated *in situ* in order to enable hydrogen-bonding interactions, which lead to the formation of highly stable molecular networks under UHV conditions as reported by *Stöhr* and co-workers.[51] In this work, the authors report the generation of a supramolecular network by the thermal dehydrogenation of 4,9-diaminoperylene-quinone-3,10-diimine (DPDI) **3** on a Cu(111) surface (Figure 2). By thermal-induced activation, the molecular modules form porous networks via self-assembled H-bond donors/acceptors. The periodic honeycomb structure is commensurate with the Cu substrate and is thermally very stable (up to > 300 °C) as a consequence of an irreversible chemical transformation and the combination of intramolecular H-bonds and strong π-bonding between the organic molecules and the surface metal atoms. Due to its structural regularity and stability, the hexagonal cavities in the network hold great potential for the local deposition and fixation of guest molecules. This has

recently been shown through the molecule-by-molecule deposition of optically active, weakly-bonded, supramolecular ZnOEP-C_{60} complexes.[52]

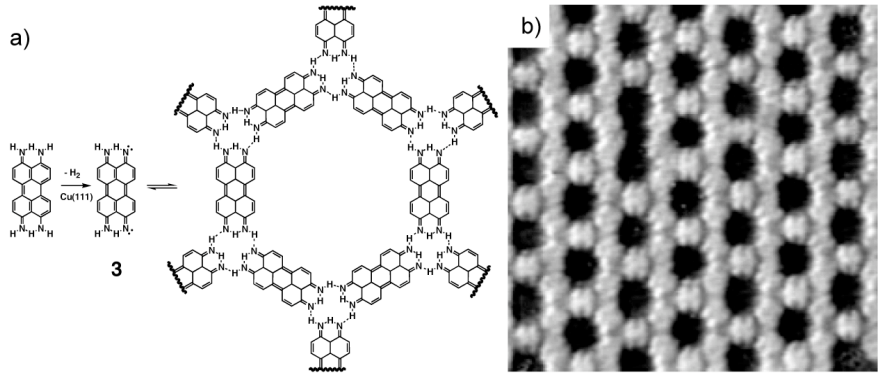

Figure 2. a) Schematic representation of the hexagonal assembly of DPDI **3**; b) STM image of the self-assembled architecture formed by perylene-derivative **3** after thermal activation on a Cu(111) surface under UHV conditions.[51]

In a recent collaborative project involving our own laboratory, the controlled formation of a bicomponent porous network at the solid-liquid interface utilising H-bonding was demonstrated.[53] The porous network was formed using melamine (**2**) and bis-uracyl (**4**) modules in a 1,2,4-trichlorobenzene (TCB) solution on highly oriented pyrolitic graphite (HOPG) surfaces (Figure 3a). Melamine, with its ability to form nine H-bonds in total, directs the self-assembly to form a hexagonal porous network in two-dimensions (Figure 3b). Each melamine molecule interacts with three bis-uracyl units by forming triple H-bonds with each one, thus giving an angle of 120 ± 12° at the apex between two bis-uracyl units. The porous network only forms with low concentration solutions (~2 μM) since at higher concentrations (~20 μM) only tightly packed monolayers of melamine (**2**) are formed. Under this conditions (*i.e.*, low concentration regime) no competitive physisorption between **2** and **4** at the HOPG-TCB interface is found and sub-monolayer coverage is achieved.

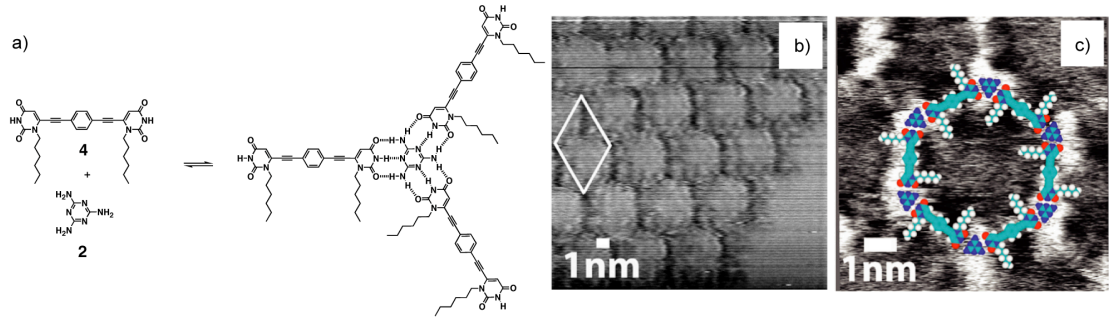

Figure 3. a) The molecular structures of melamine (**2**) and bis-uracyl (**4**) modules and the formation of the hybrid assembly via H-bonding; b) STM images of the bicomponent self-assembly showing the hexagonal porous network formed; c) proposed assembly model is shown superimposed over the close up of a single hexagonal pore.[53]

As an extension of the previous work, a comparative study of four linear linkers interacting with melamine **2** via triple H-bonds was carried out.[54] This study offered new insight into the design and versatility of pre-programmable bi-component supramolecular 2D networks at the solid-liquid interface. The ditopic imidic linkers included two molecules bearing diuracil groups in the α and ω positions, **4** and **5** respectively, naphthalene tetracarboxylic diimide **6** and pyromellitic diimide **7** (Figure 4a). The self-assembly of each linker with melamine was carried out by dissolving them in a solvent mixture of TCB/DMSO and subsequently depositing them on HOPG. By controlling the concentration and stoichiometry of the systems precisely, the formation of the desired bicomponent self-assembly could be favoured. The STM imaging experiments revealed that two-dimensional porous architectures could be formed by three, out of the four linkers, when they were co-deposited onto the HOPG surface in the presence of **2**. With two of the linkers, molecules **4** and **6**, highly ordered hexagonal structures were obtained (Figures 4b,d). The self-assembly between molecular modules **2** and **5** resulted in a distribution of various polygonal structures from pentagons to nonagons (Figure 4c). The deposition of **7** with **2** resulted in tightly packed one-dimensional supramolecular arrays (Figure 4e). When the stoichiometric ratio of **2** relative to **6**, was altered by lowering the concentration of **2**, it was observed that the hexagonal porous networks coexisted with one-dimensional supramolecular linear assemblies (Figure 4f,g), thus demonstrating the importance of controlling the concentrations and stoichiometries of the molecular systems. In fact, the occurrence of multiple phases was observed for all the bicomponent systems with concentrations below 100 μM. This comparative study confirmed that concentration-dependent polymorphism and phase segregation are hallmarks of porous self-assembled structures prepared via H-bonding interactions at solid-liquid interfaces.[55] Furthermore, the study also revealed several crucial points that have to be considered at the molecular level when designing a pre-programmed porous network. The rigidity of the linkers is very important. In the case of module **5** for example, the diethynyl moiety introduces a fair amount of conformational flexibility allowing the formation of polymorphic and glassy phases and thus is not an optimal choice when looking for a fully rigid molecular module. Peripheral functionalization of the linkers would prevent strong side-to-side interactions that lead to tightly packed bicomponent assemblies rather than porous networks and would also hinder strong adsorption in the cavities of the porous networks. Also, by designing the molecular modules in a multi-component system with complementary recognition sites, phase segregation and self-recognition can be avoided. Furthermore, another manner of avoiding such polymorphism and phase segregation at solid-liquid interfaces is to introduce a guest at the cavities of a self-assembled porous network formed by H-bonding interactions as was shown by various groups.[56-59] Thus, it was shown

that by careful investigation of the energetic contributions in crystallization, polymorphism, and phase segregation, a dramatic improvement in chemical design, and thus in the molecular engineering, can be achieved.

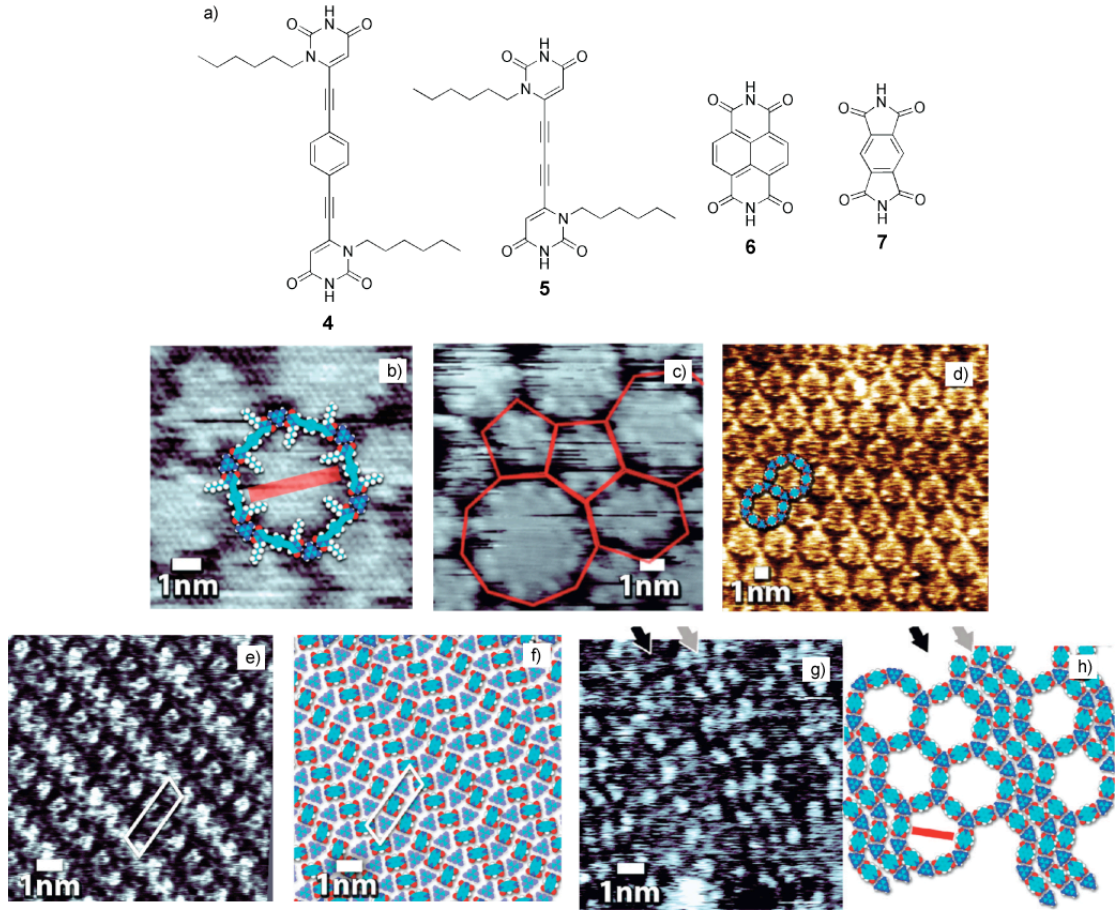

Figure 4. a) Chemical structures of the linear linkers used in the study; b) STM image of the self-assembly formed by **4** and **2**. A molecular model of the hexagonal structure formed is superimposed. The red bar corresponds to 3.2 nm; c) STM image of the self-assembly formed by **5** and **2** showing that various polygons were formed; d) STM image of the long range highly ordered hexagonal pattern formed by **6** and **2**; e,f) STM image and molecular model of the tightly packed one-dimensional supramolecular arrays formed by **7** and **2**; g,h) STM image and molecular model of the hexagonal porous networks coexisting with a one-dimensional supramolecular linear assembly formed at a lowered ratio of **2**:**6** compared to Figure 45d. The linear chain polymorph is indicated by the grey arrow, whereas the hexagonal motif is indicated by the black arrow.[54]

Following the same strategy, *i.e.*, working at sub-monolayer coverages, it has also been possible to investigate the formation of discrete assemblies featuring polygonal porous domains at the solid-liquid interface (solvent: DMSO-TCB, surface: HOPG, r.t.).[60] In order to engineer these assemblies, two types of molecular modules (1,3,6,8-tetrakis[(1-hexylurac-6-yl)ethynyl]pyrene **8** and 4,4′-[(phen-1,4-diyl)diethynyl]bis(2,6-diacetylaminopyridine) **9**,

Figure 5a) bearing complementary H-bonding sites (uracil and 2,6-di(acetylamino)pyridine, respectively) positioned at different orientations relative to each other (60° and 120° in the case of tetratopic module **8**, and 180° in the case of ditopic module **6** were deposited on HOPG. The discrete H-bonded assemblies were nucleated in solution and studied at very low-concentrated solutions (< 10 μM) (Figure 5). Given the difference in adsorption energies of the components and the tendency to minimise the occupied area, it is usually very difficult to direct the deposition of two different molecules on a surface. This approach allowed the prevention of competitive adsorption. In this manner they have shown that the arrangement of the assemblies was solely dictated by the information embedded within the molecular modules.

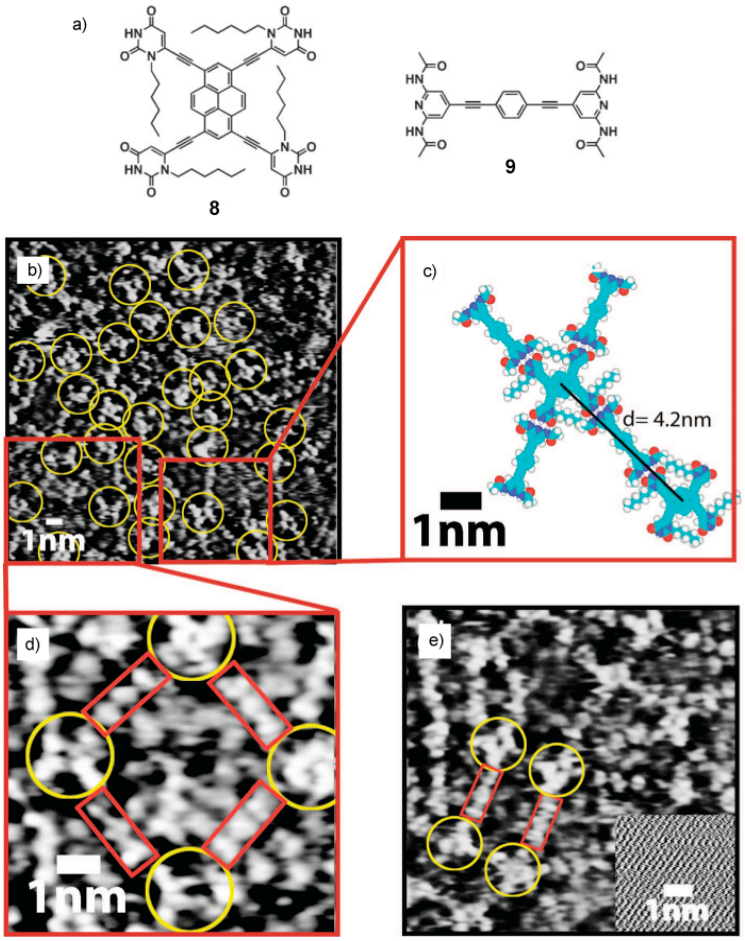

Figure 5. a) Chemical structure of molecules **8** and **9**; b) submolecularly resolved supramolecular aggregates featuring discrete oligomeric species $[(\mathbf{8})_m\cdot(\mathbf{9})_n]$ prepared from diluted equimolar solutions. Each yellow circle identifies a single molecule of **8**; c) model assembly of a hexameric hybrid complex $[(\mathbf{8})_2\cdot(\mathbf{9})_4]$ showing the distance values as estimated by MM2-based computational geometry optimization; d, e) heterogeneous **8·9** phase images highlighting the presence of rhomboidal and rectangular nanopolygons, respectively, formed as a consequence of complementary H-bonding motifs. Each yellow circle identifies a single molecule of **8** and each red rectangle a single molecule of **9**.[60]

The efforts to prepare nanostructured architectures on surfaces were not limited to the liquid-solid interface. Interesting results have also been obtained using related molecular modules under UHV conditions on metal surfaces. In a recent collaborative study using 4,4′-[(phen-1,4-diyl)diethynyl]bis(2,6-diacetylaminopyridine) (**9**, Figure 5a), it was demonstrated that a porous network could be formed upon deposition of the molecular module on a Ag(111) surface.[61] Deposition of **9** at submonolayer coverages onto the Ag(111) surface at room temperature resulted in the self-organisation into a porous hexagonal network (Figure 6a). In Figure 6b, it can be seen that each 2,6-diacetylaminopyridine moiety interacts via two H-bonds with equivalent neighbouring residues, consequently resulting in a chiral hexameric units. Each cavity was surrounded by three molecules of **9** arranged at an angle of 60° with respect to each other. This gave rise to a rhombic unit cell (shown in Figure 6b) with dimensions of 30.4 × 30.4 $Å^2$ and an angle of 60°. Astonishingly, annealing the sample to 420 K caused a phase transition transforming the hexagonal porous network into a close-packed 2D rhombic arrangement (unit cell: 20.2 × 10.0 $Å^2$ with an angle of 68.2°, Figure 6c,d).

The first clue to the cause of this dramatic change was provided by the fact that the intensity of the two acetyl units of terminal 2,6-diacetylaminopyridine moieties differed, with one of the residues appearing brighter than the other. This clearly indicated that there was a conformational difference between the two acetyl groups. An explanation for this phenomenon is that in principle the amidic functional groups can exist in both the *cis* and *trans* conformations, with the *trans* being preferred, as was the case in the hexagonal porous network. However, theoretical calculations (Figure 6e) showed that the conformations could be switched if sufficient energy was provided. It was therefore postulated that following the annealing, one of the two acetyl units of the terminal 2,6-diacetylaminopyridine moieties was in the *cis*-conformation, with the other remaining in the *trans*-conformation, enabling the formation of four H-bonds (see Figure 6e) between neighbouring molecules in a head-to-head fashion. This H-bonding was designated as $(DADA)_2$ (where D refers to a H-bonding donor moiety and A refers to a H-bonding acceptor moiety) according to the scheme in Figure 46e. These results showed that the hexagonal porous network was kinetically controlled, whereas the rhombic assembly was the thermodynamically stable phase.

In another set of experiments, a three-component assembly was prepared under UHV conditions.[22] The three molecular modules used are shown in Figure 7a. Two of the modules, **4** and **9**, have been used in experiments described above, and a new module, an anthracene bearing a uracilic H-bonding moiety **10**, was introduced to act as a molecular stopper. Before attempting the three-component assembly, several assemblies were investigated for comparison purposes. First, **4** was deposited on Ag(111) and was investigated under UHV conditions at 77 K. At submonolayer coverages, two types of close-packed arrays were

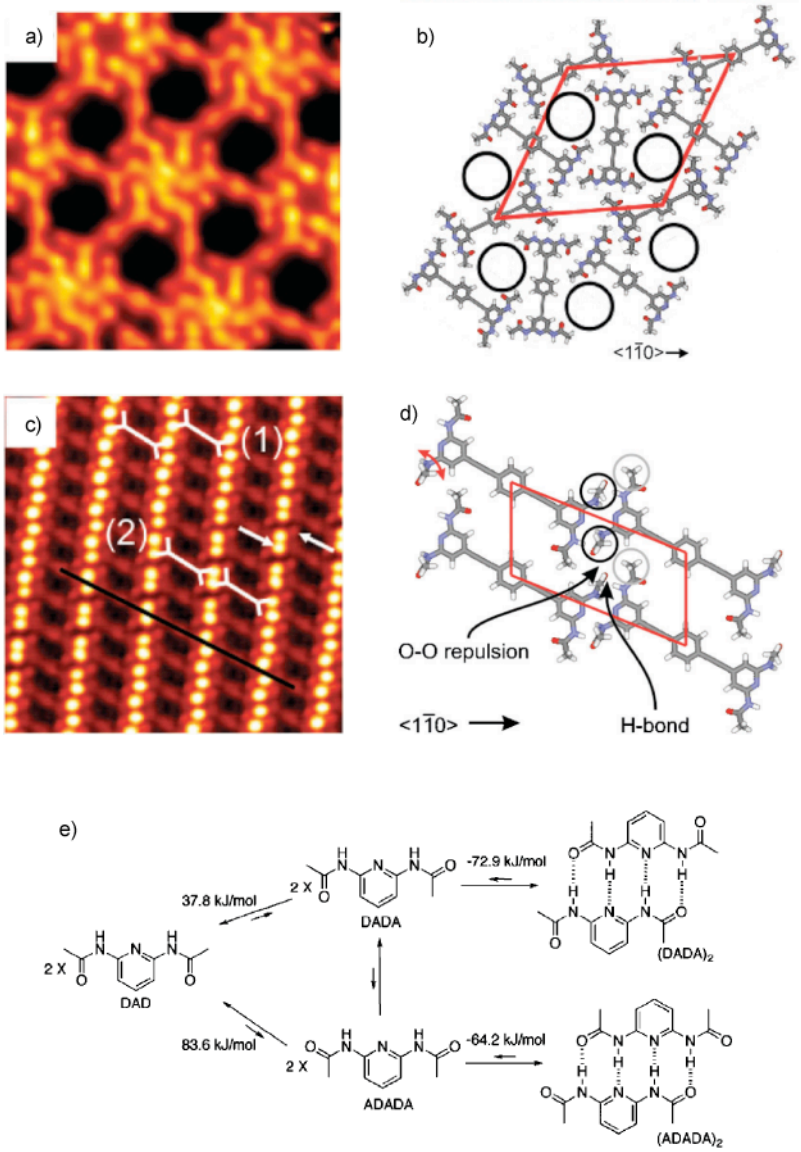

Figure 6. a,b) STM image (7 × 7 nm^2) and proposed model of the hexagonal porous network of **6** on Ag(111) at room temperature under UHV conditions; c,d) STM image and proposed model of the close-packed rhombic pattern (10 × 10 nm^2) formed upon annealing at 420 K on Ag(111); e) scheme showing the influence of the cis and trans conformers and calculated ΔH° for conformational changes and dimerisation in the vacuum using MP2/6-311G** level of approximation on B3LYP/6-311G**.[61]

observed (Figure 7b-d). It has to be noted that depending on the relative spatial disposition, the hexyl chains on the uracilic moities could display two configurations, *cis*-**4** or *trans*-**4**, where the alkyl chains lie on the same or opposite sides of the molecular backbone, respectively. In the first packing motif, two adjacent rows of *cis*-**4** interact via double head-to-head H-bonds using the uracil moities and also via Van der Waals interactions between the alkyl chains to form molecular wires with double rows (Figure 7c). In the second motif, two lateral rows of *cis*-**4** molecules are linked through *trans*-**4** molecules. The intermolecular interaction between the *trans*-**4** molecules with the *cis*-**4** molecules occurs via the interaction of the NH group of the *trans*-**4** molecules with the free carbonyl on the the *cis*-**4** molecules

(Figure 7d). As expected, an attempt to assemble **4** and **10** resulted in disordered phases due to the lack of complementary H-bonding sites. On the other hand, sequential deposition of **4** and **6** resulted in the formation of very regular extended linear bimolecular wires, which were only disrupted at the terraces of the silver substrate (Figure 7e-g). The two modules alternate to form the wires, with each molecule able to form two sets of triple H-bonds to interact with two neighbours using the pre-programmed complementary recognition groups DAD and ADA available on the 2,6-diacetylaminopyridine and uracilic residues on **9** and **4**, respectively. In this assembly, generally molecule **4** was found in the *cis*-**4** conformation in order to minimize the free surface energy by forming the most densely packed arrangement possible. Indeed in this array, the *trans*-**4** conformation was very rarely observed. Next, the three-component assembly was attempted by sequential sublimation of the three modules onto the Ag(111) surface. In this case, the extended wires observed between **4** and **9** were not observed. As predicted, the monouracil conjugate **10**, acted as a molecular stopper exposing the anthracyl moiety as the end point of the assembly preventing the molecular wires from reaching the terraces of the silver substrate as occurred in the absence of **10** (Figure 7h-j). This was therefore the first example of a tricomponent miniature assembly. A mixture of short linear trimeric structures, [**10** · **9** · **10**] (Figure 7j), pentameric structures, [**10** · **9** · **4** · **9** · **10**] (Figure 7i) and long oligomers, [**10** · **9** · (**4** · **9**)$_n$ · **10**] (Figure 7h) were observed by STM. Since **4** and **10** bear the same H-bonding motifs, they were expected to compete equally for interactions with **9**, however, clearly this was not the case since long oligomers predominated the assembly system. The reason for this is that the filling of empty space on the surface reduces the free surface energy which is the general tendency for any system on a surface.[62] Molecular stopper **10** does not allow such minimization in the occupied area per assembly as effectively as molecule **4**. This is because it only bears one H-bonding moiety that is able to make energetically favoured H-bonds compared to the two possessed by **4**. The anthracyl moiety can only interact via van der Waals interactions, however assemblies formed by these interactions are energetically less favoured compared to H-bonding. The existence of voids within the intermixed regions (Figure 7h, left dotted rectangle) and the formation of aggregates of **10** as small disordered islands (Figure 7h, right dotted rectangle) support this hypothesis. Although precise control of the length of the molecular wires was not achieved in this study, it is postulated that by controlling the ratio of the molecular modules it could result in regular monodisperse self-assembling architectures on surfaces.

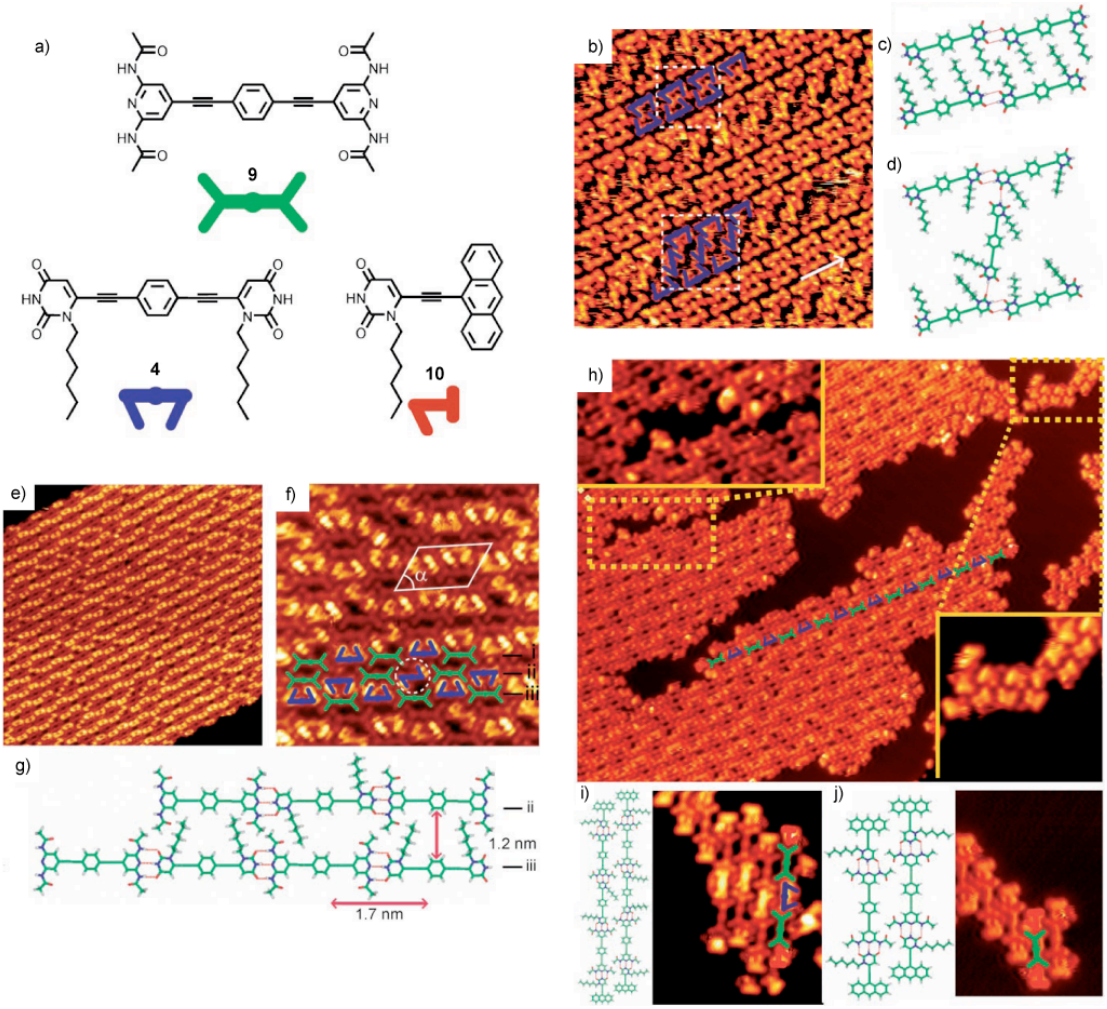

Figure 7. a) Chemical structures of the molecular modules used in the study; b) STM image of the self-assembly of **4** on Ag(111) under UHV conditions (16 × 16 nm^2) and c,d) the proposed models for the two types of packings; e,f) STM images of the self-organised molecular wires formed by molecules **4** and **9** on Ag(111) under UHV conditions following annealing at 383 K. (41.5 × 41.5 nm^2 and 12 × 12 nm^2 respectively) and g) the proposed model for the linear molecular wire assembly; h) STM image of the tricomponent submonolayer architecture formed upon sequential sublimation of **4**, **9** and **10** onto Ag(111) under UHV conditions (50 × 40 nm^2). The lower right inset shows an aggregate of **10** (7.7 × 7.7 nm^2); i, j) proposed models and zoom in STM image of trimeric and pentameric assemblies, respectively.[22]

1.1.1.2 Dipole-Dipole interactions and Van der Waals contacts

One of the first examples of a 2D porous network, prepared using self-assembled porphyrin derivatives on a metal surface, was constructed by taking advantage of dipole-dipole intermolecular interactions.[63, 64] This supramolecular assembly, described by *Spillmann et al.,* was formed using **11** a zinc-porphyrin bearing two 3,5-di(*tert*-butyl) phenyl groups and two 3-cyanophenyl substituents (Figure 8a). Precedently, *Yokoyama* and co-workers described the formation of trimeric, tetrameric and linear polymeric arrays combining different porphyrins bearing cyano substituents.[65]

Under UHV conditions, porphyrin **11** self-organised upon vapour deposition onto a Ag(111) surface (Figure 8b). The primary driving force for the formation of this porous network was the dipole-dipole and van der Waals interactions mainly contributed by the 3-cyanophenyl moieties. As shown in Figure 8, trimeric units with a central cavity with a diameter of about 1.2 nm were formed. Furthermore, the Ag (111) substrate is thought to direct the formation of the hexagonal pores as the cyano functional groups can act as donating ligands, which are well-known to strongly bind to silver ions. The cavities in this self-assembly were subsequently exploited to host C_{60} guests.

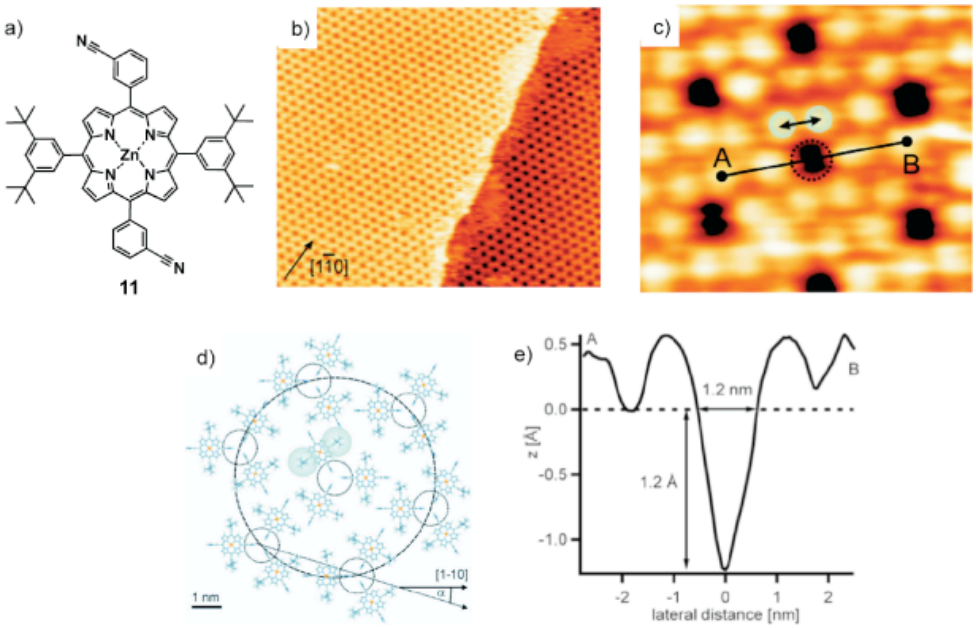

Figure 8. a) Chemical structure of the porphyrin derivative **11** studied; b) STM image of the porous network formed by the self-assembly of **11** on Ag(111) surface; c) zoom-in of the STM image indicating where the profile scan for Figure 8c was performed; d) proposed model of the self-assembled porous network. The small circles indicate where the pores are formed *i.e.*, in the centre of the trimeric units formed by the cyano moieties; e) the cross-section profile of a single pore scanned from A to B in Figure 8c.[63]

As an extension of the precedent work, *Diederich*, *Jung* and co-workers recently reported a systematic study on the influence of different alkoxyphenyl substituents on the porosity of porphyrin-based assemblies on Cu(111) at the solid-vacuum interface.[66] The self-organisation of three different porphyrin derivatives (**12**, **13** and **14**) shown in Figure 9 was analysed. All derivatives present two 4-cyanophenyl substituents in diagonally opposed *meso*-positions of the porphyrin core, but differ in the nature of the other two *meso*-alkoxyphenyl substituents. Such dissimilar functionalisation controls the dimensionality of the resulting structure and alters the pore-to-pore distance (3.09 ± 0.2 nm, 3.35 ± 0.12 nm and 4.89 ± 0.14 nm for assemblies **12**, **13** and **14** respectively) in the observed networks without significantly affecting the pore size. Specifically, at coverages below 0.8 monolayer, porphyrin **12** self-

assembles into a nanoporous hexagonal network (Figure 9a), while molecules **13** and **14** form one-dimensional wires. At higher coverages (> 0.8 monolayer), the latter porphyrin assemblies evolve into two-dimensional porous assemblies (Figure 9b and 9c, respectively). Besides the known dimeric and trimeric supramolecular modules involving the dipolar interactions between two or three cyanophenyl groups (assemblies a and b in Figure 9), a new trimeric asymmetric non-covalent motif was observed in the network shown in Figure 9c with the isopentyloxy substituents. One of two cyanophenyl groups of neighbouring porphyrins forms a C–N···H–C *H*-bond with the *ortho* polarised C-H residue to the electron-withdrawing alkoxy groups of a third neighbour. The different assemblies have been discussed in terms of the compensation of entropic losses, due to the increased restriction in the flexibility of the alkoxy chains as the length increases (from an isobutyloxy to isopentyloxy chain).

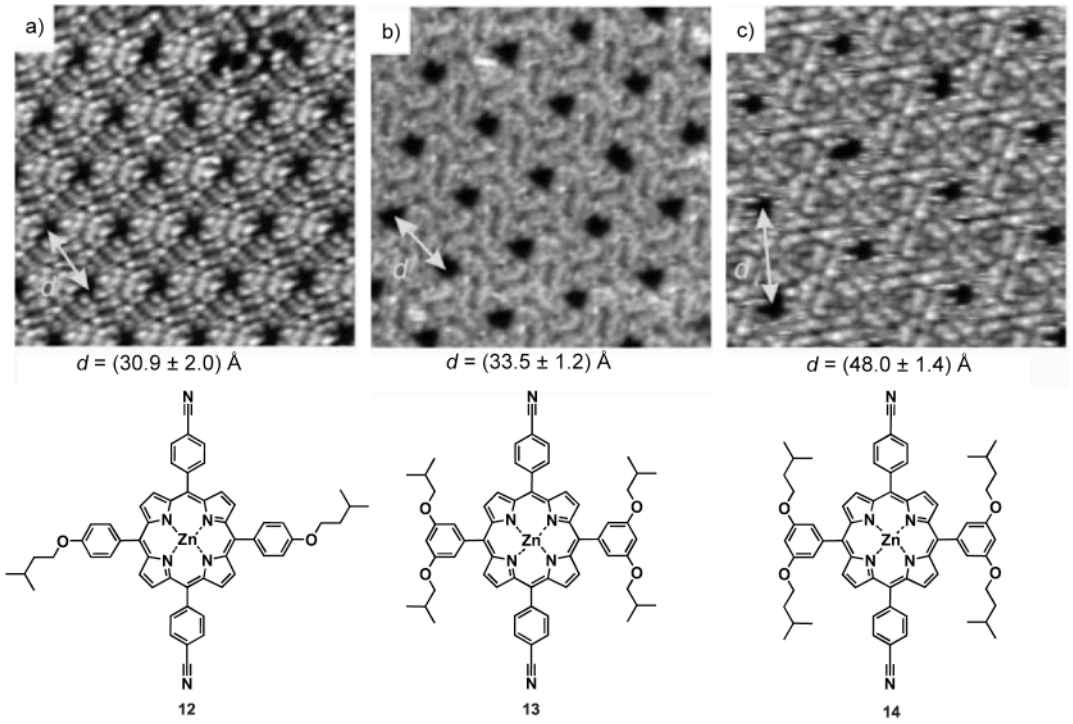

Figure 9. a-c) STM images (all 15×15 nm^2) of the nanoporous networks formed on Cu(111) by the porphyrins **12**-**14** sketched below the respective images. The coverages are close to one monolayer in each case.[66]

In quite a few cases, van der Waals interactions between long alkoxy chains have been exploited for the construction of surface-supported porous networks.[67-71] It has been demonstrated that it is possible to tune the pore size by changing the length of the alkyl chains. However, the formation of supramolecular networks with giant pores is thermodynamically unfavoured because of the low surface coverage of the molecular networks. As a method to overcome this obstacle, *Tahara et al.* demonstrated that it is

possible to obtain 2D networks featuring giant pores at the solid-liquid interface (up to 7 nm) by high dilution of the adsorbate concentration.[72] Substituted dehydrobenzo[12]annulene (DBA) **15** (Figure 10a) dissolved 1,2,4-trichlorobenzene at very low concentrations (5.0×10^{-6} mol L^{-1}) was deposited on a HOPG surface resulting in porous honeycomb networks (Figure 10b). The hexagonal voids were formed by the interdigitation of the alkyl chains (Figure 10c). Exclusively 2D porous networks were not obtained in their experiments due to the formation of regions where molecule **15** was densely packed (dark stripes in Figure 10b), demonstrating that a 7 nm pore size (edge-to-edge distance, Figure 10d) is near to the upper limit for the formation of porous networks using Van der Waals interactions between long alkyl chains. In further experiments, the authors were able to employ the giant pores to host 'molecular spoke wheels' as guests. In the section on cavity-confined host–guest recognition (Section 1.2.1), more examples of supramolecular networks held together by Van der Waals interactions and their versatility and dynamicity towards guest recognition will be discussed.

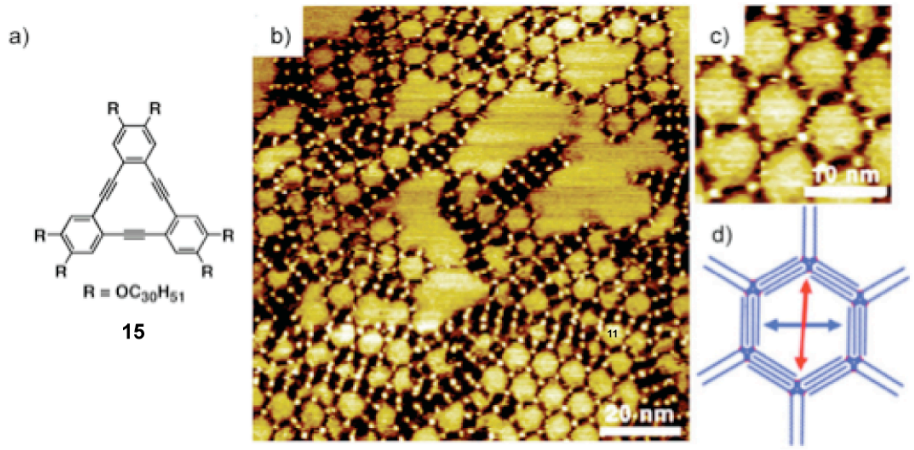

Figure 10. a) Chemical structure of dehydrobenzo[12]annulene **15** studied; b, c) STM images of the self-assembly of **15** at the TCB-graphite interface; d) schematic representation of the assembly displaying the interdigitation of the alkyl groups. The red arrow indicates the corner-to-corner distance (7.5 nm) and the blue arrow shows the edge-to-edge distance (7.0 nm).[72]

1.1.1.3 Metal-ligand Coordination

The coordination of organic molecules by transition metals has also been used for the fabrication of surface supported metal-organic coordination networks (MOCNs) as widely reported by *Barth*, *Kern* and co-workers.[73-77] In the most recent example, they reported the formation of honeycomb nanomeshes with very regular size and shape over large areas (of the order of μm^2, Figure 11a), in which pore dimensions could be varied by changing the ditopic organic linkers.[78] The molecular linkers used were oligophenyldicarbonitrile molecules consisting of three, four or five phenyl rings (*i.e.*, molecules **16**, **17** and **18**, respectively,

Figure 11). Co (III), with its ability to coordinate three nitrile groups at 120° with respect to each other, was the transition metal of choice to template the formation of the porous networks. The STM experiments were performed at ~10 K under UHV conditions on Ag(111) surfaces. The molecular linkers deposited onto the surface at submonolayer quantities were exposed to a beam of Co atoms, which allowed the nanomesh formation once a balanced stoichiometry of the constituents was achieved. Both depositions were carried out at 300 K, after which the surface was cooled to 10 K in order to capture the STM images. Extended, highly regular, hexagonal arrays were obtained, and depending on the choice of the organic linker, they were able to tailor the size of the pores to 10, 15 and 20 nm^2 (Figure 11b, c and d respectively) with the latter having a pore diameter of 5.7 nm. In subsequent experiments, the authors were able to demonstrate that guest molecules could also be spatially confined within the nanocavities. The lateral movement of the guests from one cavity to the next was restricted even upon STM-induced excitation by increasing the tunnelling current.

Very few examples of 2D porous networks formed by metal-ligand coordination at the solid-liquid interface exists,[79] including those formed by the deposition of preorganised metallocyclic cavities (see Section 1.1.3). So far, metalloorganic 2D arrays have mainly been formed at the solid-liquid interfaces by the deposition of laterally-packed metal-ligand coordination chains.[80] However, it has to be noted that in all these cases, no porous networks were formed as a direct result of the metal-mediated coordinative interactions, and only tight-packed structures have been observed to date.

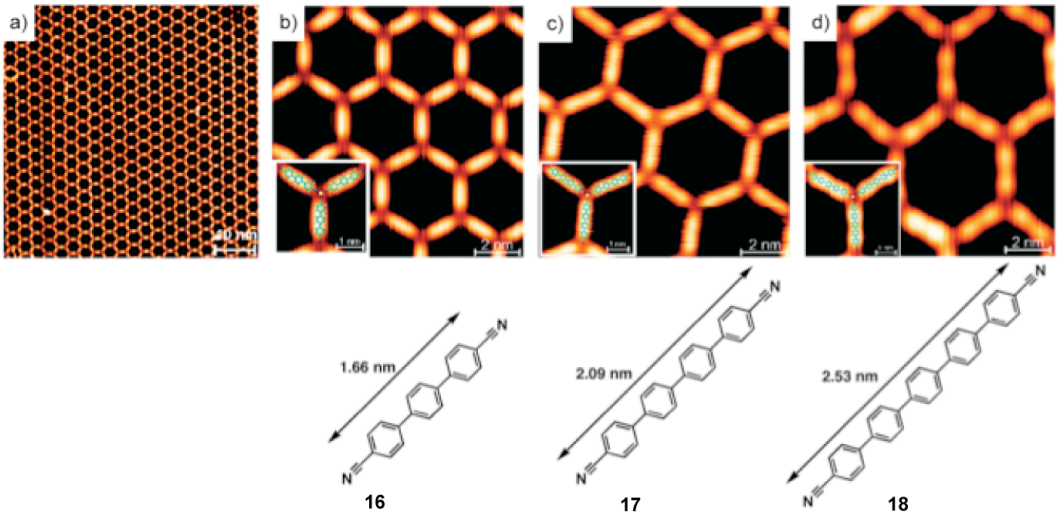

Figure 11. a) UHV STM image of the extended nanomesh formed using linker **16** and Co atoms on a Ag(111) surface; b)-d) arrays formed with increasing the length of the oligophenylene organic linkers. Chemical structures of molecules **16**, **17** and **18**.[81]

1.1.2 Porous Networks Formed By Surface-Confined Covalent Reactions

All the networks described in the previous section were assembled taking advantage of intermolecular weak interactions, which may lack stability for nanotechnological applications.[82] Consequently, a lot of effort has been focused on the engineering of covalently bonded networks on surfaces (*i.e.*, surface covalent organic frameworks, SCOFs) displaying higher stability.

The first work describing covalently bonded 2D porous networks on surfaces was published by *Grill et al*.[83] Porphyrin building blocks bearing 4-substituted bromophenyl moieties were used to form arrays on Au(111) surfaces under UHV conditions. The covalent bonds at predetermined points were formed by thermal dissociation (> 590 K). Such dissociation performed by either heating the porphyrin modules on the surface after sublimation, or by heating them in the evaporator prior to sublimation lead to intermolecular coupling between the monomeric species (Figure 12). Prior to the thermal dissociation, a control experiment at lower temperature (sublimation at 550 K) was done. Intact tetra(4-bromophenyl)porphyrin **21** units formed highly ordered islands (up to 100 nm in diameter) with a close-packed structure (Figure 12a). Various nano-architectures could be formed in a controlled manner by thermally activating the Br functions of mono-, di-, and tetra-bromo-substituted tetra(phenyl)porphyrins (TPPs) **19**, **20** and **21**, respectively (Figure 12b-d). As expected, porphyrin **19**, bearing only one Br atom, formed dimers upon activation of the reactive sites (Figure 12b). Dibromophenyl porphyrin **20** lead to the formation of long, linear chains, whereas tetrabromophenyl porphyrin **21** formed 2D networks.

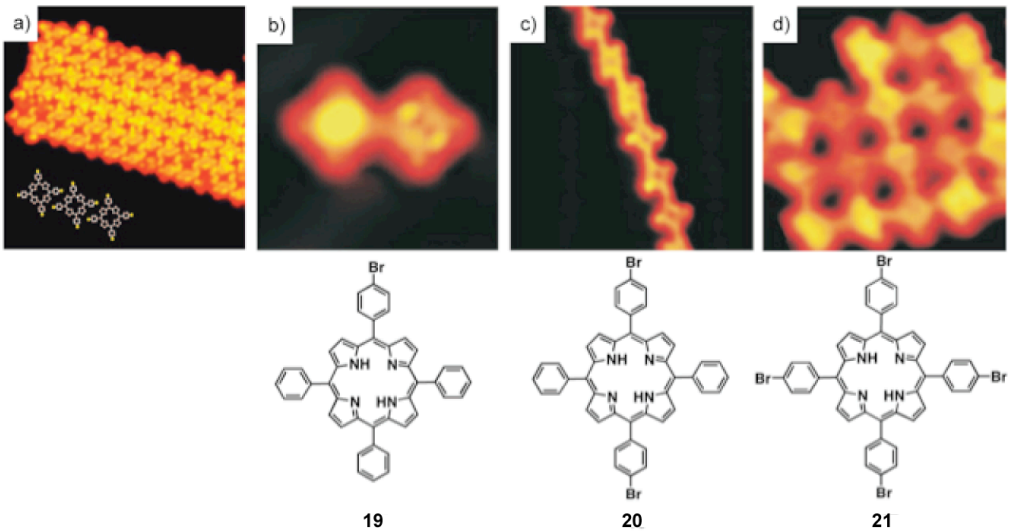

Figure 12. a) STM image (20×20 nm^2) of islands formed by unactivated **21** molecules on Au(111) after sublimation at 550 K; b)-d) results obtained after the activation of bromophenyl porphyrins **19**, **20** and **21**, respectively. Image size b) 5×5 nm^2, c) 10×10 nm^2, d) 8.5×8.5 nm^2.[83]

In another example, SCOFs formed under UHV conditions on Ag(111) surfaces were reported by *Zwaneveld et al*,[84] exploiting condensation reactions between boronic acid derivatives. Condensation reactions involving 1,4-benzenediboronic acid **22** led to six-membered B_3O_3 rings (Figure 13a) arranged into ordered porous hexagonal arrays with cavities diameters of 1.5 ± 0.1 nm (sublimation of **22** at 300-500 K, surface coverages ranging from <1% to near-complete monolayer). The stability of the assembly was tested by thermal annealing at 750 K. No degradation was observed after 5 min, however, following prolonged periods (12 h) significant degradation occurred and only small islands of the intact assembly were observed. Hexagonal networks with larger pore sizes (2.9 nm) were also obtained upon co-deposition of **22** and 2,3,6,7,10,11-hexahydroxytripenylene **23**, and once again, annealing at 750 K did not degrade the network, thus confirming the covalent nature of the assembly (Figure 13b).

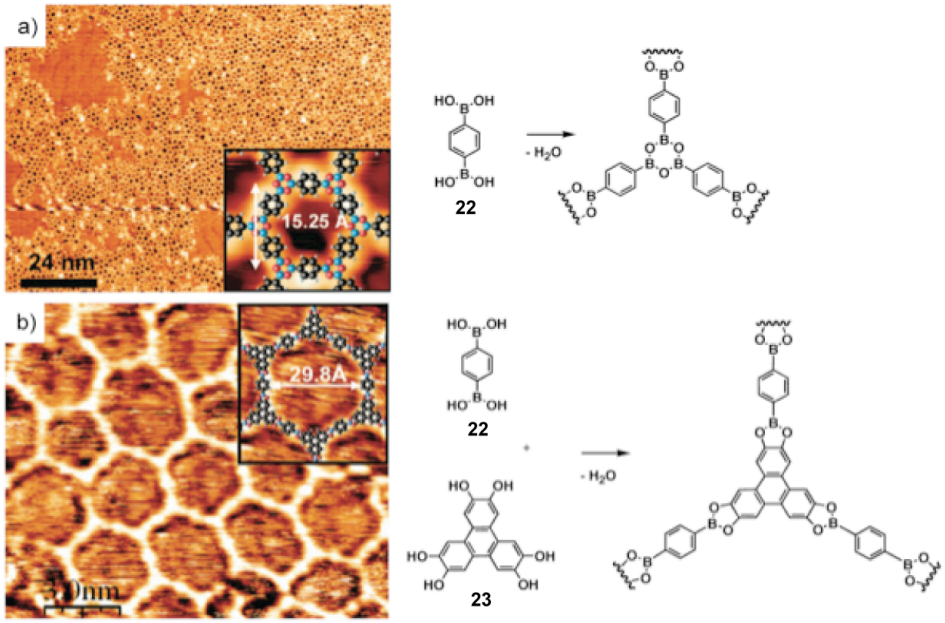

Figure 13. a) STM image of a covalent network formed upon deposition of **22** on Ag(111) at near-complete monolayer coverage; b) STM image of the SCOF formed upon co-deposition of **22** and **23** on Ag(111). The insets in both images show the theoretical pore diameter obtained by density functional theory (DFT) calculations.[84]

Using a different approach, *Linderoth* and coworkers[85] combined the use of surface-confined covalent reactions to form 2D porous networks between Van der Waals pre-organised precursor modules (**25**). In particular, three separate experiments, each resulting in a different surface assembly, were performed by condensation of trialdehyde **24** with octylamine (Figure 14) under UHV coniditions. The control experiment involved performing the reaction shown in Figure 14 in solution, and then sublimation of triimine **25** directly onto the Au(111) surface under UHV conditions. The close-packed self-assembly obtained

consisted of rows of bright protrusions separated by a lamellar arrangement (Figure 14b). This corresponds to the molecule having two 'spokes' adsorbed on the surface, with the third one protruding upright, *i.e.*, perpendicular to the surface. The assemblies obtained when the reaction was performed *in-situ*, *i.e.* on the surface, were entirely different (Figure 14c-d). Two different reaction conditions, leading to different assemblies, were investigated. In the first experiment, octylamine molecules were dosed with a high flux at low temperature onto a substrate pre-covered with molecule **24**. In this case, a densely-packed structure with complete conformational order was obtained (Figure 14c). In the second experiment, when octylamine was sublimed onto the pre-covered substrate at room temperature with a lower flux, a less ordered porous network was observed (Figure 14d). In the first case, it is suggested that the low temperature did not allow the disruption of the underlying trialdehyde assembly, and thus the reaction product inherited the organisational information of the underlying layer resulting in the close-packed assembly. In the second experiment, the thermal energy was sufficient to render the trialdehyde layer unstable. Therefore, following the completion of the reaction between the freely diffusing reactants on the Au surface, a 2D porous network was formed. The same condensation reaction was also used to construct other surface-confined assemblies.[86, 87]

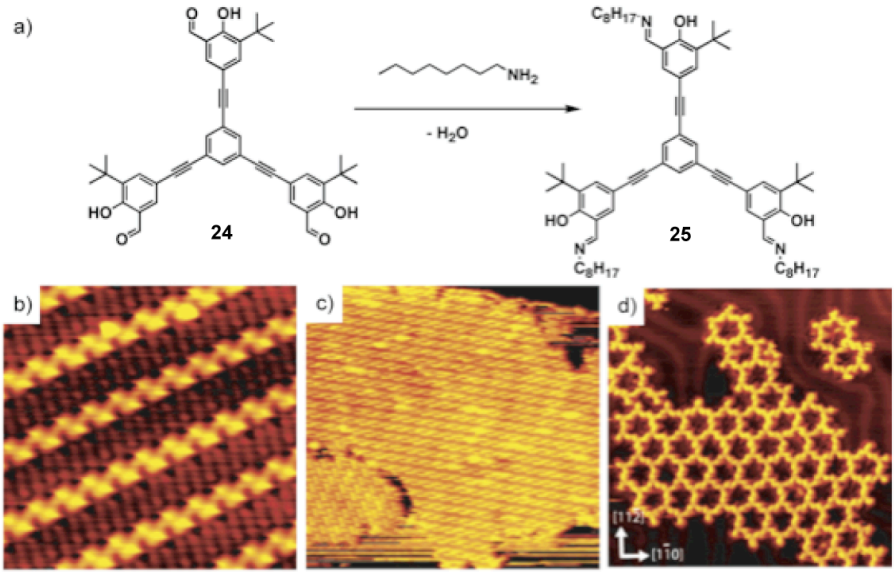

Figure 14. a) Formation of triimine **25** between condensation of trialdehyde **24** and octylamine; b) STM image (12×12 nm^2) of the rectangular structure formed on Au(111) under UHV conditions by the deposition of **25** prepared previously in solution; c-d) STM images (85×85 nm^2 and 40×40 nm^2, respectively) of the different organisation patterns formed by the triimine **24** prepared *in-situ* on the surface by a condensation reaction following c) deposition of octylamine at low temperature and high flux on preassembled islands of trialdehyde **24** or d) deposition of octylamine at r.t. and low flux on preassembled islands of **24**.[85]

1.1.3 PREORGANISED CAVITIES: THE MACROCYCLE APPROACH

One of the first examples of deposition of macrocyclic cavities on surfaces for the accommodation of guest molecules was reported by *Wan*, *Bai* and co-workers.[88] They demonstrated that calix[8]erene macrocycles can form well-organised arrays on Au(111) surfaces and that their cavities can accommodate guest molecules such as [C_{60}].

In a more recent example *Freyland, Höger* and co-workers[89] reported the formation of 2D supramolecular assemblies using the macrocyclic structure **26** bearing long alkyl chains (Figure 15a) under ambient conditions at the liquid-HOPG interface (solvent: TCB). Macrocycle **26** organised into rows held together by interdigitation of the alkyl chains forming two types of cavities, A (blue octagon, ~1.4 nm) and B (red octagon, ~2.5×1.8 nm^2) (Figure 15b). The π-conjugated structure, and the extraannular phenyl moieties (circled in green) are clearly visible in the STM image. Surprisingly, when combined with C_{60}, the carbon cages nested atop of the macrocyclic structures rather than in the cavities, probably due to donor-acceptor interactions.

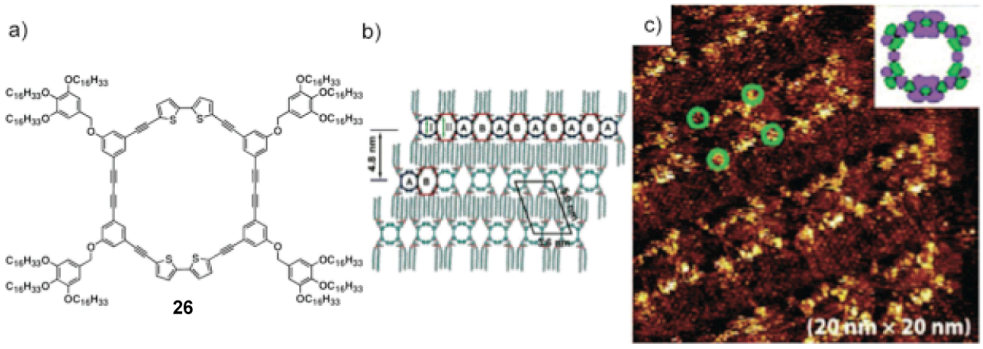

Figure 15. a) Chemical structure of macrocycle **26**; b) proposed structural model of the assembly showing the two types of cavities, A and B (blue and red octagons respectively); c) STM image of the array formed by macrocycle **26** at the HOPG surface under ambient conditions. The four extraannular phenyl moieties are highlighted with circles.[89]

Similar extended macrocyles were also deposited onto HOPG under ambient conditions (Figure 16a) by *Müllen* and co-workers who were able to observe the organisation of **27** at the air-surface interface (spin-coating of a THF solution on HOPG).[90] The STM images (Figure 16b) revealed hexagonal packed, highly organised monolayers of the ring-shaped carbazole macrocycle **27** spanning over several hundred nm^2. Due to the externally appended alkyl chains, each macrocycle is spaced from its neighbour by ~ 0.4 nm in each direction, thus preventing any close packing. Notably, all macrocycles are slightly distorted (with an elliptical shape) towards different directions. This was attributed to slight distortion of the linear geometry of the ethynyl linkers bridging the rigid conjugated carbazole-based trimers. Upon the introduction hexa-*peri*-hexabenzocoronene (HBC) by pulsed laser

deposition under UHV, the HBC molecules could be finally inserted into the pre-organised cavities.

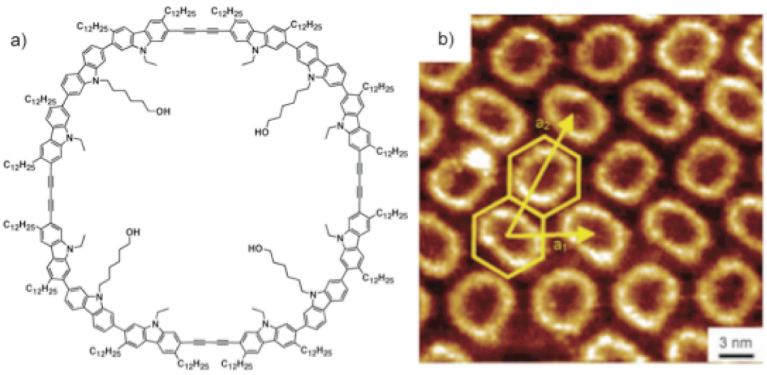

Figure 16. a) Chemical structure of conjugated carbazole macrocycle **27**; b) STM image of the self-assembly of **27** following spin coating at the air-HOPG interface. The direction of the elliptical distortion of the neighbouring macrocycles is shown by the yellow arrows.[90]

In the same context, *Bäuerle* and *Osteritz* described the organisation of macrocyclic α-conjugated oligothiophenes.[91, 92] Such structures combine the typical electron-donating properties of conjugated thiophenyl oligomers with the availability of hollow sites capable of accommodating guest molecules such as C_{60}.[93] Such cyclic molecules (Figure 17) spontaneously organised at the 1,2,4-trichlorobenzene-HOPG interface in large hexagonal patterned porous domains (up to 1×1 μm^2) featuring diameters of ~0.91 nm and ~1 nm for macrocycles **28** and **29**, respectively. Each second thiophenyl module constituting the macrocyle is decorated with two butyl appends at the β-positions. Due to the presence of the alkyl chains, the cyclic structures were not lying flat on the surface, but rather they showed a "spider-like" conformation, with the butyl substituents bent downwards with respect to the conjugated ring.

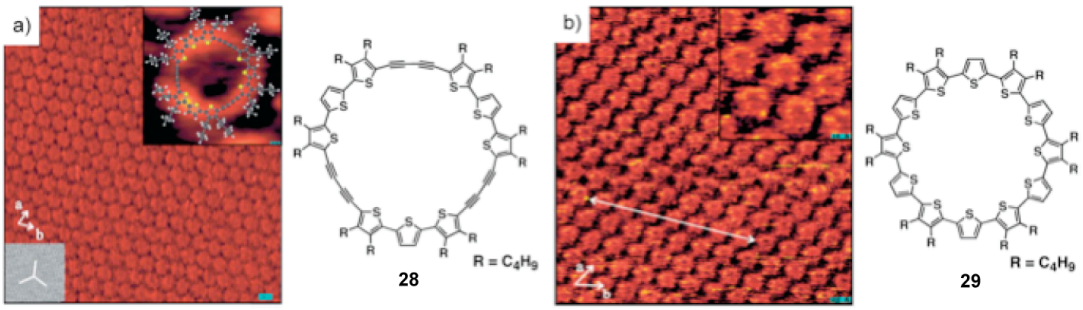

Figure 17. a) STM image of the long-range ordering of macrocycle **28** at the TCB-HOPG interface (60×60 nm^2). The inset (bottom left) shows the underlying graphite. The second inset (top right) shows the STM image of an individual macrocycle; b) long-range ordering of **29** adsorbed on HOPG with a zoomed (inset) region.[93]

Metallo-macrocyclic assemblies are appealing materials for their versatile electronic, magnetic, optical, and catalytic applications as their properties can be tailored by the coordinated metal.[94, 95] The assembly of such compounds on solid supports represents therefore an important step toward their exploitation in devices. *Lehn* and coworkers,[96-98] first reported on the study of 4,6-bis(2',2''-bipyridyl-6-yl)pyrimidine derivatives in combination with either Fe(II), Co(II) or Zn(II) to form [2×2]-square-like complexes, which were then deposited onto HOPG surfaces at the solid-liquid interface. The assembled complexes on the surface revealed to regularly pack as grid-like monolayers. In 2004 *Safarowsky et al.* reported on the organisation of a self-assembled metallo-supramolecular square complexes on a Cu(100) surface[99] through a reinforcing layer of chloride anions, that was able to enhance their interaction with the substrate. It was observed that the complexes assembled in a flat orientation exposing their open cavities toward the solution phase, and thus potentially able to accommodate guest molecules.

In parallel *Stang*, *Wan* and co-workers reported the self-organisation of supramolecular rectangles, square and three-dimensional cages at the $HClO_4$-Au(111) interface.[100] The STM images of both supramolecular rectangle **30** and square **31** (Figure 18a and 18b, respectively) revealed that the coordination complexes form well-ordered 2D networks with each single molecule lying flat on the surface, with its molecular plane parallel to the surface, and an empty cavity in the center of each structure. Specifically, the dimensions of the metallamacrocycles were consistent with those measured by X-ray

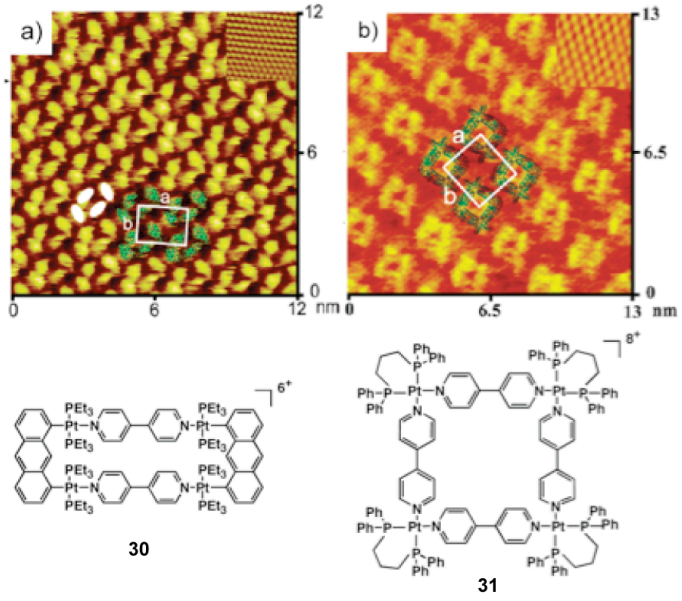

Figure 18. a) High-resolution STM image of [1,8-bis(*trans*-Pt(Et_3)$_2$)anthracene)(4,4'-byp)]$_2$(PF_6)$_4$ **30** rectangular adlayer and showing the underlying Au(111)-(1×1) lattice in the upper right corner; b) high-resolution STM image of [Pt(dppp)(4,4'-byp)]$_4$(CF_3SO_3)$_8$ **31** adlayer. In the upper right corner the underlying Au(111)-(1×1) lattice is shown.[100]

diffraction, 2.0×1.2 nm^2 and 2.1×2.1 nm^2 for **30** and **31**, respectively, showing that the cages do not suffer structural changes upon deposition on Au(111) surfaces.

1.1.4 Single Pore Assemblies: An Enhanced Level of Control in Surface Self-assembly

In order to move towards a higher level of control and predictability of supramolecular self-assemblies on surfaces, two recent publications[101] investigated the formation of single pore assemblies using porphyrin scaffolds to increase the understanding of the molecule-molecule and molecule-substrate interactions on surfaces. The first of the reports was published by *Diederich*, *Stöhr* and *Jung* and co-workers,[101] which expanded on the work of *Yokoyama et al.*[65] reporting the self-assembling of two bis-cyanobiphenyl porphyrin derivatives (bearing two 4'-cyanobiphenyl and two 3,5-di(tert-butyl)phenyl subtiutents in *cis*-like **32** and *trans*-like **33** orientations, respectively (Figure 19a), on a Cu(111) surface under UHV conditions. Surprisingly, in the case of the *cis*-like isomer, various discrete supramolecularly-assembled macrocyclic oligomers were observed, ranging from dimers to hexamers (Figure 19c-h). This large variety in the observed assemblies was attributed to two facts: a) the presence of other contributions than dipolar bonding interactions which direct the formation of other favourable geometries and b) Cu(111) surfaces has a stronger interaction with large aromatic systems in comparison to Au(111), thus the porphyrins adsorbed on the surface tended to align to principle directions of the substrate, altering the balance in strength between the adsorbate-adsorbate and adsorbate-substrate interactions. Despite the large variety of the observed architectures, the most common assemblies were trimers and tetramers. In the trimeric species (Figure 19d), each of the three porphyrins had its central axis rotated of 120° with respect to the next, and thus each one was favourably aligned to the principle directions of the Cu(111) surface. As no bending of the cyanobiphenyl moieties was apparent in the STM images and the structural alignment between neighbouring cyano groups was estimated at an angle of 150°, the interaction was postulated to be a hybrid between antiparallel dipolar and hydrogen-bonding interactions. Two types of tetramers were observed (Figures 19e,f) due to the fact that porphyrins can form conformational enantiomers upon deposition on surfaces. The meso-phenyl substituents were rotated away from their preferred perpendicular orientation relative to the porphyrin core, causing a saddle shape to form in the porphyrin core with two opposing pyrrole rings pointing upwards, and the other two pointing downwards. This can occur in two axes (Figure 19b), leading to type A and type B. One of the tetramers was formed by two type A and two type B porphyrins (Figure 19e). The interactions of the CN groups in this case were at 180°, the optimal angle for antiparallel dipolar interactions, and furthermore, all the porphyrins are

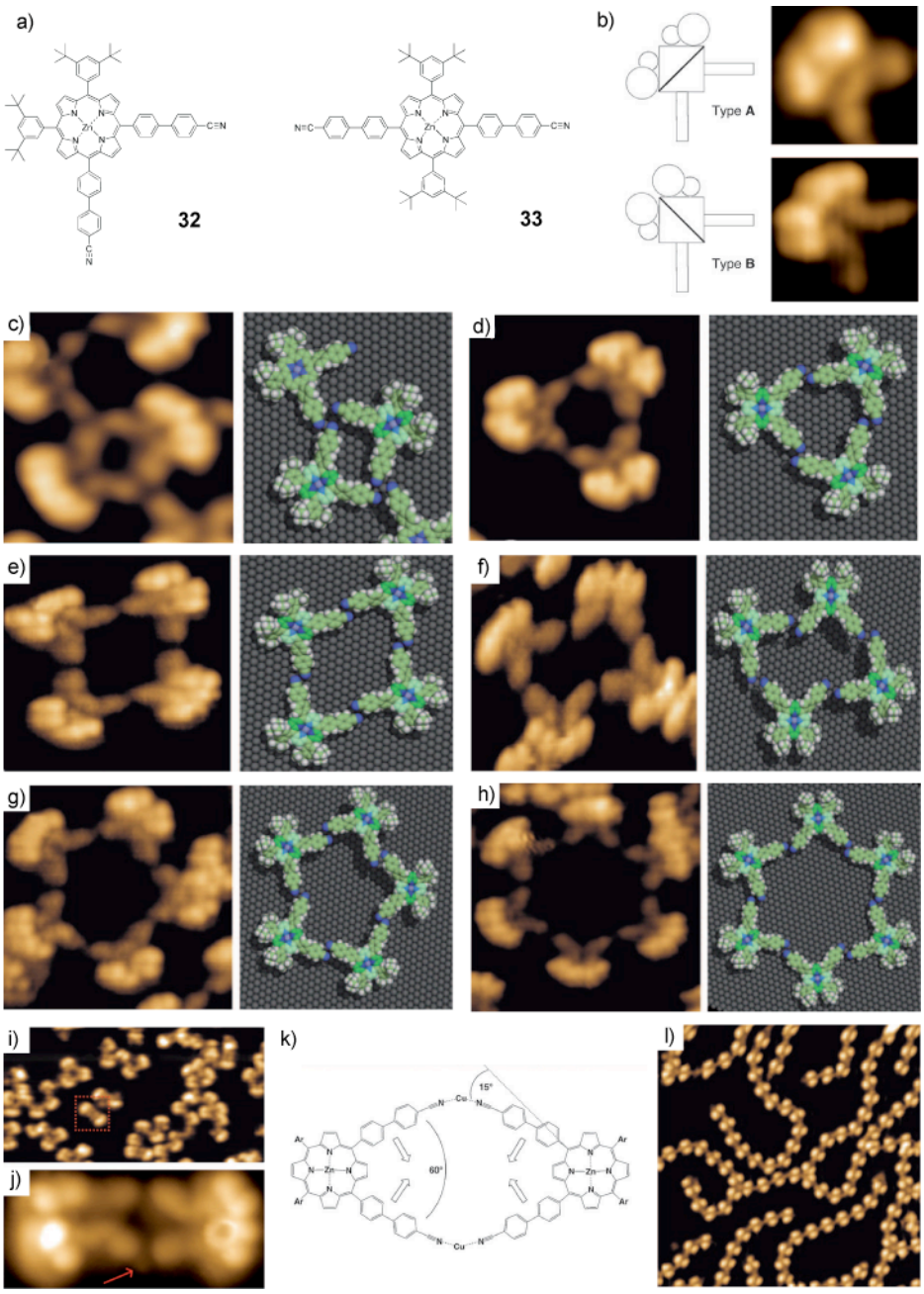

Figure 19. a) Molecular structures of porphyrins **32** and **33**. b) Conformational isomers, type A and B of **28**. c-h) High resolution STM images with the corresponding molecular models of the various self-assembled macrocyclic oligomers: c) dimer (5.0 × 5.0 nm); d) all type A trimer (6.3 × 6.3 nm); e) mixed type tetramer (6.4 × 6.4 nm); f) all type B tetramer (6.2 × 6.2 nm); g) pentamer (7.6 × 7.6 nm); h) hexamer (8.2 × 8.2 nm). i) STM image (50 × 26 nm) for submonolayer coverage of **32** on Cu(111) annealed at 150°C. The dimer marked by a square is enlarged in Figure j. j) High resolution STM image (5.5 × 2.5 nm) of a dimer. k) The proposed model for the dimer showing that the 4'-cyanobiphenyl groups bend together by ~15° to enable coordination with Cu atoms. Ar = 3,5-di(*tert*-butyl)phenyl. l) STM image showing the branched linear chains formed at low coverages by **33** on Cu(111).[101]

aligned with the Cu(111) surface axes. In the second type of tetramer (Figure 19f), the porphyrins were all of the B type, and in order to maintain their alignment on the Cu substrate's axes, the 4'-cyanobiphenyl substituents bent (inwards in two of the porphyrins and outwards in the other two) to be able to interact intermolecularly. Pentamers were also observed (Figure 19g), but very rarely because the formation does not correctly fit the Cu(111) lattice nor the 90° angle of the cyano groups of the porphyrins. Hexameric structures conform to the Cu(111) lattice, however due to the large cavities, they are generally less favoured and very infrequently observed (Figure 19h). The most interesting result obtained with porphyrin **32** was related to the dimer formation. The bonding interaction for the dimer was expected to be similar to that of the trimeric arrangement, where the CN group of one porphyrin would interact with the phenyl hydrogens of the neighbouring porphyrin macrocycle as this arrangement would conform to the geometry of molecule **32** (Figure 19c). However, another dimeric system was observed when the assembly was annealed above 150°C, causing a distortion of the 4' cyanobiphenyl substituents, closing to approximately 60°. This extreme distortion was thought to be caused, firstly, by the aforementioned Cu-substrate-induced saddle shape of the tetrapyrrolic core permitting the meso-substiutents to move laterally, an effect that was even more pronounced at elevated temperatures; and secondly, and more significantly, the elevated temperatures allowed for the mobilisation of Cu adatoms from the Cu step edges making them available for the coordination of two cyano groups, and hence the formation of dimers as it is shown in Figure 19i-k. The number of such dimers increased further upon heating to 200 °C. In the case of *trans*-enantiomer, **33**, deposition on the Cu(111) surface at low coverages led to linear chains formed by the antiparallel dipolar interactions of the cyanophenyl moieties (Figure 19l).

Analogous discrete multi-porphyrin assemblies as those in the above example were obtained in parallel in a work involving our own laboratory. *Heim et al.*[102] investigated the assemblies of three porphyrins bearing pyridyl substituents on a Cu(111) surface under UHV conditions. As shown in Figure 20a, one porphyrin bears a single phenyl-acetylene-pyridyl substituent and three 3,5-di(tert-butyl)phenyl substituents in the meso-positions (**34**). The other two porphyrins are difunctionalised with respect to both types of substituents, bearing the pyridyl moieties in a *cis*-like (**35**) and in a *trans*-like orientation (**36**). Deposition of porphyrin **34** at submonolayer coverage resulted mainly in dimer formation (Figure 20b,c), with few scattered individual porphyrins present. The dimers are coupled in an antiparallel head-on configuration, in which the pyridyl moieties are facing each other. Instead, performing the same deposition on Ag(111), it did not result in dimerisation, but in densely packed islands where the pyridyl groups avoided each other, thus inferring that the Cu(111) substrate plays a role in the dimer formation. Through careful analysis of theoretically

calculated distances compared with the distances obtained experimentally by STM, it was suggested that the most plausible mechanism of dimer formation is the coordination of the pyridyl groups with Cu adatoms originating from the substrate resulting in a pyridyl-Cu-pyridyl motif. This Cu-pyridyl coordination interaction was reported in detail by *Barth* and coworkers using a tetrapyridyl-porphyrin on a Cu(111) substrate.[103] The coordination brings the hydrogen atoms of neighbouring pyridyl groups in close proximity causing steric repulsions, consequently preventing a trimeric coordination from forming as in the case of the cyanophenyl-bearing porphyrin. Furthermore, this repulsion prevents the strong deviations from the optimal 180° angle of the head-on configuration. Although the 180° angle is required for interaction, the phenyl-acetylene-pyridyl functions display some conformational flexibility allowing for some lateral bending. This accounts for the fact that the axis connecting the two porphyrins in the dimeric species does not always follow the direction of atomic lattice of the underlying Cu(111) substrate, but it can vary with an angle of up to ±15° from it. Deposition of cis-dipyridyl porphyrin **35**, on the Cu(111) surface resulted in various discrete supramolecular assemblies (Figure 20d). Triangular and rhombic shaped assemblies were mainly observed. The trimeric assembly (Figure 20e) dominated at low coverage, whereas, the tetrameric species at higher coverages (Figure 20f), with the pentameric (Figure 20g) and hexameric assemblies (Figure 20h) also appearing at the increased coverages. This tendency demonstrates that the spontaneous self-assembly and the structural properties of the architectures depends on a combination of the pyridyl-pyridyl interactions, the conformational flexibility of the molecular modules and also the influence of the Cu substrate (as also shown by *Fendt et al.*[101]). Surprisingly, it has been observed that perpendicular angles between the substituents were very rarely observed on the surface, as the 3,5-di(tert-butyl)phenyl substiutents were generally found to have angles of 60° (type A porphyrin) or 120° (type B porphyrin) with respect to each other, and the pyridyl substituents were at opening angles of 80 ± 5° (type A) or 100 ± 5° (type B). In the triangular assembly all the porphyrin units were of type A and due to the substrate atomic lattice, the triangles could only be found in two orientations on the surface, which followed the Cu orientations (indicated by arrows in Figure 20d), and were at 180° with respect to each other. The tetrameric macrocycles involved two A-type and two B-type porphyrins resulting in rhombic shapes, and could be found in the three orientations on the surface respecting the Cu atomic lattice directions. The pentameric and hexameric assemblies were made up of B-type porphyrins only. In the case of *trans*-substituted porphyrin **36**, deposition resulted in extended chains (Figure 20i) as expected. Further investigations involving the deposition of a bicomponent mixture of porphyrins **35** and **36** (in 3.6:1 ratio), led to the formation of various large unprecedented cyclic structures incorporating both porphyrins (Figures 20k-l). Further to these results, the work also

demonstrated that the assemblies could be singularly manipulated using the STM tip (Figures 20m-p), displaying unprecedented flexibility and robustness.

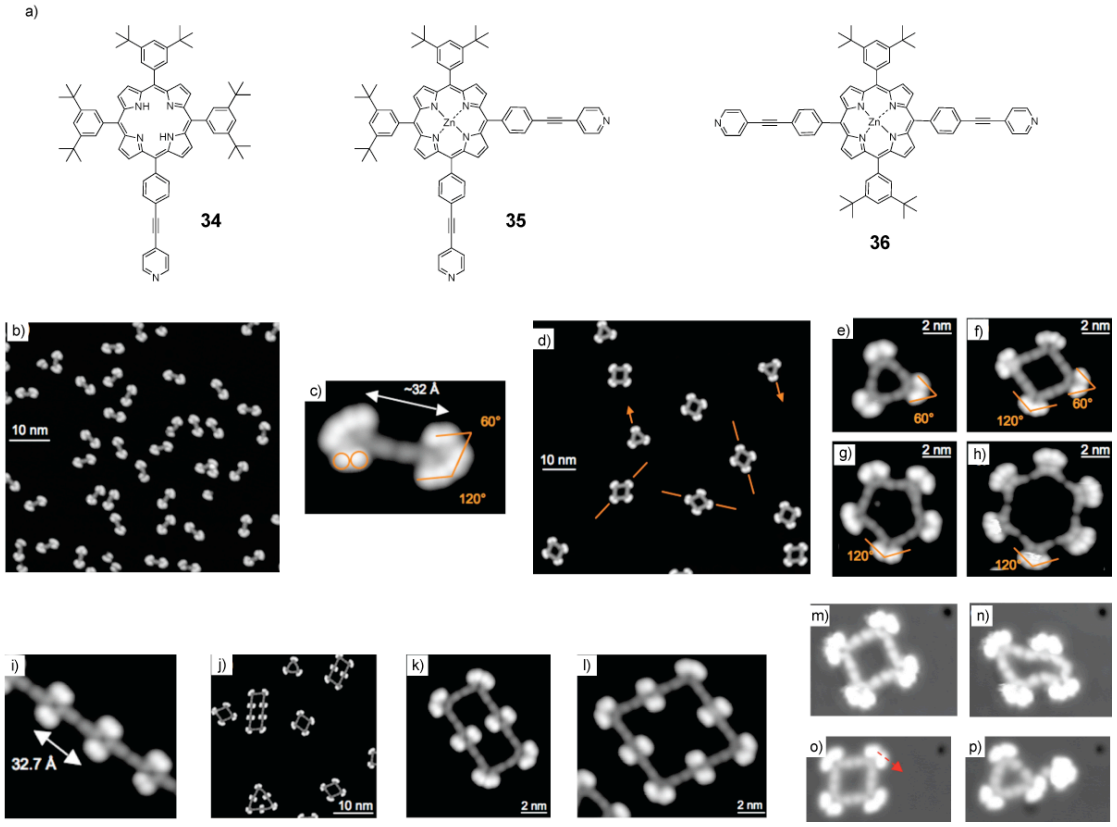

Figure 20. a) Molecular structures of pyridyl-substituted porphyrins **34**-**36**. b) STM image of the self-assembled dimers formed by porphyrin **34** on a Cu(111) surface. c) Detailed view of a single dimer. Each of the bright double lobes (circles) represents a *t*-Bu_2Ph group. The head-on aligned pyridyl-substituents can also be seen in grey. d) STM image of the triangular and rhombic supramolecules formed by porphyrin **35**. The lines and arrows mark the azimuthal orientations of the assemblies. e-h) Detailed STM images of the supramolecular cycles $(\mathbf{35})_n$ (e, n = 3; f, n = 4; g, n = 5; h, n = 6). The opening angles of the *t*-Bu_2Ph groups are indicated. i) STM image of the 1D molecular wires formed upon deposition of **36** on Cu(111). j) STM image showing the coexistance of homomolecular assemblies and bicomponent rhombic and triangular architectures formed following a mixed deposition of **35** and **36**. k, l) Detailed view of the bicomponent cyclic assemblies. m-p) Molecular manipulation experiment where the STM tip using low tunnelling resistance was used to distort a tetramer of **35** without break the intermolecular bonds (m to n) and also to extract one molecule converting a tetramer into a trimer (o to p).[102]

1.2 EXPLOITING THE CAVITIES OF POROUS NETWORKS

As anticipated in the previous Section (1.1), the voids of 2D porous networks can act as selective hosting sites for the preferential accommodation of guest molecules. An increasing number of studies are currently focusing on the specificity and guest selectivity of templated networks. Such specific recognition is essential for the immobilisation and study of functional molecules at the single molecule level of precision. This section, focuses on recent

advances in the preparation of 2D porous networks that can be regarded as molecular sieves, since they are able to selectively accommodate guest species in their cavities depending not only on their size and shape but also, in some cases, on their electronic properties. Section 1.2.1 will discuss host-guest recognition in the cavities. This will be followed by a discussion of flexibility and guest-induced structural transformation shown by some non-porous and porous hosting networks (Section 1.2.2). A sub-section is also devoted to biomolecular hosting (Section 1.2.3), and the final section discusses covalent surface functionalisation using the porous network as a template (Section 1.2.4).

1.2.1 CAVITY-CONFINED HOST-GUEST RECOGNITION

During the last years, several porous networks formed by various components of different nature, and stabilised by means of various interactions, have proved to be excellent hosts for C_{60} molecules. In a recent work, *Wee*, *Chen* and co-workers presented a strategy to fabricate regular porous nanoarrays from pentacene under UHV on Ag (111), which were used to selectively accommodate guest C_{60} molecules.[104] As shown in Figure 21a after deposition of 0.7 ML pentacene **37** on Ag(111) and annealing to 380 K (1 ML corresponds to a close-packed molecular layer) a loosely brick-wall-like structure was obtained (inter-row distance: 1.03 nm). The arrangement of this structure was significantly modified by the deposition of 0.7 ML of C_{60}, which after annealing at 360 K gave rise to the formation of an extended 2D network with well-ordered cavities. The C_{60} adsorption induced structural rearrangement of the pentacene array into pentacene pairs surrounded by C_{60} molecules (Figure 21b). The new array was constituted by a regular arrangement of C_{60} molecular chains (interchain distance: 1.82 nm) with an intermolecular distance between the nearest hosted neighbouring C_{60} molecules of 1.05 nm. The skeleton of the C_{60} nanomesh was stabilised by the strong molecule-metal interfacial interactions [C_{60}-Ag(111) and pentacene-Ag(111)] and the pentacene-C_{60} donor-acceptor coupling. Figure 21c-d clearly reveals that the C_{60} molecules exclusively adsorb in the nanocavities of the nanomesh template, and upon increasing the coverage from 0.05 ML (Figure 21c) to 0.2 ML (Figure 21d) a full occupation was achieved.

Structural modification of a Zn-porphyrin macrocycle through the introduction of 4-cyanophenyl moieties at the 1,10-positions (**38**), led to the formation of regular homochiral nanoporous domains on Cu(111) surfaces under UHV.[105] As shown in Figure 22 each pore appears as a chiral windmill-shaped structure consisting of six wings, each associated with the two *tert*-butyl residues of the 3,5-di(*tert*-butyl)phenyl substituents. These networks further displayed self-hosting properties towards unbounded single porphyrin guests, which nested atop of each windmill-like cavity (Figure 22c,d). From various STM sequences at different

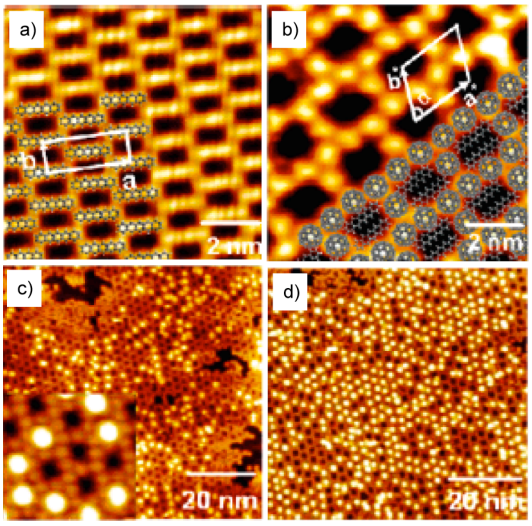

Figure 21. a) STM image of long-range ordered pentacene superstructures on Ag(111); b) detailed image of the C_{60} nanomesh together with its proposed model superimposed on the image; c-d) STM images of the coverage dependent evolution of C_{60} assembled within the nanomesh: c) 0.05 ML, d) 0.2 ML.[104]

temperatures it has been observed that the porphyrin guests can thermally switch from one stable position to another. The horizontal line in Figure 22c,d indicates that the nested molecule switched into a new position. The thermally induced rotation of the guest molecules revealed to be faster than the time-resolution of the STM, and thus the shown images are a superposition of all possible arrangements that can be taken on a single pore. As the guest molecule is embedded onto a nanoporous network, each device could also be selectively addressed and switched upon applying a local voltage by placing the tip above the porphyrin guest under scanning conditions. By applying short pulses (~1 second), a single switching event could be triggered. Although this method revealed to be successful in inducing a switching event, a preferential direction of rotation (*i.e.*, clockwise or counterclockwise) has not been achieved so far.

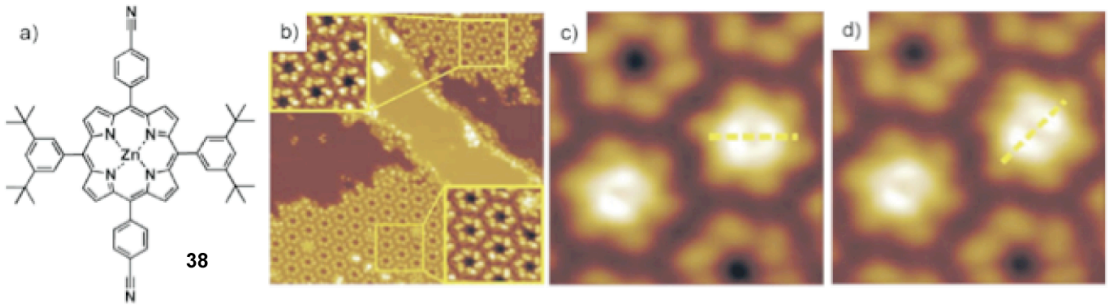

Figure 22. a) Structure of the 4-cyanophenyl substituted porphyrin **33;** b) STM image (50×50 nm^2) of the self-assembled network of **38** on Cu(111). The insets (9.1×9.1 nm^2) show that two homochiral domains were observed; b,c) STM images (6.5×6.5 nm^2) showing the controlled rotation of the nested guest molecules induced by the STM tip.[105]

In a recent work from the groups of *Attias*, *Charra* and co-workers it has been shown that deposition, at the phenyloctane-HOPG interface, of star-shaped tris-phenylene ethynylene derivative **39**, leads to honeycomb structures generating empty cavities (diameter ~ 1.3 nm) suitable for hosting guest molecules (Figure 23a).[106] With the aim to test the guest selectivity, the authors studied the confinement of several polycyclic aromatic hydrocarbons (PAHs) within the porous network. After deposition of coronene **40**, benzo[*rst*]pentaphene **41** and hexabenzocoronene **42** into the hosting network, the appearance of a circular bright spot at the center of each pore, confirmed the trapping of the guest molecules (Figure 23b-d). In contrast, when pentacene or other stilbenoid derivatives were added, they were never found to adsorb inside the cavities due to their larger size in comparison with that of the pore, thus demonstrating the size and shape selectivity of the hosting arrays.

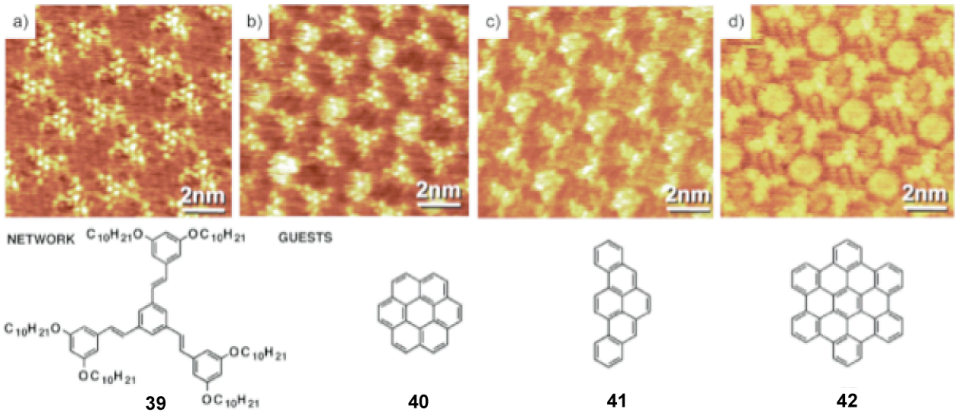

Figure 23. STM images on HOPG of a) self-assembled monolayer of the matrix formed trough self-assembly of (1,3,5-tris[(*E*)-2-(3,5-didecyloxyphenyl)-ethenyl]benzene **39**; the host matrix after addition of b) **40**; c) **41**; d) **42**.[106]

Another example of selective assembly has been obtained with bis(3,5-diacidic)diazobenzene **43**, which formed 2D porous networks at the liquid–solid interface (solvent: heptanoic acid, surface: HOPG, r.t.), with two types of cavities (A and B) of different sizes (pore diameters: 1.2 and 0.86 nm, respectively) and symmetries through double intermolecular H-bonds between frontal carboxyl groups.[58] This open Kagomé array offering two different types of binding sites can serve as a two-dimensional molecular template to accommodate functional molecules with site selectivity. Whereas the experimental results indicate that C_{60} molecules have been hosted in both sites displaying no selectivity (Figure 24a-d), larger fullerenes, such as C_{80} and $Sc_3N@C_{80}$ were exclusively accommodated in the larger cavities (*i.e.*, those with 1.2 nm of diameter) as shown in Figures 24e-f. In addition, as the caged metal atoms increase the electronegativity, endohedral fullerenes such as $Sc_3N@C_{80}$ showed enhanced binding to the **43**–graphite network compared to pristine C_{60}.

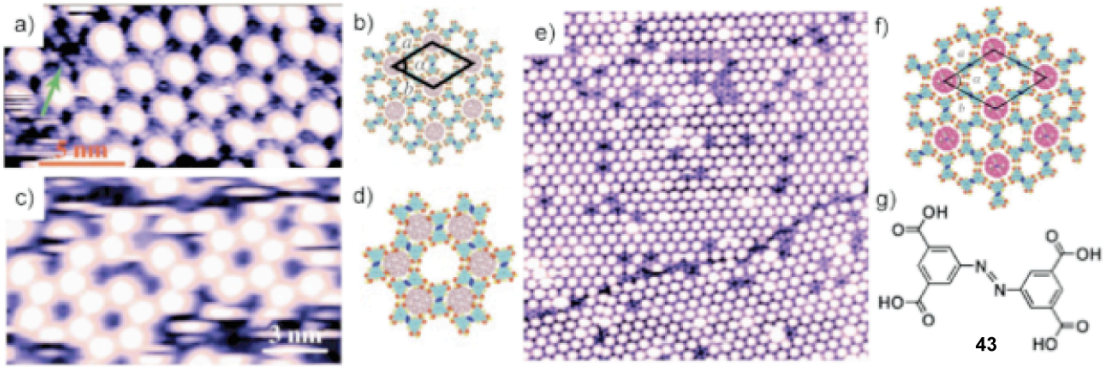

Figure 24. High-resolution STM view showing the detailed C_{60}–**43** host–guest structure with C_{60} trapped within a) the A-type network, c) the B-type network; b), d) suggested molecular models of the assembly structures for a) and c), respectively; e) STM image (68×68 nm^2) of the $Sc_3N@C_{80}$ trapped within the A-type of the diazobenzene **43** network on HOPG surface; f) proposed structural model; g) chemical structure of diazobenzene **43**.[58]

As described in Section 1.1.3, another approach towards the formation of regular hosting networks is the use of preformed molecular cavities. By means of this method, *Tobe*, *De Feyter* and co-workers obtained regular porous networks from the deposition of butadiyne-bridged planar macrocycles (pore diameter ~1 nm) at the TCB/graphite interface (Figure 25).[107] Three different macrocycles were studied: pyridinophane **44** bearing four peripheral octyl esters, and cyclophanes **45** and **46** bearing four octyl ester and four (octyloxy)methyl substituents, respectively. Although the aromatic units on the macrocycles did not show any difference in the organisation, cyclophane **46** forms a more densely packed linear pattern than macrocycles **44** and **45** probably due to the absence of H-bonding interactions between the adsorbed macrocyles. Site-selective guest inclusion was tested with tropylium (Tr) cation **47**, which is known to have high binding affinity to pyridine via ion-dipole interactions.[108] As expected, *in-situ* and *ex-situ* complexation experiments on the molecular host network **44** with guest **47** (1:13 molar ratio, in TCB/CH_3CN/$CHCl_3$ 10/9/1) showed accommodation of **47** inside the macrocycle cavities, while similar experiments on networks **40** and **41** did not reveal any complexation. Upon mixture of two similar macrocyles (**44** and **45**) with guest **47** (1:1:13 molar ratio, in TCB/CH_3CN/$CHCl_3$ 20/9/1) only some macrocycles showed bright spots inside the cavities suggesting that the remaining empty pores where those from cyclophane **45** (Figure 25a). On the other hand, mixture of **44**, **46** and **47** (1:1:13 molar ratio, in TCB/CH_3CN/$CHCl_3$ 20/9/1) showed, in addition to pure domains of the complex (Linear A, Figure 25b), a new molecular network (Linear C) formed by alternated macrocycles exhibiting bright (**44** + **47** complex) and dark cores (guest free **46**) (Figure 25b-d). The driving force for this preferred alternation and alignment on the surface has been attributed to attractive dipolar interactions between adjacent ester and ether groups along the macrocycle rows.

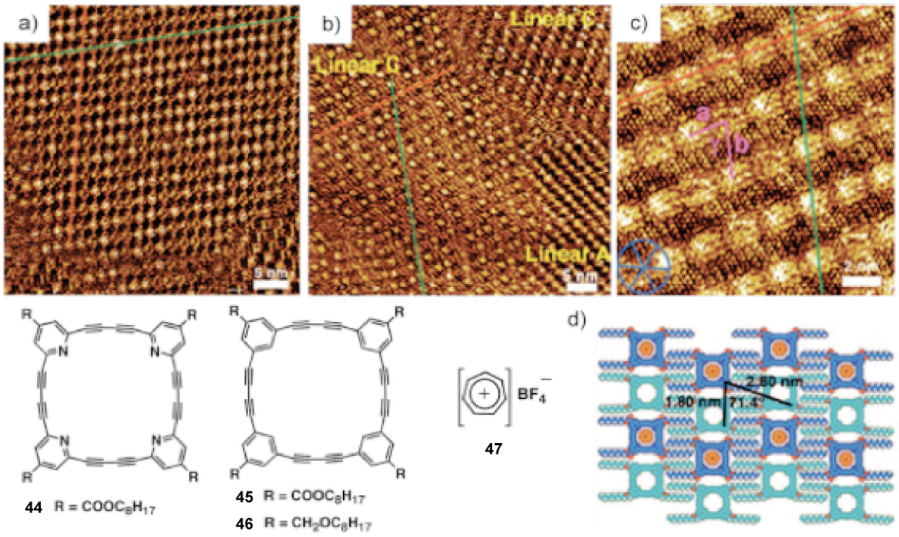

Figure 25. a) STM image of the monolayer formed by a mixture of **45** and **44** + **47** complex; b) STM image of monolayer formed by a mixture of **46** and **44** + **47** complex; c) high resolution image of the linear C structure; d) tentative model of the ideal alternating linear C structure consisting of **44** (blue), **46** (turquoise), and Tr cation (orange) **47**.[107]

1.2.2 GUEST-CONTROLLED NON-COVALENT CONFINEMENT

Given that all the networks described so far constructed via supramolecular interactions are not covalently bound to the surface, a certain degree of dynamicity during the recognition process is expected. In this section, the flexibility and the guest-induced structural transformation shown by some non-porous and porous hosting networks will be discussed.

One of the first examples of structural transformation, from a linear nonporous structure into a honeycomb porous network, as a response to the addition of guest molecules was described by *De Feyter*, *Tobe* and co-workers (Figure 26).[109] Recently, they have studied a series of dehydrobenzo[12]annulene (DBA) derivatives which by interdigitation of the alkyl chains generate well-ordered arrays on HOPG surfaces under ambient conditions. Remarkably, it has been observed that upon increasing the length of the alkyl chains present in the DBA cores, a transition from honeycomb networks to linear networks occured.[68] Some of these systems have additionally shown concentration-dependent polymorphism.[70] In particular, at low concentrations 2D porous honeycomb networks are formed, while at high concentrations, the same systems organise in dense-packed linear patterns. In spite of this, in both cases, the dense-packed linear patterns can be transformed into porous networks by addition of a proper guest molecule (Figure 26).[69]

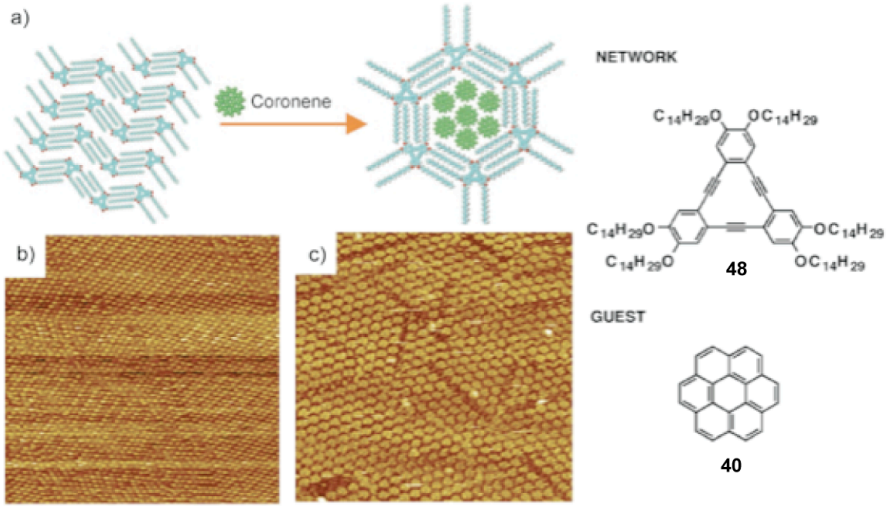

Figure 26. a) Tentative reorganisation model of **48** from a linear DBA network into a honeycomb network after addition of coronene **40**; b) STM images on HOPG of a linear network **48** without coronene and c) honeycomb structure after the addition of **40**. Image size (96×96 nm^2).[109]

Interestingly, they also studied the encapsulation of several guest molecules of different symmetry, size and planarity (Figure 27). It was observed that only the planar guest molecules presenting large π-conjugated cores such as coronene (**40**), hexakis(phenylethynyl)benzene (**49**) and phthalocyanine (**50**) induced a network transition from a linear structure to a hexagonal closed structure of the array. This could be attributed to the adsorption energies, which are larger than the adsorption energies of the other nonplanar or small π-conjugated molecules hexaiodobenzene (**51**), chrysene (**52**), 9,10-diphenylanthracene (**53**) and C_{60} (**54**).

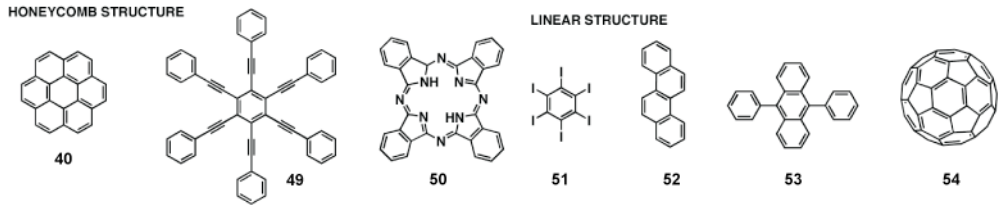

Figure 27. Guest molecules tested in order to induce structural changes on the flexible network.[109]

In a very recent work, the same authors reported a hierarchical self-assembly of three-component 2D crystalline lattices at the liquid-solid interface (solvent: 1-octanoic acid, surface: HOPG, room temperature) following a host-guest strategy, which involved specific recognition and selection processes.[57] As it can be observed in Figure 28, coronene (**40**) acted as a molecular template directing the assembly of six molecules of isophthalic acid (**55**) into a 2D H-bonded supramolecular network (Figure 28a,c). If no coronene was present, the cyclic hexamer organisation of isophthalic acid molecules would not be possible due to the

higher adsorption energy per unit area that the porous arrangement represents (Figure 28b). Using this heteromolecular cluster as a template, the assembly of an alkoxylated dehydrobenzo[12]annulene derivative **56** into a honeycomb network stabilised by van der Waals interactions was achieved (Figure 28a,d). Most notably, the network formed by **56** can be regarded as a molecular sieve. In fact, in the presence of competing guests such as trimesic acid, which is known to form well-defined bimolecular assemblies with coronene (identical to those in Figure 28c), arrays of molecule **56** exclusively hosts hetermolecular complexes composed by **40**·**55** in the ratio 1:6.

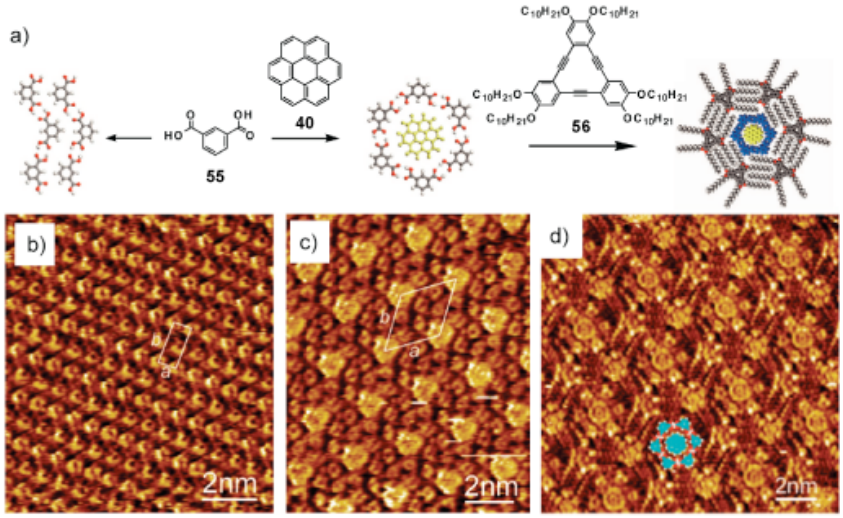

Figure 28. a) Molecular mechanics (MM)-optimised structures of (left) the "zigzag" pattern of **55** and (right) the coronene-templated assembly of **55** and model of the three-component hierarchical assembly; b,c) STM images recorded at 1-octanoic acid/graphite interface of self-assembled patterns of **55** b) in the absence of coronene and c) in the presence of coronene; d) the high-resolution image of the tricomponent architecture shows submolecular detail of the **40**·**55** (1:6) cluster.[57]

In parallel, another example of dynamic molecular assemblies was described in a systematic study performed by *Charra*, *Attias* and co-workers.[110] Exploiting the interdigitation tendency of aliphatic chains, they synthesised several molecular modules based on a 2,4,6-tristyrylpyridine central core. In particular, they showed the formation of supramolecular dimers (Figure 29a), polymers (Figure 29b), and 2D networks (Figure 29c) by absorption of mono- (**57**), di- (**58**), and trifunctional (**59**) derivatives, respectively, at phenyloctane-HOPG interfaces. The degree of functionalisation, and therefore, the number of alkylic chains (clipping functionalities) present in the central core steers the organisation of the molecules. Modules **58** and **59** have the same disposition of the alkyl chains and therefore the same organisation pattern (cyclic hexamers) was expected. However, as a result of the tendency to minimise the free surface energy, the more compact linear polymer conformation shown in Figure 29b was preferred. Still, thanks to the flexibility of the system it was possible

to induce a reorganisation of such linear polymer-like topology into cyclic hexameric blocks by addition of a hexabenzocoronene derivative (**42**) (Figure 29d). As expected, the structure of the resulting hierarchical organisation resulted to be the same as the honeycomb network using the trifunctional molecular module **59** (Figure 29c).

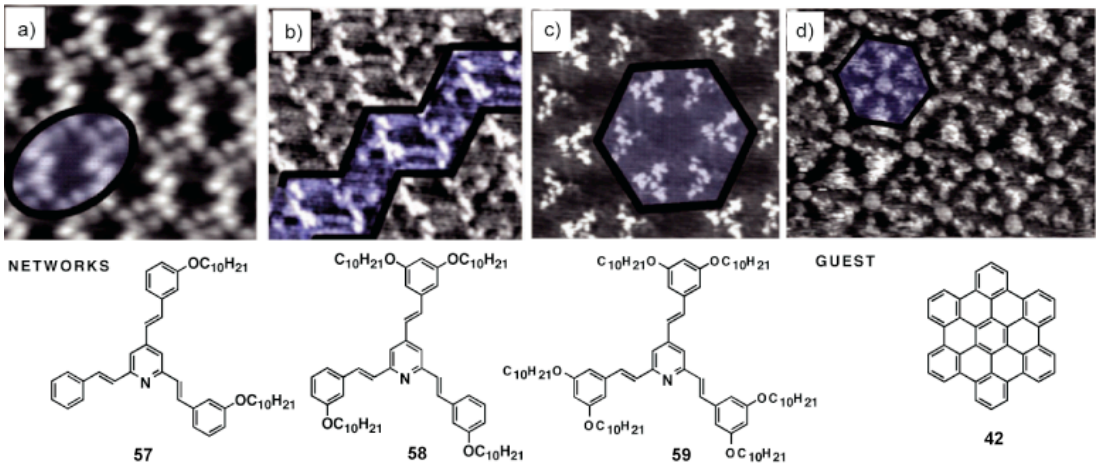

Figure 29. a-c) STM images corresponding to the monofunctional **57**, bifunctional **58** and trifunctional **59** molecules all based on the 2,4,6-tristyrylpyridine core. d) STM image after rearrangement of network b induced by addition of hexabenzocoronene (**42**). The scanned areas were a) 7.8×7.3 nm^2, b) 8.1×7.5 nm^2, c) 8.9×8.3 nm^2, d) 25.7×18.7 nm^2.[110]

In a study examining the inclusion of metallophthalocyanines (MPc) in the porous network formed by self-assembled 1,3,5-tris(10-carboxydecyloxy)benzene (**60**) on at the solid-liquid interface on HOPG under ambient conditions (solvent: toluene), it was found that the network could adapt its shape to host either one or two MPc molecules per pore.[56] Molecule **60** self-assembled into homogenous networks with almost tetragonal cavities at the toluene-HOPG interface (Figure 30a). Following this, the inclusion of different molar ratios of phthalocyanine **50** was investigated. While at a molar ratio of **60**·**50** greater than 2:1, unfilled networks were mainly observed (Figure 30a), at a molar ratio lower than 1:1, dimer-entrapped networks were formed (Figure 30c). The optimal ratio for obtaining both dimer- and monomer-entrapped network domains was 2:1. The inclusion of a single phthalocyanine in each cavity caused the bending of the flexible aliphatic moieties of **60**, and therefore a distortion of the shape of the flexible network (Figure 30b). In the domains in which dimers were entrapped, an altogether different distortion of the network was observed (Figure 30c). In this case, two MPc molecules were hosted almost side by side in a single cavity that was formed by four **60** molecules (compared to two **60** molecules in the control and the monomer-entrapped architecture). Due to the new conformation, the average number of H-bonds per unit mesh is one, compared to two in the monomer-entrapped conformation (compare the black ellipses drawn in Figure 30b and 30c). This results in weaker interactions (9.6 kcal mol^{-}

[1]) and thus a larger cavity was able to form. This establishes that the porous network formed by molecule **60** depends on H-bonding interactions for its stability and at the same time the H-bonds endow the system with a certain degree of flexibility. Once again, van der Waals interactions are thought to be the main contributor for the host-guest inclusion.

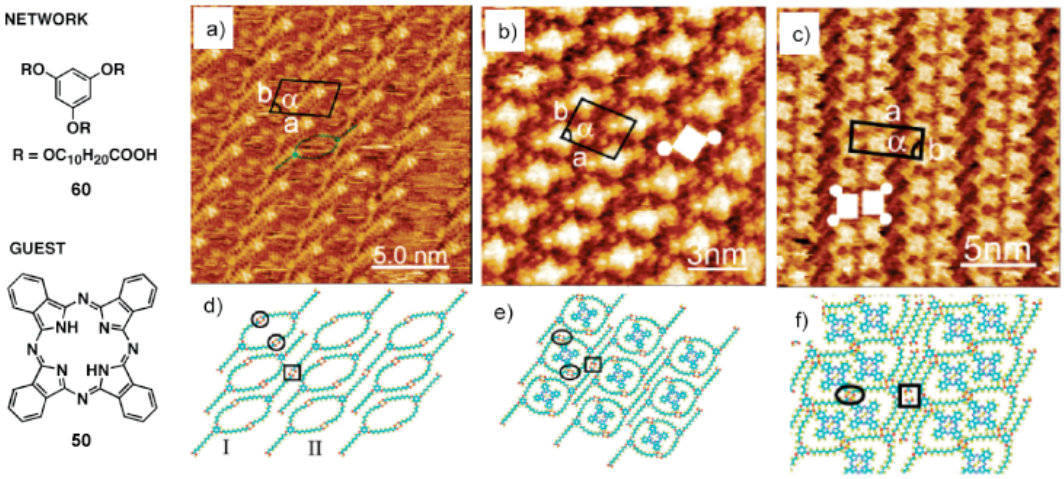

Figure 30. a) STM image of the self-assembly of **60** on a HOPG surface; STM images of the self-assembled **55** molecules hosting b) a single **50** molecule per cavity c) a dimer of **50** molecules in each cavity. The white shapes in b) and c) indicate the location of **50** as squares and the phenyl groups of **60** as circles; e-f) each STM image is accompanied by the proposed molecular model with identified H-bonding locations.[56]

Along this section the dynamicity that some systems show under solid-liquid conditions has been thoroughly demonstrated, however there are very few reports showing flexible networks studied under UHV conditions. In 2007 *Yokoyama* and co-workers reported the formation of a flexible network formed by the self-assembly of a porphyrin derivative on a Au(111) surface, which after the adsorption of C_{60} leads to the formation of a nanoporous structure that is able to accommodate the guest molecules.[111] In a similar way, *Calmettes* and co-workers reported the formation of metastable open 2D hosting networks of 2,3,9,10,16,17,23,24-octachlorozinc phthalocyanine (**61**) on Ag(111) under UHV conditions (Figure 31). The latter network could be used as flexible templates for the controlled insertion of guest molecules, in particular 1,3,5,7,9-penta-*tert*-butyl-corannulene (**62**).[112] The presence of eight chlorine atoms in **61**, which are able to establish relatively weak H-bonding and van der Waals interactions, leads to the kinetic control of the self-assembly process on the substrate. In particular, three different networks were obtained depending on the packing density (0.33 mol nm^{-2}, 0.38 mol nm^{-2}, 0.44 mol nm^{-2}, respectively) tailored by time and thermal annealing. The low packing density and the flexibility of the weak intermolecular interactions of networks N1 and N2 (Figure 31a,b), allowed the accommodation of **62** due to an aperture within the initial organisation. In the case of N1, the self-assembly of molecules

results into a chessboard-like structure (Figure 31c) and in the case of N2, both components align in separate parallel lines (Figure 31d). Remarkably, it has been shown that it was possible to modify the aforementioned arrays by removing individual **62** molecules by using the STM tip, leaving the new phthalocyanine-templated pattern almost undamaged.

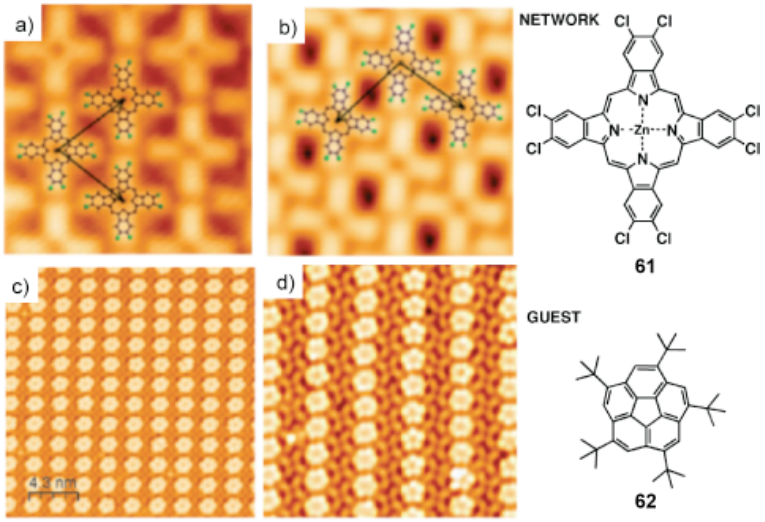

Figure 31. STM images (5×5 nm^2) at the liquid-helium temperature (T = 4.6 K) of two 2D packings of **61** on Ag(111): a) network 1 (N1), observed immediately after molecule evaporation; b) network 2 (N2), after annealing at 230 K; c) STM image a **61**-N1 network observed at T = 77 K after evaporation of **57**; d) bicomponent network obtained from the evaporation of **62** onto a **61**-N2 lattice.[111]

1.2.3 Towards Biomolecular Hosting

The organisation and immobilisation of biomolecular systems on surfaces is a requirement toward the fabrication of bionanodevices.[38] In this section, some examples of molecular confinement of aminoacids and peptides at porous hosting surfaces will be illustrated.

In this context, *Stepanow* et al. reported the first example of surface supported metallosupramolecular receptors to bind biomolecules (cystine (**64**) and diphenylalanine (**65**)) through non-covalent interactions.[113] The receptor nanocavities (1 nm opening) were prepared on Cu(100) substrate in UHV, by hierarchical self-assembly of Fe atoms and trimesic acid (**63**) (Figure 32a).[73] Addition of cystine to the nanocavities resulted in the appearance of two protrusions, each of them associated to a single cystine anchored to the Cu substrate in an upright position, inside the cavities (Figure 32b). The binding of cystine molecules was observed to be reversible, since after thermal annealing a progressive removal of the trapped molecules occurred (at 430 K one cystine was removed and at 490 K the remaining molecule was released), and the empty cavities presented their original structure. The trapping of diphenylalanine (**65**) was also observed (Figure 32c). In contrast to cystine, only one Phe-Phe molecule per cavity was found to adsorb, and because of the bulky phenyl

rings at both terminals and the length (1.3 nm), the complete inclusion of the molecule within the cavity was excluded. The Phe-Phe guests were also reversibly released at 450 K. Once more, the nanocavities remained unchanged after complete desorption of the guest molecules, indicating the reversibility of the host-guest binding.

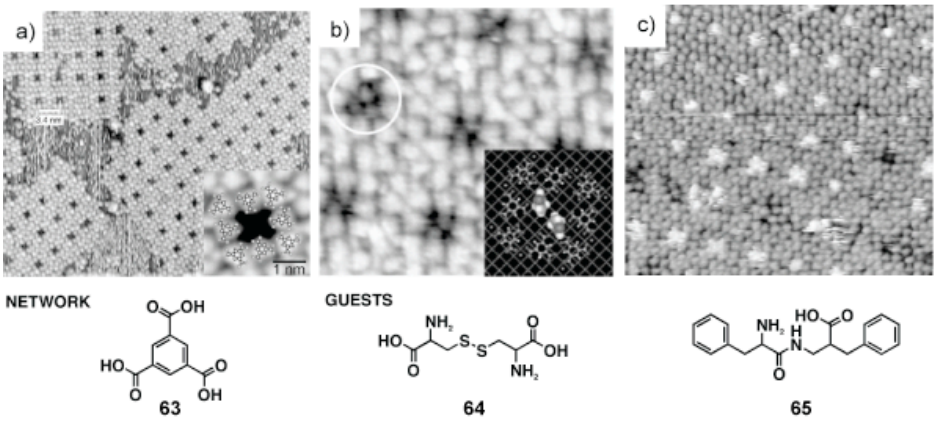

Figure 32. a) 2D metallosupramolecular nanoarrays of trimesic acid (**63**) and Fe atoms on a Cu(100) substrate; b) binding of cystine (**64**) in the receptors after deposition at 300 K. Image size 10×9 nm^2; c) binding of Phe-Phe (**65**) inside the cavities. Image size 25×22 nm^2.[113]

Under ambient conditions, *Wan* and co-workers also reported the controlled adsorption of peptides within an oligomeric template.[114] By adsorbing an oligo-(phenylene-ethynylene) OPE (**66**) bearing an end-carboxyl functional group on a HOPG surface (under ambient air conditions) a regular template was formed (Figure 33). The molecules interact with each other via H-bonds through the carboxyl groups and via interdigitation of the alkyl chains. It was observed that after the inclusion of coronene (**40**) on the OPE templated array, the guest molecules were trapped within the free spaces available among the alkyl chains. In a similar way, tripeptide Tyr-Gly-Gly (**67**) was uniformly distributed at the vacancies of the OPE template. In Figure 33b an arrow indicates the positioning of two peptide molecules between the neighbouring conjugated backbones. A careful observation reveals that molecules **67** appear at every other row and are interdigitated into the OPE template.

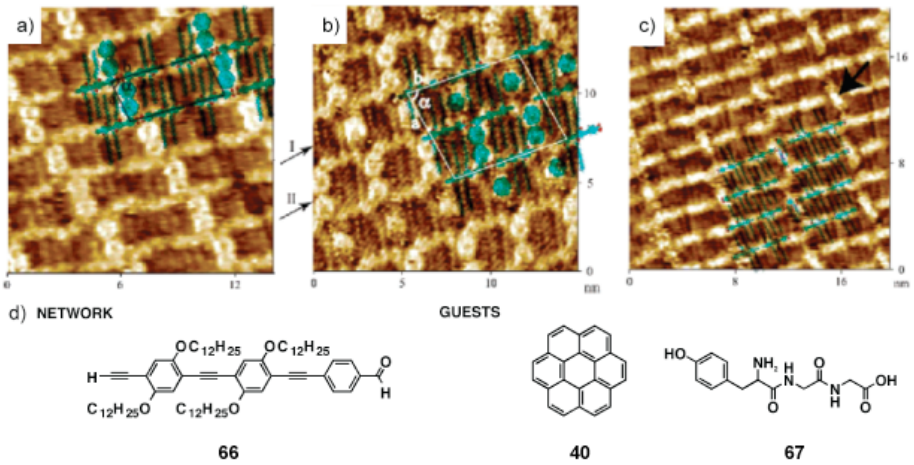

Figure 33. a) High-resolution STM image of a **40**/**66** (1:1) mixture; b) high-resolution STM image of peptide **67** dispersed within OPE template; c) chemical structure of the molecules that compose the network: OPE **66**, and of the guests: coronene **40** and tripeptide **67**.[114]

1.2.4 PORE-TEMPLATED SURFACE FUNCTIONALISATION

As thoroughly discussed in this introduction, in order to obtain useful platforms for biotechnological or electrooptical applications, the periodic organisation of functional molecules on templated surfaces is necessary. However, it is not always possible to direct the adsorption of guest molecules inside the assembled pores. In this section it will be illustrated how the use of covalently modified 2D networks could guide the encapsulation of the targeted guests within the hosting pores.

Recently, *Beton*, *Champness* and co-workers have shown that the bi-molecular hosting network depicted in Figure 1 could also be formed if molecule **1** was replaced by perylene-derived molecules (R_2-PTCDI) bearing lateral groups.[115] In particular, they have described the self-assembly and hosting properties of Br-bearing **68** (Br_2-PTCDI) and propylthio **69** (di(propylthio)-PTCDI) functionalised perylene derivatives with melamine **2** (Figure 34b) under UHV conditions (surface: Au (111)/mica). While for unfunctionalised PTCDI, it was not possible to observe complete coverage of bimolecular hexagonal arrays when combined with melamine, for Br_2-PTCDI **68** the existence of only homogeneous bimolecular hexagonal networks was found (Figure 37a). The C_{60}-entrapment properties of the new **68·2** network resulted to be the same as the one observed for the **1·2** system, namely the formation of C_{60} heptamers within the pores, indicating the relatively short steric hindrance of the Br atoms (Figure 34c). Similarly to **68**, di(propylthio)-PTCDI **69** was completely converted into a bimolecular hexagonal array when combined with melamine. However, the deposition of C_{60} onto the hexagonal network did not result in the heptameric clusters within the pores as before, but rather fullerene guests were adsorbed in an irregular fashion (Figure 34d). Such observation was attributed to the presence of the propylthio chains in the cavities, which restrained the entrapment of C_{60} within the pores.

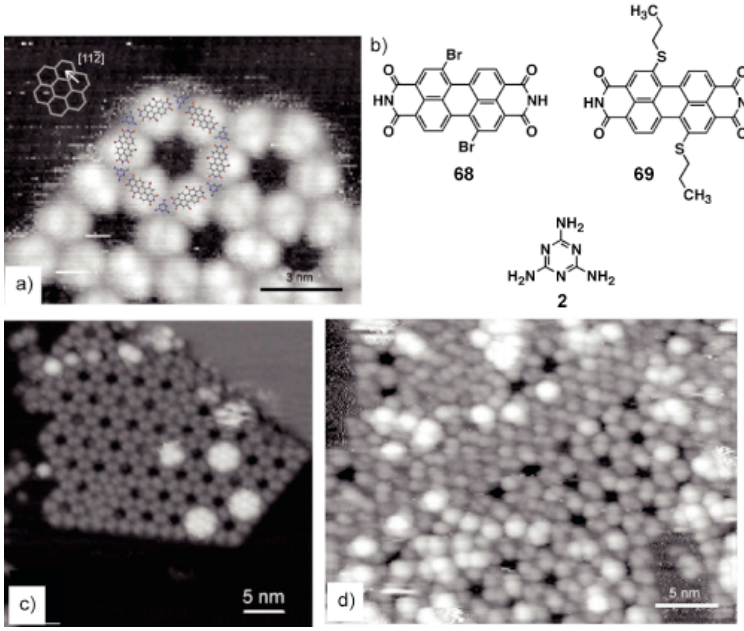

Figure 34. a) UHV STM image showing hexagonal supramolecular structures formed with Br_2-PTCDI and melamine on a Ag-Si(111)$\sqrt{3}\times\sqrt{3}R30°$ surface. The protrusion from each Br_2 is apparent; b) chemical structure of the molecules used for the network formation; c) image showing three captured C_{60} heptamers within the cavities of **68·2** network; d) STM image after deposition of C_{60} onto the bimolecular honeycomb network formed after sublimation of melamine onto adsorbed **69·2**.[115]

In a very recent work, it has been shown that the same PTCDI-melamine supramolecular honeycomb network as that described by *Beton* and co-workers[48] in Figure 1 can also be formed at the liquid-solid interface under ambient conditions. It also demonstrates sufficient robustness to act as a template to precisely guide the self-assembly of thiol-based monolayers.[116] *Buck* and co-workers have shown that different self-assembled monolayers (SAMs) consisting of adamantine **70**, dodecane **71** and ω-(4'-methylbiphenyl-4-yl)propane **72** thiols could be selectively confined inside the hexagonally patterned cavities (Figure 35). Such SAMs revealed to be so robust in the liquid environment that they could even be processed further, as it was demonstrated through electrochemical deposition experiments of Cu. Specifically, they have shown that a monolayer of Cu can be grown between the Au substrate and the thiol-derived molecules without disrupting the hybrid structure. To date, this is the first example in which a non-covalent network has been used to template the patterning of SAMs at the molecular level, providing an exact definition of structures in the substrate plane. The combination of the 2D network with the SAMs offers considerable design flexibility, with the network and the SAM each permitting separate surface modifications.

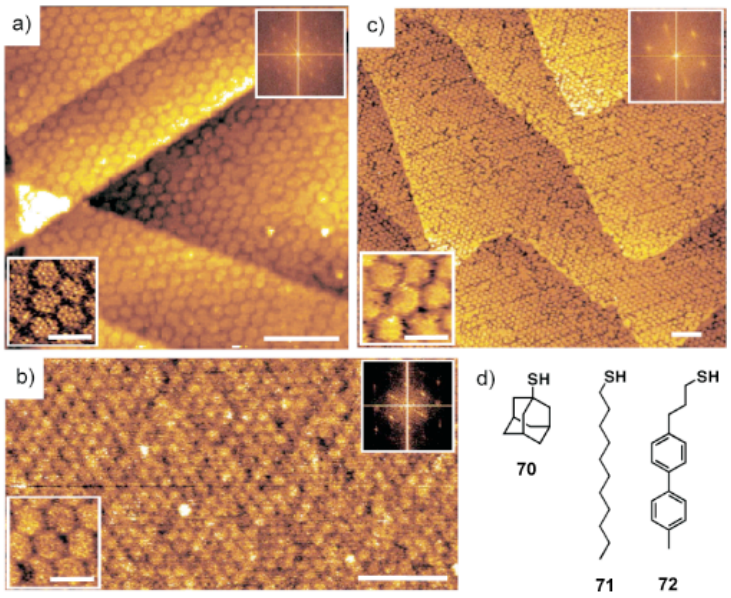

Figure 35. a–c) STM images of the hybrid structures on Au(111)/mica: network filled with **70** a), **71** b) and **72** c). The insets at the lower left and upper right corners of the STM images show high- resolution images and Fourier transforms, respectively. Scale bars, 20 nm (large-scale images) and 5 nm (insets); d) structures of the studied thiols.[116]

1.3 TOWARDS THE THIRD DIMENSION: FROM STRUCTURES TO FUNCTIONALITY

Extension of supramolecular assemblies on surfaces into the third dimension has also been explored in recent years. This section describes recent works that demonstrate that the third dimension can be used to introduce structural features, and also that it can be exploited to prepare functional molecular devices.

Porphyrins are commonly used in these experiments due to: (i) their ability to form stacks via π-π interactions e.g. *Friedlein et al.* were able to achieve films with a thickness of several nanometres by the self-assembly of porphyrins into vertical columnar stacks that were perpendicular to the basal plane of the substrate;[117] and also, (ii) because introducing the appropriate metal in the porphyrin core allows for axial coordination, perpendicular to the planar macrocycle of the porphyrin, thus extending the supramolecular assemblies on surfaces into the third dimension. The latter approach is more commonly used.

Using the axial coordination approach, *Otsuki* and co-workers[118] synthesised three double-decker complexes of cerium(IV) with porphyrin or phthalocyanine ligands (**73**-**75**, Figure 36a), and subsequently investigated their self-assembly at the 1-phenyloctane/HOPG interface by STM. All three complexes shared a common porphyrin, 5,10,15,20-tetrakis(4-docosyloxyphenyl)porphyrin (C_{22}OPP), bearing long alkoxy chains to ensure the adsorption on HOPG of both heteroleptic complexes (**73** and **75**) and to ensure the formation of robust

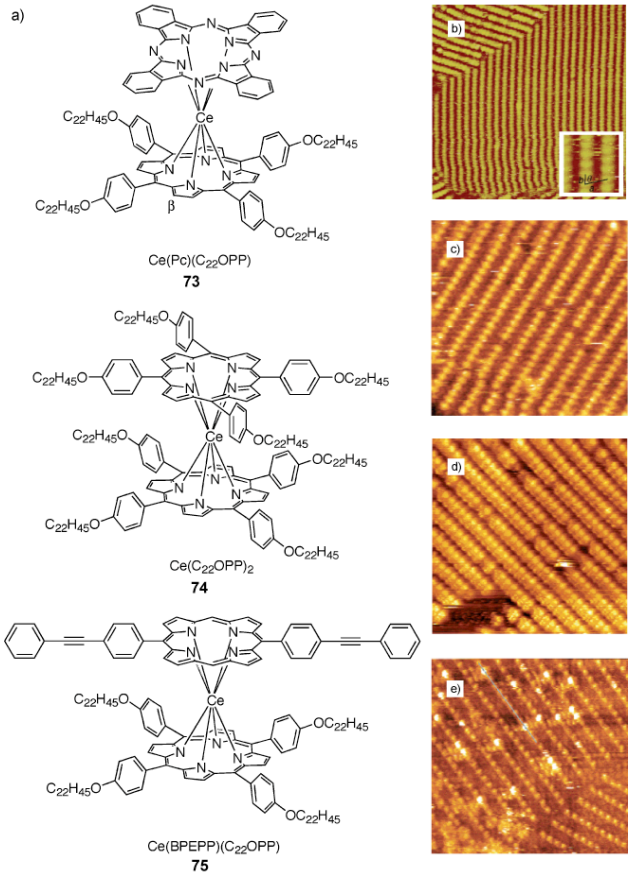

Figure 36. a) Molecular structures of the investigated double-decker porphyrins **73**, **74** and **75**. b) STM images (100 × 100 nm^2) of **73**, c) (50 × 50 nm2) of **74**, d) (50 × 50 nm^2) of **75**, e) STM image (50 × 50 nm^2) of **75** mixed with two eq. of $H_2(C_{22}OPP)$ at the 1-phenyloctane-HOPG interface.[118]

assemblies through close-packed arrays on HOPG. The other macrocycle in complex **73** was phthalocyanine (Pc), in **74** it was $C_{22}OPP$, whereas in **75**, it was 5,15-bis-[4-(phenylethynyl)phenyl]porphyrin (BPEPP). Ordered monolayers of each of the three complexes were observed upon deposition of their solutions onto HOPG. Complex **73** formed rows of bright circular spots corresponding to the Pc moieties, separated by dark rows corresponding to the interdigitated aliphatic chains adsorbed to the surface (Figure 36b). Homoleptic complex **74** formed a similar stripped self-assembly with the bright protrusions having a square shape with the corners likely to correspond to the phenylene groups (Figure 36c). Complex **75** also assembled in rows with the bright protrusions having an elliptical shape representing the BPEPP moiety (Figure 36d). In a final experiment, a mixed solution of **75** and free-base porphyrin $H_2(C_{22}OPP)$ was deposited on the HOPG surface, showing the presence of the double-decker complexes among the free-base porphyrins as bright protrusions (Figure 36e). The height profile of the STM image indicated that the average height of the $H_2(C_{22}OPP)$ molecules was ~0.2 nm, whereas that of molecule **70** was 0.7-0.8 nm. Additionally, it was observed that when complex **70** was flanked by free-base porphyrins,

the shape was no longer elliptical, but isotropic, probably indicating a rotation of the upper macrocycle.

Shimizu and co-workers[119] also investigated the assembly of 3D coordinated porphyrins on HOPG surfaces. Four related porphyrins, bearing long alkoxy chains, were investigated (Figure 37a). Two free-base porphyrins were synthesised, 5,10,15,20-tetrakis(4-octadecyloxyphenyl)porphyrin ($H_2(C_{18}OPP)$, **76**) and tetrakis(4-triacontyloxyphenyl)porphyrin ($H_2(C_{30}OPP)$, **77**), as well as their counterparts possessing a rhodium chloride metal centre coordinating a pyridine molecule, abbreviated as [$Rh(C_{18}OPP)(Cl)(Py)$] (**78**) and [$Rh(C_{30}OPP)(Cl)(Py)$] (**79**). Depositions of **76** and **77** onto HOPG (Figures 37b, c) resulted in the highly ordered self-assembled rows of porphyrin cores (bright) separated by interdigitated alkoxy chains (dark). Only noisy STM images were obtained for the deposition of **78**, although glimpses of the self-assembled structure were observed (Figure 37d). Deposition of **79** did not present such problems, presumably since the presence of longer alkyl chains results in a higher adsorption energy (Figure 37e). A comparison of the average height profiles of the bright protrusions in the assemblies of porphyrins **77** (0.20 ± 0.03 nm) and **79** (0.43 ± 0.04 nm) confirmed that the pyridine molecule was indeed coordinated to the porphyrin central core in the assembly of **74**. Two mixed deposition experiments of **76** with **78**, and **77** with **79** resulted in the assemblies shown in Figures 37f and 37g, displaying a nice contrast of dark spots and bright spots in both cases. Height profile examination confirmed that the dark spots corresponded to the free-base porphyrins in both cases, and the bright spots represented the pyridine coordinated porphyrins, further confirming the successful formation of a three-dimensional assembly.

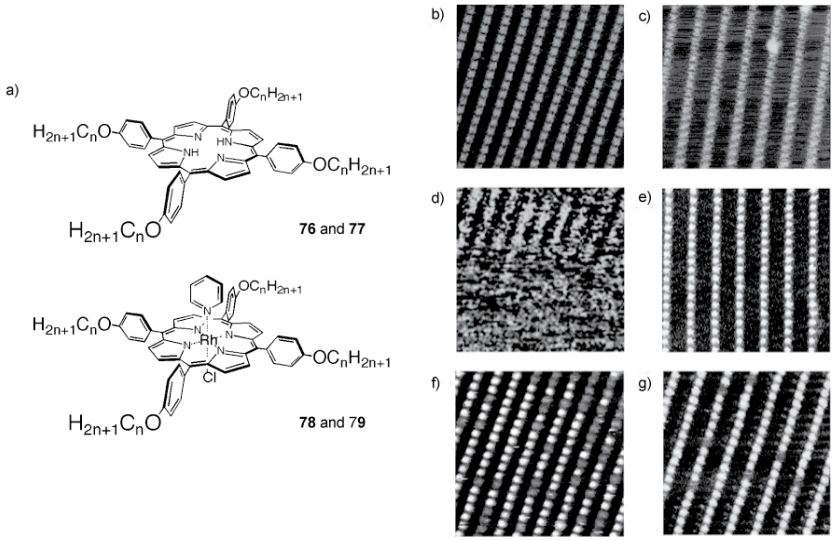

Figure 37. a) Molecular structures of the investigated porphyrins, **76** (n = 18), **77** (n = 30), **78** (n = 18) and **79** (n = 30). b-g) STM images (35 × 35 nm^2) of the monolayers at the liquid-HOPG interface of: b) **76**; c) **77**; d) **78**; e) **79**; f) 1:9 mixture of **76**/**78**; g) 1:9 mixture of **77**/**79**. Solvents: 1-phenyloctane for **76** and **78**, and 1,2-dichlorobenzene for **77** and **79**.[119]

Similar experiments involving the construction of 3D systems under UHV conditions have also been performed. *Lambert* and co-workers, in 2004, reported that zinc tetra-(3,5-di-*tert*-butylphenyl)porphyrin (**80**) deposited onto Ag(100) could be reversibly capped by 1,4-diazabicylco[2.2.2]octane (DABCO, **81**) coordinating to **80** via one of the nitrogen atoms.[120] In subsequent work, the same group have reported the construction of chemically switchable molecular pinwheel using the same porphyrin with 4-methoxypyridine (**82**) as ligand.[121] Upon sublimation of pyridine ligand **82** onto a submonolayer coverage of **80** (at 123K), the four-lobed porphyrin structures became 'doughnut'-shaped (height ≈ 4 Å, diameter ≈ 25 Å, Figure 38b). Heating the assembly to 298K, the system returned to the original state, indicating the selective desorption of ligand **82**. The interesting feature of this assembly is that even though the apparent height of the assembly increased as expected, the height profile bore the same characteristic shape as a bare porphyrin molecule. Figure 38c shows a comparison of the height profiles of bare **80**, **80** with DABCO coordinated and with 4-methoxypyridine. There is a clear difference between the profiles of the two coordinated porphyrins. Tetrapyrrolic module **80** in the presence of DABCO appeared as a circular bright protrusion (Figure 38c) indicating that the DABCO coordinated to the upper face of **80**. In contrast, molecule **80** in the presence of **82** displayed a distinct central depression (Figure

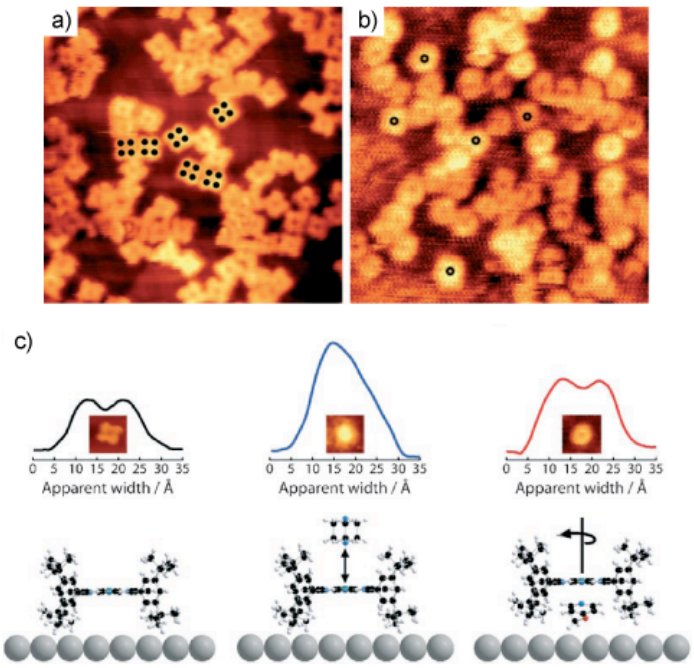

Figure 38. a, b) STM images (20 × 20 nm^2) showing a submonolayer coverage of **80** adsorbed on Ag(100): a) before and b) after the addition of 4-methoxypyridine on **82**. c) Height profiles and structural scheme for: (left) bare **80** on Ag(100); (middle) the effect of capping **80** with DABCO, **81**; (right) the effect of inserting the 4-methoxypyridine "axle".[120]

38c), therefore it is unlikely that the pyridyl ligand is coordinated to the upper face of the porphyrin macrocycle. Consequently, the authors concluded that ligand **82** is located beneath the porphyrin macrocycle acting as a tether, coordinating to the Ag surface with the oxygen atom, and to the Zn-porphyrin with the aromatic nitrogen atom. This would enable the lifting of the porphyrin by ~1 Å, weakening its interaction with the surface, consequently allowing the macrocycle to rotate, resulting in the time-averaged 'doughnut'-shaped protrusion observed in the STM image, resembling a molecular pinwheel device with ligand **82** acting as a pivotal axis (bottom right of Figure 38c).

Further works utilise coordinative interactions to metalloporphyrins in the third dimension to introduce other types of functionality such as catalysis. An example of such work was reported by *Itaya* and coworkers,[122] where highly organised adlayers of Co(II) tetra-meso-phenylporphyrin (**83**) were prepared on Au(111) electrode surfaces. In a study of the electrocatalytic activity for O_2 reduction to H_2O_2, it was found that Au electrodes with adsorbed monolayers of porphyrin **83** were able to enhance the reduction process in comparison to bare Au electrodes. Cyclic voltammograms (CVs) for the reduction process using both types of electrodes were obtained in 0.1 M $HClO_4$ solution saturated with O_2. Bare Au(111) electrode (top, Figure 39) showed that the O_2-centered cathodic current started at approximately 0.55 V and gradually increased until -0.1 V. In contrast, the CV of the electrode bearing the monolayer of **83** (bottom, Figure 39) showed that the O_2-centered cathodic current started at around 0.55 V during the scan and gave a clear electrocatalytic reduction peak for O_2 at 0.32 V, which after 0.3 V remained quite constant as the process was limited by the gas diffusion. The enhancement of current intensity at 0.32 V demonstrated that the self-assembled metalloporphyrin-based monolayer was catalysing the reduction of O_2 to H_2O_2.

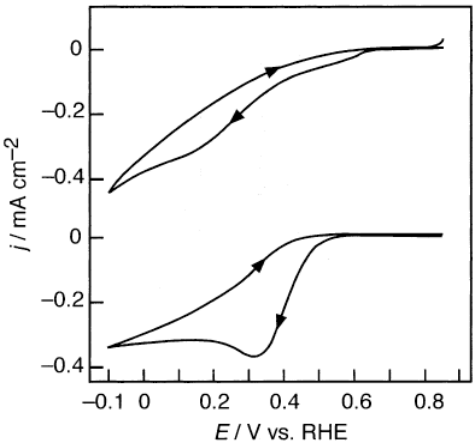

Figure 39. Cyclic voltammograms for the O_2 reduction at the bare Au(111) electrode (top) and the electrode with **78** adsorbed (bottom). The CVs were performed in 0.1 M $HClO_4$ saturated with O_2 with potential scan rate of 50 mV s^{-1}.[122]

In a more recent work published by *Itaya* and co-workers,[123] adlayers of Co(II) 5,10,15,20-tetrakis(α,α,α,α-2-pivalamidophenyl)porphyrin (**84**, Figure 40a) were prepared on Au electrodes. This porphyrin, nicknamed as 'picket-fence' porphyrin, is particularly interesting as its O_2 binding affinity is higher than that of native myoglobin.[124, 125] Adlayers of **84** were prepared on both Au(111) and Au(100)-(hex) surfaces. Nanobelt arrays were formed in both cases (an example is shown in Figure 40b). However, when the deposition of O2-adducted **84** molecules was attempted, nanobelt arrays were only formed on the Au(100)-(hex) surface. No ordered arrays were observed on Au(111), thus signifying that the adlayer formation is dependant on the crystallographic orientation of Au. It is suggested that underlying Au atoms can act as axial ligands assisting the formation of O_2-adducted **84** molecules. Nonetheless, on both surfaces, a mixture of bright and dark spots corresponding to porphyrin macrocycles was observed in the STM images (an example is shown in Figure 40c). The bright spots are attributed to the O_2-adducted **84** molecules. Time-dependent STM images showed that the coordinated oxygen molecules were highly mobile, having the ability to move from one 'picket-fence' to another. Further investigation of the system showed that potential manipulations enabled the electrocatalytic reduction of the oxygen molecules in the cavities of **84** molecules. Moreover, small stepwise negative shifts in the potential (0.80 V,

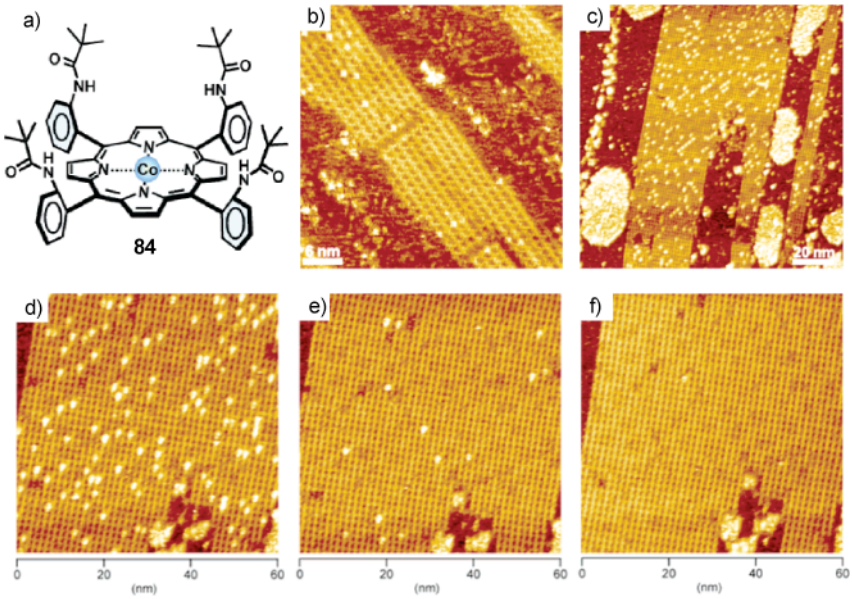

Figure 40. a) Structure of 'picket-fence' porphyrin **84**. STM images of the nanobelt arrays formed b) (40 × 40 nm^2) by **84** on Au(111), c) (125 × 125 nm^2) by **84** on Au(100)-(hex) at 0.8 V vs RHE in 0.1M $HClO_4$, after immersion in an O_2 saturated solution. The bright spots indicate porphyrins with axially complexed O_2 molecules. d-f) Potential dependent STM images (60 × 60 nm^2) of the array shown in c) at d) 0.78 V; e) 0.73 V and f) 0.68 V vs RHE in 0.1M $HClO_4$, showing a gradual reduction in coordinated O_2 molecules.[123]

0.78 V, 0.73 V and 0.68 V, Figures 40d-f) led to the gradual reduction in coordinated oxygen molecules in the nanobelt array assembled on Au(100)-(hex), until at 0.65 V no more bright spots were observed in the STM images, thus indicating that all the O_2 had been released into solution. This final experiment indicates that the described system could function as a nanoscale oxygen storage device.

Oxidative catalytic activities have also been achieved using the axial coordination capacity of metalloporphyrins adsorbed as monolayers on surfaces. *Hulsken et al*.[126] were able to monitor the oxidation process of stilbene molecules in real time using STM at the liquid-solid interface. A Mn(III)-porphyrin was used in this study (**85**, Figure 41a) as these metalloporphyrins are known to catalyse the oxidation of alkenes to epoxides.[127] Self-assembly of **85** was initially investigated at the *n*-tetradecane/Au(111) interface under an Ar atmosphere. A regular patterned monolayer resulted, in which the porphyrin units adsorb face-on to the surface (Figure 41b). The introduction of O_2 into the system led to the appearance of brighter spots, mainly in pairs, which corresponded to O_2-coordinated porphyrin **85** (Figure 43c). This pairing is explicable as follows: O_2-Mn binding requires the metal's reduction, which in this case is thought to involve the Au substrate that coordinates to **85** axially allowing a chlorine radical to dissociate, reducing Mn(III) to Mn(II). Molecular O_2 then binds and reacts with the Mn(II) causing homolytic dissociation of O_2 to form two mono-oxygen-coordinated species, one of which coordinates to the closest adjacent **85** molecule. This results in a pair of reactive Mn(IV)=O species which can subsequently act as heterogeneous catalysts for the epoxidation reaction. The cycle is summarized in Figure 43d. The epoxidation reaction using cis-stilbene was followed in real time and space by STM. Starting from a monolayer prepared under Ar, the number of oxidised **85** molecules in a fixed area of the surface were counted. O_2 molecules were then introduced to the system, causing an increase in the number of oxidised **85** molecules. Next, cis-stilbene was introduced, causing a significant drop in the number of oxidised **85** molecules. Gas chromatography analysis of the solution in the STM liquid-cell confirmed the presence of both cis-stilbene oxide and trans-stilbene oxide signifying that the surface catalytic device was functional. The monolayer was monitored for several days during which the number of oxidised **85** molecules remained constant following the reaction, demonstrating that the surface-bound catalysts were stable and also possess the potential for long-lasting activity.

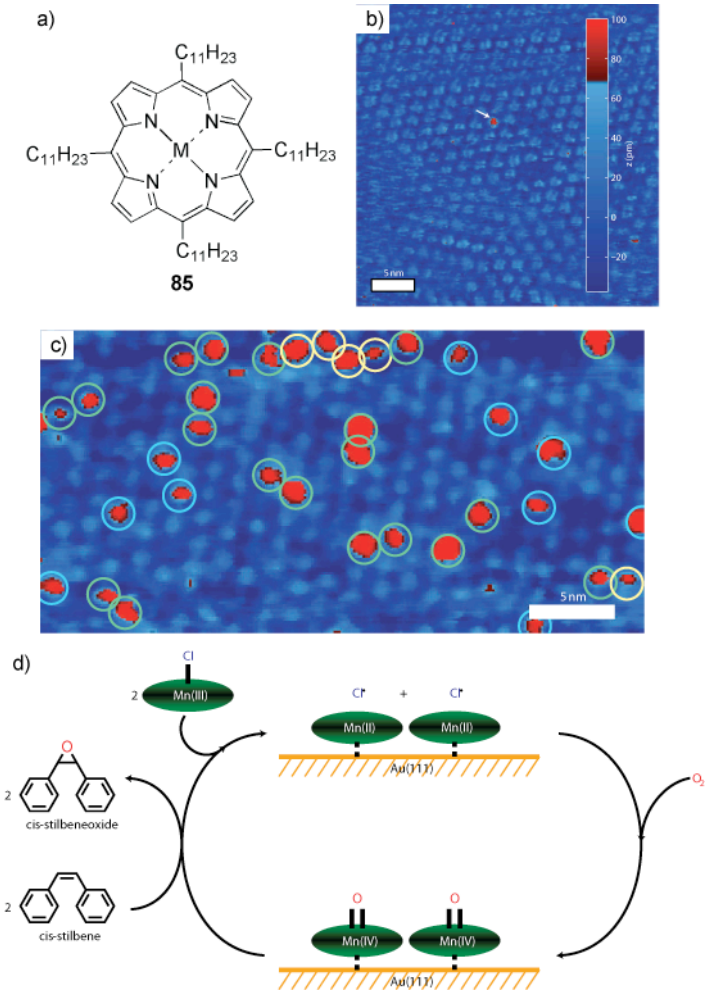

Figure 41. a) Molecular structure of porphyrin **85**, M = MnCl. b) STM image of a monolayer of **85** self-assembled at an interface of Au(111) and an argon-saturated *n*-tetradecane liquid phase. c) STM image of a monolayer of **85** self-assembled 4h after the introduction of O_2. The overall population of bright spots corresponding to **85** with complexed O_2 is approximately 8%. d) Proposed catalytic cycle of the epoxidation reaction.[126]

1.4 THE BIOMIMETIC APPROACH

The formation of porous networks on surfaces can also be achieved using a biomimetic approach. Biomolecules such as DNA can be exploited in material science due to their selective recognition ability. Section 1.4.1. discusses the self-assembly of DNA oligomers on surfaces in 2D and also 3D assemblies. Section 1.4.2. introduces Peptide Nucleic Acids (PNAs) and discusses the work that has been done using these DNA mimics on surfaces.

1.4.1 DNA

Another approach to the formation of porous networks on surfaces is to use a biomimetic strategy.[128, 129] In this case, biomimetic oligomers are exploited for their

recognition properties to prepare supramolecular architectures. The use of DNA for the self-assembly of 2D crystals on surfaces stems from the seminal work of *Winfree* and coworkers.[130] They recognised that the specificity of the H-bonding interactions of DNA's Watson-Crick complementary base pairs[131] would be suitable for the construction of nanostructures via self-assembly, hence 'Structural DNA Nanotechnology'[129] was born. In their work, striped lattices were produced on mica surfaces and were imaged by atomic force microscopy (AFM). In order to construct the lattices, either two or four individual DNA units ('tiles') bearing sticky ends were used in the self-assembly. The tiles were composed of either three or four strands of DNA, each one carefully sequenced in order to form the desired 'tile' upon self-assembly in solution. Furthermore, the DNA sequences allowed for the protrusion of short single-stranded DNA strands from the 'tile', thus providing the so-called complementary 'sticky ends', required for the self-assembly of the 'tiles' on the mica surface to form the nanoscale lattices. During the years following their work, the field of structural DNA nanotechnology grew, and by developing their ideas, more complex nanostructures were constructed,[129] and also the level of control which could be achieved was clearly demonstrated by *Rothemund* in his article about DNA origami.[132] The developments also led to formation of 2D porous networks, and, below, several recent examples are reported.

Liu et al. have described finite-size DNA arrays wherein the boundaries, and as a consequence the size of the array, can be defined and controlled.[133] They constructed two types of networks using two different DNA 'tiles' bearing different symmetries, C_2 and C_4. Since both assemblies are similarly constructed, only the former will be discussed here. A 5×5 tile array was constructed using a total 25 DNA tiles bearing C_2 symmetry (Figure 42). Only 13 unique tiles were required to form the assembly since several tiles could be used in multiple positions in the array. Each tile was 16.9×14.2 nm^2 and consisted of 8 DNA helices

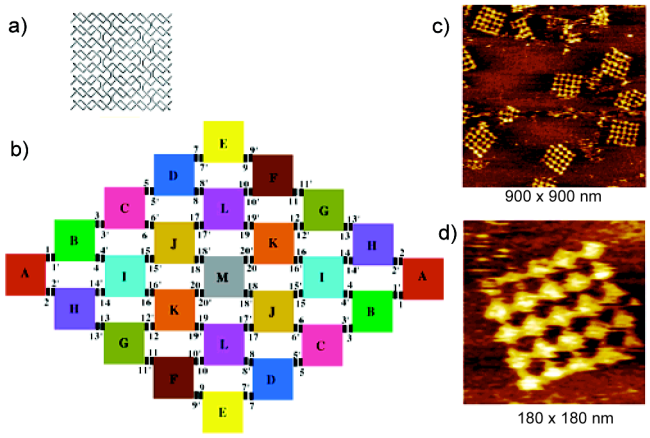

Figure 42. a) The 8-helix tile showing the crossover points; b) the array design utilising 13 unique tiles (each bearing different sticky ends) to form the 5×5 array in a predictable and controllable manner; c,d) AFM images of the 25 tile array.[133]

joined together in a plane with two crossovers to connect to the adjacent helices (Figure 42a). The same core strand sequences were used in all the 13 unique tiles; the only differences in the tiles were the sequences of the sticky ends emerging from the helical axis of the tiles. These were required for the specific inter-tile H-bonding interactions *i.e.*, they acted as the pre-programmed instructions required for the self-assembly of the finite array. The arrays were constructed in a stepwise manner. The individual tiles were formed by cooling a stoichiometric mixture of the component DNA strands from 90 ºC to 40 ºC. The 13 tiles were then mixed in the correct proportions at 40 ºC and, upon cooling the solution to 10 ºC, the arrays were formed. A sample of the solution was deposited onto a mica surface and was imaged by Atomic Force Microscopy (AFM) (Figure 42c, 42d). The total size of the array was 110×110 nm^2.

Park et al.[134] compared two methods to construct finite-size DNA arrays: MD (minimal depth) – a one step assembly method, similar to the one used by *Liu et al.,* that required that every tile was unique and MSS (minimal sequence set) – a stepwise hierarchical assembly technique which required less unique tiles. The cross-shaped tiles were identical in sequence at the core of the tile, but differed in the sequences of the five base pairs that formed the sticky ends. The individual tiles were formed by mixing the appropriate DNA strands, annealing to 95 °C and cooling slowly to 20 °C. The DNA nanoarrays were then formed by

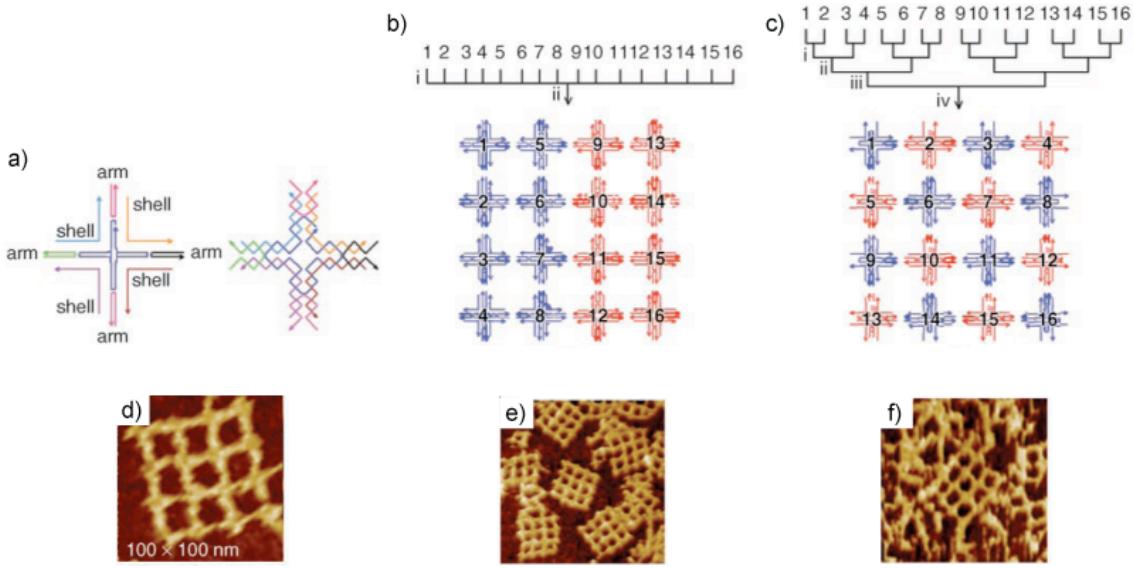

Figure 43. a) Schematic drawings of the cross tiles with DNA strand names marked (arm, shell, and loop). b) MD strategy. A converging-stream diagram of the two-step assembly that starts with 16 tubes with one tile each (i), which goes directly to one tube of 16 tiles (ii), resulting in the sixteen tile array. c) MSS strategy. A converging-stream diagram of the four-step assembly process starting with eight tubes of two tiles each (i) and concluding with one tube containing all 16 tiles (iv). d) AFM image (100 x 100 nm) showing a zoom in of a complete 4 x 4 tile DNA nanoarray. e,f) AFM images (300 x 300 nm and 200 x 200 nm respectively) showing the contrast of the results obtained via the MD strategy and the MSS strategy. The MD strategy produced higher yields of the properly assembled target structures and fewer partially assembled "waste" products.[134]

mixing the tiles in the appropriate manner depending on the MD and MSS strategies, annealing to 43 °C (to break the hydrogen bonding of the sticky ends only), and cooling to 20 °C. The MD strategy involved mixing the contents of 16 tubes with one tile each (Figure 43b, i) in one step resulting in one tube containing all 16 tiles (Figure 43b, ii). The MSS strategy began with eight test tubes containing two complementary tiles each (Figure 43c, i), then it proceeded to four tubes of four tiles (Figure 43c, ii), two tubes of eight tiles (Figure 43c, iii), and finally one tube containing all 16 tiles (Figure 43c, iv). The DNA nanoarrays were then investigated by AFM imaging in both cases. The images obtained revealed that both strategies produced the target assembly, however, the MD strategy produced higher yields of the properly assembled target structures and fewer partially assembled "waste" products (Figures 43e,f).

In contrast to the above examples, *Mao* and co-workers have used DNA to construct non-finite 2D porous networks that can form extended arrays with domains as large as 1mm in length.[135] The individual units used to form the networks resembled a three-point star and were made up of seven DNA single strands (Figure 44a). At the apices of the three-point star, palindromic sequences were used as the sticky ends. This was done to ensure that the H-bonding interactions between the units in all directions would have equal strengths. The DNA strands were mixed in the appropriate proportions in a tris-acetic-EDTA-Mg^{2+} buffer and were cooled stepwise from 90 ºC to 4 ºC. Following the deposition of the buffer solution onto a mica surface, it was observed by AFM investigation that extended, highly ordered, hexagonal 2D crystalline arrays had resulted (Figure 44b, 44c). The diameter of the pores observed was of 29.9 ± 0.1 nm.

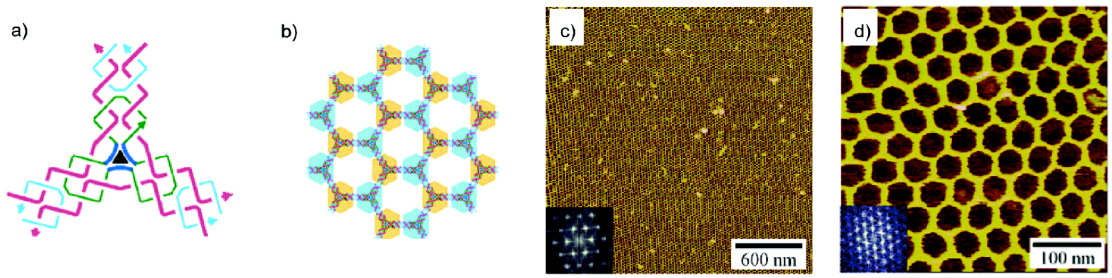

Figure 44. a) The three point star motif made up of seven DNA single strands; b) Model of the 2D array formed by the assembly of the individual tiles; c,d) AFM images of the self-assembly showing the hexagonal porous network on a mica surface.[135]

As an extension of the previous work, *Mao* and co-workers[136] developed a strategy for *in situ* DNA self-assembly on solid surfaces using the same three point star motif (Figure 44a). Since DNA assemblies are delicate and fragile, they tend to deform or break into small pieces due to the shear forces that occur during the transfer from the solution to the surface, therefore, it was desirable to directly perform DNA self-assembly on the solid surfaces. The

strategy involved the assembly of the individual tiles by cooling the single stranded DNA strands from 95 to 60 °C in solution and then assembling the tiles into the 2D array directly on the mica surfaces by incubating at 50 °C for 16 h (Figure 45a). The critical temperatures in this two step assembly process were 60 °C and 50 °C. Cooling to 60 °C in solution was important because it was low enough to allow the formation of the individual tiles but it was too high to prevent further assembling into the large 2D arrays. At 50 °C, it was observed that no appreciable inter-tile 2D arrays formed in solution, however, on the solid mica surface, the surface stabilization of DNA tiles resulted in nuclei that initiated further DNA tile assemble on surface. Consequently, large 2D arrays formed, covering the entire surface (Figure 45b) resulting in a similar assembly as shown in Figures 44c and 44d.

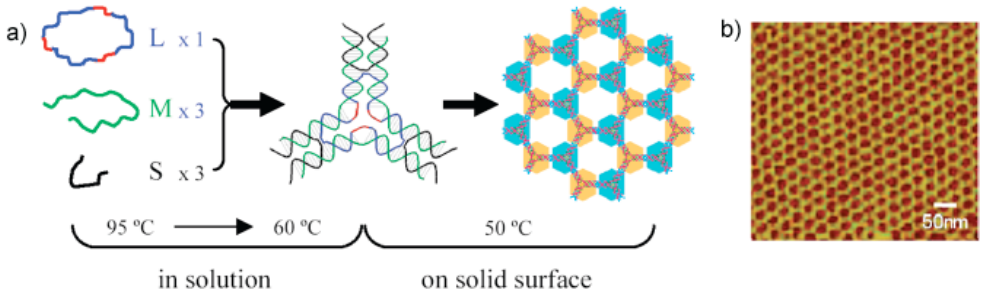

Figure 45. a) Schematic representation of the assembly of the 2D array in two steps. First the individual tiles are formed in bulk solution from 95 to 60 °C, and then the large 2D crystals are assembled on solid surfaces. The 3-point-star tile contains seven DNA strands: a long DNA strand (L), three identical medium length strands (M), and three identical short peripheral strands (S). b) AFM images of the self-assembly of DNA showing the porous network on a mica surface.[136]

Similar to the results obtained by *Mao* and coworkers in the above examples, non-finite porous networks on surfaces have also been observed by varying the DNA tile to a 4-point star,[137] 5-point star[138] and 6-point star.[139] Extending the work from these 1-tile non-finite porous networks is the recent report from *Seeman* and coworkers[140] in which two double-layer DNA-origami tiles with two orthogonal domains underwent self-assembly into well-ordered two-dimensional DNA arrays (up to 10 μm in diameter). In this work, two complementary tiles were prepared, with each one consisting of two helix axes that propagated in two independent directions perpendicular to each other (Figure 46a). The dimensions of each tile was approximately 100 x 100 nm^2 (Figure 46b). The key feature of this system was that there were two domains to each tile, one in a plane above the other. Bringing the two tiles together, the two layers of each tile have opposite orientations relative to the tile plane, thus each tile interacts with the adjacent one oriented at 90° with respect to each other so that the top layer of one tile was bonded to the bottom layer of the next. The resultant alternating self-assembly has the appearance of a braided pattern (Figure 46c,d). The

annealing temperature required for the formation of the desired self-assembly was 53 °C. Lower temperatures resulted in aggregates of the tiles and higher temperatures damaged the tiles preventing the self-assembly from forming.

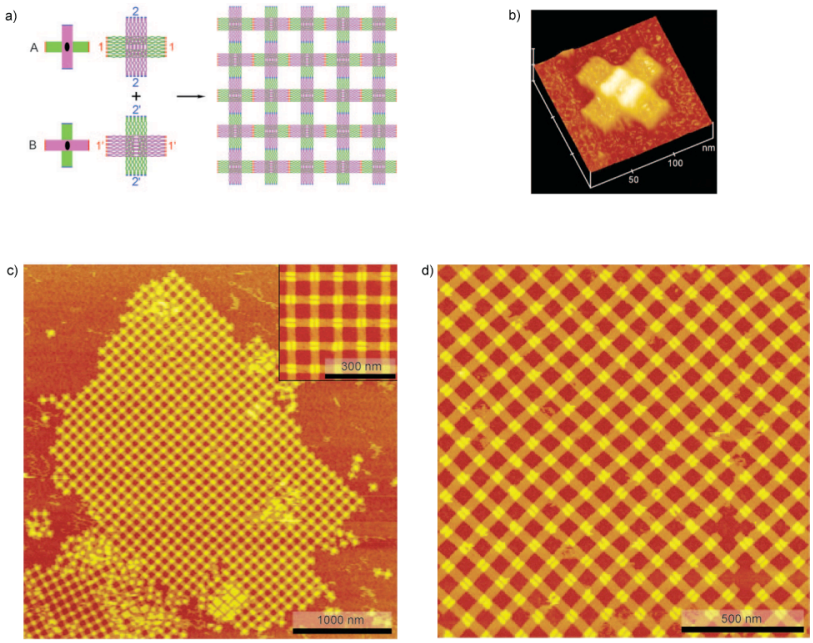

Figure 46. a) Schematic structure of the tiles (A and B), showing their two-fold axes, with the purple rectangular domain lies above the green rectangular domain in both tiles. Apart from the sticky ends, both tiles are identical. When the tiles are brought together, the self-assembly results in the woven pattern shown on the right. b) AFM image of an individual tile. c,d) AFM images of the self-assembled porous network formed by the two tiles on a mica surface upon annealing at 53 °C.[140]

Moving away from the crossover junctions used in the above examples, *Hamada and Murata*[141] demonstrated that the assembly of a variety of structures on surfaces (1D ladders, 2D porous networks and polar coordinated wheels) was possible using single-duplex-based T-shaped junction tiles. This was the first report to introduce T-junctions (Figure 47a) into the field of DNA nanotechnology. Unlike the more commonly used crossover junction, the T-junction is right-angled providing the possibility of preparing a larger variety of DNA nanostructures. Also, it a more rigid junction, therefore the resultant assemblies have lattices with higher stabilities. Furthermore, the individual tiles can be of a smaller size, therefore, the resultant assemblies can have a higher resolution *i.e.* smaller unit cells and thus greater nanoscopic detail. Figures 47b-e show two types of 2D self-assembled DNA arrays that were observed upon the mica-assisted self-assembly of two types of tiles with T-junctions.

Supramolecular self-assemblies on surfaces using DNA are not limited to two-dimensional networks only. Recent work has shown that features in the third dimension can

be introduced into the two-dimensional arrays, and also that three-dimensional DNA nanoarchitectures can be deposited onto surfaces. These works demonstrate the versatility and complexity of the biomimetic strategy. Selected examples of these works are described below.

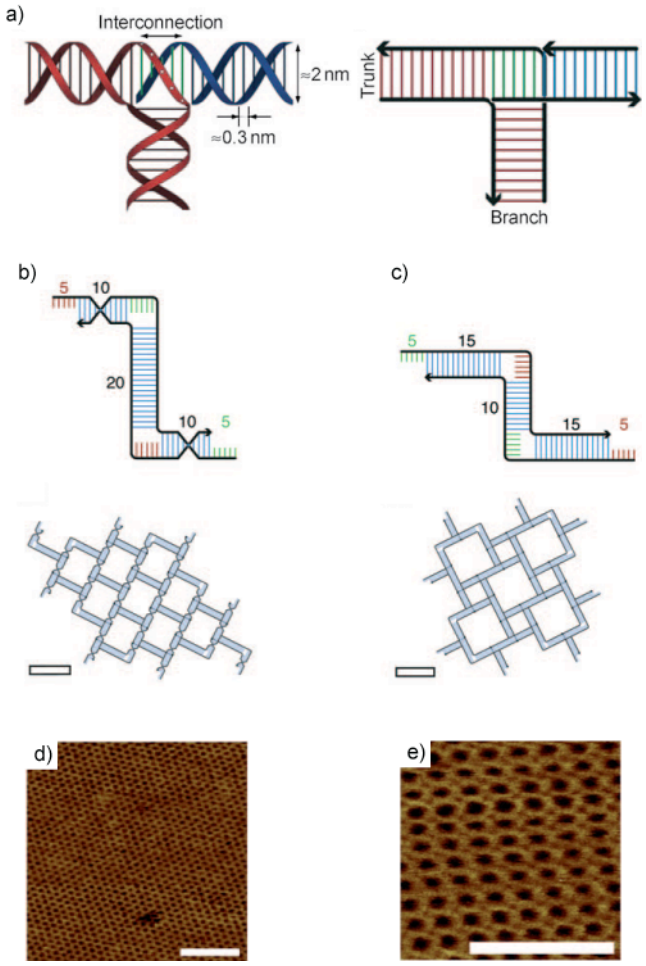

Figure 47. a) Helical and schematic representations of the single-duplex-based T-shaped junction. b) Schematic representation of the T-shaped junction tile used to form the 2D brick-wall lattice and the model of the self-assembled structure following annealing and cooling. c) Schematic representation of the T-shaped junction tile used to form the 2D windmill lattice and the model of the self-assembled structure following annealing and cooling. d,e) AFM images (scale bar = 100 nm) of the self-assembled structure on mica surfaces.[141]

Self-assembled 2D DNA lattices have recently been used to organise gold nanoparticles into periodic patterns. *Kiehl* and co-workers[142] organised 6 nm gold nanoparticles functionalised with multiple T_{15} sequences into periodic striped patterns by *in situ* hybridization to a preassembled DNA lattice on a surface. Extending this work, *Yan* and co-workers[143] used a DNA nanogrid to organise gold nanoparticles into a periodic square-like configuration. First, two complementary cross-shaped DNA tiles (A and B) were

assembled in solution. The A tile was modified to include a hybridization site, *i.e.* an A_{15} sequence protruding perpendicular to the tile surface. The two tiles were then allowed to self-assemble into a nanogrid in solution that was subsequently deposited onto a mica surface. Gold nanoparticles functionalised with T_{15} sequences were then added to the surface resulting in their binding to the hybridization sites on the DNA nanogrids. Figure 48 summarizes this process, and also shows the AFM images of the nanogrid without and with the hybridized gold nanoparticles. The distance between neighbouring gold nanoparticles was found to be 38 ± 1 nm as expected.

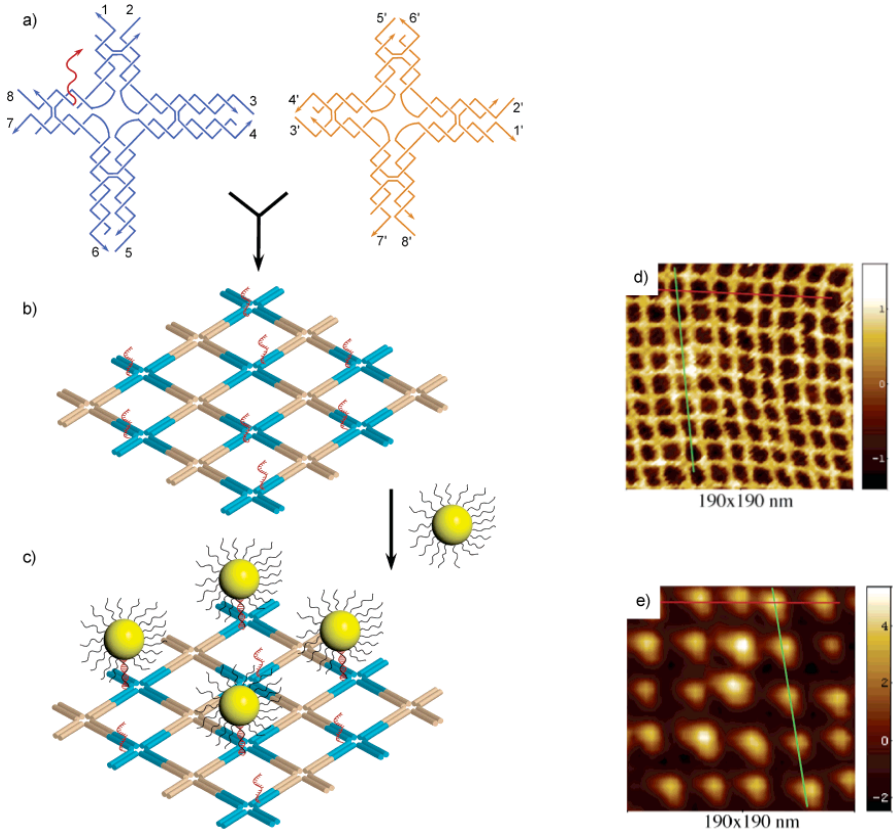

Figure 48. a) The two cross-shaped tiles used for the self-assembly, A (left) and B (right). Tile A bears an A_{15} hybridization sequence shown in red protruding perpendicular to the plane of the tile. b) The 2D DNA nanogrid showing the positions of the hybridization strands (red) pointing out of the plane. c) Assembly of the gold nanoparticles functionalised with T_{15} sequences (black) on the DNA grids at the hybridization sites. d) AFM image showing the 2D DNA nanogrid formed following the self-assembly of the two tiles. e) AFM image showing the gold nanoparticles periodically assembled on the DNA grid.[143]

Moving to the construction of three-dimensional architectures, the same research group were able to assemble 3D DNA tubules through the effect imposed by the integration of gold nanoparticles.[144] Four double-crossover tiles (Figure 49a) were used in the study, with the first tile modified in its central strand to include a thiol group, which was used to covalently attach a gold nanoparticle. The self-assembly of the tiles resulted in a 2D array

with the gold nanoparticles adjacent to each other resulting in parallel rows of nanoparticles with a periodicity of ~64 nm (Figure 49b). The strong electrostatic and steric repulsion due to the close proximity of the nanoparticles in the 2D array resulted in the curvature of the array to avoid direct contact between the particles. The curling of the array resulted in tubules in which the nanoparticles were organised as stacked rings, single spirals, double spirals or nested spirals (Figures 49c,d) depending on how the edge tiles associated with corresponding edge tiles at the opposite side of the array (Figures 49c,d). A stacked ring structure resulted when the array curled into a tube without any offset. When the corresponding edge tiles that associate were offset at neighbouring lines, tubes displaying a spiral of nanoparticles resulted. A single spiral was the outcome of an offset of one line, a double spiral resulted with an offset of two lines and nested spirals were created when the offset was greater than three lines. All varieties of tubules were observed, however the stacked rings and single spirals were the most common. Furthermore, depending on the size of gold nanoparticles attached to the DNA array, the type of tubules formed could be controlled.

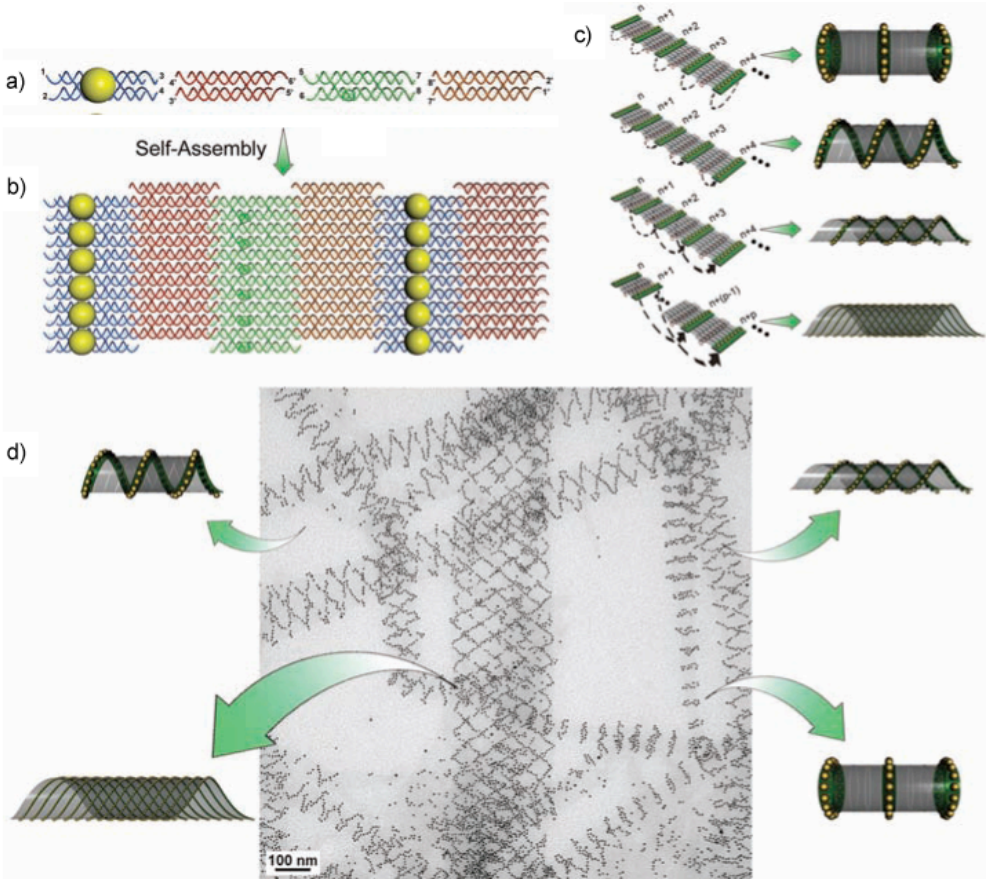

Figure 49. a) The design of the double-crossover tile system. The position of the gold nanoparticle on top of the first tile is shown. b) The 2D array formed upon self-assembly of the four tiles is shown. The parallel rows of gold nanoparticles are clearly displayed. c) The four possible ways for the corresponding edge tiles on opposite sides of the 2D array to associate and lead to the formation of tubes displaying patterns of gold nanoparticles in stacked rings or spirals. d) TEM image of all four types of tubules.[144]

Another type of 3D architecture is the metal-DNA cage reported by *Yang et al*.[145] The preparation of the cages was a stepwise process (Figure 50). First six DNA strands incorporating two bis-2,9-diphenyl-1,10-phenanthroline (dpp) ligands were synthesized. Next, two triangular faces (T1 and T2) were prepared using three of the DNA strands in each triangle. This brought the dpp ligands in close proximity for metal coordination. The two triangular faces were then brought together into a DNA prismatic cage (TP-S) by hybridization with three linking DNA strands. The area of the linking strands that remained single-stranded were hydridized again with complementary strands to rigidify the DNA triangular prism (TP). The coordination of various metals in the TP cage was explored, and it was found that it was an excellent coordination environment for Cu^{+}, Ag^{+}, Zn^{2+}, Co^{2+}, Cd^{2+}, Au^{2+} and Eu^{2+}, which were all incorporated stoichiometrically. The metallation was found to stabilise the TP cages towards chemical and thermal denaturation. Although not reported, the authors conclude that the cages could be used to host guests and that the presence of the transition metals in close proximity to the guests could be exploited for redox, photoactivity, magnetic and catalytic properties.

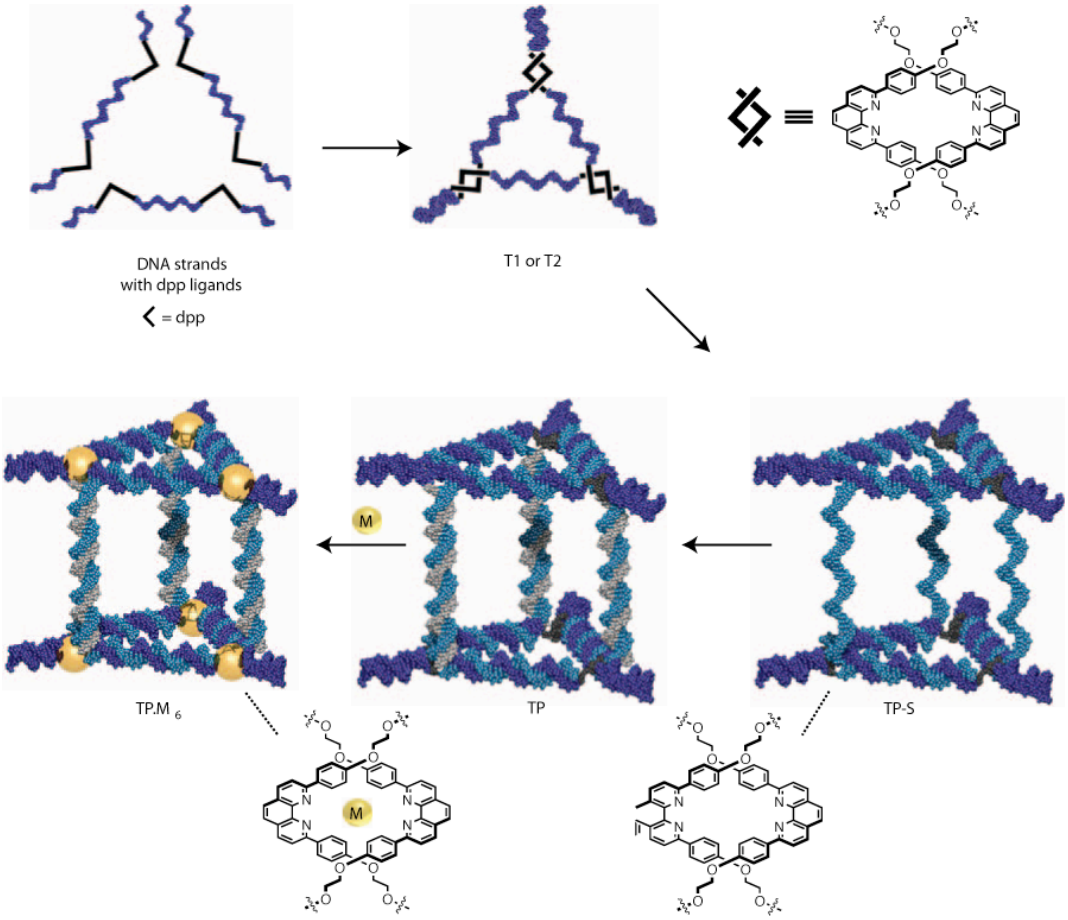

Figure 50. Schematic representation of the stepwise construction of the three-dimensional DNA prism TP and the subsequent site-specific metallation.[145]

Demonstrating an even higher level of complexity and control than the above examples, *Andersen et al.* reported the self-assembly of a nanoscale DNA box with a controllable lid.[146] The construction of the DNA box was done using a single-stranded DNA genome of the M13 bacteriophage, which was folded to form six interconnected DNA origami sheets. Subsequently, the cuboid was obtained upon the introduction of staple strands that bridged the edges of the box. AFM images (Figures 51b-d) show the interconnected DNA sheets, the closed box and the open box respectively. The open box was obtained by omitting the staple strands of three edges. Next, the authors investigated the opening of the lid of the DNA box in solution. They incorporated two fluorescent dyes in close proximity on the box (Figure 51e), which displayed efficient fluorescence resonance energy transfer (FRET) in the closed state (~0.22). Moreover, the lid was functionalized with two lock-key systems,

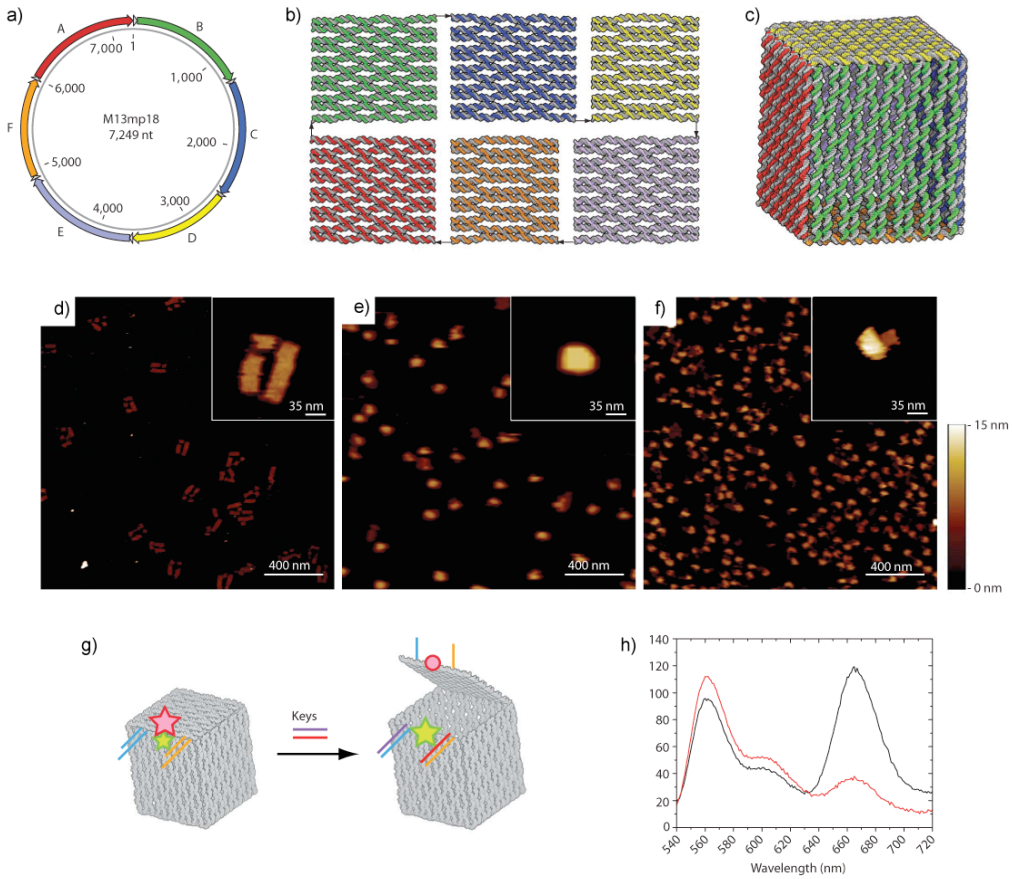

Figure 51. a) The circular, single-stranded DNA genome of the M13 bacteriophage with regions used to fold the six DNA sheets shown as coloured arrows. b,c) Molecular models of the six DNA sheets in the flat and cubic structures, respectively. d-f) AFM images displaying the six DNA sheets folded to form (d) the flat structure, (e) the closed box and (f) the box with the open lid. g) Schematic representation of the controlled opening of the box lid. The fluorescent dyes are represented by the green and red stars. Loss of emission of the dye is represented by a circle. The lock-key systems are denoted by the blue and orange lines. Upon adding the keys (shown in violet and red), duplex displacement occurs allowing the box to open. h) Ensemble FRET measurements of the closed box before (black curve) and 35 min after (red curve) the addition of the keys.[146]

which consisted of DNA duplexes holding the lid closed. The two DNA duplexes bore sticky ends to provide a 'toehold' for hydridization with external 'key' oligonucleotides. Upon addition of the appropriate 'key' oligonucleotides, they hydrogen bonded to the 'toehold' to form a duplex with on of the strands of the 'lock', consequently denaturing the original 'lock' duplex and resulting in the opening of the lid. The opening was monitored by the reduction of the FRET efficiency due to the increased distance between the two dyes. The FRET efficiency decreased by 90% to ~0.02. A kinetic study of the opening process showed that the FRET signal decreased biexponentially, with an initial fast decay time of 40 seconds upon key addition.

1.4.2 Peptide Nucleic Acids (PNAs)

PNA was first described by *Nielsen et al.* in 1991.[147] It is a DNA analogue in which the phosphate backbone is replaced by *N*-(2-aminoethyl)glycine units. The structure of PNA in comparison to that of DNA is shown in Figure 52. The properties of this recently discovered class of molecules are quite remarkable. As reported by *Hyrup* and *Nielsen*,[148] PNA has several advantages over DNA: (*i*) PNA oligomers can be synthesized using established techniques from peptide chemistry i.e. solid phase peptide synthesis; (*ii*) organic moieties can be covalently attached to the C-terminal carboxylic acid group or the N-terminal amino group of the oligomer; (*iii*) PNA is achiral, so all enantiomeric purity problems are avoided; (*iv*) the PNA peptidic backbone is neutral compared to DNA's negatively charged sugar-phosphate backbone, therefore, no electrostatic repulsion exists when PNA hybridizes with another PNA or DNA oligomer; and (*v*) due to the lack of electrostatic repulsion, PNA-PNA duplexes have a higher thermal stability relative to DNA-PNA and DNA-DNA duplexes *e.g.* PNA decamers containing all four nucleobases form duplexes with very high thermal stability: PNA-PNA T_m = 67 °C; PNA-DNA T_m = 51 °C; DNA-DNA T_m = 33.5°C for identical decamer sequences.[149] Furthermore, PNAs have a high biostability, since they are not degraded by nucleases nor proteases,[150] and also are chemically resistant to strong acids and weak bases.[151] These properties make them an appealing candidate for a number of applications, including material science.

PNA has mainly been used for biological applications[148, 151, 152] such as diagnostics, biotechnology and pharmaceuticals. PNA oligomers have been exploited as bio-drugs to inhibit translation (antisense agents),[153-155] transcription and replication (antigene agents),[153, 156] and ribonucleoprotein interactions (inhibitors of enzymes such as telomerase).[157-159] Although the results with PNA in cell-free systems were encouraging, their poor cellular uptake is the main obstacle for their effective therapeutic use.[160] PNA is also used as a molecular probe for diagnostics and detection[161-172] because of the high sensitivity of PNA to

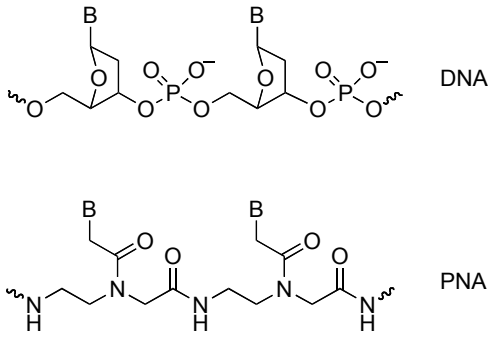

Figure 52. A comparison of the structures of DNA and PNA. 'B' represents the nucleobases (adenine, thymine, cytosine and guanine).

a single mismatch, the high duplex stability, and also the ability to cause strand invasions in double-stranded DNA. Thus, using PNA *vis-à-vis* DNA as a molecular probe gives more specific, more sensitive, and more accurate results for the detection of target sequences. Further *in vitro* applications of PNA oligomers includes their use as molecular tools in PCR clamping,[173-178] modulation of enzymatic cleavages,[179-182] and sequence-specific purification of nucleic acids[183-186] for use in molecular biology and functional genomics.

Apart from the biological applications, PNA has also been introduced very recently into the field of supramolecular chemistry.[187] *Janssen et al.* utilised a single-stranded oligothymine PNA decamer to template the assembly of an oligo-(*p*-phenylenevinylene) diaminotriazine derivatives in solution. Nanostructure helices were obtained in which the size was controlled by the PNA template. AFM analysis of the structures drop-casted onto an HOPG surface confirmed uniform small particles with a height of 3-4 nm were obtained.

To date, no reports of 2D self-organised nanoporous architectures on surfaces utilising PNA-mediated interactions have been published. However, self-assembled monolayers (SAMs) of PNA have been prepared by covalent attachment of modified PNA oligomers to various surfaces (*e.g.* gold, pyrite, glass) with the intention of preparing microarray biosensors.[188-194] In the most recent example, *Calabretta et al.*[194] reported the patterning of PNA on glass surfaces using reactive microcontact printing. Glass surfaces were modified with aldehyde functional groups, and the PNA oligomers were functionalised with an amino group attached via a short aminoethyl ethoxy linker. To pattern the surfaces, a freshly oxidized polydimethylsiloxane (PDMS) stamp was 'inked' with a 20 μM solution of PNA in acetonitrile for 5 minutes, it was dried with nitrogen and then was brought into contact with the aldehyde modified glass surface for 15 minutes. This allowed the amino groups to react with the aldehyde functional groups forming an imine linkage between the PNA and the glass substrate. The imine bonds were then reduced to the corresponding amines with $NaBH_4$. This process is summarized in Figure 53a. Fluoresence microscopy of a glass surface printed with a fluorescein-bearing PNA oligomer confirmed the micropattern of

covalently-bound PNA on the glass surface (Figure 53b). The patterned surfaces were then hydribized with complementary and single-base mismatched dye-labeled DNA oligomers to test their ability to recognize complementary DNA sequences. It was shown that both sequences hybridized successfully to the PNA, however, the mismatched sequence's PNA/DNA duplex displayed a lower melting temperature (~5 °C less) compared to the fully complementary sequence, therefore, confirming that the microarray biosensor could be used to selectively detect sequence mismatches and point mutations in DNA.

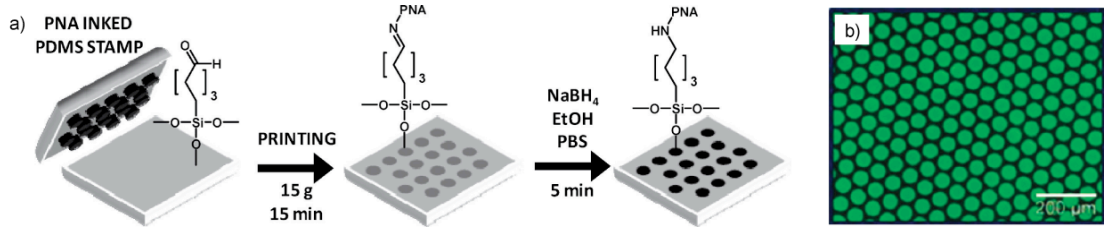

Figure 53. a) Schematic representation of the patterning of amino-capped PNA ligomers onto aldehyde-functionalized glass slides via reactive contact printing. b) Fluorescence microscope image (scale bar: 200 µm) of a glass surface following microcontact printing with fluorescein-labelled PNA.[194]

1.5 PROJECT OBJECTIVES

1.5.1 PRAIRIES OBJECTIVES

The project described in this thesis formed part of a collaborative EU Marie Curie research training network named Supramolecular Hierarchical Self-Assembly of Organic Molecules onto Surfaces towards Bottom-Up Nanodevices: A Host-Driven Action (acronym: PRAIRIES). The aim of the PRAIRIES research network was to gain a basic understanding and develop protocols for the controlled fabrication of organic nanopatterned surface networks featuring hosting properties, ultimately targeting the construction of superior organic materials for nanotechnological devices. This was achieved by gaining full control over the physico-chemical properties of the complex architectures constructed from a diversity of different functional molecules. In this manner, synthetic materials with controlled nanoscopic properties, which would be switchable in response to a specific external stimulus, would be implemented within the architectures (Figure 54).

Specifically, the PRAIRIES project required the synthesis of new types of organic materials, that would take advantage of the supramolecular approach to engineer, in a controllable fashion, extended two-dimensional organic networks on solid substrates featuring receptor sites (controllable both in shape and size) able to host functional organic molecules. The intention was to explore the self-assembly on surfaces of a large variety of programmed

rigid molecular modules (*e.g.*, porphyrins, benzenes, and phenanthrenes) bearing unidirectional connectors (*e.g.*, phenyl-acetylene linkers), alternatively functionalized with

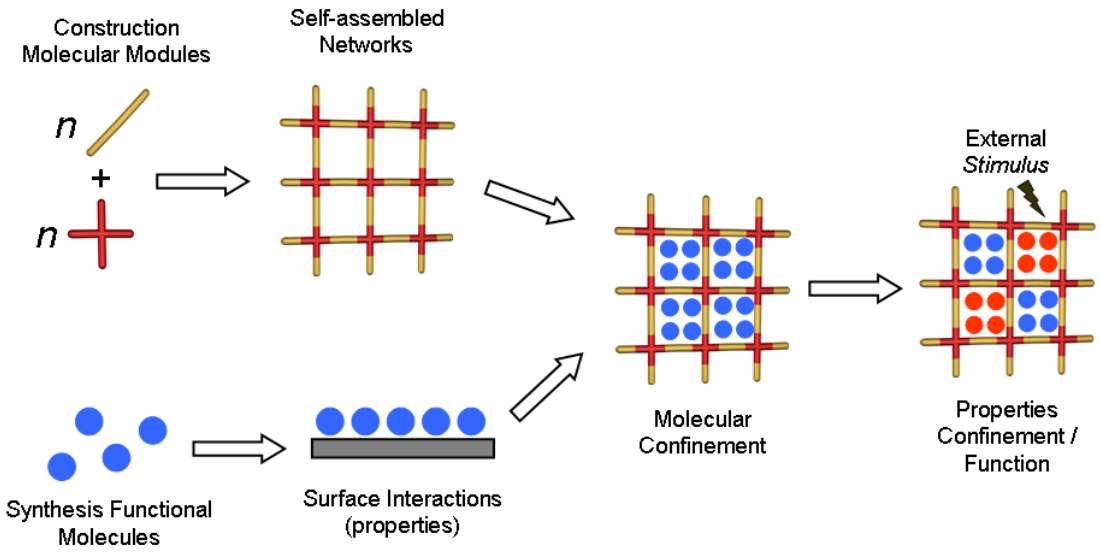

Figure 54. A schematic representation of the objectives of PRAIRIES.

multiple hydrogen-bonding donor and acceptor sites. The interaction of the modules would then result in the formation of supramolecular networks featuring periodic receptor sites. Particular attention was given (*i*) to the design of the molecular modules so that the suitable geometrical requirements were achieved to form two-dimensional self-assembled networks showing recognition sites of defined size (~1-10 nm) and geometry (*e.g.* hexagonal, square); (*ii*) to the fundamental understanding of the interaction between both the network molecules and the hosted substrates; and (*iii*) to the exploitation of the hosting properties and thus the potential applications.

Prior to the host-guest interaction studies of the networks and their receptor cavities, the initial focus of our research group was placed on the synthesis of the organic modules and the construction the self-assembled networks on surfaces. The focus was to synthesize two classes of molecules: (i) angular units (represented in red in Figure 54), which control the geometry of the arrays and (ii) rigid linear units (represented in yellow in Figure 54), which link the angular units together. To this end, several investigations have already been published and were described in Section 1.1.1.1 (Figures 3-7).

Our idea in this project, and thus the focus of this doctoral dissertation was to prepare bi-dimensional networks on surfaces featuring larger pores. Inspired by the self-assembly of DNA into nanoporous arrays on surfaces presented in Section 1.4.1, it was postulated that the Watson-Crick base pairing of oligonucleotide's nucleobases would be ideal in preparing porous networks with large receptor cavities. The idea was to covalently attach

complementary single stranded oligonucleotides to rigid angular and linear unit core modules respectively, and then perform the two units' self-assembly on surfaces. Instead of using DNA oligonucleotides, it was postulated that the use of peptide nucleic acid (PNA) oligonucleotides would result in more robust architectures due to the aforementioned advantageous properties of this class of biomimetic molecules (described in Section 1.4.2).

1.5.2 Design of the Angular and Linear Units

The necessary angular and linear units had to be designed bearing in mind that the key feature was to use the units to build rigid and stable nanoscale supramolecular assemblies on surfaces by utilising hydrogen bonding interactions to *directionally* link the building blocks together. Therefore, both the angular and linear units needed to consist of rigid organic modules in the core of the unit, which possessed the capacity to bear the required number of covalently-bonded, single-stranded PNA oligomers. Additionally, the link between the two units, *i.e.,* the PNA duplex formed via the *H*-bonding interactions of the two complementary single strands would have to have the highest thermal stability possible to ensure that the resultant supramolecular structure was rigid and stable. Finally, the duplex would have to be approximately one helical turn in length to maintain the optimal geometry of the supramolecular array on the surface. The number of base pairs required for a full helical turn of a duplex is 10.5 base pairs for DNA_2 (in solution),[195] 13 base pairs for DNA·PNA (in solution)[196] and 18 base pairs for PNA_2 (crystalline).[197]

Since the *H*-bonding recognition of PNA was the main feature in the construction of the desired supramolecular, the choice of the sequences of the complementary oligomers was fundamental. *Sen* and *Nielsen*[198] investigated the stability of various PNA_2, DNA·PNA and DNA_2 decamer duplexes. Their results showed that the most stable duplex was a PNA_2 decamer, which had a melting temperature of 73.4 °C. The same sequence was chosen for this project due to its high thermal stability. Although the decamer sequence chosen for the project did not satisfy the full helical turn of the PNA duplex, it was decided that initially the angular and linear units would be prepared using the decamer sequences to prove that the self-assembly concept functions. Upon obtaining this proof, larger porous networks could be prepared later using 18mer PNA sequences. Figure 55 shows the angular and linear unit designs diagrammatically, indicating the chosen base sequences for the PNA oligomers for the two complementary sequences, PNA_A and PNA_B. It must be noted that for simplicity, only one PNA oligomer is shown on the angular unit. The dashed lines represent further Spacer-PNA_A moieties. Figure 56 diagrammatically shows how the linear unit forms two duplexes with two angular units to form the supramolecular assembly. This assembly would extend in two dimensions since each angular unit core would bear several Spacer-PNA_A moieties. The

geometry and the shape of the receptor cavities of the resultant supramolecular porous network would depend on the type of angular unit core. Specific molecular details of the angular and linear units are shown below in Section 1.5.3.

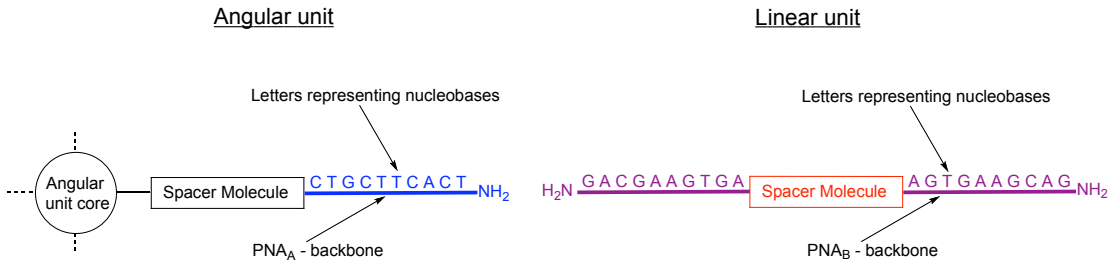

Figure 55. Diagram showing the angular and linear unit designs. The sequences of the complementary PNA oligomers (PNA_A and PNA_B) are shown. Only one PNA oligomer is shown on the angular unit for simplicity. The dashed lines represent further Spacer-PNA_A moieties.

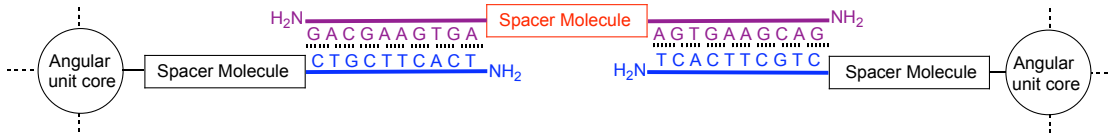

Figure 56. Diagram showing how the linear units' PNA_B oligomers recognise their complementary sequence, PNA_A, on two angular units to form two PNA duplexes. One linear unit links two angular units. Only one linkage is shown for simplicity, however, the assembly extends in two dimensions along the dashed lines in the same manner.

1.5.3 TARGET SUPRAMOLECULAR ASSEMBLIES

The intention of the project was to prepare several types of self-assembled porous networks, each one, with a differently shaped receptor cavity (Figure 57). Figure 57a would be constructed using a 1,3,5-trisubstituted benzene as the angular unit core and would result in a honeycomb structure made up of hexagonal cavities. The angle of the substituents on the angular unit core bearing the PNA oligomers is 120° with respect to each other. Figure 57b shows the supramolecular array that would result if a 5,10,15,20-tetrasubstituted porphyrin would be used as the angular unit core. A grid-like structure made up of square-shaped pores would result. The angle of the substituents on the angular unit core would be 90° with respect to each other. The third target assembly (Figure 57c), would utilise a 1,3,6,8-tetrasubstituted pyrene as the angular unit core to construct a rhombus-grid structure. The substituents on the angular unit core would be either 60° and 120° with respect to each other. A similar rhombus-grid could also be constructed using a 5,6,5',6'-tetrasubstitued [bis-1,10-phenanthroline-Cu(I)] complex as the angular unit (Figure 57d).

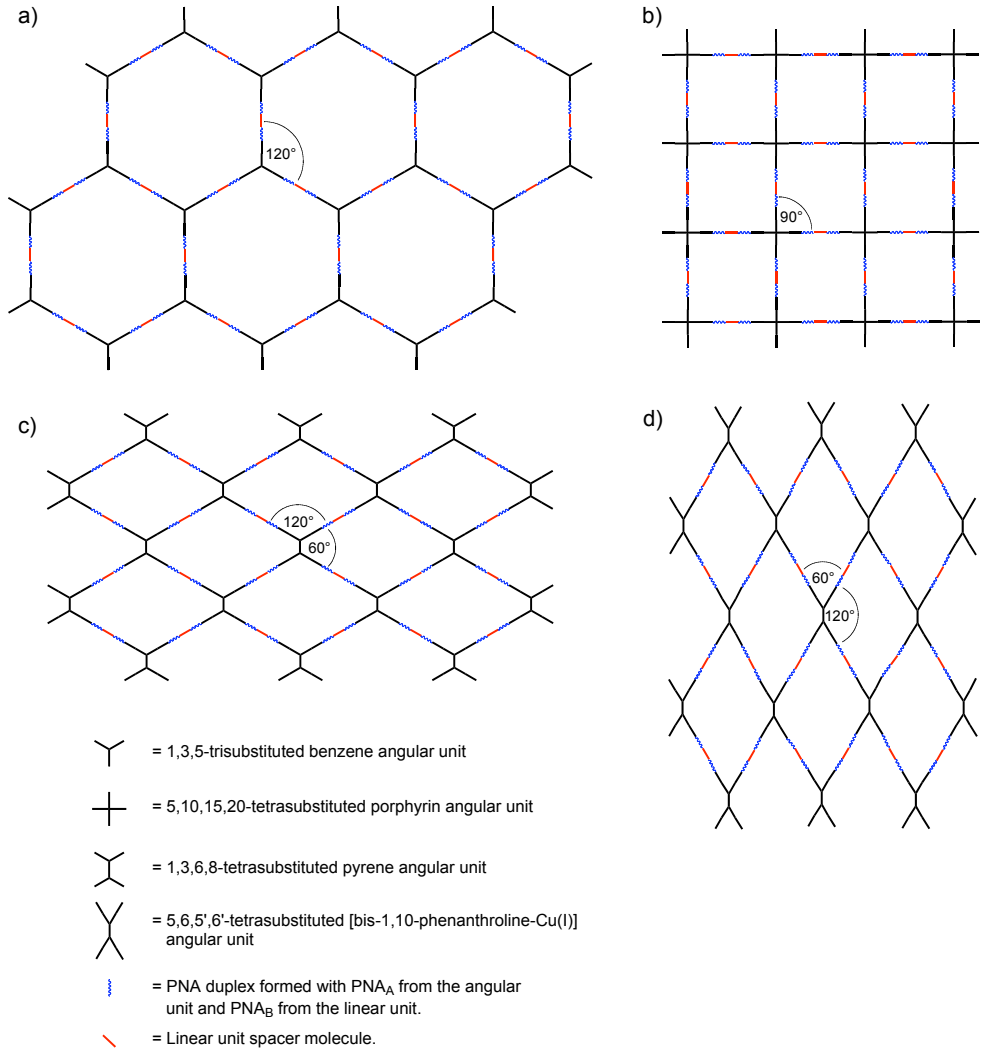

Figure 57. Diagram showing the various target self-assembled networks that can be formed by varying the angular unit core molecules. a) Hexagonal network envisaged to form when the angular unit core is a 1,3,5-trisubstituted benzene; b) Grid-shaped network envisaged to form when the angular unit core is a 5,10,15,20-tetrasubstituted porphyrin; c) Rhombic-shaped network envisaged to form when the angular unit core is a 1,3,6,8-tetrasubstituted pyrene; Rhombic-shaped network envisaged to form when the angular unit core is a 5,6,5',6'-tetrasubstitued [bis-1,10-phenanthroline-Cu(I)] complex.

The molecular designs of the angular and linear units are shown in Figures 58 and 59 respectively. The angular units (Figure 58), as already mentioned, would consist of a 1,3,5-trisubstituted benzene, a 5,10,15,20-tetrasubstituted porphyrin, a 1,3,6,8-tetrasubstituted pyrene or a 5,6,5',6'-tetrasubstitued [bis-1,10-phenanthroline-Cu(I)] complex. The substituents of these core modules would be PNA oligomers in each case. The linear unit (Figure 59) would consist of an aromatic core unit bearing two acetylene-phenyl-alkoxyamino units. The amino groups would serve as the attachment point for the PNA$_B$ oligomers.

Prior to synthesizing and assembling the complex molecular targets described above, a similar, yet simpler system was designed to be able to prove the concept that the bi-dimensional arrays could be formed on surfaces via PNA duplex formation. The decision was to omit the linear unit initially and simply use angular units functionalized with self-complementary PNA oligomers. The PNA sequence that was selected was the following dodecamer: TTAATTAATTAA.

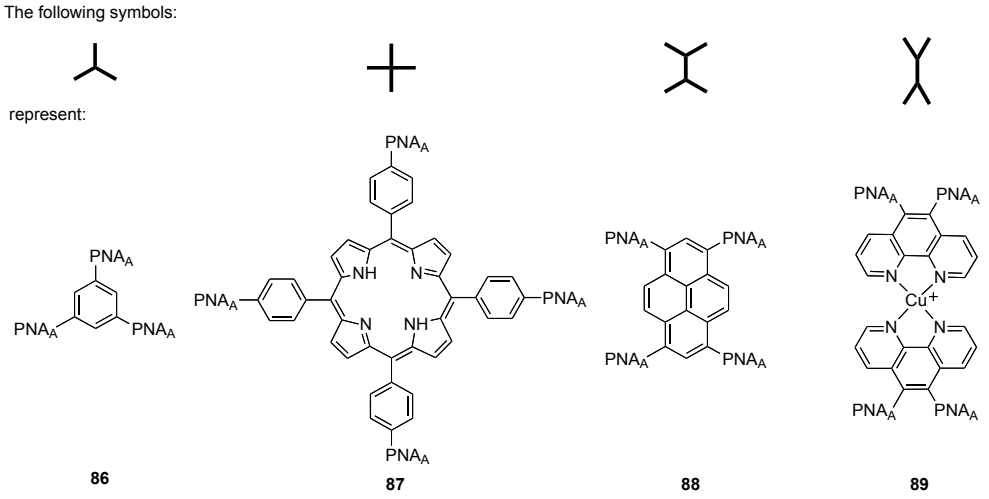

Figure 58. The molecular structures of the angular units including a 1,3,5-trisubstituted benzene (**86**), a 5,10,15,20-tetrasubstituted porphyrin (**87**), a 1,3,6,8-tetrasubstituted pyrene (**88**) and a a 5,6,5',6'-tetrasubstitued [bis-1,10-phenanthroline-Cu(I)] complex where the substituent group is a PNA_A oligomer.

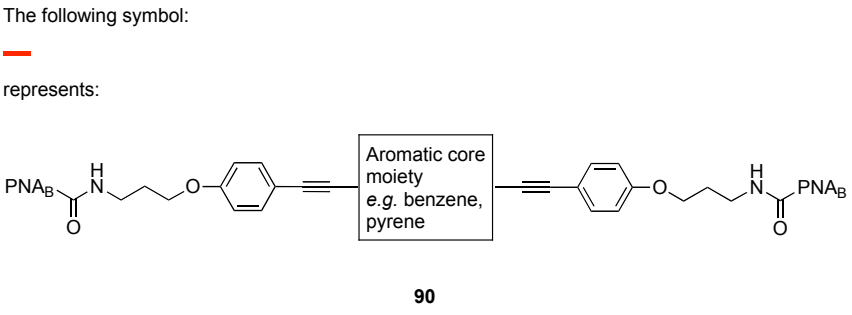

Figure 59. The structure of the linear unit. The core of the unit is an aromatic moiety (*e.g.* benzene, pyrene). The substituents are acetylene-phenyl-alkoxyamino unit, which would serve as the attachment points for the PNA_B oligomers.

Results and Discussion

Our interest in this project was to synthesise molecular scaffolds, based on rigid chromophores bearing complementary PNA oligomers, which by means of hydrogen bonding interactions could self-assemble and generate 2D porous nano-architectures on surfaces. The design of the angular and linear units bearing complementary PNA oligomers, required for this purpose are shown in Section 1.5.2 and 1.5.3. However, prior to synthesizing these molecules, a proof of principle was required to confirm that the PNA duplexes could be formed on surfaces and in the presence of chromophoric moieties (*e.g.* porphyrin, pyrene). The design of this proof of principle would take advantage of a self-complementary PNA dodecamer as the hydrogen-bonding recognition unit. This chapter describes the synthetic steps taken towards the preparation of the PNA oligomer and thereafter, our efforts to prepare PNA-chromophore adducts. This chapter is divided into four sections.

Section 2.1 describes the synthesis of the target self-complementary PNA oligomer (sequence: TTAATTAATTAA). This includes a description of the retrosynthesis and existing solid phase synthesis strategies to prepare PNA oligomers; a discussion of the orthogonal protecting group strategy required in this project; the synthesis of the monomers and finally the synthesis of the target oligomer.

Section 2.2 deals with our efforts to prepare PNA-chromophore adducts. Attempts to covalently attach a porphyrin moiety to the resin-bound oligomer via an amide linkage failed, possibly due to steric hindrance. Subsequently, a copper-catalysed 1,3-dipolar cycloaddition was attempted, but also this approach did not yield the target adduct. These unsuccessful results paved the way to the development of a copper-free 1,3-dipolar cycloaddition that enabled the attachment of chromophores to the PNA oligomer.

Section 2.3 discusses the results obtained in a preliminary study into the deposition of PNA onto mica surfaces and their subsequent imaging by AFM.

2.1 PNA SYNTHESIS

The correct assembly of the angular and linear units designed for this project depends on PNA as the functional supramolecular recognition system. For this reason, PNA was the central focus of this project at the initial stages. The successful synthesis of PNA oligomers was crucial to the success of the project.

An important consideration that must be accounted for when synthesizing PNA is the protecting group orthogonality. Whilst many protecting group strategies had been reported,[148, 151] when this project was started in 2006, all the reported strategies involved the deprotection of the nucleobase protecting groups during the resin cleavage step (Section 2.1.1). This was undesirable in this project since the oligomers had to be used in further reactions following the cleavage step, therefore a strategy had to be developed in which the nucleobase protecting groups were maintained following the resin cleavage.

After designing the protecting group strategy (Section 2.1.2), the required monomers were prepared (Section 2.1.3) and then several methods of PNA oligomer synthesis were evaluated (Section 2.1.4). Reports of rapid and successful solid phase peptide synthesis in the microwave,[199] several methods of PNA oligomerisation using various microwave methods were attempted, however all the methods resulted in complex mixtures from which the target product couldn't be isolated (Section 2.1.4.2). Reverting to manual solid phase synthesis, the desired PNA oligomer was isolated in its protected form (Section 2.1.4.3).

After obtaining the protected PNA dodecamer, several methods to deprotect the nucleobase protecting groups in solution were evaluated (Section 2.1.4.4). After several trials, a successful and reproducible method was developed, thus yielding the desired deprotected PNA dodecamer.

2.1.1 INTRODUCTION TO PNA SYNTHESIS STRATEGIES

In order to successfully synthesize the desired PNA oligomer, a review of the existing methods to prepare the monomer and oligomer was required.

The core of the monomeric unit is an *N*-(2-aminoethyl)glycine (AEG) moiety protected at the terminal amino group. Three main retrosynthetic routes (A-C) have been described for this unit (Figure 60). Route A involves an S_N2 reaction between a mono-protected ethylenediamine species and an α-halogenated acetic acid or its esters (route A), which is one of the most convenient and inexpensive methods.[200-203] Route B and C both involve a reductive amination reaction.[204, 205] In route B the reaction is performed between the mono-protected ethylenediamine and a glyoxalic ester. In route C, protected glycinal and glycine synthons are used. The completion of the PNA monomers is then performed by coupling a (protected) nucleobase modified with a carboxymethyl moiety with the secondary

amine of the AEG unit. This is normally done using peptide coupling reagents (e.g. *N*,*N*'-dicyclohexylcarbodiimide [DCC]). Due to this coupling reaction, the carboxylic group of the AEG is normally protected as an ester. The protected monomer is then selectively deprotected at the carboxyl group to produce the monomer required for oligomerisation. The choice of the protecting groups on the amino group and on the nucleobases depends on the strategy used for oligomer synthesis.

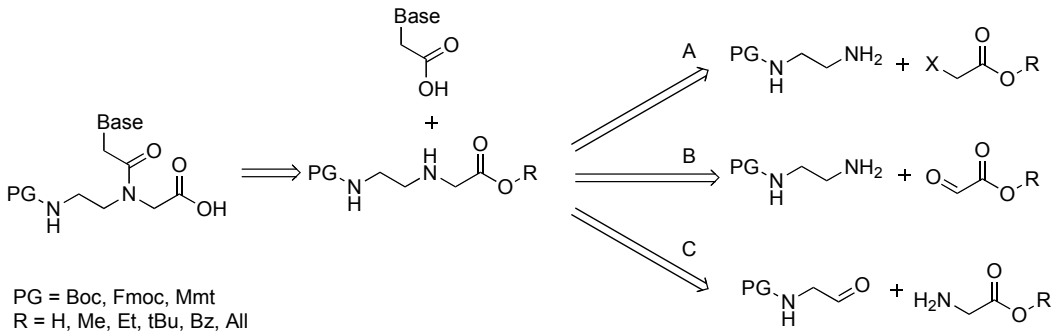

Figure 60. Retrosynthesis of the PNA monomer showing routes A-C to obtain the *N*-(2-aminoethyl)glycine unit.

The carboxymethyl nucleobases required for coupling to the AEG unit are shown in Figure 61.[151] Carboxymethylthymine is synthesized by alkylation of N^1 of thymine with bromoacetic acid and is generally used in its non-protected form. The carboxymethyl adenine and cytosine derivatives are generally prepared in two steps by protecting the exocyclic amino group first, followed by alkylation with bromoacetic acid derivatives. Guanine is the most difficult base to work with due to its lack of solubility. Generally the synthesis utilizes 2-amino-6-chloropurine as the starting material, where alkylation at the N^9 position is performed first with a bromoacetic ester. This is followed by protection of the exocyclic amino group and *in situ* saponification and hydrolysis to give the desired guanine derivative.

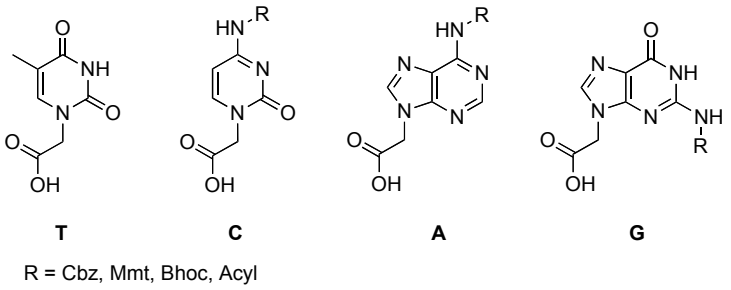

Figure 61. Nucleobase derivatives used for PNA synthesis. Thymine, cytosine, adenine and guanine derivatives are shown from left to right.

PNA monomers feature a protected *N*-terminus and a free carboxylic group, thus in this respect, they are comparable to the amino acids used to prepare peptides, therefore, PNA

oligomerisation can be performed with the same synthetic procedures commonly used for peptides *i.e.* solid phase synthesis. A general scheme for the synthesis of PNA oligomers on solid phase resins is shown in Figure 62.[151] In the first step, a monomer is loaded onto the free amino groups of the resin. Subsequently, the elongation takes place by repeated cycles of deprotecting the *N*-terminus of the anchored monomer and coupling of the following *N*-protected monomer to the deprotected *N*-terminus. The coupling reactions are carried out with coupling reagents such as HBTU, which are expected to give yields above 99%. As mentioned above, the exocyclic amino groups present on cytosine, adenine and guanine are protected to prevent interference with the oligomerisation synthesis. At the desired length of oligomer, the final cleavage can be carried out to release the oligomer from the resin yielding the crude product.

The most common strategies used in PNA synthesis involve the *N*-terminal Boc[147, 151, 206-209] and the Fmoc[203, 210-214] protecting groups. The Boc strategy was applied first to the synthesis of PNA.[147, 208] Homothymine sequences were synthesized first and later, the strategy was optimized for mixed sequences.[209] The solid phase resin chosen in these cases was a methylbenzhydryl amine (MBHA) derivatised polystyrene (PS) resin to which the first PNA monomer is linked by an amide bond. The amino groups on the nucleobases were protected with benzyloxycarbonyl derivatives (Cbz), therefore, this protecting group combination is referred to as the Boc/Cbz strategy. The Boc group was deprotected with trifluoroacetic acid (TFA) during the oligomer elongation, whereas, the final cleavage of PNA from the resin, with simultaneous deprotection of the exocyclic amino groups of the nucleobases, was carried out using HF or with a mixture of trifluoroacetic and trifluoromethanesulphonic acids (TFA/TFMSA). Such drastic cleavage conditions limited the range of PNA oligomers synthesized according to the Boc protocol.

A search for milder conditions led to the development of the Fmoc strategy of PNA synthesis. The *N*-terminal Fmoc protecting group is cleaved under mild basic conditions using piperidine. This makes the Fmoc strategy compatible with a wider variety of resin linkers (e.g. Rink amide, chlorotrityl groups) which can be cleaved under less acidic conditions (*e.g.* TFA). In the first paper reporting the use of a Fmoc strategy,[203] Cbz groups were used to protect the nucleobases, so HF was still used to carry out the final cleavage and nucleobase deprotection. However, later on *Uhlmann* and co-workers[210] introduced the monomethoxytrityl (Mmt) protecting group, which is easily deprotected during the final TFA cleavage. Similar to the Fmoc/Mmt strategy is the Fmoc/Bhoc strategy since it also allows the final cleavage and deprotection to be carried out *in situ* under acidic conditions.[213] A strategy including acyl protecting groups (*e.g.* acetyl, isobutyryl, anisoyl, benzoyl, *tert*-butylbenzoyl) for nucleobases has also been described.[214]

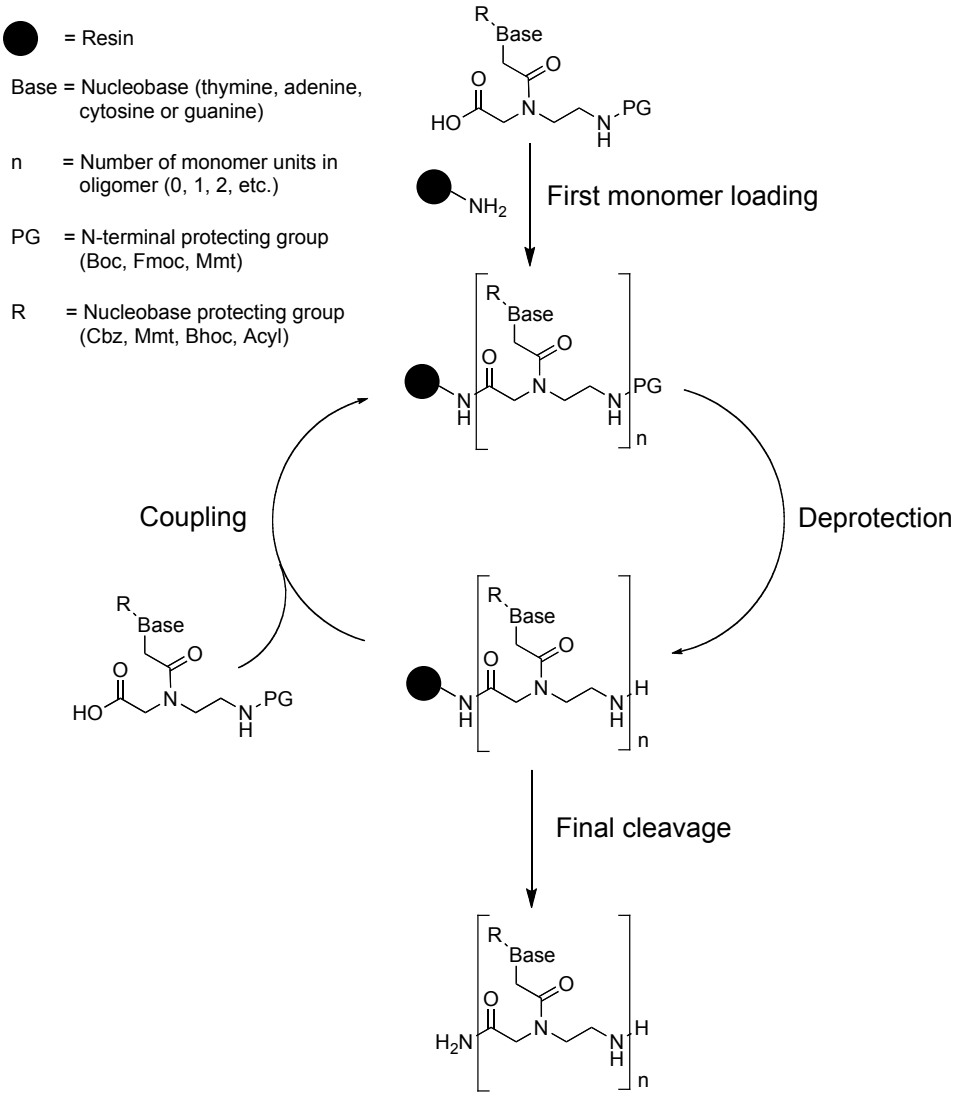

Figure 62. General scheme for the synthesis of PNA oligomers on solid-phase resins.

In addition to the Boc and Fmoc protection, another widely used *N*-terminal protecting group is Mmt.[200, 215-217] The Mmt group is acid-labile, but is cleaved in much milder conditions compared to the Boc group. Treatment with 3% trichloroacetic acid is sufficient.[200] In the Mmt strategy, the exocyclic amino groups of the nucleobases are usually protected with acyl groups.

Besides these three 'classic' strategies, which were introduced in the early years of PNA synthesis (1991-1999), several other strategies have been developed recently using a range of protecting groups. In 1999, a thiol-labile dithiasuccinate (Dts) group developed by *Barany* and coworkers was used in conjunction with the Cbz protecting group on the nucleobases to prepare PNA oligomers.[218] Further alternative protecting groups for the terminal nitrogen atom were introduced from 2001-2005. These included the Dmt,[219] N_3,[220] Alloc,[221] Dde[222] and Nvoc[223] protecting groups.

An interesting method introduced in 2007 by *Lee et al*.[224] utilised cyclic monomers bearing a Bts/Cbz protecting group combination. The benzothiazole-2-sulfonyl (Bts) group was particularly interesting because it played a dual role in the PNA synthesis in that it served as a protecting group for the *N*-terminus, and also, as an activating group for the coupling reactions. This meant that no coupling agent was required during coupling steps, consequently, the excess monomers could be recovered following the reactions. The Bts group is deprotected using 4-methoxybenzenethiol.

The most recent developments in protecting group strategies for PNA synthesis were published by *Winssinger* and coworkers in 2008.[225] In this work entitled 'Expanding the scope and orthogonality of PNA synthesis', several new protecting group strategies were introduced. Six types of protecting groups were evaluated for the terminal nitrogen atom: Alloc, Teoc, 4-N_3Cbz, Fmoc, 4-OTBSCbz and Azoc, in combination with five types of protecting groups on the nucleobases: Cl-Bhoc, F-Bhoc, Teoc, 4-OMeCbz and Boc. One interesting strategy was the use of the Alloc/Cl-Bhoc protecting group combination with a 2-chlorotrityl resin linker. This strategy allowed the final cleavage to yield a fully protected oligomer. All other strategies described above generally result in a completely deprotected oligomer. Control of the final cleavage/deprotection step was of particular importance in our project, since we required protected PNA oligomers following the resin cleavage. All the above-mentioned protecting groups have been summarized in Table 1.

Type	Protecting group	Structure	Typical reagents for amine protection	Typical reagents/ conditions for deprotection	Ref.
Acid-labile	**Boc** *tert*-Butyloxy carbonyl	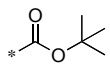	Di-*tert*-butyl dicarbonate	TFA or HCl/dioxane	147, 151, 206-209, 229
	Cbz Benzyloxycarbonyl	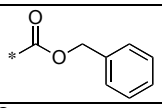	Benzyl chloroformate	H_2/Pd-C, TFMSA, or TMSI	203, 229
	4-OMeCbz 4-Methoxy benzyloxycarbonyl	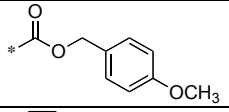	Carbonyldiimidazole & 4-methoxybenzyl alcohol	5% TFA	225
	Mmt Monomethoxy trityl	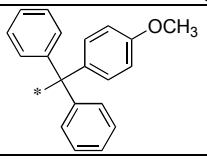	4-Methoxytrityl chloride	5% Trichloro-acetic acid	210, 229

	Dmt Dimethoxy trityl	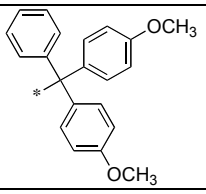	4,4'-Dimethoxytrityl chloride	1% TFA	219
	Bhoc Benzhydryloxy carbonyl	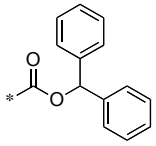	Carbonyldiimidazole & diphenyl-methanol	1% TFA	213
	Cl-Bhoc 4,4'-dichloro benzhydryl oxycarbonyl	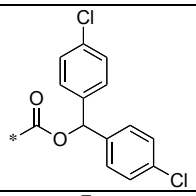	Carbonyldiimidazole & 4,4'-dichloro benzhydrol	5% TFA	225
	F-Bhoc 4,4'-difluoro benzhydryl oxycarbonyl	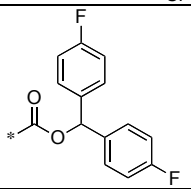	Carbonyldiimidazole & 4,4'-difluoro benzhydrol	5% TFA	225
Base-labile	**Fmoc** 9-Fluorenylmethyl oxycarbonyl	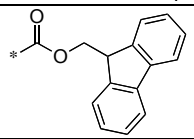	N-(9-Fluorenyl methoxy carbonyloxy) succinimide	20% Piperidine	203, 210-214, 229
	Acyl *e.g.* acetyl, isobutyryl, benzoyl	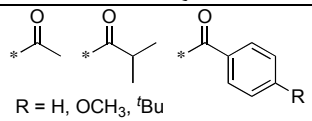	Acyl chlorides *e.g.* acetyl chloride, benzoyl chloride	Ammonia	214
	Dde 1-(4,4-Dimethyl-2,6-dioxocyclo-hexylidene)ethyl	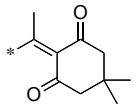	2-Acetyldimedone	2% hydrazine in DMF	222, 229
Catalytic cleavage	**Alloc** Allyloxycarbonyl	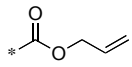	Allyloxycarbonyl chloride	Catalytic $[Pd(PPh_3)_4]$	221, 225, 229
Thiol-labile	**Dts** Dithiasuccinoyl	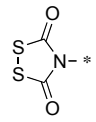	Bis(ethoxy-thiocarbonyl)sulfide, *N*,*O*-bis(trimethylsilyl-acetamide) & (chlorocarbonyl) sulfenyl chloride	2-Mercapto-ethanol, NEt_3	218, 229
	Bts Benzothiazole-2-sulfonyl	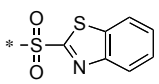	Benzothiazole-2-sulfonyl chloride	4-Methoxy benzenethiol	224
Azide protecting groups	**N_3** Azide		Sodium azide	Reduced to azaylide using trimethyl phosphine	220
	Azoc Azidomethyloxy carbonyl	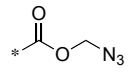	Chloromethyl chloroformate & sodium azide	1M trimethyl phosphine	225

	4-N_3Cbz 4-Azidobenzyl oxycarbonyl	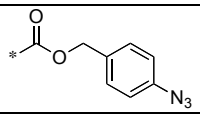	Phenyl (4-azido benzyloxy) formate	1M trimethyl phosphine	225
Silyl protecting groups	**Teoc** 2-(Trimethylsilyl) ethoxycarbonyl	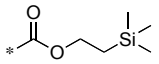	1-[2-(trimethylsilyl) ethoxycarbonyloxy] pyrrolidin-2,5-dione	TBAF	225
	4-OTBSCbz 4-(*tert*-butyl dimethylsilyloxy)-benzyloxycarbonyl	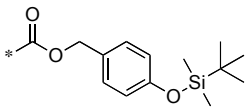	Phenyl [4-(*tert*-butyldimethyl silyloxy)benzyloxy] formate	TBAF	225
Photo-cleavable	**Nvoc** Nitroveratryloxy carbonyl	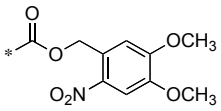	4,5-Dimethoxy-2-nitrobenzyl chloroformate	UV photo-cleavage (350 nm)	223

Table 1. Protecting groups used to protect *N*-terminal amino groups and nucleobase exocyclic amino groups in PNA synthesis.

Another important consideration during PNA synthesis is the selection of the appropriate resin and linker. The resin used as the solid support may range from a very apolar polymer (*e.g.* polystyrene) to very polar one (*e.g.* poly(ethylene glycol)/dimethylacrylamide copolymer).[226] Each of these resins presents its own advantages (Table 2) and all of them have been used to prepare PNA, however, polystyrene (PS) resins and polystyrene/diviylbenzene-poly(ethylene glycol) graft copolymer (PS-PEG) resins are most commonly used for PNA synthesis.

Apart from the resin, an important factor in PNA solid phase synthesis is the linker used to attach the growing oligomer to the resin. Linkers must be orthogonal to the protecting group strategy. In particular, they must be stable to the conditions used to perform the deprotection of the *N*-terminal protecting group, the coupling of the monomers to the growing oligomer and the capping step. On the other hand, the last step of PNA oligomerisation usually involves the simultaneous cleavage of the resin and deprotection of the nucleobases' amino-protecting groups, therefore linkers are chosen according to conditions required to cleave it. For this reason, generally acid-labile and base-labile linkers have been used in PNA synthesis, even though many other types of linkers exist[226] (*e.g.* photo-cleavable linkers). The main linkers that have been used in PNA synthesis as well as their cleavage conditions are summarized in Table 3.

Polymer support	Comments	Polarity
PS Polystyrene with 1-2% divinylbenzene (DVB) cross-linking	- Gel-type structure. Readily allows penetration of reagents and solvents into the beads to sites where chemistry is taking place. - 1-2% DVB cross-linking provides a balance between a good stability of the resin whilst maintaining swelling ability. 5% DVB cross-linking provides greater stability, but swelling is limited. - Very apolar resin.	Low
PS-PEG Polystyrene/DVB-poly(ethylene glycol) graft copolymers	- Distances reactive sites from apolar resin core to give more 'solution-like' conditions at the reactive sites. - Ideal when using polar solvents. - Enhanced swelling ability compared to PS. - *e.g.* Tentagel and Argogel	
PA Polyacrylamide-based	- These two supports are generally used in continuous flow solid phase peptide synthesis and in oligonucleotides synthesis. - The high polarity of these resins makes them hydrophilic.	
CPG Controlled-pore glass		
PEGA Poly(ethylene glycol)/dimethy-lacrylamide copolymer	- Very polar resin. - Unparalleled swelling properties in water. - Flexible interior enables access to large macromolecules including enzymes.	High

Table 2. Classes of resins used in solid phase synthesis.[226]

Type	Linker	Structure	Typical reagents for resin cleavage	Ref.
Acid-labile	**MBHA** 4-Methylbenzhydryl amine	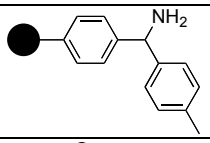	TFA or TFMSA	206
	Breipohl linker	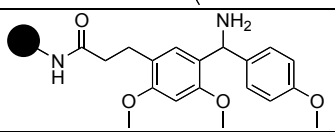	95% TFA	210
	Rink	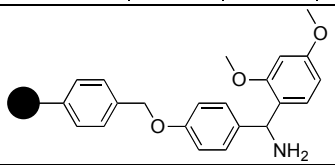	80% TFA	203
	PAL 5-[3,5-Dimethoxy-4-(aminomethyl)phenoxy]pentanamide	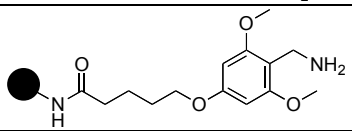	50% TFA	224
	Wang [4-(Hydroxymethyl) phenoxymethyl]	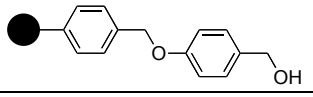	50% TFA	219

	2-Chlorotrityl	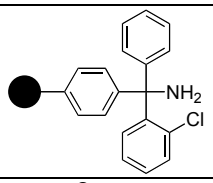	1% TFA or acetic acid	225
Base-labile	**12-hydroxy-dodecanamide**	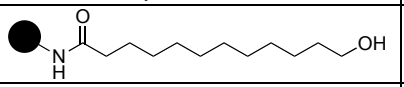	NH_3/EtOH	214
	Aminohexyl succinate	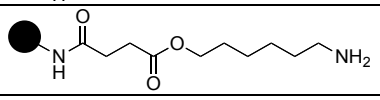	NH_3/H_2O	215

Table 3. Linkers used to attach growing PNA oligomers to resin support polymers.

2.1.2 ORTHOGONALITY AND THE PROTECTING GROUP STRATEGY

In order to successfully synthesize the desired PNA oligomer, both the monomer and the oligomer synthesis required protecting groups that could be orthogonally deprotected when required. Furthermore, the linker between the solid phase resin and growing PNA oligomer also had to be orthogonal to the protecting groups. As mentioned above, a further complication to our system was the requirement that the PNA oligomers needed to be cleaved from the solid support without removing the nucleobase protecting groups. This is contrary to what is normally reported in PNA synthesis in the literature[148, 151] *i.e.* normally nucleobase deprotection and resin cleavage is carried out simultaneously in one step. Also, adding further complication was the fact that the synthetic design had to be compatible with all the chromophores (*e.g.* porphyrins, pyrene), which were going to be attached to the PNA oligomers. This meant that it would have been desirable that the nucleobase deprotection step in particular would be carried out under the mildest conditions possible.

After reviewing all these requirements, the following system was proposed. The monomers would be synthesized using a Fmoc/Mmt strategy *i.e.* Fmoc protection on the terminal nitrogen of the AEG moiety and Mmt protection on the exocylic amino groups of the nucleobases. A methyl ester was suggested to protect the carboxylic moiety of the AEG unit. This strategy had been used for synthesizing PNA monomers previously by *Breipohl et al*.[210] Fmoc chemistry is commonly used for solid phase peptide synthesis (SPPS), thus the PNA oligomer synthesis could be prepared using well-established procedures.[203, 210] Having decided the protecting group strategy, attention was shifted towards the design of the linker for the oligomerisation process. The linker chosen for the SPPS was base-labile under strong basic conditions. It was chosen to prevent cleavage of the oligomer from the resin during the mild base deprotection of the Fmoc protecting group (20% piperidine in DMF).[227] Also, the use of a base cleavable linker would ensure that the Mmt protection of the nucleobases would remain intact during the resin cleavage step. The Mmt group was chosen because it is cleaved under very mild acid conditions (5% chloroacetic acid[228] or 2% TFA is sufficient[229]) and

thus would ensure that the chromophores attached to the PNA would not be effected.

Unfortunately, this strategy was abandoned following failure of the chosen base cleavable linker (Section 2.1.4.1). During the early stages of the oligomerisation process, a resin cleavage attempt was performed to evaluate whether the solid phase synthesis cycle was working correctly. Unfortunately, the resin cleavage did not yield any crude product. The test was attempted several times without success, therefore an alternative strategy was designed.

The alternate strategy that was designed maintained the Fmoc protecting group to protect the terminal nitrogen atom. The nucleobases' exocyclic amino groups were to be protected with the very robust Cbz protecting group. The Cbz group is stable to basic conditions and also acidic conditions up to pH 1.[230] It is generally deprotected by hydrogenation in the presence of palladium on activated carbon, strong acids (*e.g.* trifluoromethanesulfonic acid), or nucleophilic substitution (with silyl derivatives). Since the Cbz group is stable to TFA, a *tert*-butyl ester was proposed as the protecting group for the carboxylic moiety of the AEG unit. *Thomson et al.* had previously reported this protecting group strategy.[203] The Fmoc/Cbz protected monomers could then be used to prepare the oligomer using the commercially available Rink MBHA resin. This resin is stable to basic conditions, therefore, the oligomer elongation using Fmoc chemistry is compatible. Oligomers can be cleaved from this resin using acidic conditions. Due to the robustness of the Cbz protecting groups, TFA resin cleavage[220] allows the oligomer to retain the Cbz protection of the nucleobases. With the nucleobase protection, the oligomer could be used for further reactions in solution, and when required the Cbz deprotection could be carried out in solution using trimethylsilyl iodide (TMSI). This strategy is summarized in Figure 63.

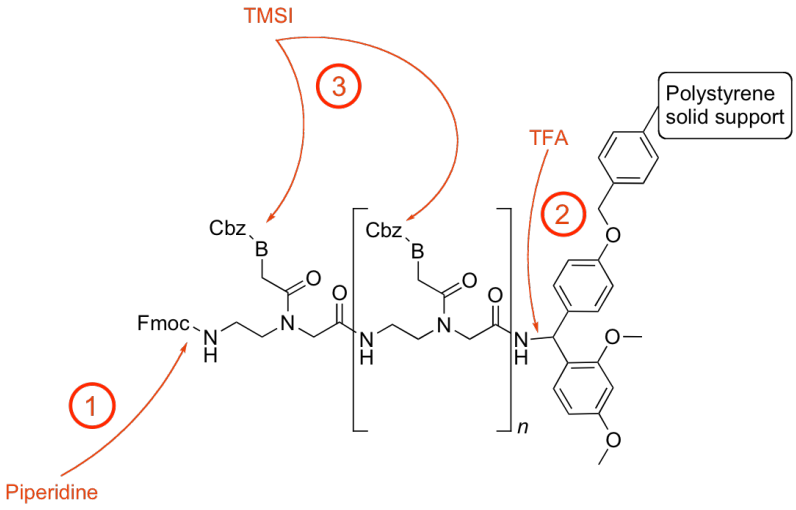

Figure 63. The orthogonal strategy proposed for the PNA oligomerisation using Fmoc/Cbz protected monomers. The *N*-terminal Fmoc protecting groups can be deprotected with piperidine, without affecting the base-stable Rink MBHA resin and the Cbz protecting groups. The oligomer can be cleaved from the resin using TFA without deprotecting the Cbz protecting groups, which can be deprotected later, in solution, using TMSI.

2.1.3 SYNTHESIS OF PNA MONOMERS

This section presents the synthesis of the thymine and adenine monomers required for the solid phase synthesis of the target PNA dodecamer (sequence: TTAATTAATTAA). The structures of the target monomers are shown in Figure 64. In order to prepare the required PNA oligomer, the PNA monomers had to be prepared on a multi-gram scale. The monomers were prepared using a convergent synthesis where the carboxymethyl nucleobase derivatives and the AEG unit were coupled together. The thymine monomer was prepared first and was used to test the solid phase oligomerisation. Two adenine monomers are shown in Figure 64 because a change in strategy was required due to the failure of the base cleavable linker used during solid phase oligomerisation process in the Fmoc/Mmt strategy (discussed in Section 2.1.4.1). The synthesis of Fmoc/Mmt adenine monomer **92**, was not completed due the abandonment of the strategy.

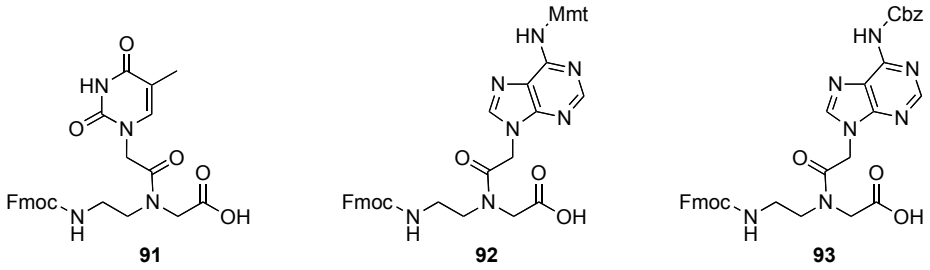

Figure 64. The structures of the target monomers.

2.1.3.1 Synthesis of the thymine monomer

Two components were required to prepare thymine monomer **91**, the carboxymethyl functionalized nucleobase and the AEG unit. The nucleobase's synthesis was tackled first, followed by the synthesis of the AEG unit. The two synthons were coupled together to form the protected monomer, which following deprotection of the carboxylic ester moiety yielded **91**.

Two methods to synthesize thymine-1-acetic acid **95** were evaluated. In the first method (Scheme 1a), commercially available thymine **94** was treated with bromoacetic acid to give product **95** in 64% yield.[231] The second method (Scheme 1b) gave **95** with a similar yield (62%). The reaction involved the addition of methylbromoacetate to thymine **94** followed by saponification without isolating or purifying the ester intermediate.[207] The latter method was preferred despite the longer synthetic route and marginally lower yield because the isolated product, **95**, did not contain traces of the starting material as an impurity as was observed in the product formed by the method shown in Scheme 1a.

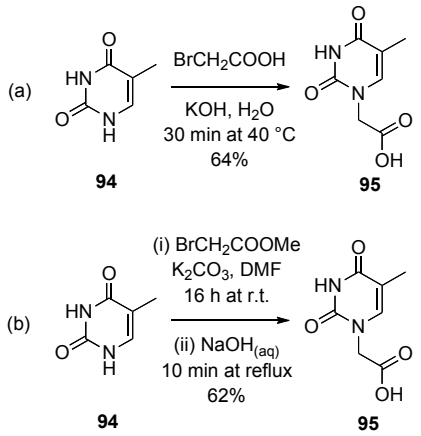

Scheme 1

Having obtained **95**, the completion of thymine monomer **91** was done according to a procedure published by *Thomson et al.*[203] The synthesis involved the addition of *tert*-butylbromoacetate to ethylenediamine **96**, with the latter in large excess during the reaction, to give **97**. This was followed by treatment with Fmoc-OSu to Fmoc-protect the remaining primary amine of the ethylenediamine moiety, yielding Fmoc/^{t}Bu-protected AEG unit **98** in 48% yield over two steps. Although the yield was modest, the important point in the preparation of **98** was that no chromatography was required to obtain the pure product and that the reactions were scalable to multi-gram quantities. The next step was the coupling of thymine derivative **95** to the secondary amino group of AEG unit **98**. This was carried out in the presence of EDC with a slight excess of **95** yielding **99**, the protected thymine monomer, which was purified by silica gel chromatography. The thymine monomer **91** required for the PNA oligomerisation *i.e.* bearing a free carboxylic group was isolated upon treatment with TFA.

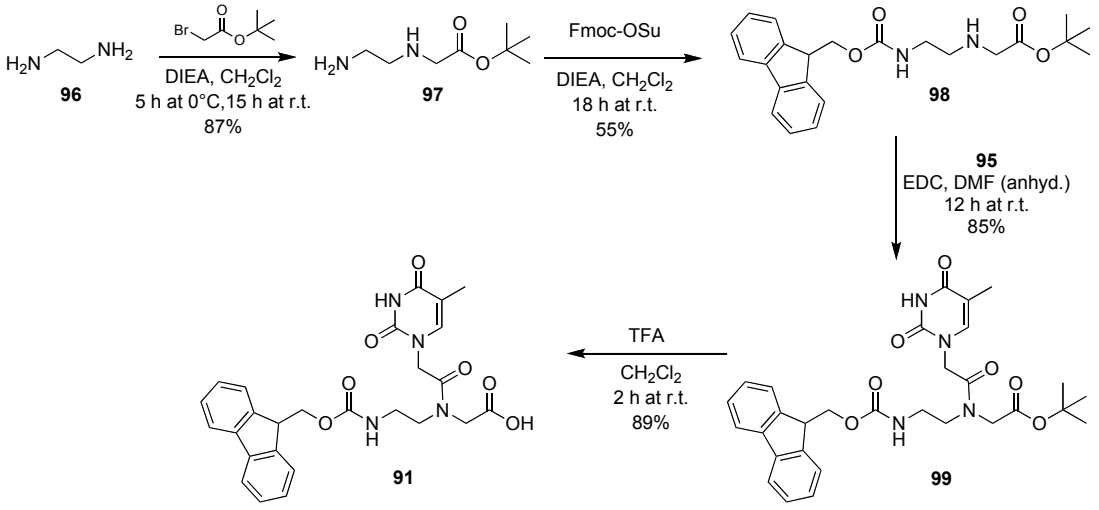

Scheme 2

Once thymine monomer **91** was obtained, subsequent work focused on testing and optimizing the solid phase oligomerisation synthesis (Section 2.1.4.1) and also, in parallel, synthesizing the adenine monomer (2.1.3.2).

2.1.3.2 Synthesis of the adenine monomer

In the initial stages of this project, the focus was on using a Fmoc/Mmt strategy to prepare a protected PNA oligomer. To this end, the synthesis of a Fmoc/Mmt protected adenine monomer was required (Section 2.1.3.2.1). However, due to the failure of the base cleavable linker used in the solid phase synthesis, the overall PNA synthesis strategy was altered to utilise a Fmoc/Cbz strategy, therefore the synthesis of a Fmoc/Cbz protected adenine monomer is reported (Section 2.1.3.2.2).

2.1.3.2.1 Synthesis of the Fmoc/Mmt protected adenine monomer

The synthesis of the Fmoc/Mmt protected adenine PNA monomer required careful selection of the protecting group for the carboxylic moiety of the AEG unit. Since the Fmoc group is labile under mild basic conditions and Mmt is labile under mild acidic conditions, the carboxyl group of the AEG unit could not be protected with the most commonly used esters in PNA synthesis *i.e.* the *tert*-butyl ester or methyl ester due to the strong acidic and basic conditions, respectively, required for their hydrolysis. To circumvent this problem, an allyl ester was chosen to protect the AEG carboxylic acid functional group. The allyl ester was chosen since it is catalytically cleaved under neutral conditions in the presence of a palladium catalyst. As with the thymine monomer, the preparation of adenine monomer **92** required two synthons: the protected AEG unit and the carboxylmethyl functionalized nucleobase.

The required nucleobase derivative **102** was synthesized in three steps as shown in Scheme 3. Deprotonation of adenine **100** followed by treatment with methylbromoacetate yielded the methyl ester derivative **101**.[207] Then Mmt-protection of the exocyclic amine ensued, using Mmt-Cl in a mixture of pyridine and dichloromethane in the presence of N-ethylmorpholine (NEM) as a base.[232] Finally, saponification of the ester gave the desired MMT protected adenine derivative **102**.

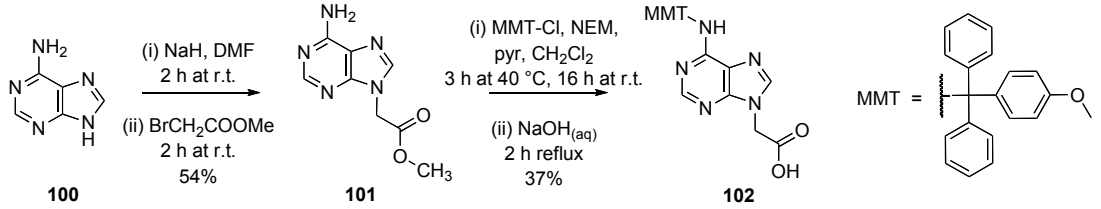

Scheme 3

Scheme 4 displays the next steps towards the synthesis of the adenine monomer with Fmoc/Mmt protection **92**. The Fmoc/allyl-protected AEG unit was prepared using a published procedure.[233] The reported procedure required compound **98** as the starting material, therefore, the first two steps were the same as previously shown in Scheme 2. At this point, the *tert*-butyl-protecting group had to be switched to the allyl-protecting group. This conversion was achieved by converting the ester to the carboxylic acid by treating compound **98** with TFA, and then, by dissolving the resultant crude product in allyl alcohol and treating with thionyl chloride. The desired product *i.e.* Fmoc/allyl-protected AEG unit **103** was obtained in 84% yield from **98**. AEG unit **103** was then coupled with Mmt-protected adenine derivative **102**. The coupling was done by activating the carboxyl group of **102** using TOTU as the activating agent, and then introducing **103** as the nucleophile to give the protected adenine PNA monomer **104** in reasonable yield (62%). The final step in the preparation of required Fmoc/Mmt-protected adenine monomer **92** was the deprotection of the allyl group. It was expected that the reaction would proceed using $[Pd(PPh_3)_4]$ as the catalyst.[234] However, the final reaction to prepare monomer **92** was never attempted since this monomer was no longer required due to a change in the overall PNA synthesis strategy caused by the aforementioned problems encountered in the oligomerisation process (discussed in Section 2.1.4.1).

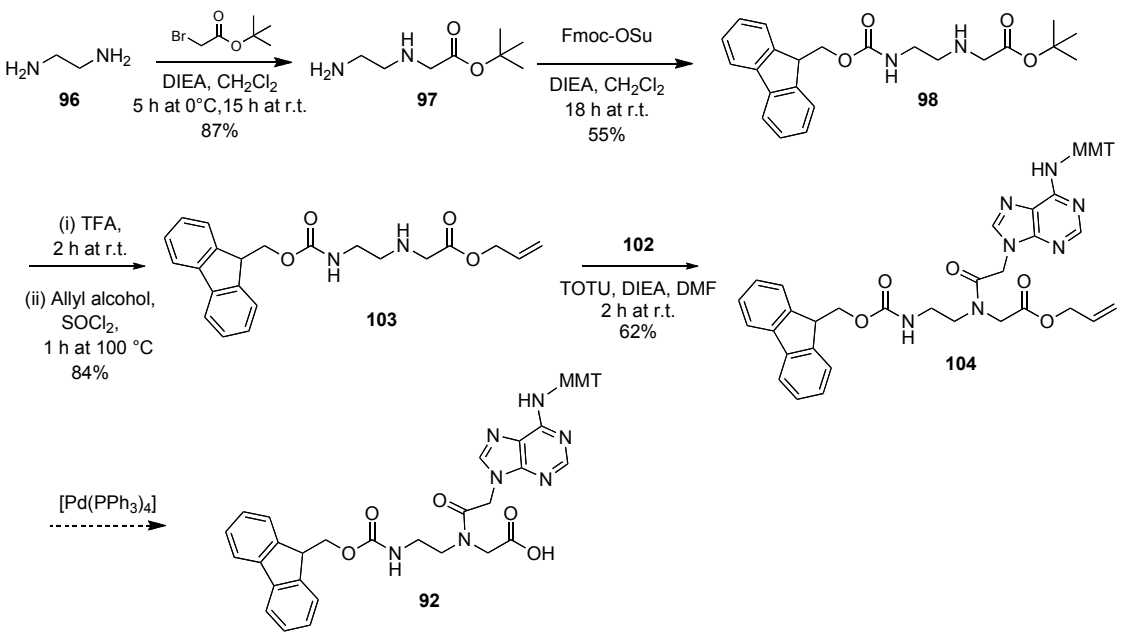

Scheme 4

2.1.3.2.2 Synthesis of the Fmoc/Cbz protected adenine monomer

The change in the overall PNA synthesis strategy, also included a change in the resin used for the solid phase synthesis. Rink amide MBHA resin was selected as the solid support, which required strong acidic conditions for the final cleavage step. Consequently, the Mmt group had to be replaced by a more robust protecting group to ensure that a protected PNA oligomer was isolated following the resin cleavage. For this purpose, the Cbz group was selected since it is resistant to TFA. This section describes the synthesis the Fmoc/Cbz-protected adenine monomer.

First, the Cbz-protected adenine nucleobase derivative **107** was synthesized (Scheme 5). The first step involved the deprotonation of adenine **100** using sodium hydride, followed by the protection of the exocyclic amine using Cbz-Cl. Next, alkylation introduced the *tert*-butyl acetate moiety to give **106**, which was subsequently deprotected using TFA to give Cbz-protected adenine derivative **107** that was ready for coupling to the AEG unit. Although **107** was successfully isolated using the synthetic steps described in Scheme 5, another procedure was evaluated (Scheme 6) to determine if the overall yield could be improved.

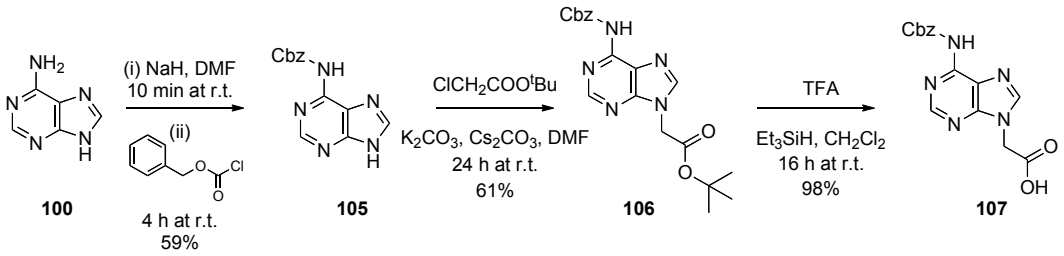

Scheme 5

A procedure reported by *Debaene* and *Winssinger*[220] offered an alternative method that could be used to prepare **107**. The pathway is described in Scheme 6. The introduction of the *tert*-butyl acetate moiety to adenine **100** to give **108** was achieved by deprotonation using sodium hydride, followed by the slow addition of *tert*-butyl chloroacetate to the reaction mixture. The crude solid of **108** was then treated with carbonyldiimidazole followed by benzyl alcohol yielding **106** in 81% yield. Deprotection of the *tert*-butyl group using TFA

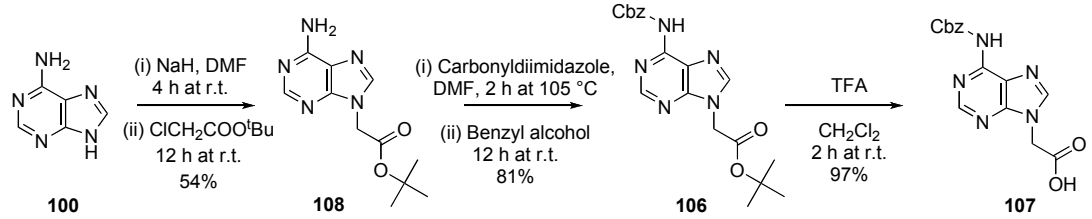

Scheme 6

gave target compound **107**. This synthetic route gave a better yield overall yield (42%) compared to the route described in Scheme 5 (35%), therefore, it was the preferred method.

Having obtained Cbz-protected adenine derivative **107**, the coupling to AEG unit **98** ensued (Scheme 7). Initially, this was performed in a manner analogous to that of protected thymine monomer **99**. The carboxyl group of **107** was activated using HBTU in the presence of DIEA as the base. AEG unit **98** was then added to the activated adenine derivative yielding **109**, the protected adenine monomer in 57% yield. Treatment of **109** with TFA, yielded adenine monomer **93** required for the solid phase synthesis.

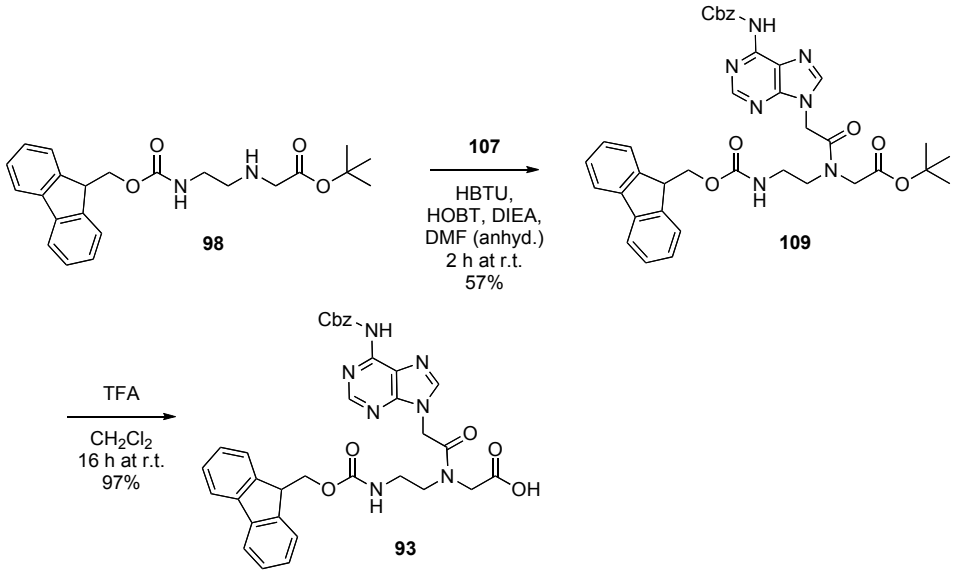

Scheme 7

Optimisation of the condensation reaction between **98** and **107** using a procedure reported by *Debaene* and *Winssinger* yielded **109** in 69% yield.[220] The reaction (Scheme 8) involved activating the carboxyl moiety of **107** using pivaloyl chloride to form an asymmetric acid anhydride, and then, *in situ*, introducing AEG unit **98** to form the desired coupling product **109**. Higher yields with this reaction are unlikely because the secondary amine of **98** could also react with the pivalylic carbonyl group to form a side-product, although this is not favoured due to the hindrance caused by the pivalylic *tert*-butyl moiety.

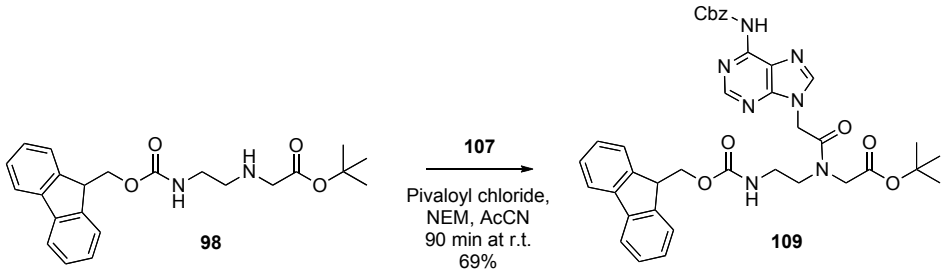

Scheme 8

2.1.4 SOLID PHASE SYNTHESIS OF PNA OLIGOMERS

This section discusses the protocols which we have evaluated in the preparation of the target PNA dodecamer (sequence: TTAATTAATTAA). Section 2.1.4.1 presents the problems that were encountered using the Fmoc/Mmt strategy during the oligomerisation process. The following section (2.1.4.2) shifts the attention to the Fmoc/Cbz strategy and our efforts to utilize microwave-assisted solid phase synthesis to prepare the target PNA strand. In section 2.1.4.3, the target dodecamer sequence was finally isolated using the classic manual solid phase synthesis technique and in the final section (2.1.4.4) the development of a solution phase Cbz-deprotection method for the oligomer's nucleobases is described.

2.1.4.1 Solid phase PNA synthesis using the Fmoc/Mmt strategy

In parallel to the preparation of Fmoc/Mmt-protected adenine monomer **92** (Section 2.1.3.2.1), thymine monomer **91** was used to evaluate the PNA oligomerisation conditions for the Fmoc/Mmt strategy. The resin chosen for the oligomerisation was TentaGel resin.

TentaGel resins are grafted copolymers consisting of a low cross-linked polystyrene matrix on which polyethylene glycol (PEG) is grafted.[235] Since PEG is a polymer with both hydrophobic and hydrophilic properties, the graft copolymer shows modified physico-chemical properties. It combines the benefits of the soluble polyethylene glycol support with the insolubility and handling characteristics of the polystyrene bead. These characteristics allow the resin to mimic solution phase reaction conditions at the reactive sites, whilst maintaining the benefits of solid phase resin *i.e.* purification involves washing the resin following reactions. The resin was selected due to the fact that the reactions take place in polar, solution-like conditions on the TentaGel resin, which was thought to be beneficial for the polar conditions used in PNA synthesis. Furthermore, synthesis of PNA using Tentagel had been reported previously.[236]

In order to initiate the solid phase synthesis, the base-cleavable linker required to attach the PNA oligomer to the Tentagel resin had to be prepared. The linker, which was reported as cleavable under concentrated aqueous ammonia conditions[215] was synthesized as

shown in Scheme 9. The amino group in 6-aminohexan-1-ol **110** was first protected using Mmt-Cl to give **111** in 53% yield as reported.[215] Then, nucleophilic attack of the alcohol moiety on succinic anhydride introduced an ester and a carboxylic acid moiety to give **112** in 79% yield. The ester provides the cleavage point in the linker *i.e.* it is hydrolyzed upon treatment with a strong base and therefore would act as the cut off point between the PNA oligomer and the resin to yield the PNA oligomer when required during the SPPS. The carboxylic acid moiety was used in the final step of Scheme 9 to attach the linker to the amino groups of the tentagel solid phase resin using TBTU as the activating agent resulting in **113**. Compound **113** provided the platform on which the PNA oligomer would be grown using established SPPS techniques.

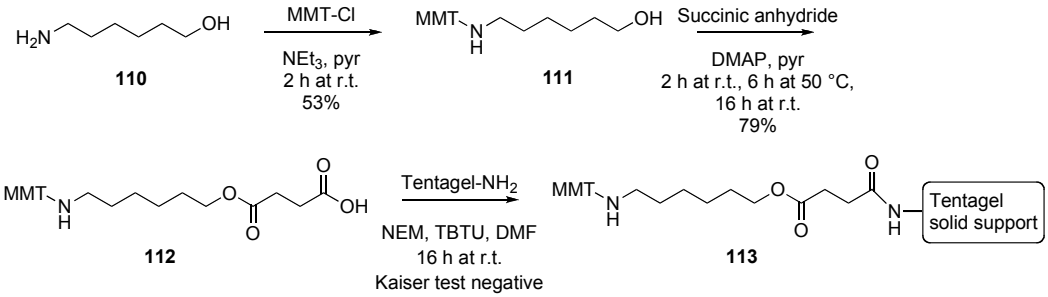

Scheme 9

Once compound **113** was prepared, the PNA oligomer synthesis was attempted (Scheme 10). The amine protecting group (Mmt) was deprotected using 3% trifluoroacetic acid in CH_2Cl_2. The deprotection was verified by a Kaiser test, which indicated that the reaction was complete (both the resin sample subjected to the test and the test solution turned blue indicating the presence of free amino groups). Next, the first thymine monomer **91** was coupled to the deprotected amine using HBTU as the coupling agent, NEM as the base and DMF as the solvent. All the reagents were added in excess to ensure efficient coupling. Following the coupling, another Kaiser test was performed, and this time the result was negative *i.e.* no colour change was observed indicating that no more free amines were present and that the coupling reaction had gone to completion. Following a successful coupling, a capping reaction using acetic anhydride was performed to ensure that if any traces of free amino groups remained following the coupling, they would be blocked from any further reaction. This is very important since it dramatically minimizes the chances of the formation of erroneously assembled (wrong sequence) PNA oligomers that would be difficult to separate from the desired oligomer during purification.

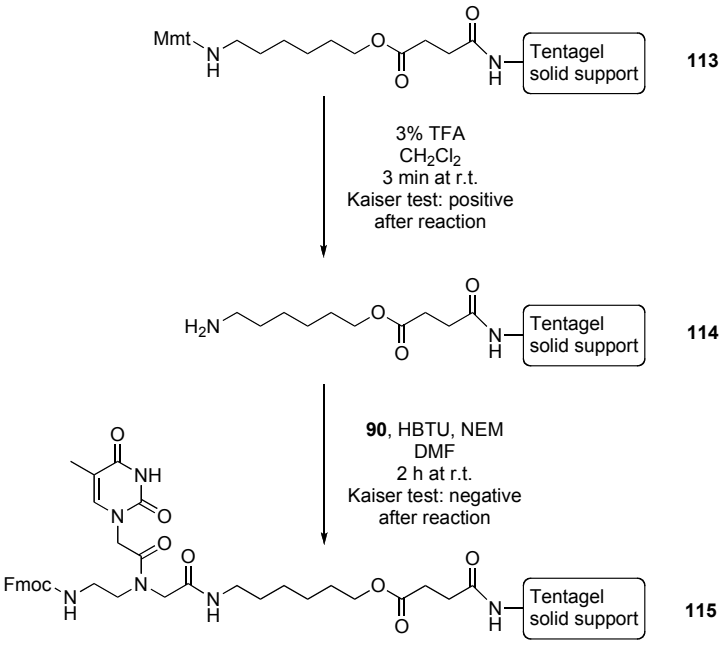

Scheme 10

At this stage a small sample of the resin was taken for analysis purposes. In order to analyse all the reactions shown in Scheme 10 had proceeded as planned, the derivatised resin sample **115** had to be subjected to cleavage, so that the target molecule **117** (Scheme 11) could be analysed by proton NMR. However, since the cleavage conditions involved treatment with a strong base, prior to the cleavage, the Fmoc group was deprotected and the resultant free amines were capped with acetic anhydride (Scheme 11). The cleavage reaction was then performed using concentrated aqueous ammonia (Scheme 11). The cleavage solution was collected and evaporated leaving a residue, which was analysed by proton NMR. The desired compound was not detected in the crude residue indicating that there was a problem occurring during the SPPS or the cleavage step. Repeating the cleavage on another sample of the resin gave the same unexpected result. The entire sequence of reactions was repeated with a fresh batch TentaGel, however, the same result was obtained yet again. Several factors in the synthesis were controlled: (i) the linker was resynthesized. It was tested following its attachment to the resin *i.e.* an Mmt deprotection was carried out and the reaction solution was analysed. The residual Mmt group was detected in the residue by proton NMR, indicating that the linker was correctly attached to the resin. (ii) The cleavage solution was changed from concentrated aqueous ammonia to hydrazine in DMF. (iii) The capping reagent was changed to Boc anhydride to increase the targets molecular mass and to improve its proton NMR detectability. (iv) Dissolution of the target compound in various polar solvents after cleavage was also attempted. Unfortunately, none of these changes yielded the desired

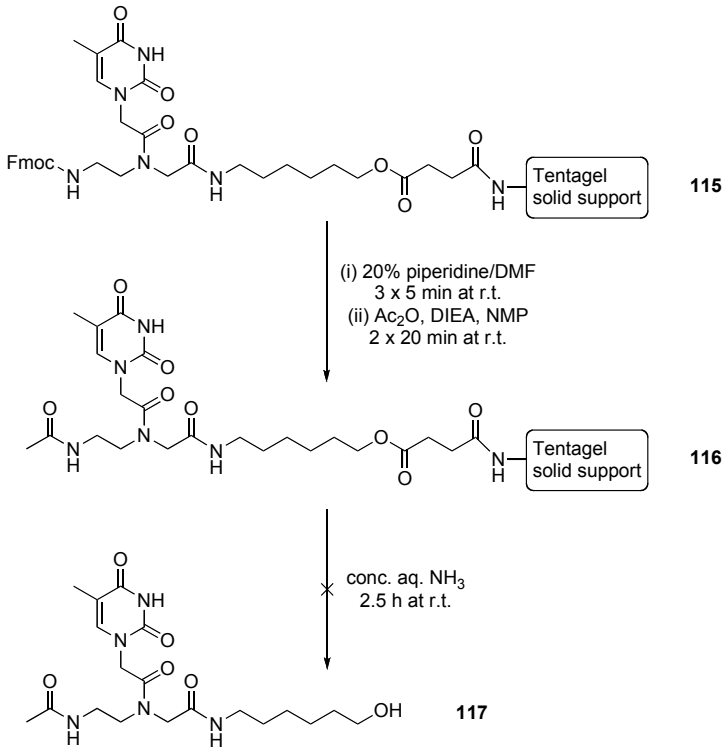

Scheme 11

product. At this point, without any clear reason as to why the desired compound was not obtained, it was decided that another resin should be evaluated, with an acid cleavable linker to determine definitively whether the base cleavable linker was the problem in this synthesis. The resin that was purchased was rink amide resin **118**. This resin was subjected to the same steps as before with the Tentagel resin (Scheme 12), with the following differences: the first step involved a Fmoc deprotection rather than an Mmt deprotection and also, a lysine was incorporated as the first monomer because it has been reported that it enhances the solubility of PNA oligomers and it also helps to induce helix formation during PNA duplex hybridisation.[237] The deprotection steps, as well as the coupling steps of the lysine and thymine PNA monomers proceeded as before (according to expected colours obtained following the Kaiser tests). A small sample of resin was cleaved using acidic conditions (4:1 TFA/*m*-cresol) and the resultant solution was dried *in vacuo* to give a white residue. The residue was analysed by proton NMR and it revealed the presence of desired compound **121**. Since the change of resin yielded the desired compound, it was decided that the PNA oligomers would be synthesized using the Rink amide resin. However, since the oligomers are cleaved from this resin in strong acidic conditions, the Fmoc/Mmt PNA synthesis strategy was no longer suitable. Thus the Mmt protecting group was replaced by the more robust Cbz-

protecting group, to ensure that PNA oligomers with protected nucleobases were cleaved from the Rink amide resin.

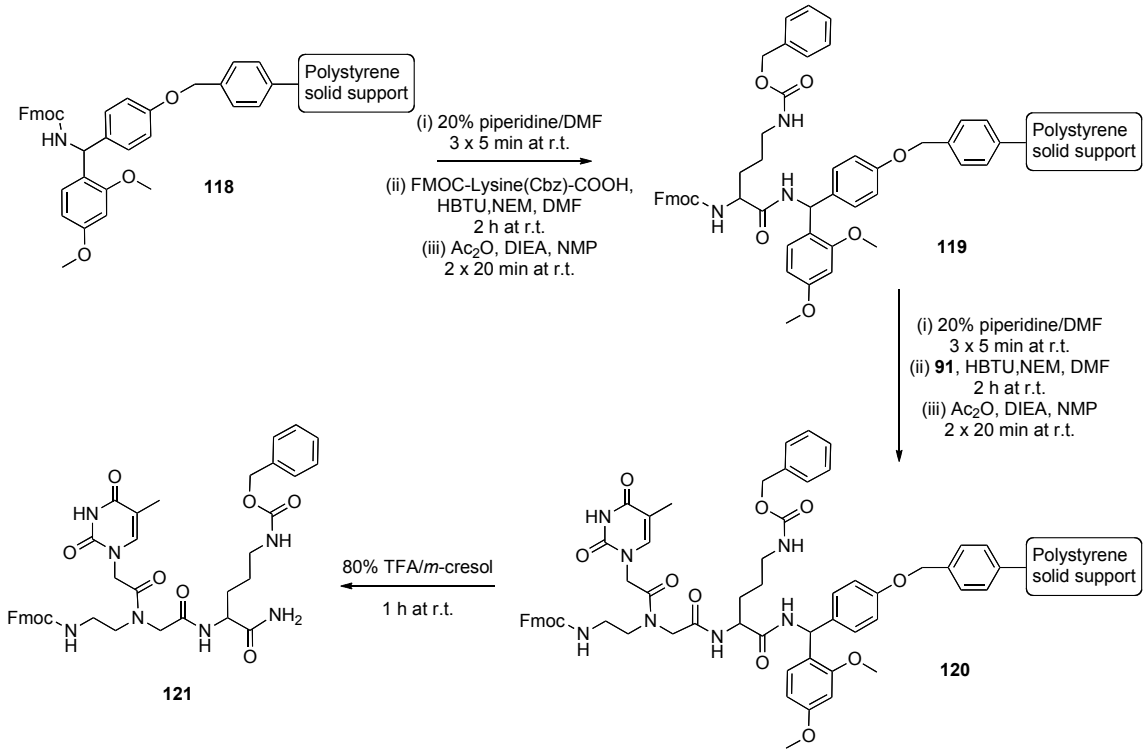

Scheme 12

2.1.4.2 Microwave-assisted PNA synthesis using the Fmoc/Cbz strategy

The recent advances in microwave assisted solid phase peptide synthesis, claiming improved purity of oligomer products using very short coupling times (*e.g.* 5 minutes),[199] led us to attempt performing the solid phase PNA oligomerisation using microwave irradiation. This was done using the Fmoc/Cbz strategy and Rink amide resin as the solid support. This section discusses our attempts to prepare the target PNA dodecamer (sequence: TTAATTAATTAA) using three different microwave systems, Biotage, CEM Discovery and CEM Liberty.

2.1.4.2.1 Oligomerisation using the Biotage microwave system

Since we did not have a microwave specifically designed for solid phase synthesis, a system was adapted in which a MacroKan (Figure 65) was filled with resin and was placed in a 5 ml microwave reactor tube designed for the Biotage microwave available in our

laboratory. The MacroKan is a polypropylene vessel designed for solid phase synthesis, which can seal the resin inside it by means of a cap. The walls of the vessel and cap are made of a mesh that allows the free flow of solutions through the walls. It was used to enable easier handling of the resin and also, it prevented any losses of resin that would have occurred during resin transfer, washing and filtration if the resin was not contained.

Figure 65

The microwave solid phase PNA oligomerisation was performed on a 200mg batch of Rink amide resin. Compound **119** was prepared as previously (Scheme 12), but then the oligomerisation cycles were performed in the microwave. Each oligomerisation cycle involved the following reactions: (i) Two deprotection reactions using 20% piperidine in DMF were carried out in the microwave at 60 °C for 30 seconds and 150 seconds respectively, with the resin being washed with DMF following every reaction. At this point, a Kaiser test was carried out on a few beads of resin to confirm that the deprotection had proceeded correctly. If the resin and solution turned blue (positive result indicating the presence of free amine functional groups), the cycle was continued. If a negative result (no colour change), or partial positive result (some beads remained colourless) was observed, then the deprotection reaction was repeated. (ii) Following the deprotection, a coupling reaction was carried out using the appropriate PNA monomer. The PNA monomer was dissolved in DMF, DIEA and HBTU were added, and upon dissolution of all the solids, the mixture was added to the resin bearing free amino groups. The reaction conditions were 5 minutes at 60 °C in the microwave. After the reaction, the resin was thoroughly washed with DMF, before a Kaiser test was carried out on a small sample of the resin once more. If any blue colour was observed, the coupling was repeated with a fresh reaction mixture. If no colour change was observed *i.e.* indicating that no more free amino groups were present on the resin, the next cycle was started. (iii) The capping step, normally used in manual SPPS, was omitted since it was reported as being unnecessary due to the high coupling yields achieved in the microwave.[199]

After preparing dimer **122** (sequence: TT, Figure 66) using two oligomerisation cycles, a small sample of the resin was taken for analysis, whilst the rest of the resin was washed with DMF, CH_2Cl_2 and Et_2O, it was dried thoroughly and stored in the freezer. The small sample of resin was cleaved by treating with TFA, yielding the crude PNA product, which was analysed by HPLC. This was done to monitor the progress of the SPPS, to ensure that no erroneous cycles occurred (relying on the Kaiser free amine test alone was insufficient). The analysis was performed by reverse phase HPLC using a gradient of 0.1% TFA in water to 0.1% TFA in acetonitrile. The HPLC chromatogram (Figure 67) obtained indicated the presence of a major peak at a retention time of 26.9 minutes. To confirm that the product was target dimer **122**, the crude sample was analysed by MALDI-TOF MS (Figure 68). The observed mass for **122** was m/z 1056.3824, which corresponded to the calculated mass of the $[M+Na]^+$ species: 1056.4192 ($C_{51}H_{59}N_{11}NaO_{13}$).

Once the structure of the dimer was confirmed, the resin was thawed, re-swollen and the oligomerisation of the PNA was continued. Another two oligomerisation cycles were performed before an analytical sample was cleaved and analysed. Surprisingly, the HPLC chromatogram indicated that a very impure tetramer crude product **123** was obtained (Figure 70) in comparison to the dimer crude product **122** (Figure 67). This meant that it was possible that the PNA was decomposing during storage on the resin. It was postulated that this could be because during the drying, the resin shrinks causing aggregation of the PNA oligomers in the pores of the resin, and subsequently decomposition. As a result of this observation, it was decided that if the resin bearing PNA had to be stored, it would be stored in the fridge in a swollen state, suspended in a mixture of 1:1 CH_2Cl_2/DMF. The latter storage method was tested, and it was confirmed (by HPLC analysis) that the PNA oligomers could be stored on the resin over several months without significant changes in the crude PNA oligomers obtained following resin cleavage.

In order to confirm whether the decomposition was due to the storage, or whether it arose due to the microwave irradiation, a small-scale trial was repeated using the same procedures. A hexamer PNA oligomer was synthesised using the microwave on a scale of 60 mg of resin. This synthesis was performed as rapidly as possible over two days reducing storage times as much as possible. 20 mg samples of the resin were taken at the dimer (Figure 66), tetramer (Figure 69) and hexamer (Figure 71) stages of the oligomer synthesis. The PNA oligomers were cleaved from these resin samples and were analysed by HPLC (Figure 72).

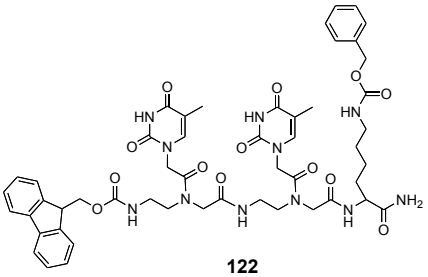

122

Chemical Formula: $C_{51}H_{59}N_{11}O_{13}$
Exact Mass: 1033.4294

Figure 66. Molecular structure of PNA dimer **122** (sequence: TT).

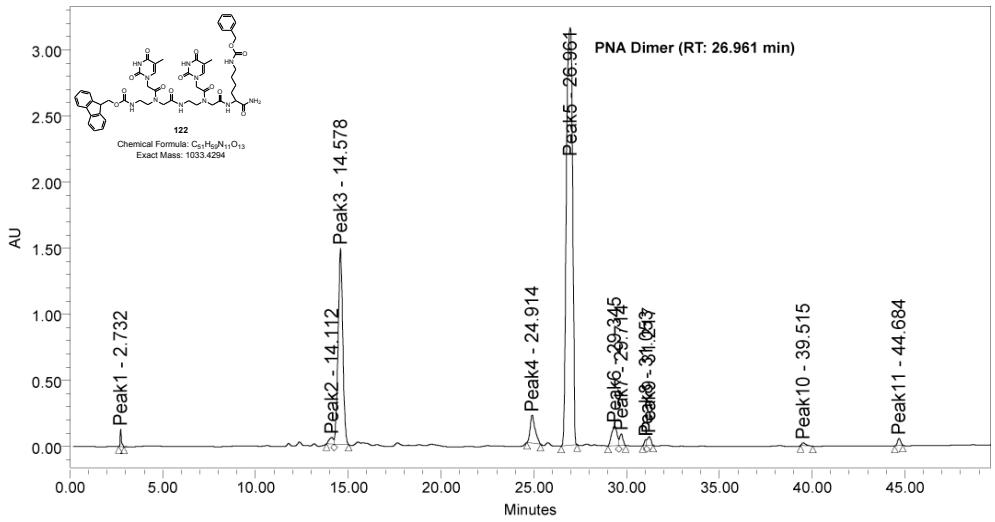

Figure 67. HPLC chromatogram of PNA dimer **122** prepared using microwave synthesis. (Agilent Zorbax SB-C18, 5 µm, 4.6 x 250 mm, gradient: 0.1% TFA in H_2O to 0.1% TFA in CH_3CN, flow: 1 mL/min, r.t.)

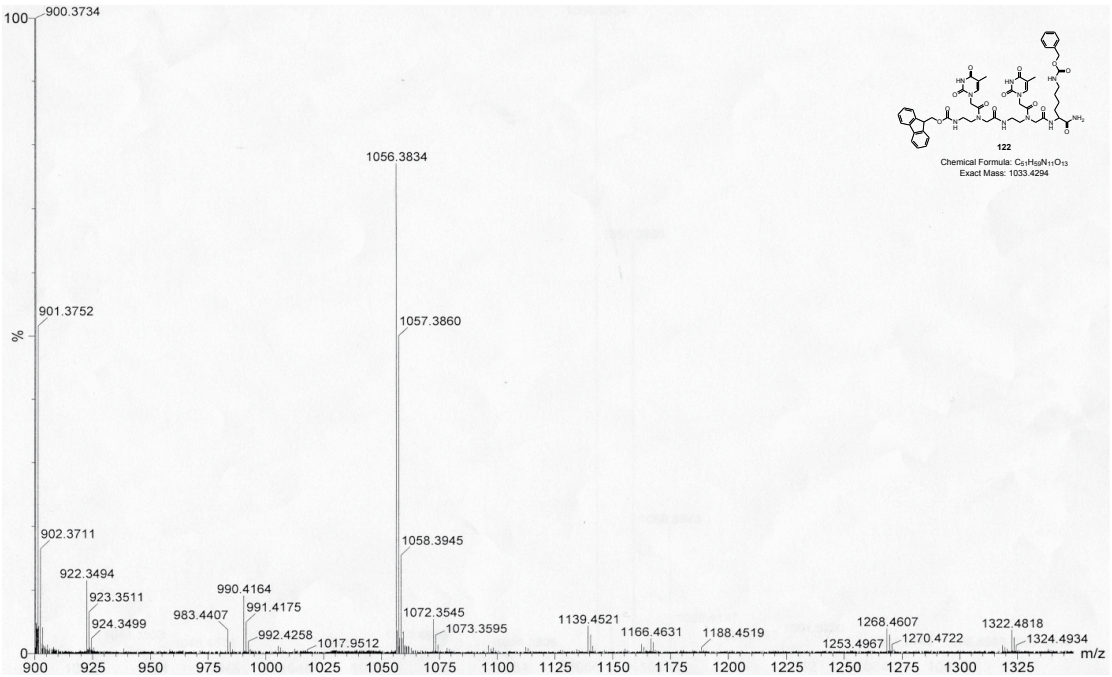

Figure 68. MALDI-TOF MS of crude PNA dimer **122** prepared using microwave synthesis.

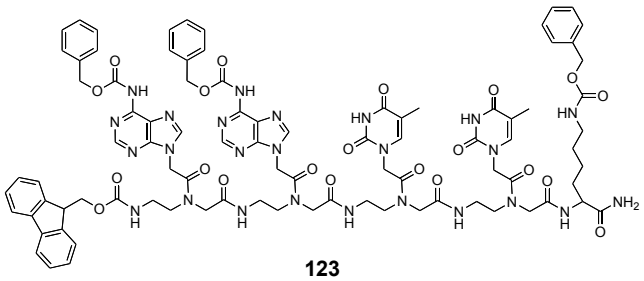

123

Chemical Formula: $C_{89}H_{97}N_{25}O_{21}$
Exact Mass: 1851.7291

Figure 69. Molecular structure of PNA tetramer **123** (sequence: TTAA).

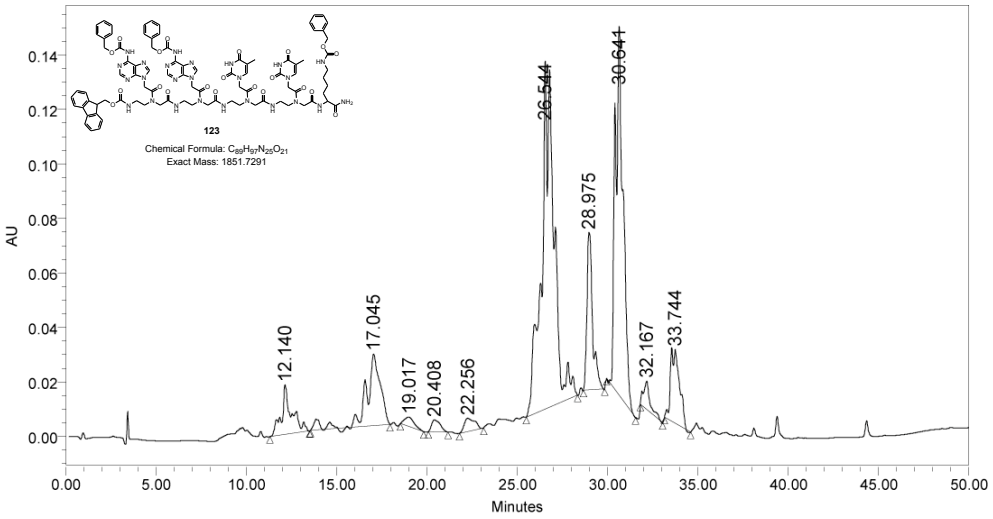

Figure 70. HPLC chromatogram of the PNA tetramer **123** prepared using microwave synthesis. (Agilent Zorbax SB-C18, 5 µm, 4.6 x 250 mm, gradient: 0.1% TFA in H_2O to 0.1% TFA in CH_3CN, flow: 1 mL/min, r.t.) Note: The resin bound PNA was dried and stored in the freezer over two days. This storage method is thought to cause the decomposition of the resin bound PNA.

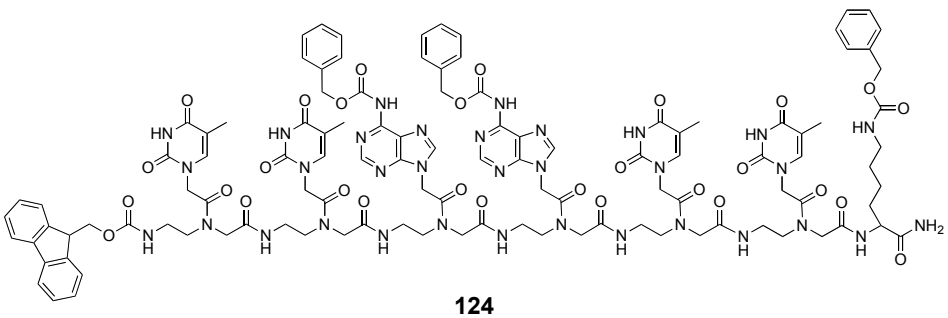

124

Chemical Formula: $C_{111}H_{125}N_{33}O_{29}$
Exact Mass: 2383.9321

Figure 71. Molecular structure of PNA hexamer **124** (sequence: TTAATT).

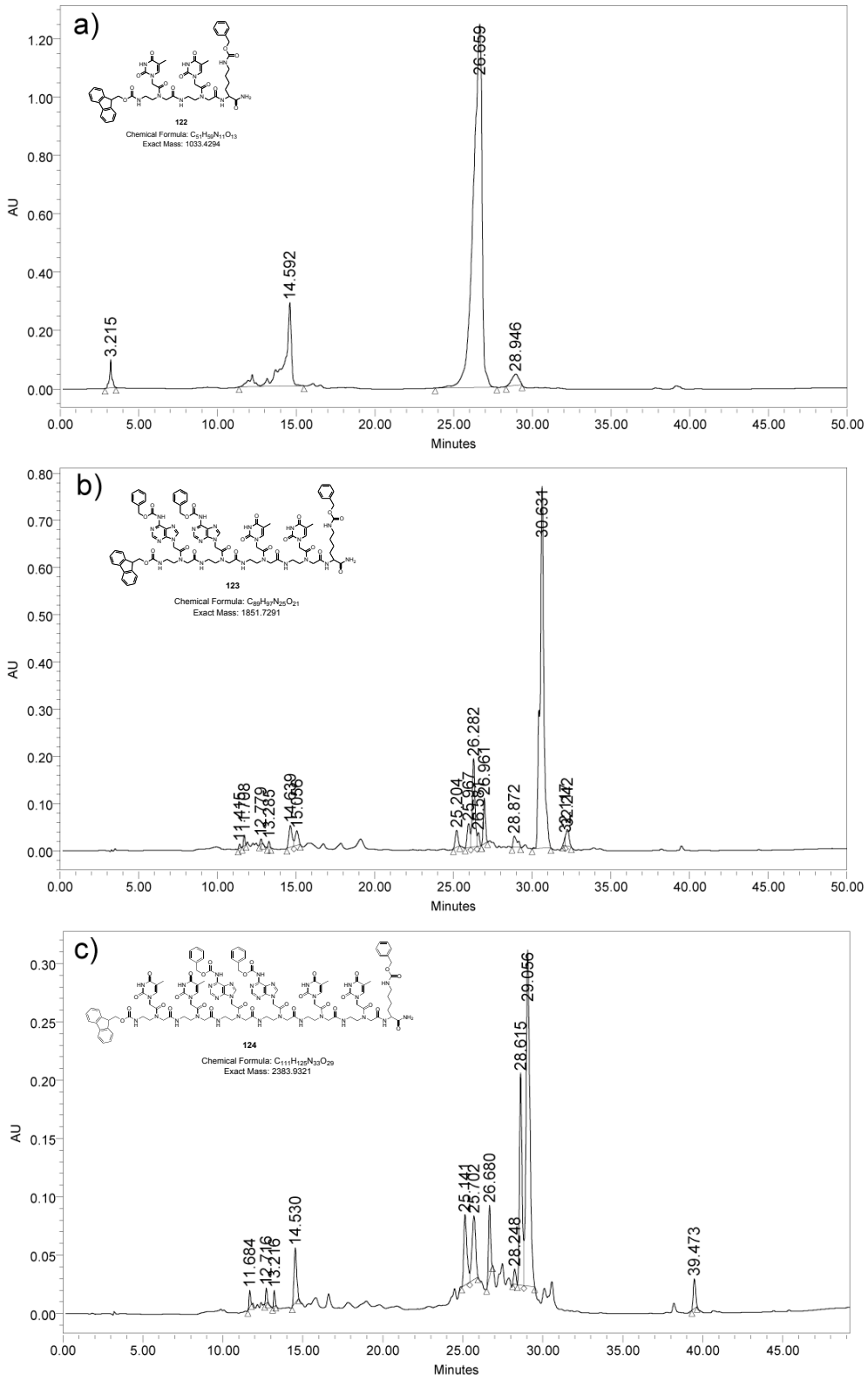

Figure 72. HPLC chromatograms of the crude PNA oligomers: (a) dimer **122**, (b) tetramer **123** and (c) hexamer **124**, prepared during the small-scale trial using microwave synthesis. (Agilent Zorbax SB-C18, 5 µm, 4.6 x 250 mm, gradient: 0.1% TFA in H_2O to 0.1% TFA in CH_3CN, flow: 1 mL/min, r.t.)

The purity of the crude tetramer **123** synthesized in the small scale trial (Figure 72b) was superior to the purity obtained in the previous attempt (Figure 70), thus confirming that the storage of the resin in the freezer was likely to have caused the decomposition in the first synthesis attempt. The HPLC chromatogram of the crude hexamer **124** indicated that there was an increase in the level of by-products in the crude material. The reduction of purity between the tetramer and hexamer was attributed to the fact that the quantity of resin had reduced to 20mg for the final two cycles in the synthesis, and in order to submerge the entire resin contained in the MacroKan in the coupling solution in the microwave reactor tube, a more dilute solution had to be used compared to the normal concentration of the coupling reagents' solution. This meant that the coupling may not have gone to completion even though the Kaiser test was negative following the coupling. If an incomplete coupling had occurred, various PNA oligomers could form after subsequent coupling cycles, and therefore could explain the increased number of peaks in the HPLC chromatogram of compound **124** (Figure 72c).

With promising results of the microwave solid phase synthesis up to the tetramer, and with a plausible explanation for the reduction in purity between the tetramer and hexamer, it was decided to attempt the dodecamer synthesis in the microwave at 200mg scale. The synthesis was performed over three subsequent days (4 deprotection/coupling cycles per day) to reduce storage time, and minimize any possible decomposition. The same procedures were used during the small-scale trial were applied, however, no dilution of the coupling solution was required to keep the resin submerged. Samples of the resin (20 mg) were taken at the tetramer **123**, octamer **125** (Figure 73) and dodecamer **126** (Figure 74) stages of the synthesis. The PNA oligomers were cleaved from the resin and were analysed by HPLC. The analysis was performed following the completion of the dodecamer sequence. Disappointingly, the analysis indicated that complex mixtures were obtained (Figure 75) in contrast to the relatively pure crude products obtained during the small-scale trial.

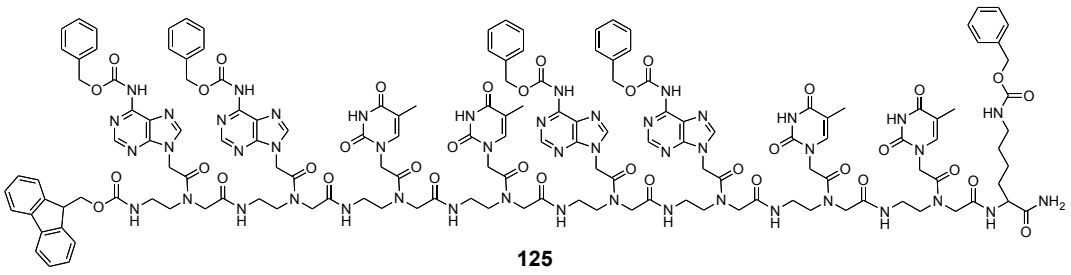

125

Chemical Formula: $C_{149}H_{163}N_{47}O_{37}$
Exact Mass: 3202.2318

Figure 73. Molecular structure of PNA octamer **125** (sequence: TTAATTAA).

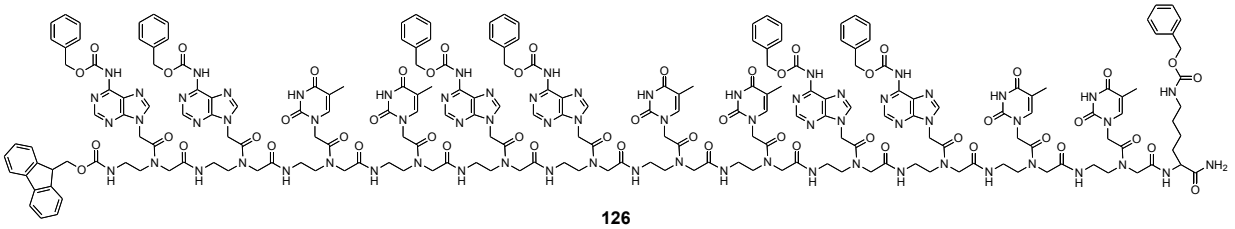

126

Chemical Formula: $C_{209}H_{229}N_{69}O_{53}$
Exact Mass: 4552.7345

Figure 74. Molecular structure of PNA dodecamer **126** (sequence: TTAATTAATTAA).

Two possible explanations were postulated: the first was that incomplete coupling caused the synthesis of many different PNA sequences. The reduction in quality of the crude products from **123** to **126**, judging from the HPLC chromatograms (Figure 75) supports this hypothesis. The incomplete coupling may have been caused by an insufficient amount of agitation of the resin within the MacroKan. The maximum stirring rate in the microwave was 900rpm. When microwave reactor set up including the MacroKan and resin was tested on a normal stirrer at this speed, the resin had a tendency to remain at the bottom of the MacroKan without significant suspension and movement. The lack of movement and suspension could have prevented the reagents in the coupling solution from reaching all the oligomers' reactive terminals in the pores of the resin, and therefore, no coupling reactions would have occurring at those sites. The second possibility was that the microwave irradiation itself, which sometimes peaked at 100W of power, could have caused the decomposition of the PNA on the resin. The procedure that was followed[199] suggested using only 10W of power during coupling reaction, however, this power was insufficient to heat the solution to the desired temperature of 60 °C in our microwave setup. It must be noted that *Bacsa et al.*[199] were using a CEM Discover SPS microwave designed for solid phase synthesis, which utilised a completely different set up, thus the power settings of the two microwaves are not directly comparable.

2.1.4.2.2 Oligomerisation using the CEM Discovery SPS microwave system

Further attempts to prepare target PNA dodecamer **126** (sequence: TTAATTAATTAA) using microwave irradiation were performed on two different CEM microwaves, the CEM Discover SPS and CEM Liberty. The CEM suppliers in Belgium made both machines available to our laboratories for a few days for testing. First, the CEM Discover SPS microwave was used. This microwave was equipped with a vessel specially designed for solid phase synthesis in the microwave (Figure 76). The vessel into which the resin was placed was designed to retain the resin on a polyethylene filter and was equipped

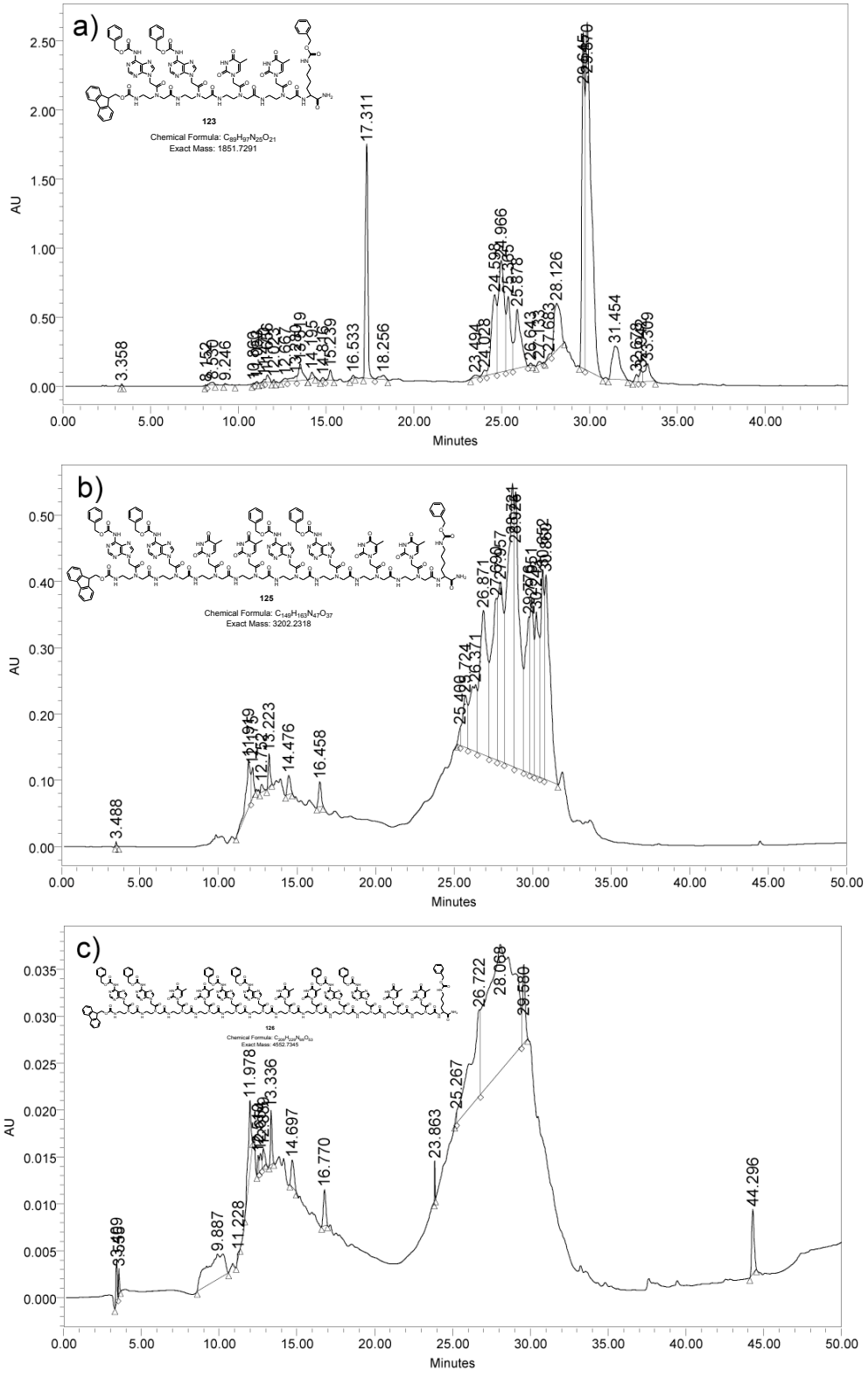

Figure 75. HPLC chromatograms of the crude PNA oligomers: (a) tetramer **123**, (b) ocatamer **125** and (c) dodecamer **126** prepared using microwave-assisted solid phase synthesis with the Biotage microwave system. (Agilent Zorbax SB-C18, 5 µm, 4.6 x 250 mm, gradient: 0.1% TFA in H_2O to 0.1% TFA in CH_3CN, flow: 1 mL/min, r.t.)

with Teflon Seal Ball to close the vessel, preventing the reaction solutions from exiting. Furthermore, it was equipped with a fiberoptic temperature probe to monitor the temperature, and also a gas inlet (not shown in Figure 76) to allow for nitrogen bubbling of the solutions with the scope of agitating the resin during reactions. The reaction vessel was removable as shown in Figure 76, and could be attached to the washing module provided with the microwave that was designed to facilitate the filtration and washing of the resin following the reactions. Using the conditions described by *Bacsa et al.*[199] including the microwave irradiation powers, the dodecamer synthesis was attempted once more on a scale of 200 mg of resin. As in the previous attempt, the synthesis was performed over three subsequent days (4 deprotection/coupling cycles per day). Samples of the resin (20 mg) were taken at the tetramer **123**, octamer **125** and dodecamer **126** stages of the synthesis. The PNA oligomers were cleaved from the resin and were analysed by HPLC. The HPLC chromatograms are shown in Figure 77.

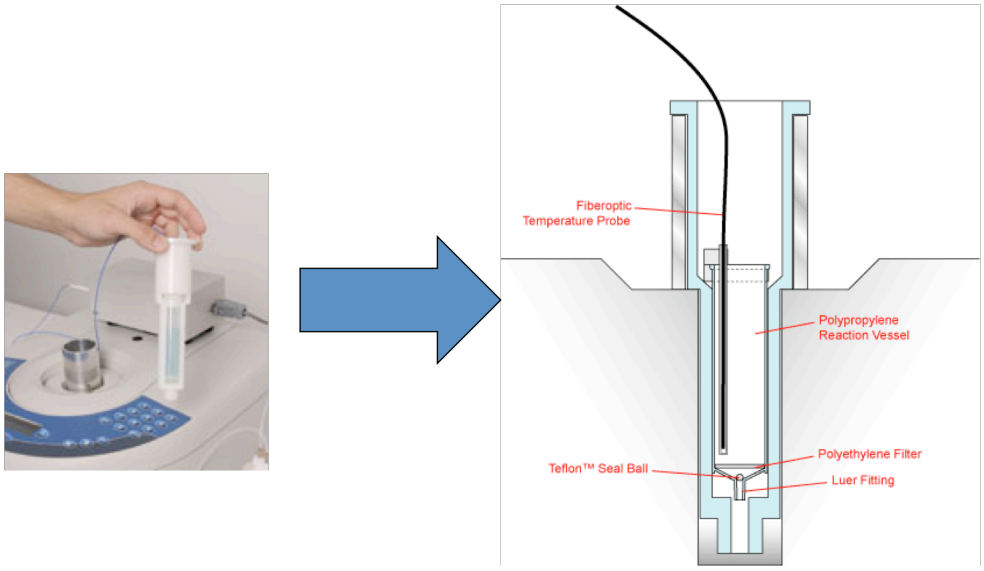

Figure 76. The CEM Discover SPS setup for solid phase microwave synthesis.

The HPLC results obtained following the oligomer synthesis using the CEM Discover SPS microwave were an improvement over the last microwave synthesis attempt (using the Biotage microwave), yet the purity was still too poor in the case of the dodecamer to carry out a purification by semi-preparative HPLC. We would have liked to repeat the synthesis using this machine, to include a capping step in the oligomerisation in an attempt to reduce the number of side products, however, since the machine was in our laboratories for only one week, this experiment could not be performed. These HPLC analysis results were discussed with the suppliers of the CEM Discover SPS and they suggested attempting the same synthesis on a CEM Liberty microwave.

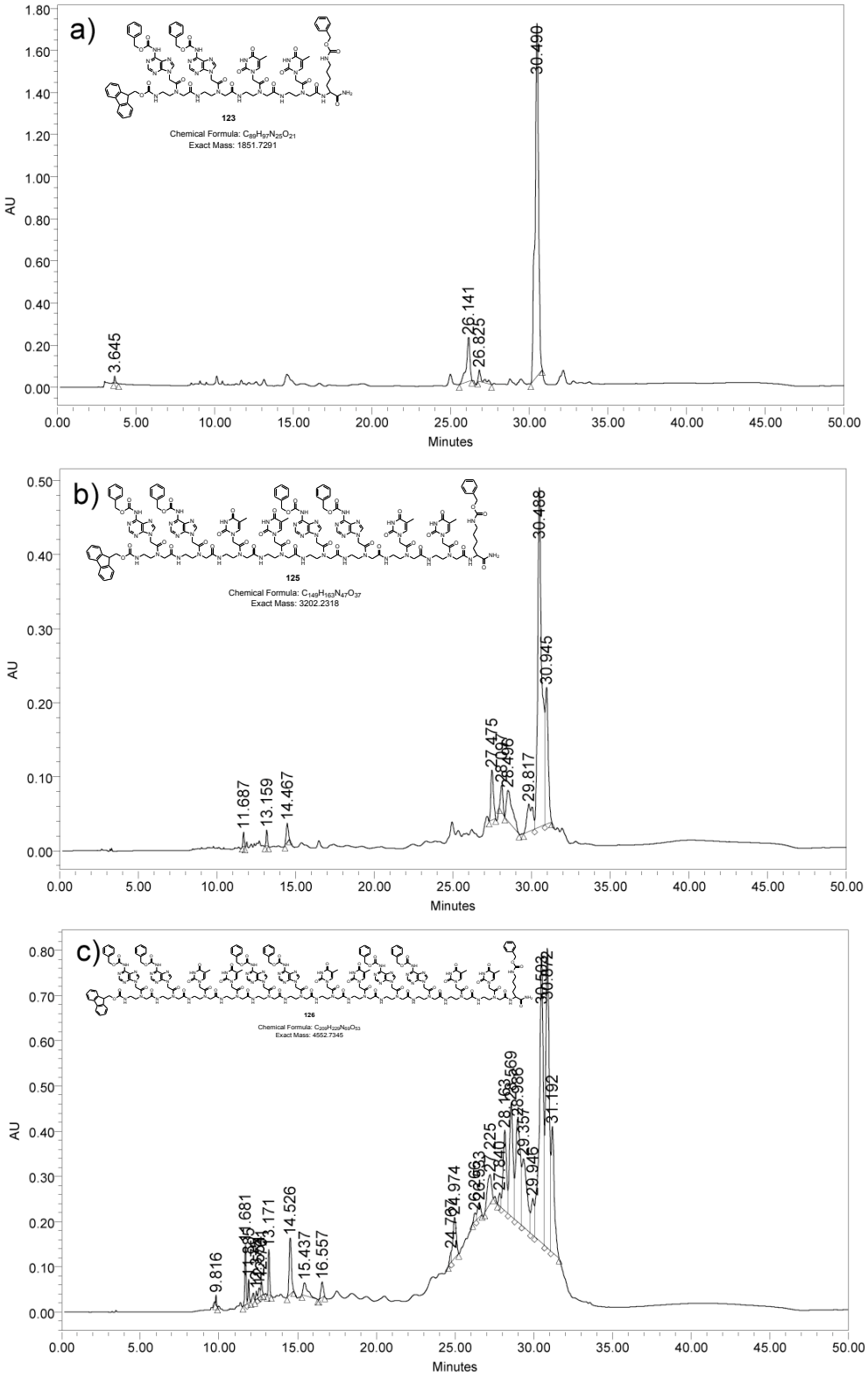

Figure 77. HPLC chromatograms of the crude PNA oligomers: (a) tetramer **123**, (b) ocatamer **125** and (c) dodecamer **126** prepared using microwave-assisted solid phase synthesis with the CEM Discover SPS microwave. (Agilent Zorbax SB-C18, 5 µm, 4.6 x 250 mm, gradient: 0.1% TFA in H_2O to 0.1% TFA in CH_3CN, flow: 1 mL/min, r.t.)

2.1.4.2.3 Oligomerisation using the CEM Liberty microwave system

The CEM Liberty microwave was based on the same setup as the CEM discover SPS microwave, however, it included an attachment making it a fully automated microwave peptide synthesizer. Using the automated machine, the synthesis time to produce target dodecamer **126** was less than 24 hours. With the assistance of the CEM technicians, the automated synthesis was set up. The oligomerisation cycle was set up to include a capping step (using 20% Ac_2O in DMF) in this trial. Since the oligomerisation was automated, samples could not be taken at the intermediate stages of the synthesis, therefore, an analytical sample of the crude dodecamer **126** was cleaved from the resin upon completion of the synthesis. The crude product was analysed by HPLC (Figure 78). Once more, using microwave irradiation during the solid phase oligomer synthesis resulted in a complex, inseparable mixture. Due to the poor results obtained using microwave irradiation, it was decided that the oligomer synthesis would be attempted by the conventional manual solid phase synthesis method during the remainder of the project. It must be noted, however, that in 2010, *Gait* and coworkers[238] optimised the microwave-assisted solid phase PNA synthesis using the CEM Liberty machine to prepare a 23mer sequence of PNA. The PNA oligomers in their case were synthesized from commercially available Fmoc/Bhoc protected monomers using Rink-Amide ChemMatrix (Matrix Innovation) solid support, and PyBOP (benzotriazol-1-yltris-pyrrolidinophosphonium hexafluorophosphate) as the coupling agent.

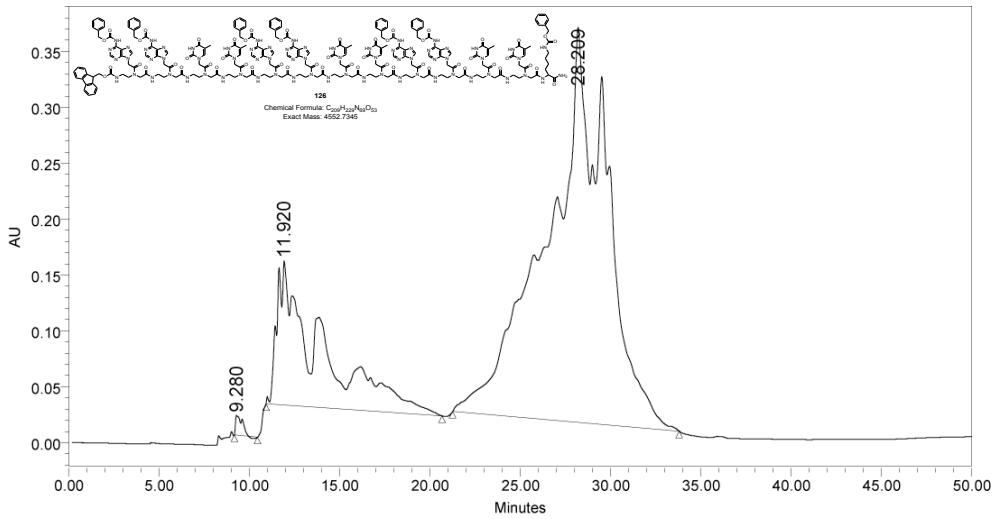

Figure 78. HPLC chromatogram of the crude PNA dodecamer **126** using microwave-assisted solid phase synthesis with the CEM Liberty microwave. (Agilent Zorbax SB-C18, 5 µm, 4.6 x 250 mm, gradient: 0.1% TFA in H_2O to 0.1% TFA in CH_3CN, flow: 1 mL/min, r.t.)

2.1.4.3 Isolation of the target oligomer via manual solid phase synthesis of PNA using the Fmoc/Cbz strategy

Following the unsuccessful microwave-assisted oligomer syntheses, it was decided that the PNA would be synthesized using the conventional solid phase synthesis method. This section describes the manual solid phase synthesis method with which protected target PNA dodecamer **126** (sequence: TTAATTAATTAA) was isolated.

Following advice obtained from a collaborating group working on peptide synthesis, several technical aspects of the synthesis were taken into consideration: (*i*) the loading of the resin with respect to the reactive amino groups was controlled to a lower value that is more suitable for PNA synthesis such as 0.4 mmol/g (instead of 0.64 mmol/g previously). The lower loading can lower aggregation of the oligomers on the resin, thus lowering the number of by-products; (*ii*) Coupling reactions were carried out in NMP instead of DMF because NMP is a better solvent for coupling agents (*e.g.* HBTU) and thus allows the concentration of the coupling solution to be higher. (*iii*) The PNA monomer was added at a slight excess with respect to the coupling reagent (HBTU) because the coupling reagent is also reactive towards amino groups and can cap these reactive sites preventing the desired coupling reactions; (*iv*) The PNA monomer was pre-activated at 45 °C for 5 minutes with the coupling agent and base prior to its introduction to resin bearing the free amino group. This ensured that all the PNA monomers' carboxyl groups were activated prior to being mixed with the free amino groups. Also, this preactivation ensured that no free coupling agent was present in the coupling solution, thus preventing its reaction with the free amino groups on the growing oligomer; (*v*) The deprotection of the Fmoc-protecting groups had to be done as rapidly as possible. This was done to minimize two known side reactions, *N*-acyl transfer[206] and *N*-terminal deletion[203] reactions (Scheme 13), since it is known that they occur under basic conditions when the terminal amino group is deprotected. These reactions can markedly reduce the purity of the crude product since new species are formed.

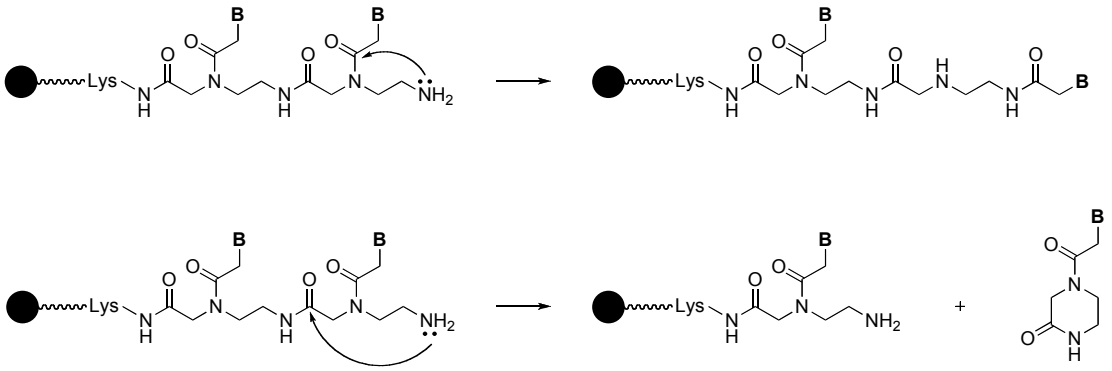

Scheme 13

Taking into consideration the factors described above, it was shown that the coupling reaction was complete after only 15 minutes at room temperature,[239] however, due to the time needed to prepare the materials for each cycle, a coupling reaction time of 30 minutes was preferred. This protocol was used to prepare the dodecamer and was completed in only two days (6 deprotection/coupling/capping cycles per day). The dodecamer was prepared on a scale of 200mg of resin. The lysine derivative of the resin **119** was prepared, however, by controlling the amount of lysine and HBTU added to the resin, the loading of the commercial Rink resin was reduced from 0.64 mmol/g to 0.4 mmol/g. Once this step was complete, the solid phase PNA synthesis was performed with repetitive cycles of deprotection, coupling and capping as summarized in Scheme 14. Deprotection of the terminal Fmoc protecting group was carried out using 20% piperidine in DMF. The reaction was carried out twice, first for two minutes, and then with a fresh solution for ten minutes. After the second exposure, the resin was washed thoroughly with DMF. At this point, a Kaiser test was carried out on a few beads of resin to confirm that the deprotection had proceeded correctly. Next, a coupling reaction was carried out using the appropriate PNA monomer. Five equivalents of the PNA monomer was dissolved in NMP, HBTU (4.5 eq) and DIEA (12 eq) were added, and mixture was activated at 45 °C for five minutes before being added to the resin bearing free amino groups. The reaction was allowed to proceed for 30 minutes, after which the resin was washed thoroughly using DMF. Once again, a Kaiser test was carried out on a small sample of the resin. If a positive test was obtained, the coupling was repeated. If a negative test was obtained, the capping procedure was performed. During the capping procedure the derivatised resin is exposed to acetic anhydride in NMP for 5 minutes at room temperature to block any minor traces of free amino groups left on the growing oligomer, thus preventing erroneous sequences from forming as by-products. Following the capping the cycle was restarted from the deprotection step. Once the desired length of the PNA oligomer was reached, the resin was cleaved using TFA to yield the crude oligomer.

Samples (20 mg) of the derivatised resin were taken at the tetramer **123**, octamer **125** and dodecamer **126** stages of the oligomer synthesis. The PNA oligomers were cleaved from the resin and were analysed by HPLC. Very good results were finally observed in the HPLC chromatograms in that the crude PNA oligomers that were obtained were relatively pure, and a major product could be identified in each case (Figure 79). Satisfied with the analytical results, the purification of all the samples was performed using semi-preparative scale HPLC. Following the purification, the samples were analysed by analytical HPLC to verify their purity (Figure 80). Once the PNA oligomers were confirmed to be pure, the samples were sent for analysis by MALDI-TOF MS.

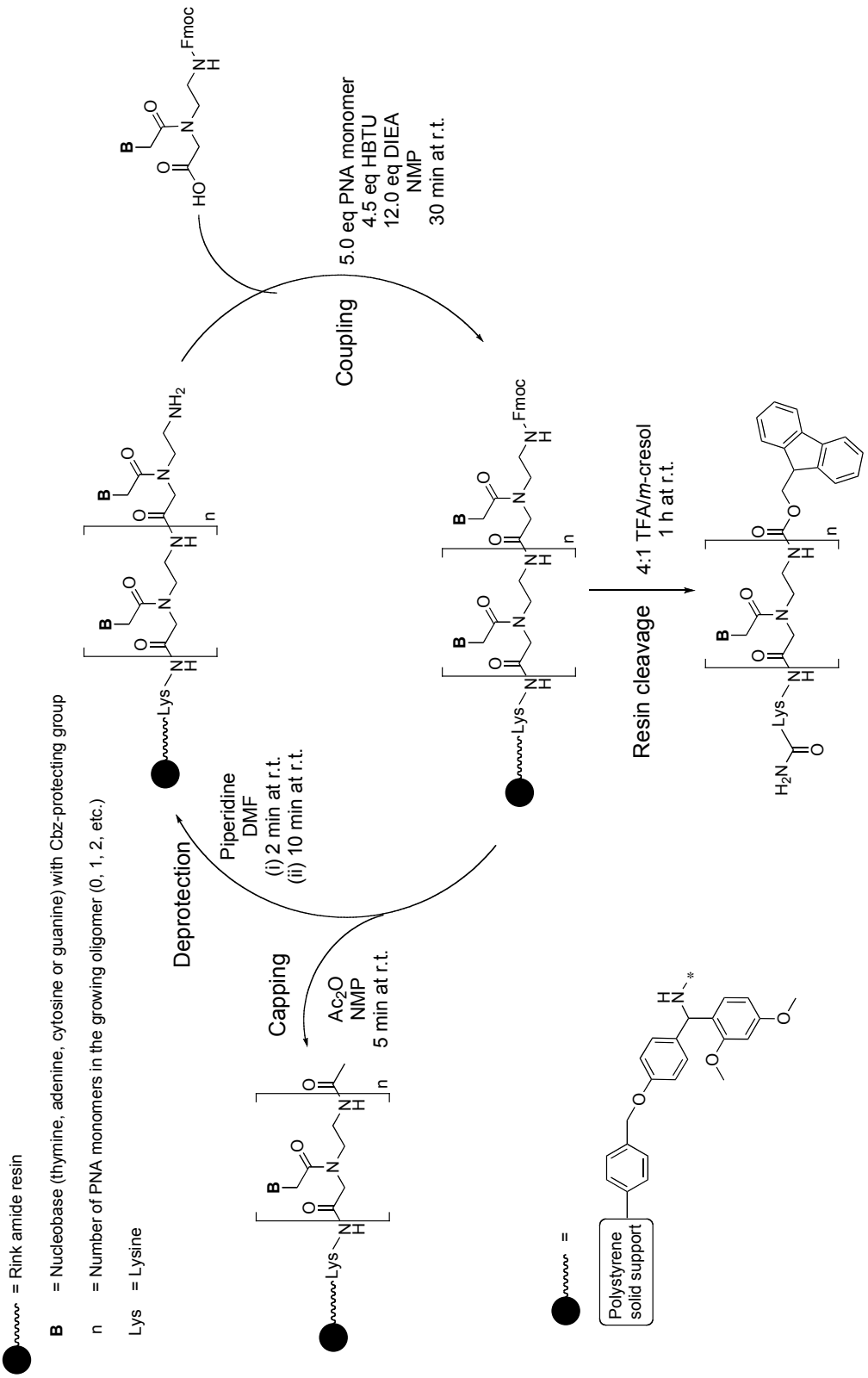
= Rink amide resin
B = Nucleobase (thymine, adenine, cytosine or guanine) with Cbz-protecting group
n = Number of PNA monomers in the growing oligomer (0, 1, 2, etc.)
Lys = Lysine
Coupling
5.0 eq PNA monomer
4.5 eq HBTU
12.0 eq DIEA
NMP
30 min at r.t.
Deprotection
Piperidine
DMF
(i) 2 min at r.t.
(ii) 10 min at r.t.
Capping
Ac2O
NMP
5 min at r.t.
Resin cleavage
4:1 TFA/m-cresol
1 h at r.t.
Polystyrene solid support

Scheme 14

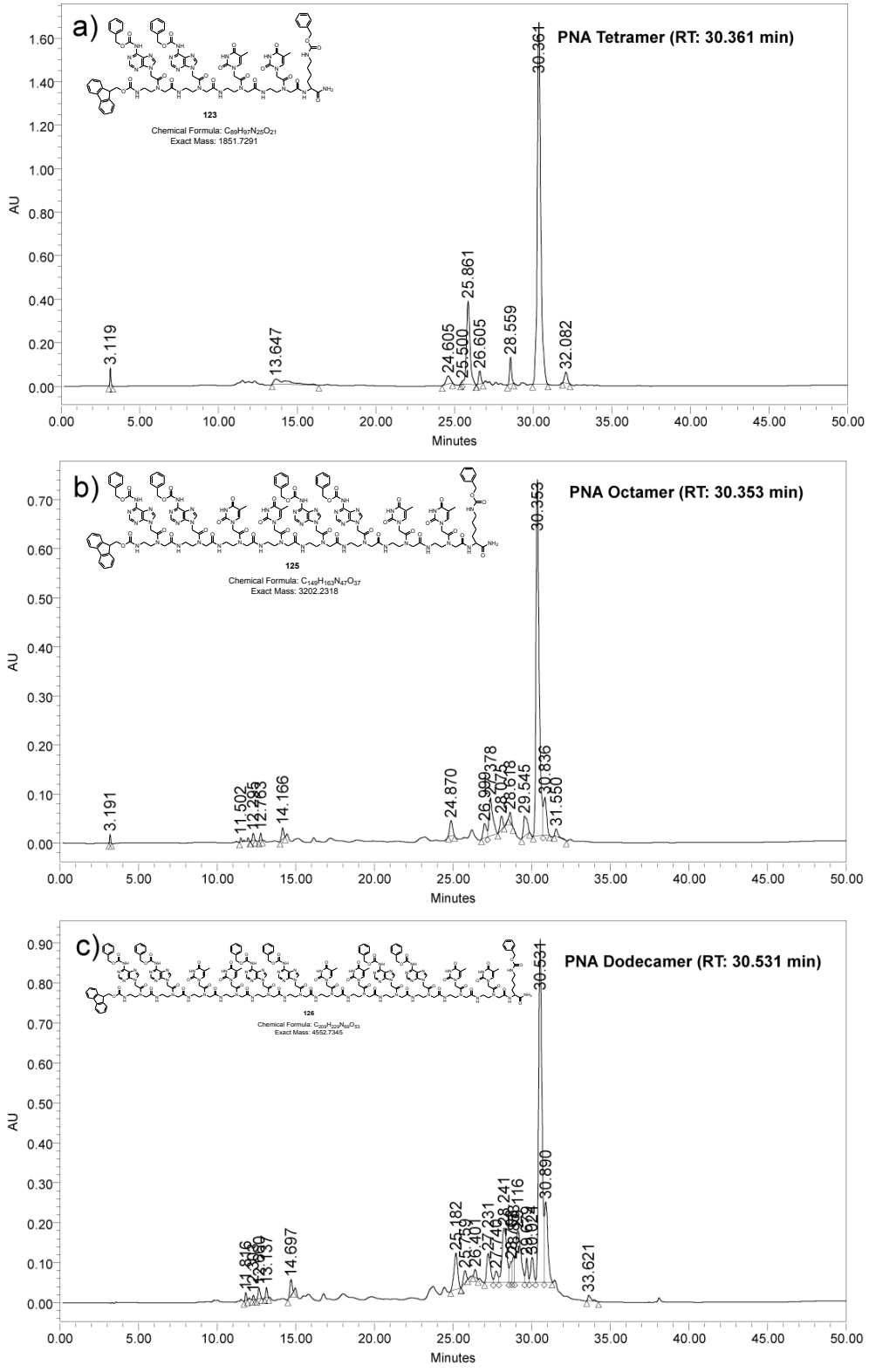

Figure 79. HPLC chromatograms of the crude PNA oligomers: (a) tetramer **123**, (b) ocatamer **125** and (c) dodecamer **126** prepared using the manual solid phase synthesis protocols. (Agilent Zorbax SB-C18, 5 µm, 4.6 x 250 mm, gradient: 0.1% TFA in H_2O to 0.1% TFA in CH_3CN, flow: 1 mL/min, r.t.)

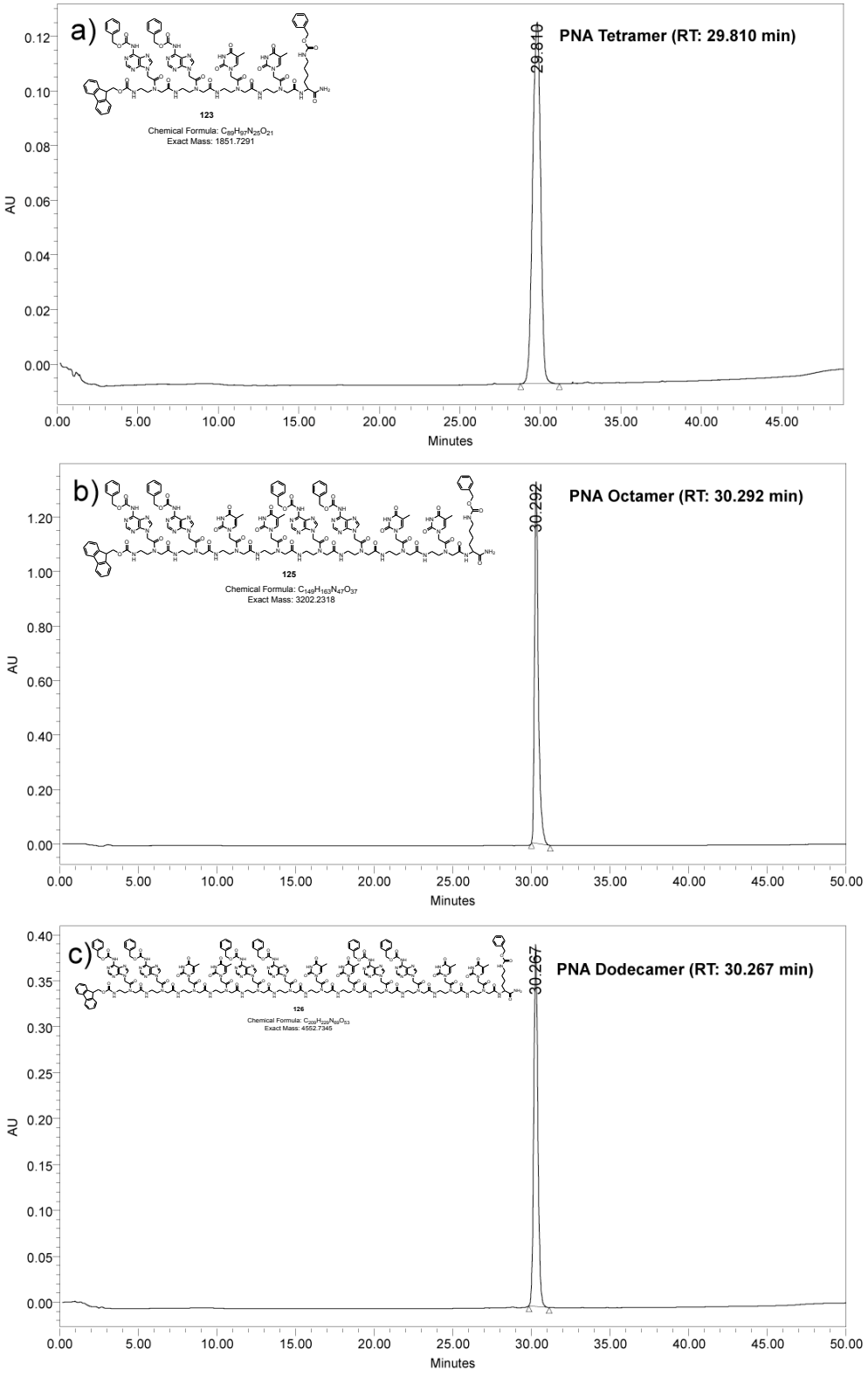

Figure 80. HPLC chromatograms of the purified PNA oligomers: (a) tetramer **123**, (b) ocatamer **125** and (c) dodecamer **126** prepared using the manual solid phase synthesis protocols. (Agilent Zorbax SB-C18, 5 µm, 4.6 x 250 mm, gradient: 0.1% TFA in H_2O to 0.1% TFA in CH_3CN, flow: 1 mL/min, r.t.)

The major peak in each of the mass spectra obtained was not the expected $[M+H]^+$ mass ion. However, on closer analysis of the spectra, it was clear that fragmentation of the compounds was occurring during the ionisation in the MALDI-TOF analysis. The fragmentation was occurring within the Fmoc and Cbz protecting groups that were cleaved at the carbon-oxygen bond of the carbamate moiety resulting in two fragments, F1 and F2 (Figure 81). However, despite identifying a fragmentation pattern, the presence of the desired PNA oligomers, still had to be conclusively confirmed. Analysis of the compounds by ESI-MS was attempted in order to obtain confirmation that the expected compounds had been obtained, however, none of the oligomers were detected by this technique. The lack of easily ionisable functional groups is a possible reason for the fragmentation observed by MALDI-TOF-MS and the lack of ionisation altogether in ESI-MS.

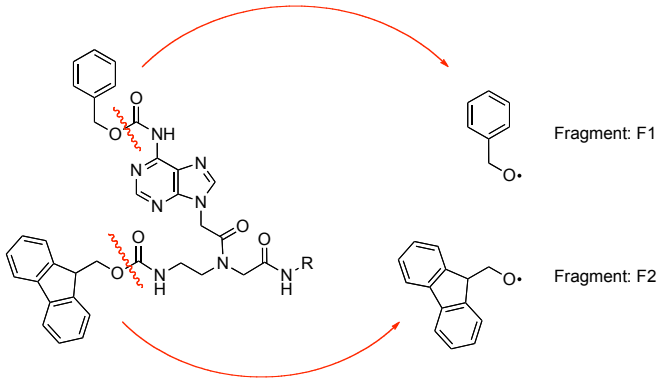

Figure 81. The fragmentation of the Fmoc and Cbz groups into fragments F1 and F2 observed by MALDI-TOF-MS.

Figure 82 shows the MALDI-TOF mass spectrum of the tetramer **123**. The mass spectrum shows the presence of this compound's $[M+H]^+$ ion (m/z 1852.81) in a minor quantity which gives confidence that the desired compound was isolated. The exact mass found for this peak was m/z 1852.7424, which corresponded to the $[M+H]^+$ peak of **123** ($C_{89}H_{98}N_{25}O_{21}$) which has a calculated mass of m/z 1852.7369. Also, two of the peaks observed in the spectrum could be assigned. The peak at m/z 1744.75 corresponded to ionisation-induced fragmentation of a Cbz protecting group at the position indicated in Figure 81, yielding the fragment of $[M\text{-}F1]^+$ or $[M\text{-}C_7H_7O]^+$. Similarly, the peak at m/z 1658.66 corresponds to the ionisation-induced fragmentation of the Fmoc protecting group at the position indicated in Figure 81, yielding the fragment of $[M\text{-}F2]^+$ or $[M\text{-}C_{14}H_{11}O]^+$. Unfortunately, the remaining peaks could not be assigned.

In Figure 83, the MALDI-TOF-MS of the PNA octamer **125** is displayed. The mass spectrum shows the presence of this compound's $[M+H]^+$ ion (m/z 3203.32) in a very minor quantity, once again giving confidence that the target molecule had been isolated. The exact mass found for this peak was m/z 3203.2512, which corresponded to the $[M+H]^+$ peak of **125**

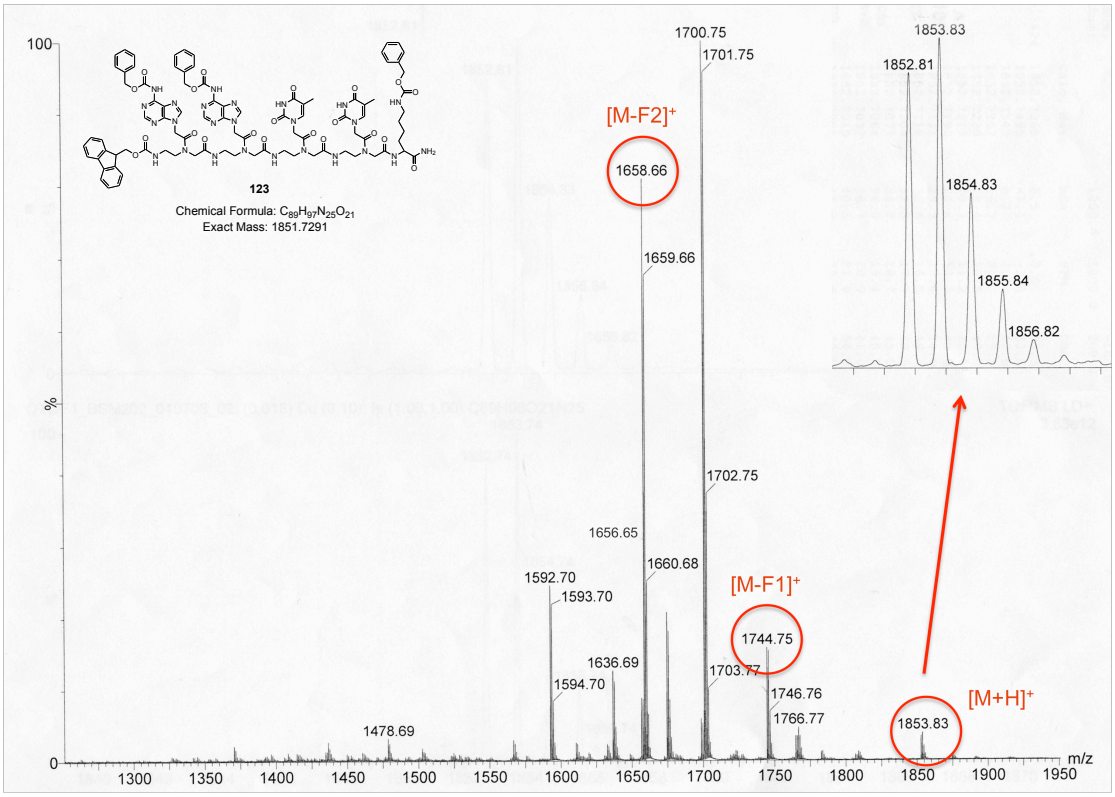

Figure 82. MALDI-TOF-MS of the PNA tetramer **123**.

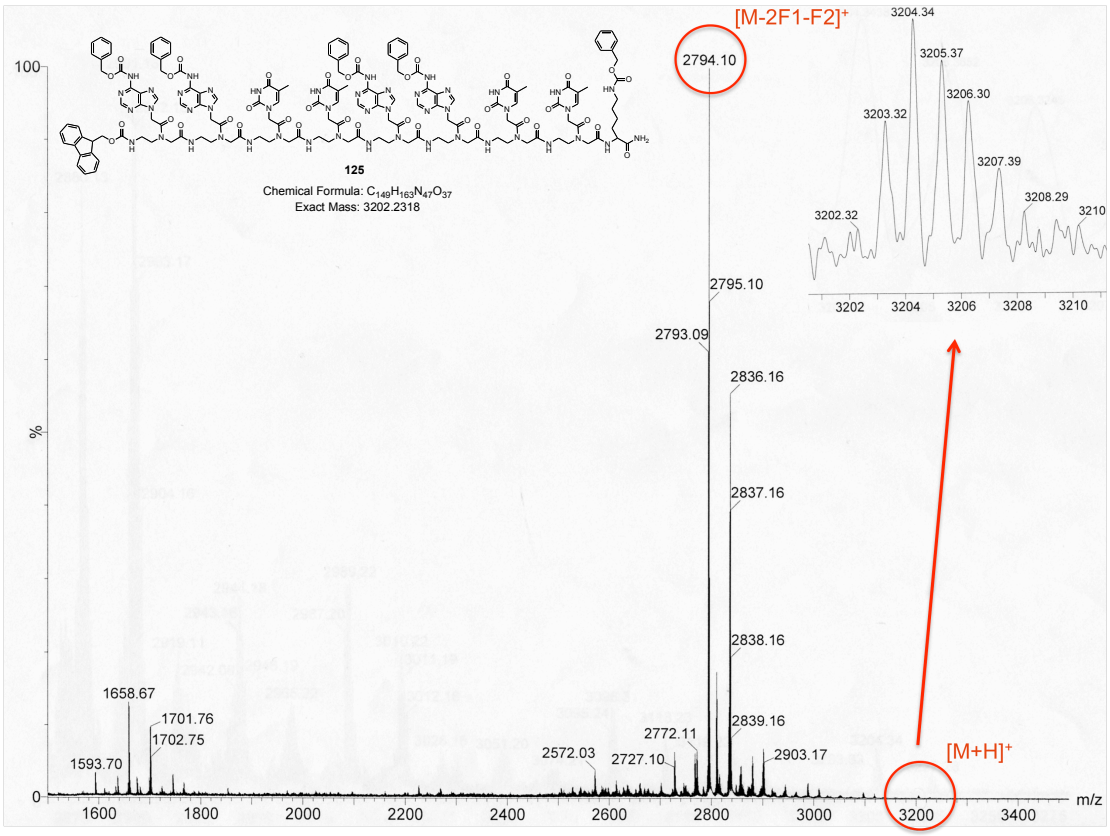

Figure 83. MALDI-TOF-MS of the PNA octamer **125**.

($C_{149}H_{164}N_{47}O_{37}$) which has a calculated mass of m/z 3203.2396. Also, another peak observed in the spectrum could be assigned. The peak was found at m/z 2794.10, and it corresponded to the ionisation-induced fragmentation of the Fmoc and two Cbz protecting groups at the positions indicated in Figure 81, yielded the species $[M\text{-}2F1\text{-}F2]^+$ or $[M\text{-}C_{28}H_{25}O_3]^+$.

The MALDI-TOF-MS of the dodecamer **126** is shown in Figure 84. The calculated mass for **126** ($C_{209}H_{229}N_{69}O_{53}$) is 4552.7345. Unfortunately, the $[M+H]^+$ ion was not observed in the mass spectrum, so the exact mass could not be confirmed. However, as with **123** and **125**, a fragmentation pattern allowed the assignment of several peaks. The mass ion at m/z 4145.63 corresponded to the ionisation-induced fragmentation resulting in $[M\text{-}2F1\text{-}F2]^+$ or $[M\text{-}C_{28}H_{25}O_3]^+$. The peak at m/z 4036.53 corresponded to the ionisation-induced fragment $[M\text{-}3F1\text{-}F2]^+$ or $[M\text{-}C_{35}H_{32}O_4]^+$. The peak at m/z 3929.47 was also assigned and it corresponded to the ionisation-induced fragment $[M\text{-}4F1\text{-}F2]^+$ or $[M\text{-}C_{42}H_{39}O_5]^+$.

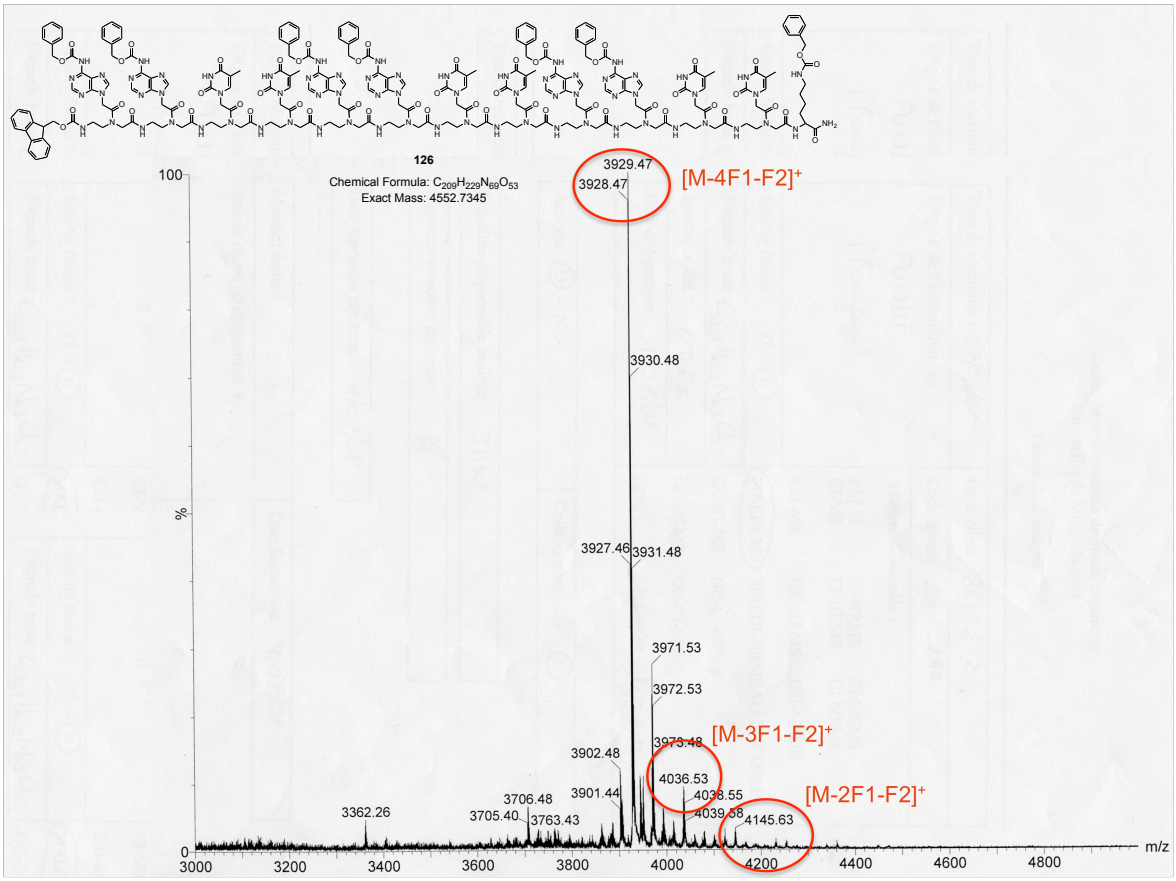

Figure 84. MALDI-TOF-MS of the PNA dodecamer **126**.

With these mass spectra of the respective oligomers, it was reasonable to suggest that the desired compounds had been isolated, however, definitive proof was still required in order to be completely certain. Since ionisation by ESI-MS was not possible for these compounds,

the only manner to be completely certain of the dodecamer was to render it more easily ionisable. This could be achieved by the complete deprotection of the dodecamer sequence.

2.1.4.4 Deprotection of the PNA dodecamer

The deprotection of PNA dodecamer **126** was required to definitively confirm that the target oligomer had been obtained, and also to establish a method for the solution phase deprotection of the PNA oligomer. This section describes the steps taken to develop a protocol to deprotect the Cbz-protecting groups on the nucleobases.

The deprotection of the purified dodecamer **126** sequence was performed in two steps. The first step was the deprotection of the Fmoc protecting group using 20% piperidine in DMF. Following the reaction, the product was isolated by precipitation and washing with Et_2O. The deprotection of Cbz protecting groups was then attempted on the crude product. Table 4 summarises the deprotection attempts leading up to the successful deprotection of the dodecamer **126**. All the conditions were tested on adenine monomer **92** before applying them to the oligomer. The first attempt, using strong acidic conditions (33% HBr in acetic) did not result in the deprotected monomer as confirmed by TLC and NMR analysis. Trifluoromethanesulfonic acid (TFMSA) in TFA was attempted next. TLC and NMR analysis indicated that the deprotection of **92** was quantitative. The same conditions were therefore attempted on **126**. HPLC analysis following the work up was promising since the product had become more polar (a shorter retention time was observed, 24.448 minutes, compared to starting material, 30.267 minutes). The product was purified and sent for MALDI-TOF-MS analysis, however, the result indicated that the deprotection of the Cbz groups was incomplete. Subsequently, other methods were attempted on monomer **92**. Palladium on activated charcoal in formic acid was attempted, however the starting material remained unchanged. Next, trimethylsilyl bromide (TMSBr) in TFA was attempted, however, incomplete deprotection was observed on the TLC, therefore, the method wasn't attempted on the oligomer. Finally, **92** was exposed to trimethylsilyl iodide (TMSI) in DMF at 50°C for 30 minutes, followed by methanol at r.t. for 15 minutes which lead to a quantitative deprotection of the Cbz group (as observed by TLC and NMR analysis). The same conditions were attempted on the dodecamer **126**, however, HPLC analysis indicated that several species were formed, indicating once again that incomplete deprotection was occurring to different extents (Figure 85a). The reaction was repeated with a prolonged reaction time. Treating the oligomer with TMSI overnight, instead of 30 minutes resulted in an HPLC chromatogram (Figure 85b) displaying a single major product at a very short retention time (15.1 minutes), indicating that the polarity of the product had increased drastically. The product was subsequently purified

and analysed by ESI-MS. The mass spectrum (Figure 86) clearly indicated the presence of the desired deprotected dodecamer **127** (Figure 86).

Conditions for reaction	Result for PNA monomer	Result for PNA oligomer
33% HBr in acetic acid	Unsuccessful	Not attempted
TFMSA in TFA	Successful	Incomplete deprotection
Pd/C in formic acid	Unsuccessful	Not attempted
TMSBr, thioanisole, TFA	Incomplete deprotection	Not attempted
TMSI, DMF, MeOH	Successful	Successful

Table 4. Cbz-deprotection conditions tested of the PNA monomer **93** and PNA oligomer **126**.

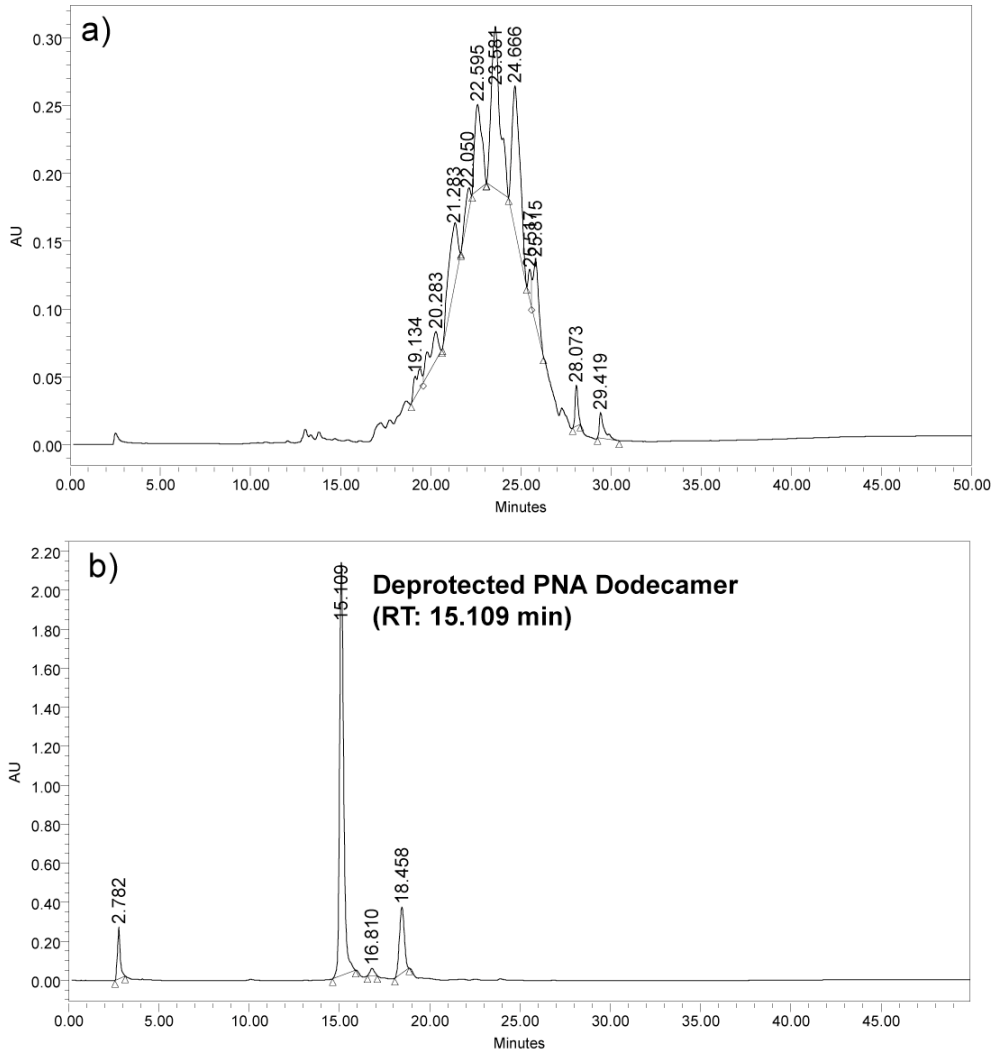

Figure 85. a) HPLC chromatogram following the treatment of **126** with TMSI for 30 minutes at 50°C. The HPLC chromatogram indicates the incomplete deprotection of the Cbz protecting groups. b) HPLC chromatogram following the treatment of **126** with TMSI for 16 hours at 50°C. The main peak represents the fully deprotected dodecamer **127** at a retention time of 15.1 minutes. (Agilent Zorbax SB-C18, 5 µm, 4.6 x 250 mm, gradient: 0.1% TFA in H_2O to 0.1% TFA in CH_3CN, flow: 1 mL/min, r.t.)

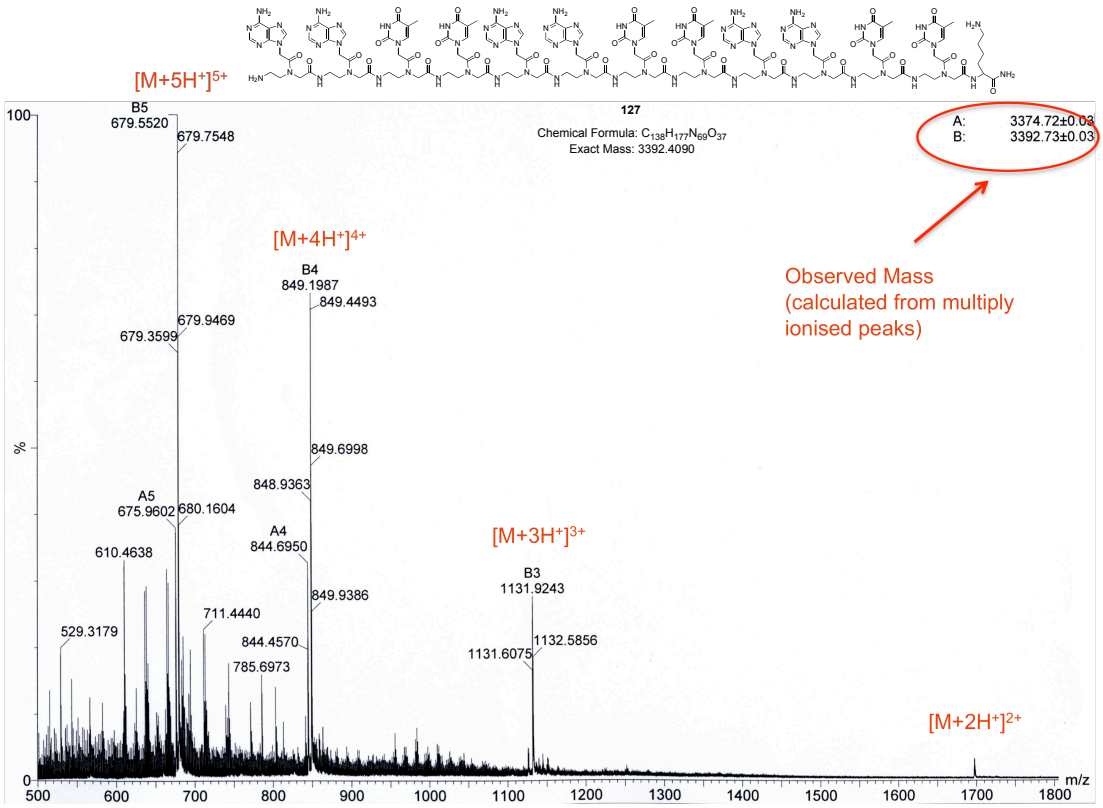

Figure 86. ESI-MS of the fully deprotected PNA dodecamer **127**.

The major peaks of the mass spectrum were all assigned to the fully deprotected dodecamer **127** ($C_{138}H_{177}N_{69}O_{37}$), which had a calculated mass of m/z 3392.4090. These included the $[M+2H]^{2+}$: m/z 1697.2134, $[M+3H]^{3+}$: m/z 1131.6075, $[M+4H]^{4+}$: m/z 848.9363 and $[M+5H]^{5+}$: m/z 679.3599 peaks as shown in Figure 86. With this data, it was finally confirmed that the solid phase synthesis was working as expected, and that the desired oligomers, protected and deprotected, were successfully synthesized.

Having obtained the target dodecamer **127**, the focus of the project was placed on the attachment of the chromophores to the PNA oligomer (Section 2.2) and also, in parallel, an evaluation of the conditions required to deposit the PNA oligomer onto a mica surface was carried out (Section 2.3).

2.2 SYNTHESIS OF PNA-CHROMOPHORE ADDUCTS

Prior to synthesizing and assembling the target angular and linear units described in the introduction (Section 1.5.3), a simpler proof of concept was required to (i) evaluate whether the PNA duplex could be formed on surfaces; (ii) to determine whether the PNA duplex can be formed in the presence of the attached chromophoric moieties, and (iii) if the duplexes do form, whether the presence of the chromophore adduct has any effect on the stability (melting temperature) of the PNA duplex. The molecule designed for this purpose, **128**, is shown in Figure 87. PNA-porphyrin adduct **128**, includes self-complementary dodecamer PNA sequence **127** (Section 2.1.4.4) as its supramolecular recognition unit. The porphyrin moiety was selected since it fulfils the aforementioned requirements. It would facilitate the STM or AFM imaging because porphyrins are easily identifiable by these techniques. Following duplex formation on the surface, the inter-porphyrin distance could be calculated and compared to computational data of the molecule to determine whether the duplex was correctly formed on the surface. Furthermore, using solution phase studies, the porphyrin moiety would assist in the determination of whether the attached organic moiety has any effect of the duplex formation or on its stability.

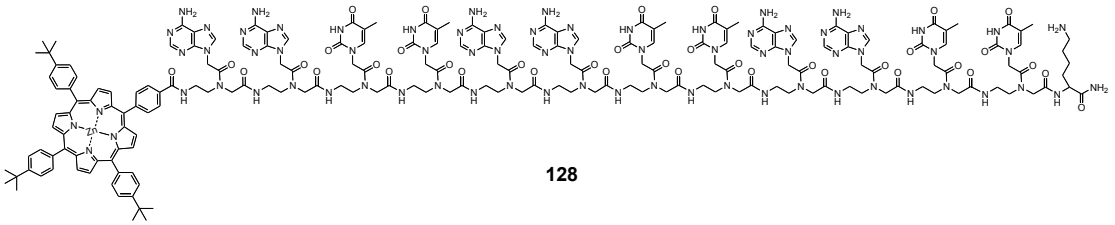

Figure 87. Molecular structure of the desired PNA-porphyrin adduct.

Initially, the addition of the porphyrin to resin-bound dodecamer **126** was attempted via a condensation reaction to form an amide bond, however, this proved to be unsuccessful (Section 2.2.1). Next, a copper-catalysed 1,3-diploar cycloaddition reaction was tried (Section 2.2.2). For this reaction, a linker featuring a terminal azide moiety was attached to the dodecamer, and an acetylene functionalised porphyrin was used. This synthetic route also failed, mainly because of problems related to the copper catalyst. The unsuccessful trials paved the way to the development of a copper-free 1,3-dipolar cycloaddition that enabled the attachment of chromophores to the PNA oligomer.

Section 2.2.3 describes the use of a Cu(I)-free 1,3-dipolar cycloaddition reaction between nitrile oxide and acetylene derivatives to prepare PNA-chromophore adducts. An introduction into the nitrile oxide-acetylene cycloaddition reaction is presented (Section 2.2.3.1). Next, using anthracene nitrile oxide precursors, various methods to generate nitrile

oxide species *in situ* were evaluated (Section 2.2.3.2) and were then applied in nitrile oxide-acetylene cycloaddition reactions with PNA to yield the first PNA-chromophore adduct (Section 2.2.3.3). Since the nitrile oxide-acetylene cycloaddition reaction was unknown with respect to porphyrins, the next step was to evaluate and optimise its use with porphyrins (Section 2.2.3.4). Once a method that was compatible with both PNA and porphyrin was found, its versatility was tested. A variety of chromophoric nitrile oxide precursors (porphyrin, pyrene, phenanthroline and fluorescein) were synthesized, and their reactions with an acetylene-functionalised PNA were examined (Section 2.2.3.5).

2.2.1 ATTEMPTS TO SYNTHESIZE PNA-PORPHYRIN ADDUCTS VIA AMIDE BOND FORMATION

The preparation of PNA-porphyrin adduct **128** was the next focus of the project. The first reaction proposed for the synthesis of this adduct was a condensation reaction between the terminal amino group of resin bound dodecamer **126** and mono-carboxylic acid functionalised porphyrin **133**.

Porphyrin **133** was prepared according to Scheme 15. The porphyrin core of **132** was prepared by the BF_3 catalysed reaction of a statistical mixture of the required aldehydes, 3 equivalents of 4-*tert*-butylbenzaldehyde **129** and one equivalent of methyl 4-formylbenzoate

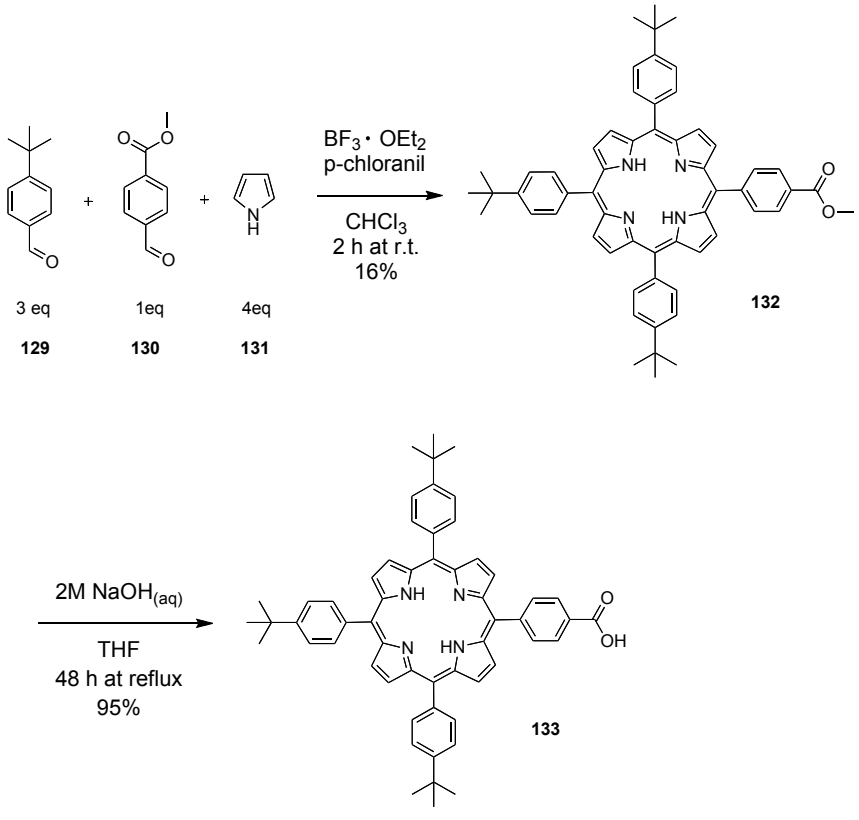

Scheme 15

130, with 4 equivalents of pyrrole **131**. The oxidation of the resultant porphyrinogen macrocycle was performed upon addition of *p*-chloranil to the solution. The reaction gave a statistical mixture of porphyrins, with **132** as the major product. The desired product was isolated by chromatography in 16% yield. Saponification of **132** yielded target mono-carboxyl porphyrin **133** in 95% yield.

Attempting to attach **133** to the *N*-terminal amino group of the PNA dodecamer was unsuccessful under several conditions (Scheme 16). The coupling was first attempted with Fmoc-deprotected PNA dodecamer still attached to the Rink amide resin **134a**, using the same conditions utilised to couple the PNA monomers to the growing oligomer, *i.e.* **133** was added in excess, with HBTU as the coupling agent, DIEA as the base and NMP as the solvent. The reaction mixture was shaken for 2 h at r.t. instead of 30 minutes. HPLC analysis of a cleaved sample of the crude product indicated that no reaction had occurred using this method. The chromatogram displayed peaks of both the unreacted PNA oligomer and porphyrin. Extending the reaction time to 16 h did not improve the result. The same conditions with 16 h reaction time were attempted with Fmoc-deprotected PNA dodecamer **134b** in solution rather than attached to the resin. However, once again HPLC analysis indicated that no reaction occurred. Finally, the reaction was performed once again in solution, but this time, it was heated to 80°C in an attempt to unbundle any aggregates of PNA. This reaction also did not yield the desired compound. Following these unsuccessful attempts to prepare **128**, the strategy was modified.

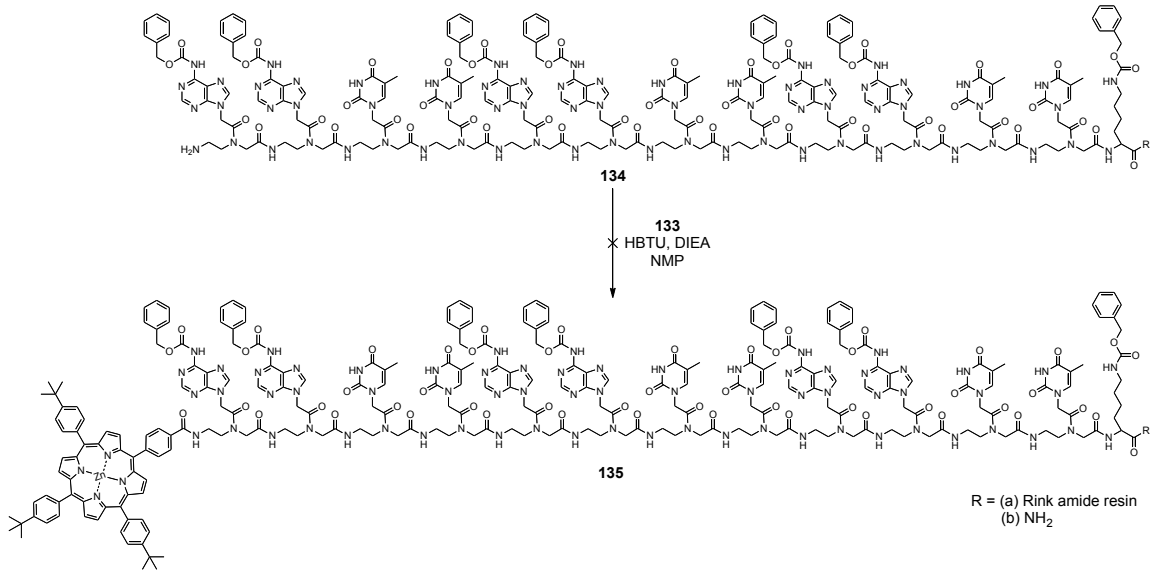

Scheme 16. The conversion of **134** to **135** was unsuccessful under solid phase and solution conditions. Solid phase conditions: (i) 2 h at r.t; (ii) 16 h at r.t. Solution phase conditions: (iii) 16 h at r.t.; (iv) 16 h at 80 °C.

2.2.2 Attempts to synthesize PNA-porphyrin adducts via Cu(I)-catalysed 1,3-dipolar cycloaddition

The alternative strategy proposed would take advantage of the increasingly popular click chemistry *i.e.* the Cu(I)-catalysed 1,3-dipolar cycloaddition between an azide and acetylene moiety.[240] When this strategy was chosen for the preparation of the PNA-porphyrin adduct, this reaction had already been used with PNA to immobilise PNA on a glass surface,[241] and to prepare a peptide-PNA hybrid derivative.[242] Using this strategy, the synthesis of two target PNA-porphyrin adducts (Figure 88) was attempted. Using solid phase synthesis, the preparation of mono-PNA-porphyrin adduct **136** was attempted, and using a solution phase reaction, the synthesis of tetra-PNA-porphyrin **137** was attempted.

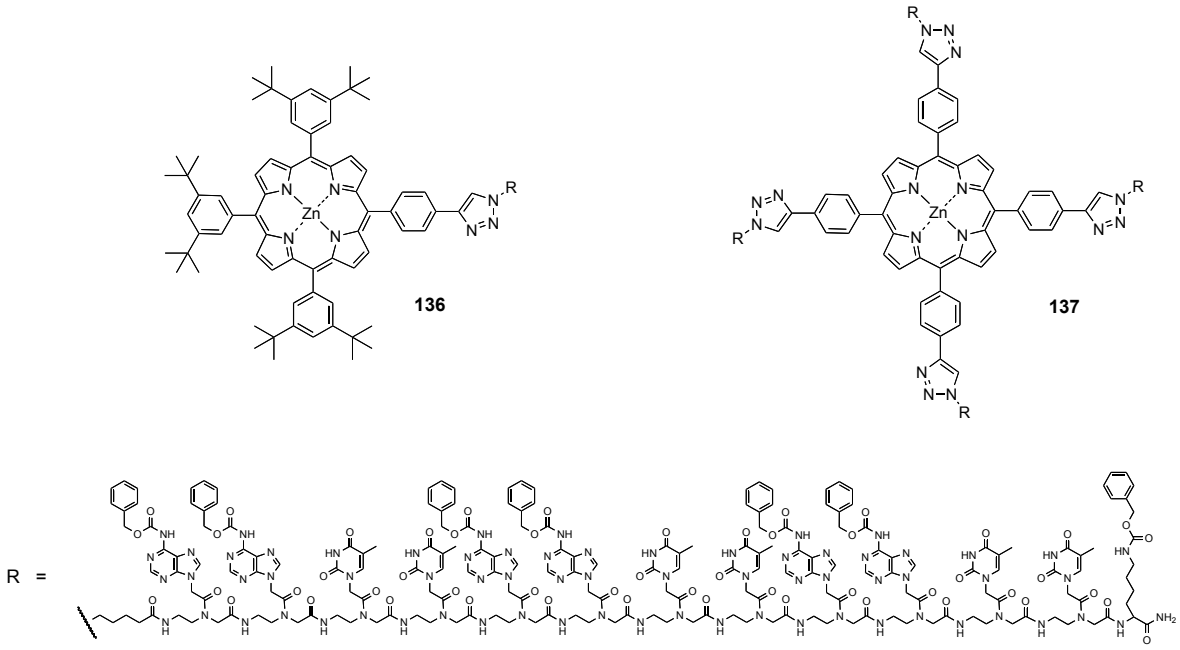

Figure 88. Molecular structure of the desired PNA-porphyrin adducts, **136** and **137**.

Three molecules were required for this new strategy (Figure 89). The first was a short linker bearing a carboxylic acid and an azide group separated by a short alkyl chain **138**. This linker would be attached to the resin-bound PNA oligomer to prepare the PNA for the click reaction. The linker was prepared according to Scheme 17. The porphyrin bearing a single acetylene moiety **139** was available in our laboratories and would be used to attempt the preparation of **136**. The last molecule required was the porphyrin derivative bearing four acetylene groups **140**, which was prepared according to Scheme 18. This molecule was required to attempt the preparation of **137**.

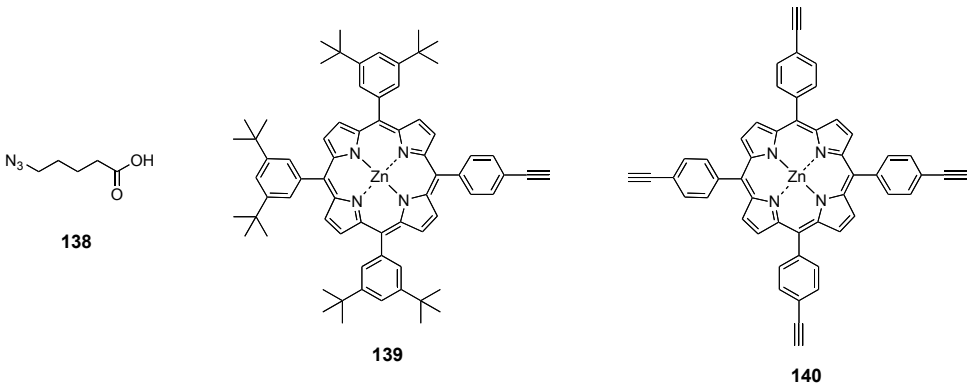

Figure 89. The molecules required for the preparation of PNA-porphyrin adducts via the Cu(I)-catalysed 1,3-dipolar cycloaddition strategy.

Refluxing bromovaleric acid **145** with sodium azide in water yielded linker **138** in 78% yield (Scheme 17). Porphyrin **140** was prepared as shown in Scheme 18. The porphyrin core was prepared by the BF_3 catalysed reaction between 4-[(Trimethylsilyl)ethynyl] benzaldehyde **142** and pyrrole **131**, followed by treatment with *p*-chloranil to oxidize the resultant porphyrinogen macrocycle. Following purification by chromatography, the tetra-acetylene porphyrin was obtained in 45% yield. Metallation with $Zn(OAc)_2$, followed by the deprotection of the trimethylsilyl (TMS) protecting groups using TBAF yielded the desired product **140**.

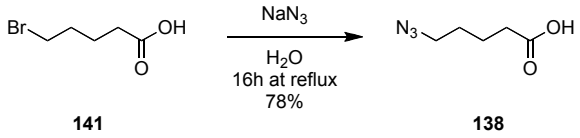

Scheme 17

Prior to attempting the Cu(I)-catalysed 1,3-dipolar cycloaddition on PNA, a test reaction between porphyrin **140** and azidovaleric acid **138** was performed to evaluate the reaction conditions. This reaction is most commonly performed in the presence of $CuSO_4 \cdot 5H_2O$ and sodium ascorbate using H_2O and *tert*-BuOH (1:1) as the solvent mixture. However, due to the lack of solubility of the porphyrin derivatives in this solvent mixture, the test reaction was performed in DMF. The two synthons were dissolved in DMF and were treated with $CuSO_4 \cdot 5H_2O$ and sodium ascorbate for 24 hours at 50 °C (Scheme 19). A quantitative conversion to the target compound **145** was achieved as observed by TLC. The isolated yield following purification by precipitaton was 86%.

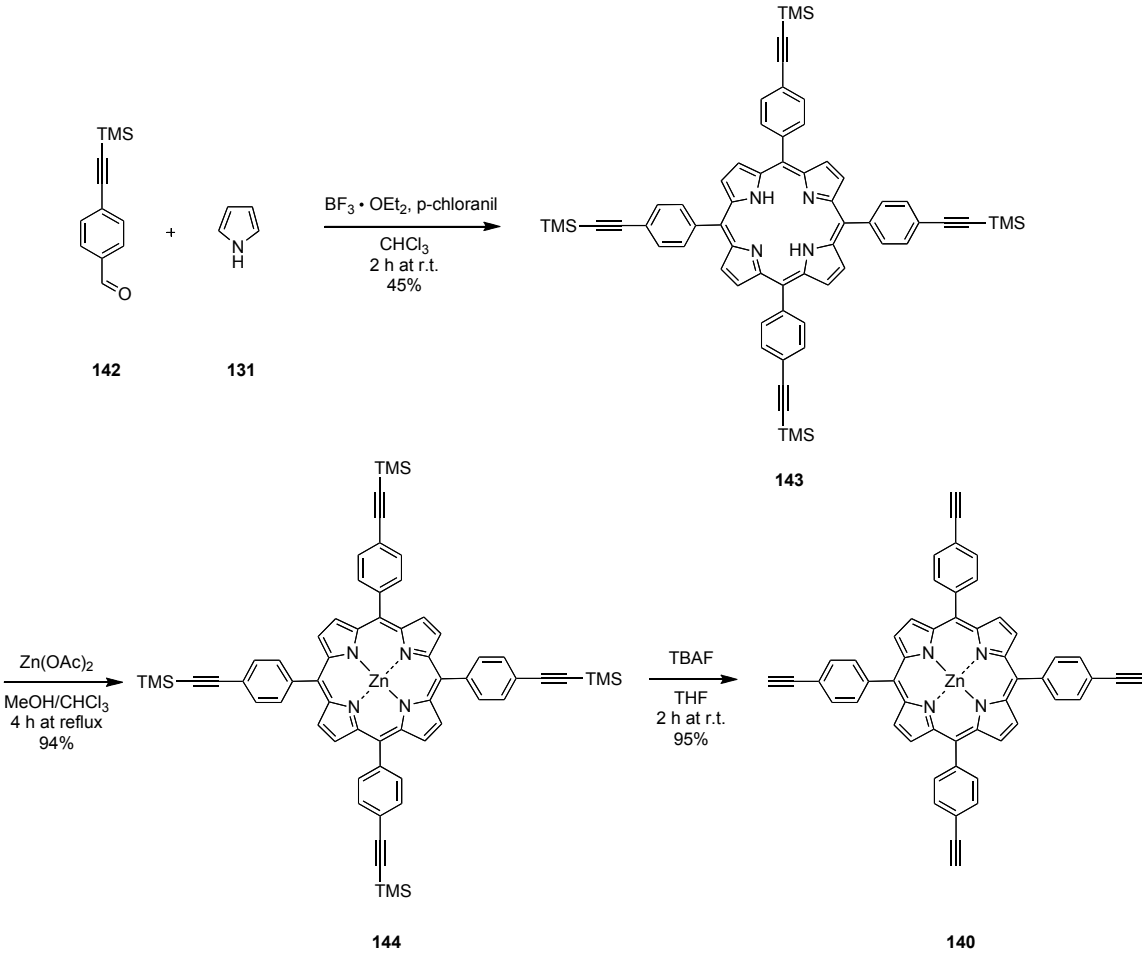

Scheme 18

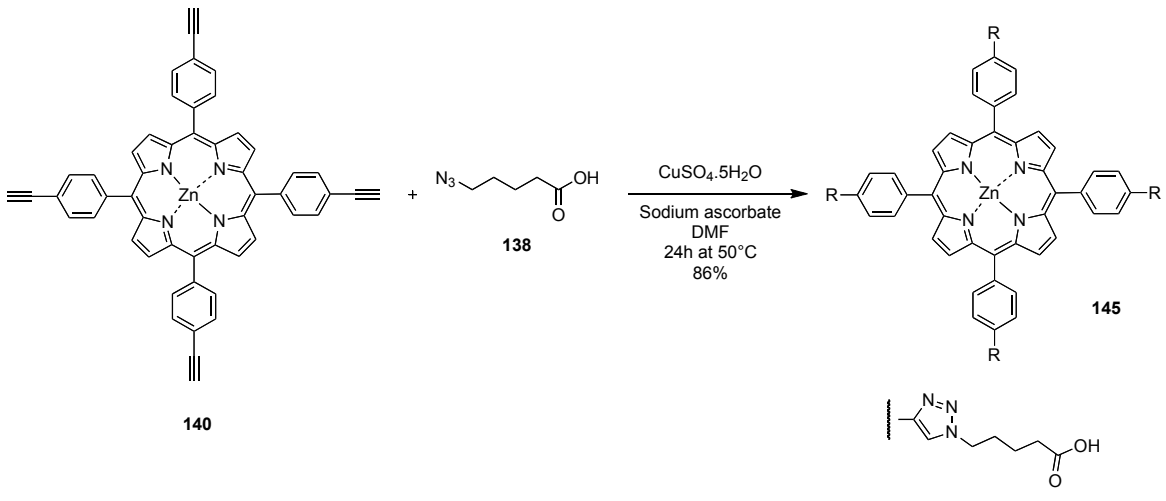

Scheme 19

The PNA oligomer was then prepared for the Cu(I)-catalyzed 1,3-dipolar cycloaddition by introducing the azide moiety. This was done by attaching **138** to the resin-bound PNA dodecamer using the standard coupling conditions. The Kaiser test indicated that the coupling reaction had succeeded. HPLC analysis of a cleaved sample of the resultant oligomer (**146**, Figure 90) indicated that the attachment of the linker was successful, since the retention time changed from 30.2 minutes (Figure 80c) to 28.3 minutes. The HPLC chromatogram of the purified azide-dodecamer **146** is shown in Figure 91. MALDI-TOF-MS was attempted on the purified product **146**, however, despite raising the laser intensity, a mass spectrum could not be obtained.

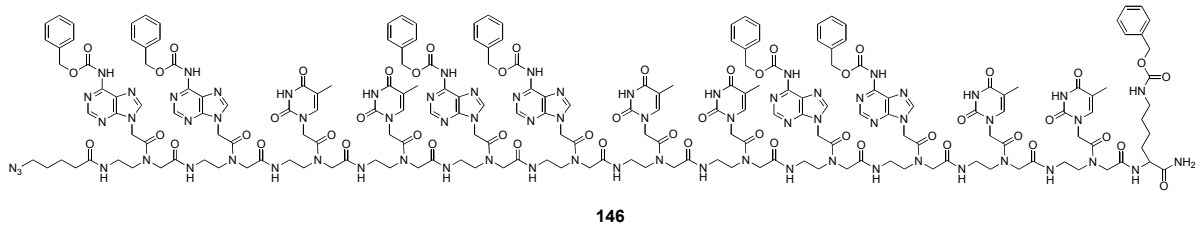

146

Figure 90. Molecular structure of compound **146**: the PNA dodecamer bearing an azide linker.

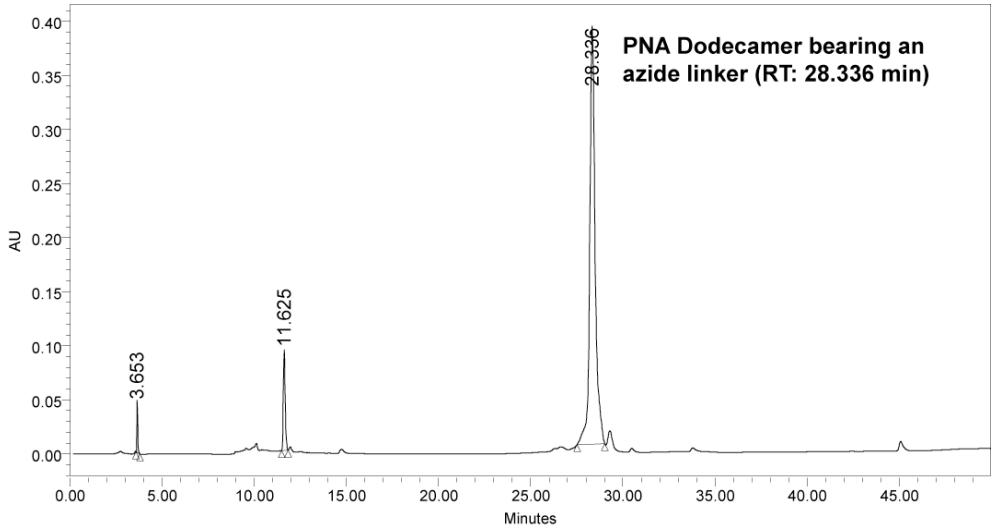

Figure 91. HPLC chromatogram of compound **146** following purification. (Agilent Zorbax SB-C18, 5 µm, 4.6 x 250 mm, gradient: 0.1% TFA in H_2O to 0.1% TFA in CH_3CN, flow: 1 mL/min, r.t.)

The preparation of PNA-porphyrins adducts was then attempted under using the same conditions utilised in the test reaction (Scheme19). The Cu(I)-catalyzed 1,3-dipolar cycloaddition was first attempted between resin-bound oligomer **146** and an excess of mono-acetylene porphyrin **139** in an attempt to prepare compound **136** (Figure 88). Following the reaction, a cleaved sample of the crude product was analysed by HPLC. The chromatogram displayed peaks corresponding to both of the starting materials, indicating that the reaction

had not worked. The reaction was then repeated at a higher temperature (80 °C), however the same result was obtained. Subsequently, the catalyst was changed to CuI, but once again HPLC analysis indicated that no reaction had occurred. The preparation of tetra-PNA-porphyrin adduct **137** was also attempted. The reaction was performed in solution between tetra-acetylene porphyrin **140** and azide-functionalised PNA oligomer **146** so that the reaction could be monitored by HPLC. Following 24 hours of reaction time, the HPLC chromatogram indicated that both starting materials remained unreacted in the reaction mixture, therefore the reaction was abandoned. The main postulated reason as to why the click reaction was not working in the presence of PNA was that the nucleobases were coordinating the catalytic quantity of copper in solution, thus preventing the activation of the acetylene and hence the 1,3-dipolar cycloaddition. Therefore, once again the strategy was modified.

Following the change in our strategy, further reports utilising the 1,3-dipolar cycloaddition in conjunction with PNAs were reported. The reports utilised the reaction to prepare DNA-PNA[243] and aminoglycoside-PNA[244] conjugates; to attach ferrocene to PNA;[245-247] to introduce a triazole *in lieu* of an amide bond within the PNA backbone[248] and also, to covalently link azide and alkyne PNA fragments using a DNA template.[243, 248] However, even though the reaction has proven to be successful, several drawbacks exist. Large excesses of a tris-triazolylamine Cu(I) ligand (*e.g.* tris-(benzyltriazolylmethyl)amine [TBTA]) had to be added to avoid complexation of the catalytic copper to the oligonucleotide's nucleobases and thus allow the cycloaddition reaction to proceed.[248] When working with PNA in the presence of DNA the reactions need to be performed in air-free conditions and in the presence of a large excess of a tris-triazolylamine Cu(I) ligand in order to avoid degradation of the oligonucleotides via the redox chemistry of copper ions.[249, 250] The solubility of the copper catalysts in organic solvents can be problematic and extensive washing is required to remove the Cu catalyst and ligand following the reaction.[251] As a consequence of these drawbacks, the development of a copper-free alternative for the functionalisation or conjugation of PNA was desirable.

2.2.3 Development of a Cu(I)-free 1,3-dipolar cycloaddition reaction to prepare PNA-chromophore adducts

This section describes the use of a copper-free 1,3-dipolar cycloaddition reaction between nitrile oxide and acetylene species to prepare PNA-chromophore adducts. This section is subdivided into five sections. First, an introduction into the nitrile oxide-acetylene cycloaddition reaction is presented (Section 2.2.3.1). It is followed by an evaluation of the various methods to prepare nitrile oxide species *in situ* using anthracene nitrile oxide precursors as model compounds (Section 2.2.3.2). Testing the nitrile oxide-acetylene

cycloaddition reaction using the anthracene model compounds with PNA, yielded the first PNA-chromophore adduct (Section 2.2.3.3), confirming that the reaction was compatible with PNA. Since the reaction was unknown in relation to porphyrins, the next step was to evaluate and optimise its use with porphyrins (Section 2.2.3.4). Finally, a method that was compatible with both PNA and porphyrin was found, therefore, to evaluate the method's utility and versatility, porphyrin, pyrene, phenanthroline and fluorescein nitrile oxide precursors were synthesized, and their reactions with an acetylene-functionalised PNA were examined (Section 2.2.3.5).

2.2.3.1 Introduction to the nitrile oxide-acetylene 1,3-dipolar cycloaddition reaction

Following the unsuccessful attempts described in sections 2.2.1 and 2.2.2 to prepare the PNA-porphyrin adducts, we decided to develop a copper-free 1,3-dipolar cycloaddition reaction to functionalise PNA strands with chromophores. Reports of copper-free 1,3-dipolar cycloadditions applied on DNA oligomers that were recently published by the groups of Heaney[251, 252] and Carell[253, 254] offered inspiration towards this goal. Their strategies involved the generation of a nitrile oxide species *in situ*, which then reacts with either an alkene or an alkyne to form an isoxazoline or an isoxazole. This cycloaddition is an attractive method since nitrile oxide dipole precursors are easily formed via a variety of methods;[255] the reaction occurs readily at room temperature since the cycloaddition has a barrier of 20.2 kcal/mol;[256] it is regioselective with alkynes forming the 3,5-disubstituted adducts;[257] and it can be performed in a variety of organic solvents (*e.g.* CH_2Cl_2, DMF, EtOH) and also aqueous media.[251-254, 258] To this end, we decided to attempt using the nitrile oxide 1,3-dipolar cycloaddition to attach apolar and polar chromophores to resin-bound PNA strands bearing a terminal acetylenic linker.

Several methods exist for the preparation of nitrile oxides *in situ*,[255] however, two of them are by far the most popular and well-established. The first is the Mukaiyama method[259] which involves the dehydration of nitroalkanes by an aryl isocyanate or another dehydrating agent (*e.g.* $POCl_3$, $MeSO_2Cl$). The second involves the base-mediated dehydrochlorination of a hydroximoyl chloride to yield the nitrile oxide.[260] Another method to prepare nitrile oxides was introduced *Carreira* and his co-workers more recently.[258] It involves the treatment of an *O*-silylated hydroxamic acid species with trifluoromethanesulfonic anhydride (Tf_2O) to yield a nitrile oxide. The three methods are shown in Figure 92.

Assessing the three methods, our first choice for the preparation of nitrile oxides was the hydroximoyl chloride method. Normally, the reaction is performed starting from a stable hydroximoyl chloride derivative, which upon treatment with a base yields the nitrile oxide,

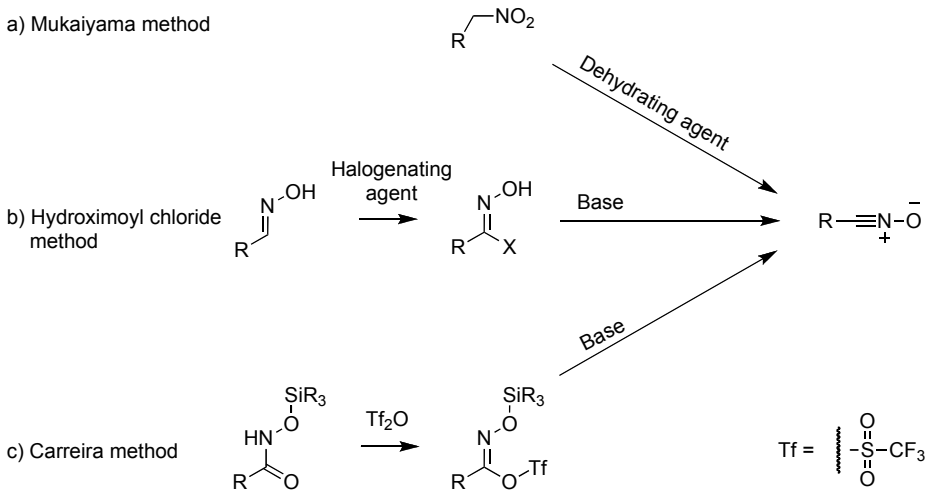

Figure 92. The preparation of nitrile oxide species *in situ* from (a) nitroalkanes, (b) oximes or hydroximoyl halides, and (c) *O*-silylated hydroxamic acids.

which then reacts with a dipolarophile. If a stable hydroximoyl chloride precursor cannot be isolated, the reaction can be performed starting from an aldoxime which is treated with an electrophilic chlorine source in the presence of a base yielding the nitrile oxide *in situ* passing via a hydroximoyl chloride intermediate. This method has been applied in numerous cycloaddition reactions[255] and was the method of choice for the Cu(I)-free cycloadditions performed on DNA.[251-254] The compatibility of this method with oligonucleotides was the one of the primary reasons why we selected to work this method. Furthermore, we were apprehensive about using strong dehydrating agents in the presence of PNA, so we decided to rule out the Mukaiyama method. The lesser-known Carreira method was also an appealing method of preparing the nitrile oxide species, therefore, it was selected as an alternative to the hydroximoyl chloride method.

2.2.3.2 Evaluation of the nitrile oxide-acetylene 1,3-dipolar cycloaddition reaction using anthracene derivatives

An evaluation of the conditions required to prepared nitrile oxide species *in situ* using the two selected methods was required prior to applying the nitrile oxide-acetylene 1,3-dipolar cycloaddition reaction to PNA oligomers. This evaluation was carried out on anthracene derivatives that acted as a model system.

The first method was the hydroximoyl chloride method. Initially, our intention was to isolate the hydroximoyl chloride derivative. For this purpose, 9-anthraldehyde oxime **147** was dissolved in DMF and treated with NCS (Scheme 20). Although TLC indicated a good conversion of the starting material to the product, the isolated yield of the product following purification by silica gel chromatography was 34%. The low yield indicated that the

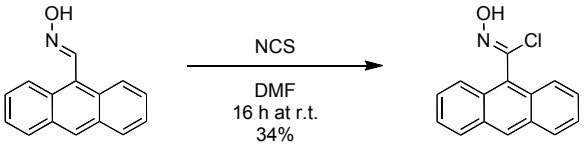

147 148

Scheme 20

hydroximoyl chloride of anthracene was not very stable. Consequently, it was decided that the nitrile oxide species would be prepared directly from the aldoxime by treating the starting material with the chlorinating agent and subsequently introducing a base to induce dehydrochlorination. Also, a dipolarophile would be added after the base to trap the highly reactive nitrile oxide species to prevent the formation of furoxans by dimerisation of two nitrile oxides (Scheme 21).

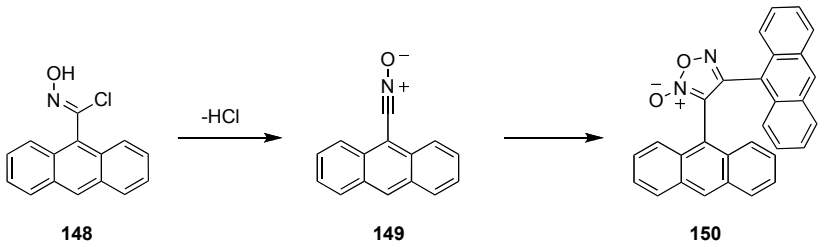

148 149 150

Scheme 21

The first trial of the new *in situ* strategy (Scheme 22) involved the reaction between **147** and a mild oxidizing agent, *tert*-BuOCl. The reaction was performed in CH_2Cl_2 for 5 minutes at -10°C, after which trimethylsilyl acetylene **151** as the dipolarophile and triethylamine as the dehydrochlorination agent were added. The mixture was then warmed to room temperature and was allowed to react overnight. The reaction resulted in target compound **152** in 45% yield, however, side product **153** in which the anthracene core was chlorinated at the 10-position was also present in significant quantities (31% yield). This trial indicated that the chlorinating agent, *tert*-BuOCl, was too strong and that an even milder chlorinating agent was required.

In the next trial, the oxidant was changed to 1-chlorobenzotriazole. This reagent had the property of acting as both the oxidizing agent and the dehydrochlorination agent because once the chlorine atom is released, the benzotriazole by-product is sufficiently basic to activate the nitrile oxide, thus the addition of the dipolarophile should follow in quick succession to the addition of the 1-chlorobenzotriazole in this reaction to avoid the formation of a large quantity of furoxan dimers **150** between two nitrile oxide species (Scheme 21).

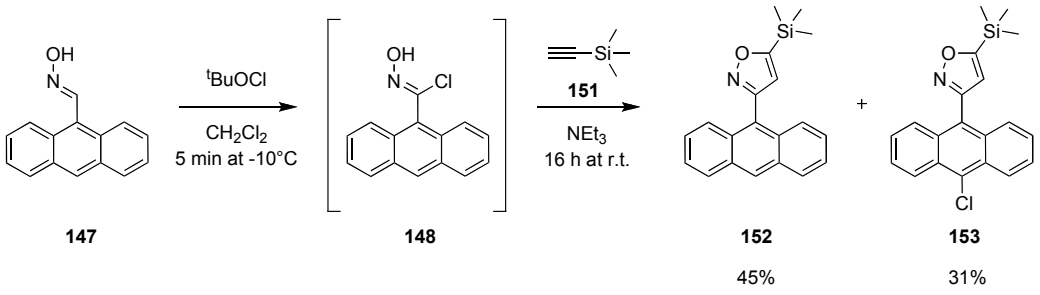

Scheme 22

Scheme 23 shows the reaction between **147**, 1-chlorobenzotriazole and **151**. The same conditions were used as in the previous reaction shown in Scheme 22. This reaction showed a marked increase in the yield of the target product **152** with no formation of the side product **166**. Following this result, the preparation of **152** using the Carreira method was attempted to compare it to the hydroximoyl chloride method.

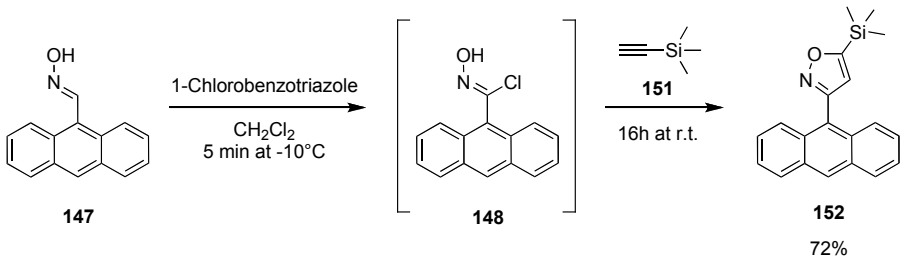

Scheme 23

The *O*-silylated hydroxamic acid of anthracene **156** was prepared in two steps starting from 9-anthracenecarboxylic acid **154** (Scheme 24). The acid chloride was prepared first using oxalyl chloride, and then the introduction of *O*-silylated hydroxylamine **155** yielded **156** in 52% overall for the two steps. Compound **156**, which was the precursor to the nitrile oxide species was stable and could be chromatographed without the loss of yield as in the case of the hydroximoyl chloride. The pure product was then exposed to trifluoromethanesulfonic anhydride for 1h at 0°C, after which the dipolarophile **151** was introduced and was allowed to react overnight at room temperature. The reaction yielded the desired product **152** with a yield of 79%, which was a slight improvement to the yield obtained using the hydroximoyl chloride method.

These trials indicated that the hydroximoyl chloride and Carreira protocols were both efficient methods in generating nitrile oxide species for the 1,3-dipolar cycloaddition reactions with acetylene to prepare isoxazole derivatives. Subsequently, using the anthracene nitrile oxide precursors described in this section, these two methods were applied to prepare PNA-anthracene adducts.

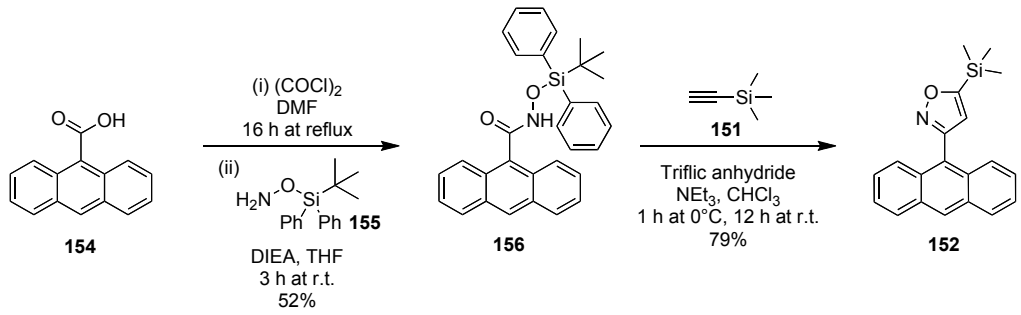

Scheme 24

2.2.3.3 Preparation of PNA-anthracene adducts via nitrile oxide-acetylene 1,3-dipolar cycloaddition reactions

This section describes the synthesis of PNA-anthracene adducts using the nitrile oxide-acetylene 1,3-dipolar cycloaddition reaction. Both methods evaluated in the previous section were successfully applied to prepare the PNA-chromophore adducts.

The dodecamer was prepared for the cycloaddition reaction by coupling 5-hexynoic acid **157** to the PNA using the standard conditions. The Kaiser test following the reaction indicated that the coupling had proceeded successfully. HPLC analysis of a cleaved sample of the PNA-acetylene product **158** (Figure 93) showed one major product at a retention time of 28.1 minutes (Figure 94a), which differed from the retention time of the Fmoc-protected PNA dodecamer **126** (30.2 minutes, Figure 80). The product was purified by semi-preparative HPLC (Figure 94b), and then, to confirm that the desired product had been isolated, **158** was deprotected by treatment with TMSI, and the resultant purified product (**159**) was analysed by MALDI-TOF-MS. The mass ion peak found for **159** was m/z 3487.65 (Figure 95), which corresponded to the calculated mass for the $[M+H]^+$ species of **159** ($C_{144}H_{184}N_{69}O_{38}$), m/z 3487.4587, therefore confirming that the PNA-acetylene products had been isolated. Having obtained the PNA-acetylene product **158**, the cycloaddition reaction with anthracene nitrile oxide **149** could be attempted.

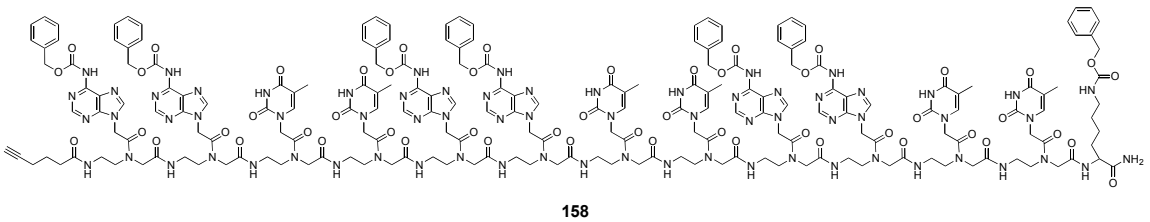

158

Figure 93. Compound **158**: the PNA dodecamer bearing an acetylene linker.

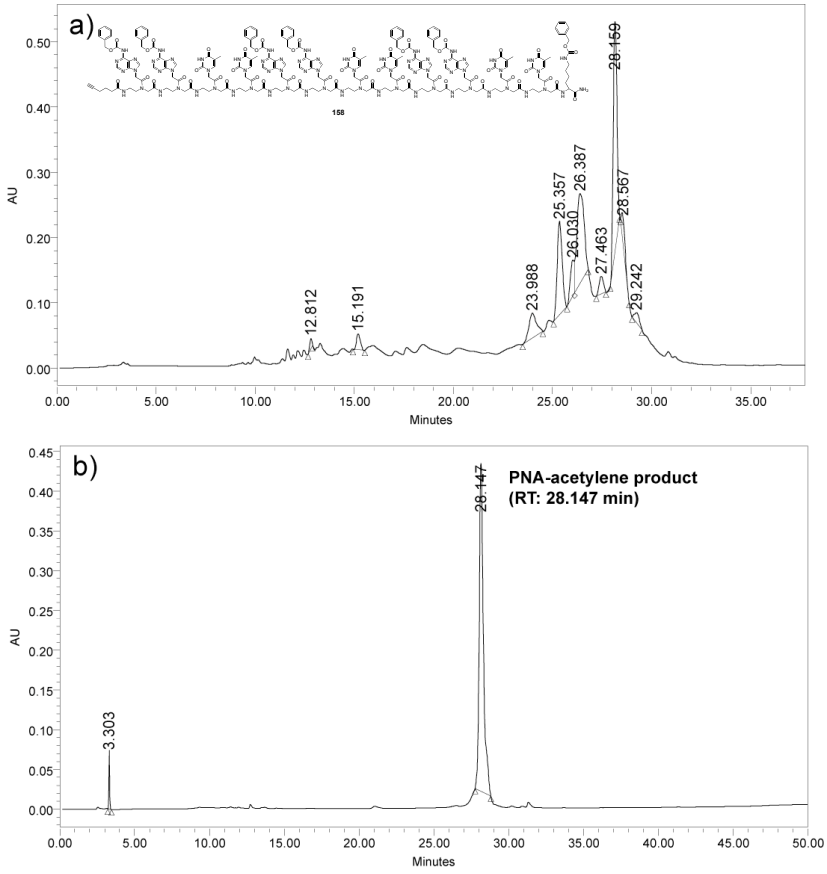

Figure 94. a) HPLC chromatograms of (a) the crude mixture of **158** isolated from the resin and (b) **158** following purification. (Agilent Zorbax SB-C18, 5 µm, 4.6 x 250 mm, gradient: 0.1% TFA in H_2O to 0.1% TFA in CH_3CN, flow: 1 mL/min, r.t.)

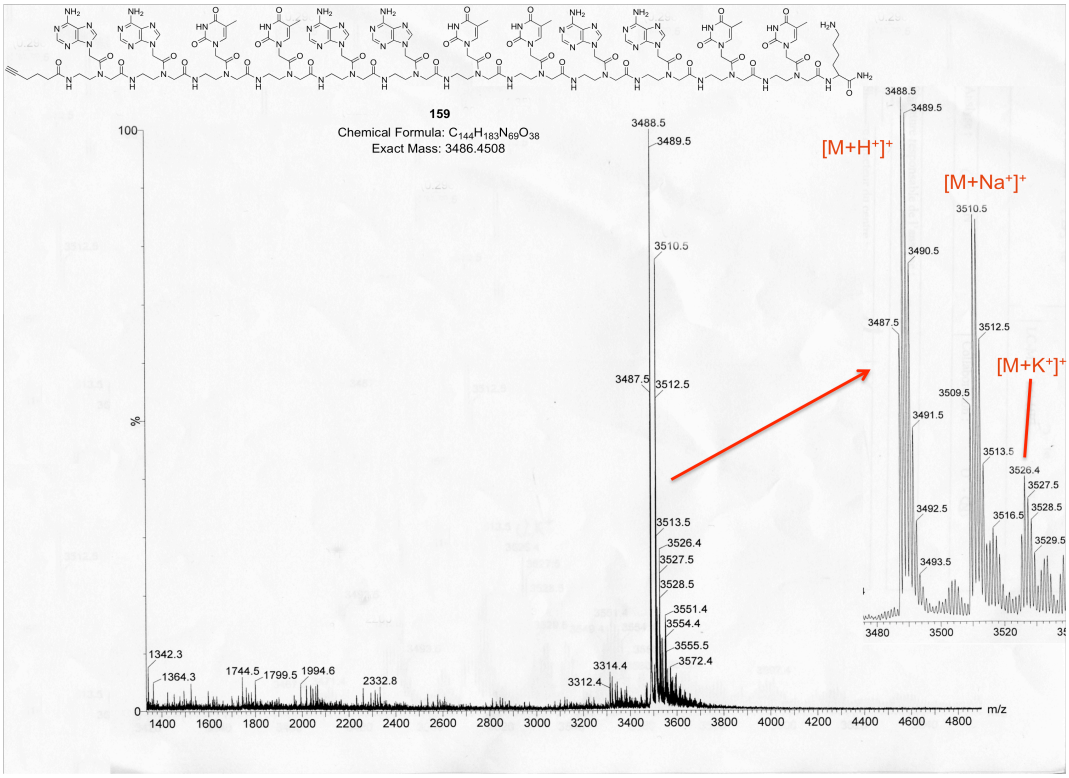

Figure 95. MALDI-TOF-MS of deprotected PNA-acetylene oligomer **159**.

The reaction between resin-bound PNA-acetylene oligomer **158** and anthracene nitrile oxide **149** was first attempted using the hydroximoyl chloride method. The reaction was performed using hydroximoyl chloride **148** rather than aldoxime **147** as the starting material, in order to avoid introducing an chlorinating agent in the presence of PNA. To this end, resin-bound PNA-acetylene oligomer **158** was suspended in a solution of **148** in DMF before Et_3N was added and the mixture was shaken overnight at room temperature (Scheme 25). The HPLC chromatogram of the cleaved crude product indicated the presence of a new compound **160** at retention time of 30.2 minutes (Figure 96), but it also showed the presence of starting material **158**, therefore optimisation of the reaction was required to achieve a quantitative conversion. The peak of **160** was also observed at a wavelength of 360nm on the HPLC UV detector, whereas the peak of **155** was only observed at 260nm. This observation was promising since it provided evidence that the new compound was potentially PNA-anthracene adduct **160**.

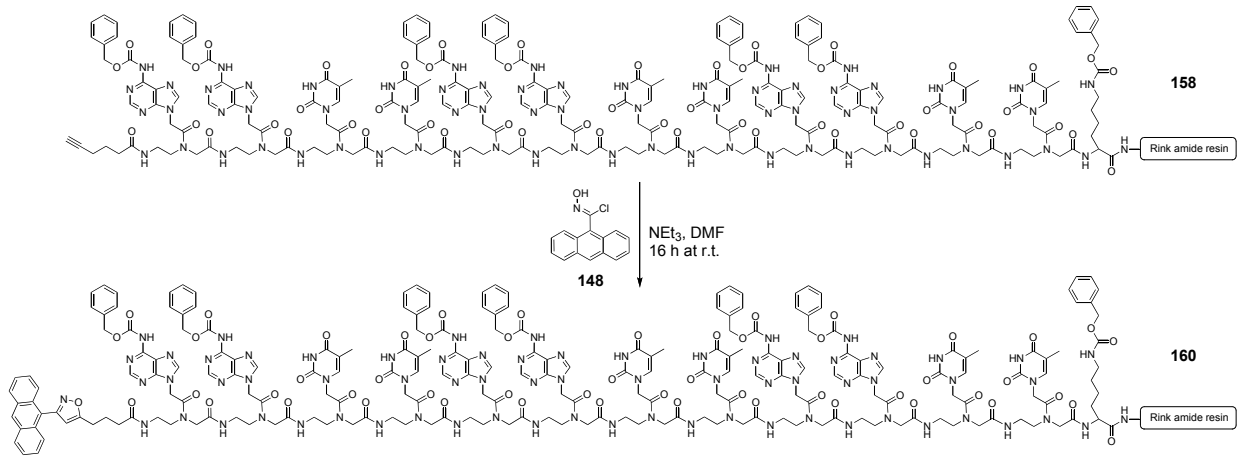

Scheme 25

At this point, the cycloaddition reaction was optimised to increase the ratio of the new product **160** versus the starting PNA-acetylene compound **158**. The reaction was first performed at a higher concentration, but this did not significantly improve the ratio between **160** and **158**. Next, the reaction was performed overnight at 50°C instead of room temperature, and this resulted in a good conversion as indicated by the HPLC analysis wherein **160** was the only major peak in the chromatogram (Figure 97). **160** was subsequently purified by semi-preparative scale HPLC, before a Cbz-deprotection using TMSI was carried out. Following purification of the deprotected PNA-anthracene **161** (Figure 98), MALDI-TOF-MS analysis was performed to confirm the presence of the target compound. The mass spectrum obtained indicated that the desired compound had been obtained (Figure 99). The mass ion peak found for compound **161** was m/z 3706.5244, which corresponded to the

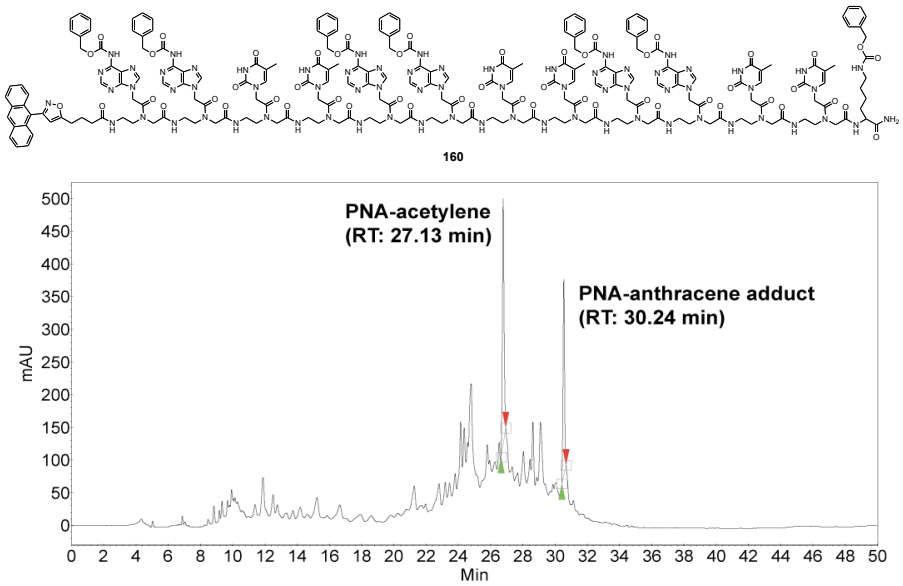

Figure 96. HPLC chromatogram of the crude mixture following the nitrile oxide-alkyne 1,3-dipolar cycloaddition performed overnight at room temperature. The mixture indicated the presence of compounds **158** and **160** as major products. The molecular structure of compound **160**, the PNA dodecamer-anthracene adduct is shown. (Varian Pursuit C18, 5 µm, 4.6 x 250 mm, gradient: 0.1% TFA in H_2O to 0.1% TFA in CH_3CN, flow: 1 mL/min, 65°C)

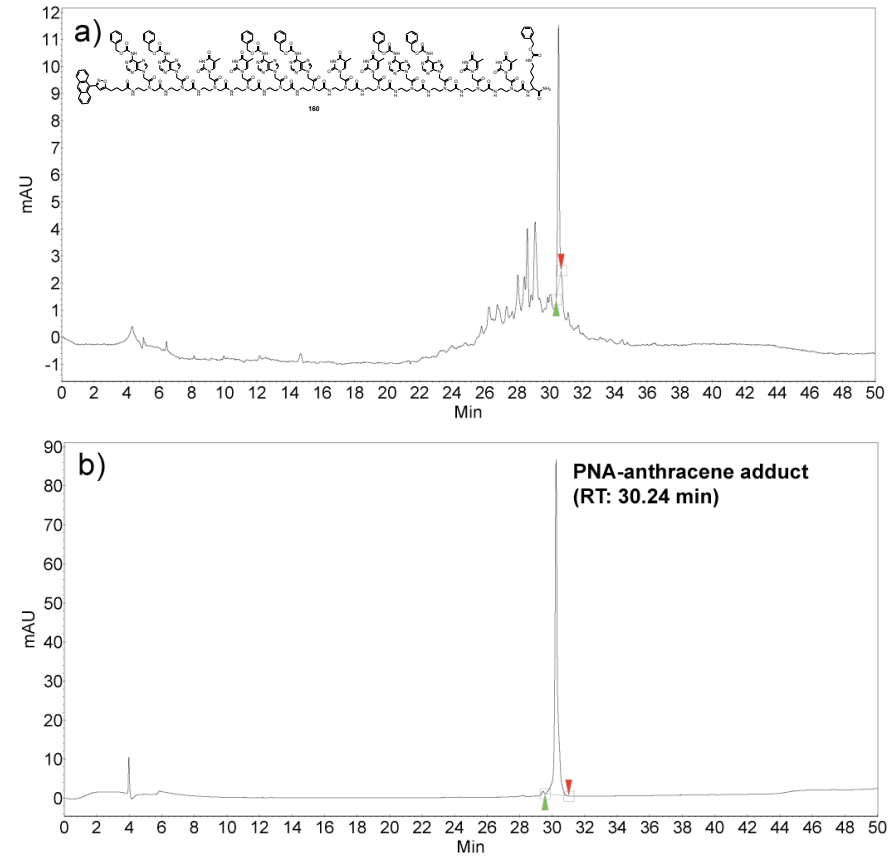

Figure 97. a) HPLC chromatogram of the crude mixture of **160** isolated from the resin following the nitrile oxide-alkyne 1,3-dipolar cycloaddition performed overnight at 50°C. b) HPLC chromatogram of **160** following purification by semi-preparative HPLC. (Varian Pursuit C18, 5 µm, 4.6 x 250 mm, gradient: 0.1% TFA in H_2O to 0.1% TFA in CH_3CN, flow: 1 mL/min, 65°C)

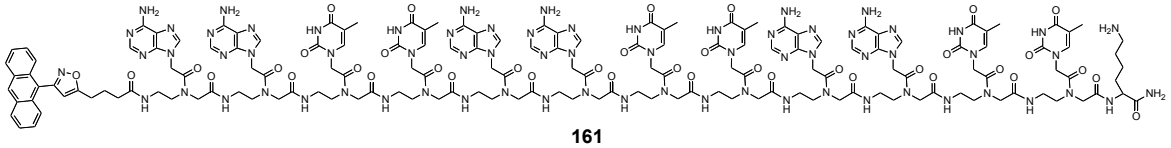

161

Figure 98. Molecular structure of compound **161**: the deprotected PNA-anthracene adduct.

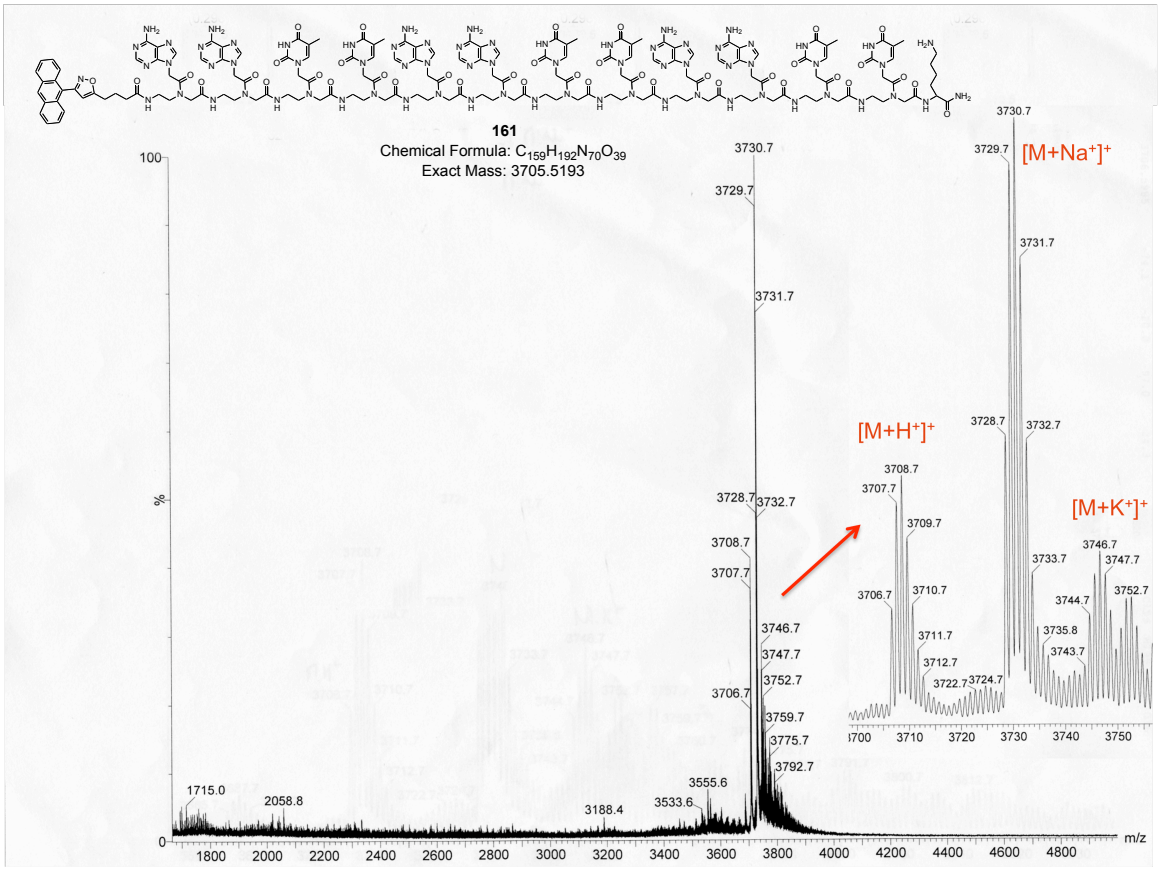

Figure 99. MALDI-TOF-MS of the deprotected PNA-anthracene adduct **161**.

calculated mass for the protonated form, $[M+H]^+$ of **161** ($C_{159}H_{193}N_{70}O_{39}$), m/z 3706.5271. This result confirmed that the nitrile oxide-acetylene 1,3-dipolar cycloaddition reaction was compatible with PNA.

Next, the preparation of PNA-anthracene adduct **160** was attempted using the Carriera method to prepare the nitrile oxide dipole (Scheme 26). Compound **156** *i.e.* the *O*-silylated hydroxamic acid derivative of anthracene was used as the nitrile oxide precursor. Since the HPLC retention time of PNA-anthracene adduct **160** was identified (30.24 min, Figure 97), the success of this method could be determined directly and rapidly by analyzing the crude PNA-anthracene product by HPLC analysis. To prepare the nitrile oxide, **156** (10 eq.) was dissolved in CH_2Cl_2, NEt_3 (30 eq.) was added and then following cooling to -40°C, trifluormethansulfonic anhydride (11 eq.) was added dropwise. After allowing the temperature of the mixture to reach 0°C in 1 h, the mixture was added to the resin-bound

PNA oligomer bearing the acetylenic linker (**158**) suspended in DMF. The suspension was then shaken for 16 h at 50°C. Analysis of the cleaved crude product indicated that PNA-anthracene adduct **160** had been prepared successfully with a quantitative conversion in the same manner as with the hydroximoyl chloride method. The product was subsequently purified, deprotected and analysed by MALDI-TOF-MS, confirming the presence of target PNA-anthracene adduct **161** (Figure 98). Obtaining a positive result from both methods, it was decided that this Cu(I)-free 1,3-dipolar cycloaddition reaction would be used to synthesize further PNA-chromophore conjugates, commencing from the PNA-porphyrin adduct.

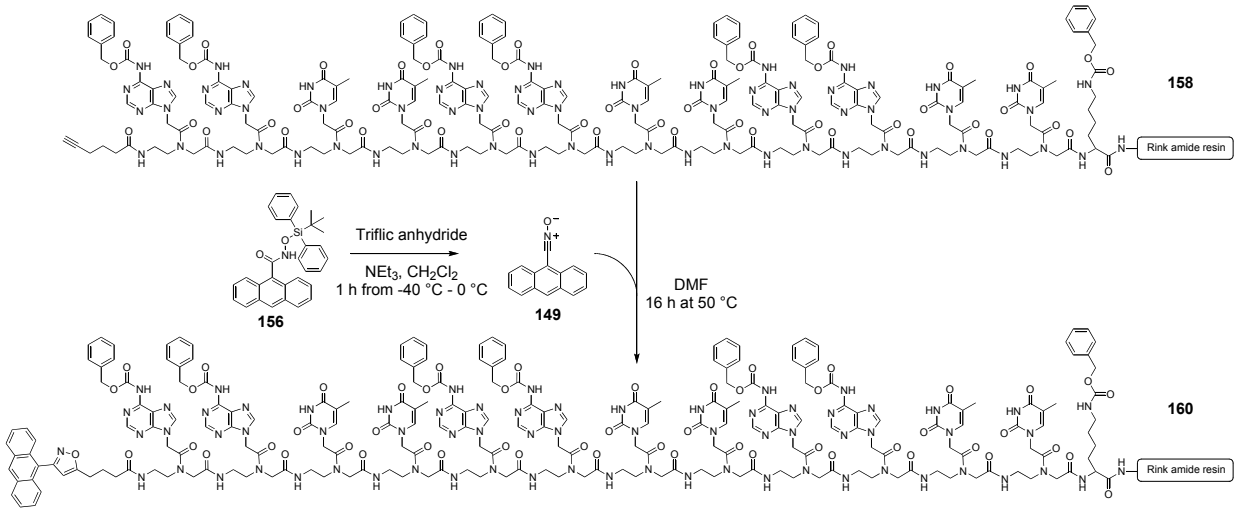

Scheme 26

2.2.3.4 Development of a porphyrin nitrile oxide precursor

Since the nitrile oxide-acetylene 1,3-dipolar cycloaddition reaction was unknown in relation to porphyrins, the next step was to evaluate and optimise its use with porphyrins. This section discusses our efforts to prepare and optimise a method to prepare a porphyrin nitrile oxide species to be used in Cu(I)-free 1,3-dipolar cycloaddition reactions. The hydroximoyl chloride and Carreira methods were evaluated to prepare the porphyrin nitrile oxide precursors. It was observed that the porphyrin macrocycle was unstable towards the chlorinating agents used in the hydroximoyl chloride method, therefore, the Carreira method was found to be the favoured method for preparing nitrile oxide precursors.

Commencing with the hydroximoyl chloride approach, the nitrile oxide precursor of the porphyrin had to be prepared. The precursor to the hydroximoyl chloride *i.e.* a mono-oxime porphyrin **164** was synthesized starting from porphyrin **132** (scheme 15). The methyl ester was reduced to the alcohol **162** using lithium aluminium hydride, after which, the

product was treated with pyridinium chlorochromate oxidizing it to the corresponding aldehyde **163**. The aldehyde was then converted to the oxime **164** using hydroxylamine in the presence of sodium acetate as shown in Scheme 27.

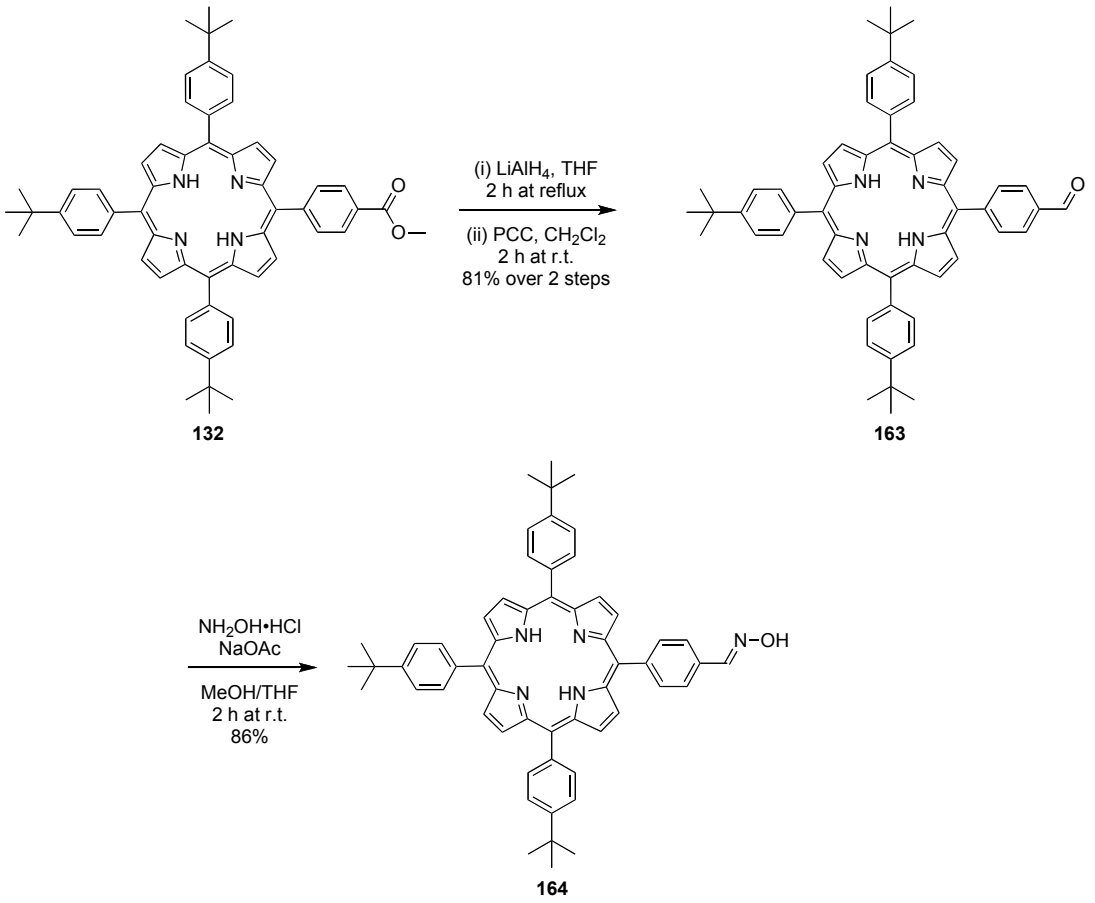

132 163 164

Scheme 27

Initially, our intention was to isolate a hydroximoyl chloride derivative of porphyrin, but the preparation of this nitrile oxide precursor from the oxime proved to be challenging (Scheme 28). Unfortunately, all attempts to chlorinate the oxime functional groups failed as is summarized in Table 5. As shown in the table, two oxidizing agents were used, NCS and *tert*-*tert*-BuOCl under various conditions. Initially NCS was used, however, despite changing the solvent, lowering the reaction temperature and shortening the reaction time, the reaction always resulted in the decomposition of the porphyrin. It was postulated that NCS was a sufficiently strong oxidizing agent to also attack the porphyrin macrocycle causing its decomposition, however this was not confirmed. At this point in the trials, the oxidant was changed to the milder *tert*-BuOCl oxidizing agent. Once again, changing the reaction time and reaction temperature when performing the reaction in DMF resulted in decomposition.

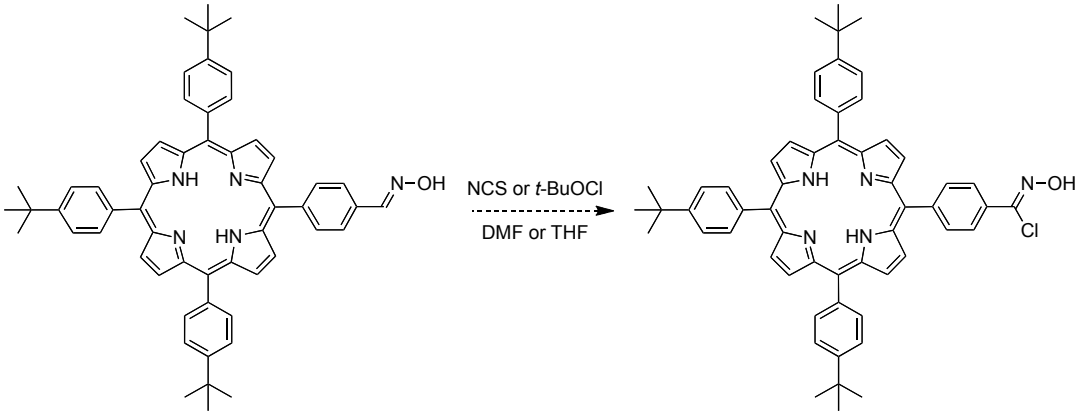

164 165

Scheme 28

Oxidant	Reaction temp.	Reaction time	Solvent	Result
NCS	r.t.	16 h	CH_2Cl_2	Decomposition of porphyrin.
NCS	r.t.	16 h	DMF	Decomposition of porphyrin.
NCS	0°C	1 h	DMF	Decomposition of porphyrin.
NCS	-48°C	1 h	DMF	Decomposition of porphyrin.
tert-BuOCl	0°C	1 h	DMF	Decomposition of porphyrin.
tert-BuOCl	-48°C	1 h	DMF	Decomposition of porphyrin.
tert-BuOCl	-48°C	15 min	DMF	Some starting material recovered. Decomposition.
tert-BuOCl	-78°C	15 min	THF	New product (TLC). Decomposition during purification.

Table 5. Reaction conditions used to attempt the synthesis of porphyrin **165**.

When the solvent was changed to THF, and the temperature was lowered further, a new product was observed to form when the reaction mixture was analysed by TLC, however, attempting to purify the product by chromatography resulted in its decomposition. This observation suggests that, similarly to anthracene hydroximoyl chloride **148**, the hydroximoyl chloride derivatives of porphyrins are not stable, therefore the pursuit of obtaining isolated hydroximoyl chloride functionalized porphyrins was discontinued. Instead, an approach similar to that used for preparing anthracene isoxazoles was used (Section 2.2.3.2), *i.e.* the chlorination of the oxime, activation to the nitrile oxide and cycloaddition with the acetylene would all be performed *in situ*.

Unfortunately, the change in strategy did not improve the results. Several conditions to obtain the target isoxazole funtionalised porphyrin **166 (**Scheme 29) were attempted (Table 6), however none of the reactions were successful. 1-Chlorobenzotriazole was used as the

chlorinating agent in these trials, since it provided the best results with anthracene aldoxime **147** (Scheme 23). The first reaction was performed at 0°C in THF. It resulted in decomposition of the porphyrin. Performing the same reaction at a lower temperature resulted in the recovery of the starting material. Changing the solvent to DMF led once more to the decomposition of the porphyrin whereas performing the reaction in a mixture of CH_2Cl_2 and pyridine gave minor traces of a new porphyrin product as observed by TLC. Following all the unsuccessful attempts to utilise the hydroximoyl chloride functionalised porphyrin as a precursor to form the nitrile oxide, we decided to abandon this approach in favour of using the Carreira method. The *O*-silylated hydroxamic acid derivative of anthracene had proved to be a stable nitrile oxide precursor, therefore it was postulated that a stable porphrin nitrile oxide precursor could be prepared using the latter method.

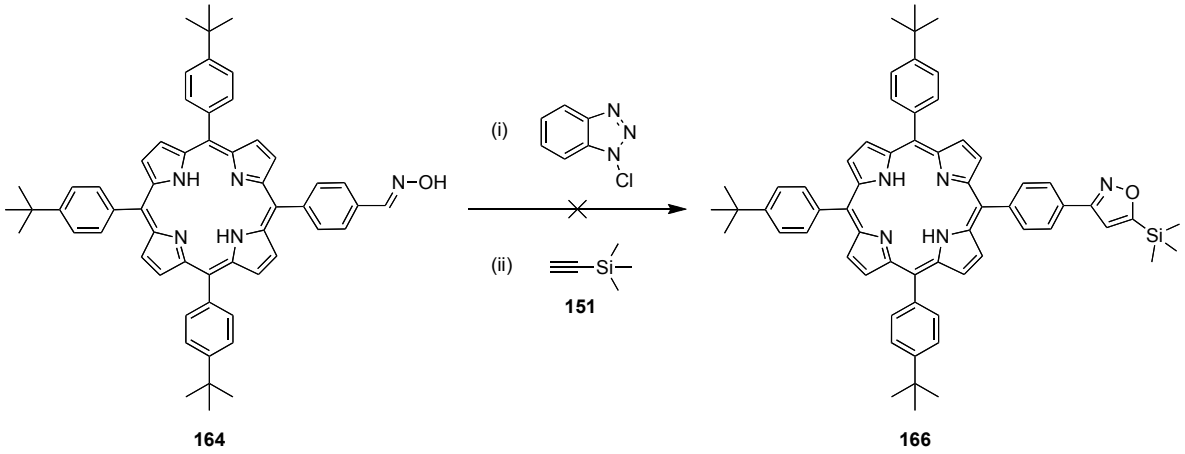

Scheme 29

Entry	Reaction temp. step i, step ii	Reaction time step i, step ii	Solvent	Result
1	0 °C, r.t.	5 min, 16 h	THF	Decomposition of porphyrin.
2	-40 °C, r.t.	1 h, 16 h	THF	No reaction. Recovery of starting material.
3	-40 °C, r.t.	15 min, 16 h	DMF	Decomposition of porphyrin.
4	-40 °C, r.t.	15 min, 16 h	CH_2Cl_2/pyridine	Traces of a new product observed by TLC.

Table 6. Reaction conditions used to attempt the synthesis of porphyrin **166**.

A tetra-*O*-silylated hydroxamic acid derivative of porphyrin was prepared from tetra-carboxyphenyl-functionalised porphyrin **167**. This was done using similar conditions as in the preparation of **156** (Scheme 24). Porphyrin **167** was exposed to oxalyl chloride to prepare the

acid chloride, which was subsequently treated with *O*-silylated hydroxylamine **155** to give porphyrin **168** in 21% yield overall following purification by chromatography. Finally, a stable porphyrin precursor to the nitrile oxide was isolated. Porphyrin **168** was then treated with trifluormethanesulfonic anhydride for 1 h at 0°C to yield the nitrile oxide functional groups, and following the reaction with trimethylsilyl acetylene **151** (200 equivalents) overnight at room temperature, the desired tetra-isoxazole porphyrin (**169**) was obtained in 62% yield, which corresponds to a yield of 89% per 1,3-dipolar cycloaddition (Scheme 30). The NMR spectrum of porphyrin **169** is shown in Figure 100.

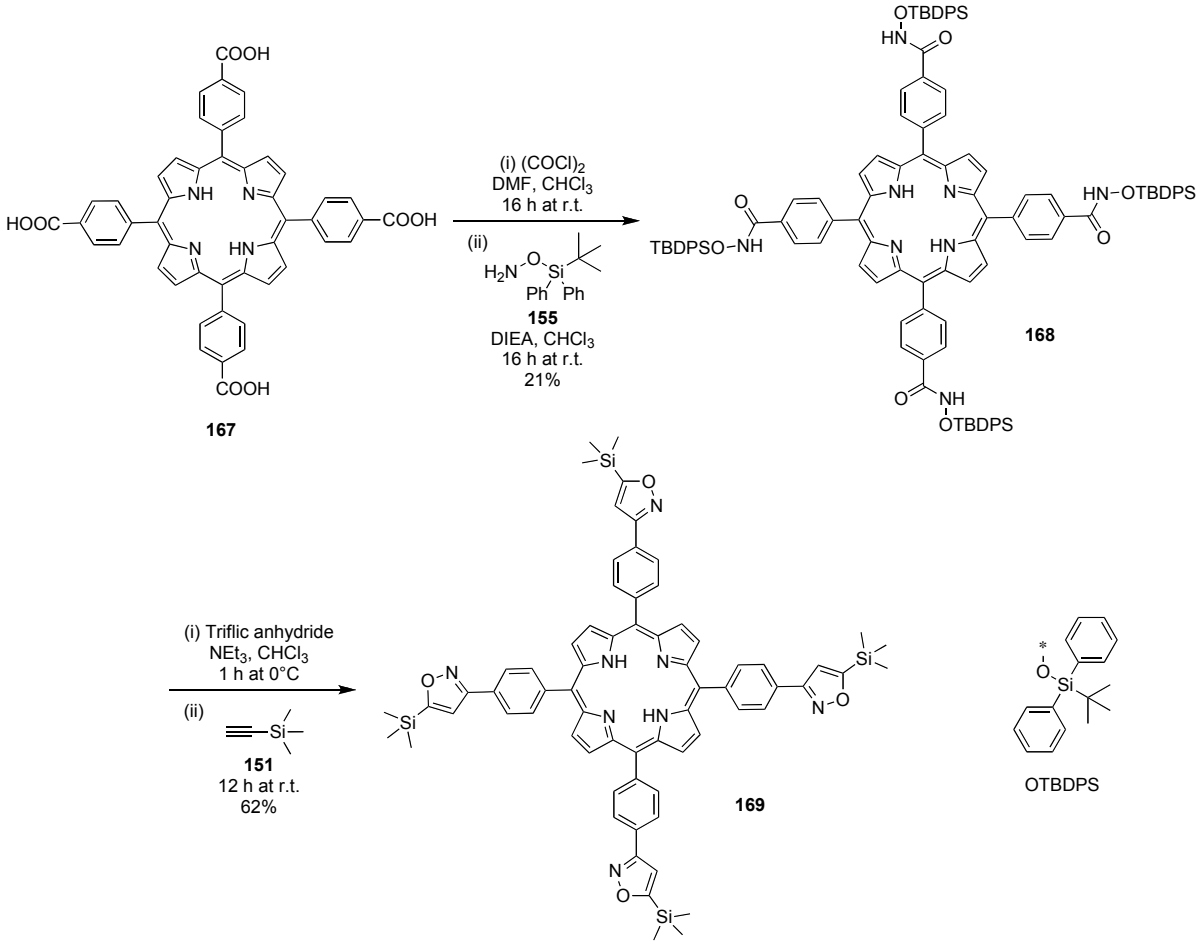

Scheme 30

Since the reaction shown in Scheme 30 required the use of a large excess of dipolarphile (200 equivalents), optimisation was required. The reaction was optimised using phenyl acetylene **170** as the dipolarophile (Scheme 31). Table 7 shows the reactions performed to lower the number of equivalents from 200 to 10, whilst maintaining a good yield. In the first entry the conditions used in Scheme 30 were applied resulting in 43% yield using **170** as the dipolarophile. Entries 2 and 3 show that reducing the number of equivalents

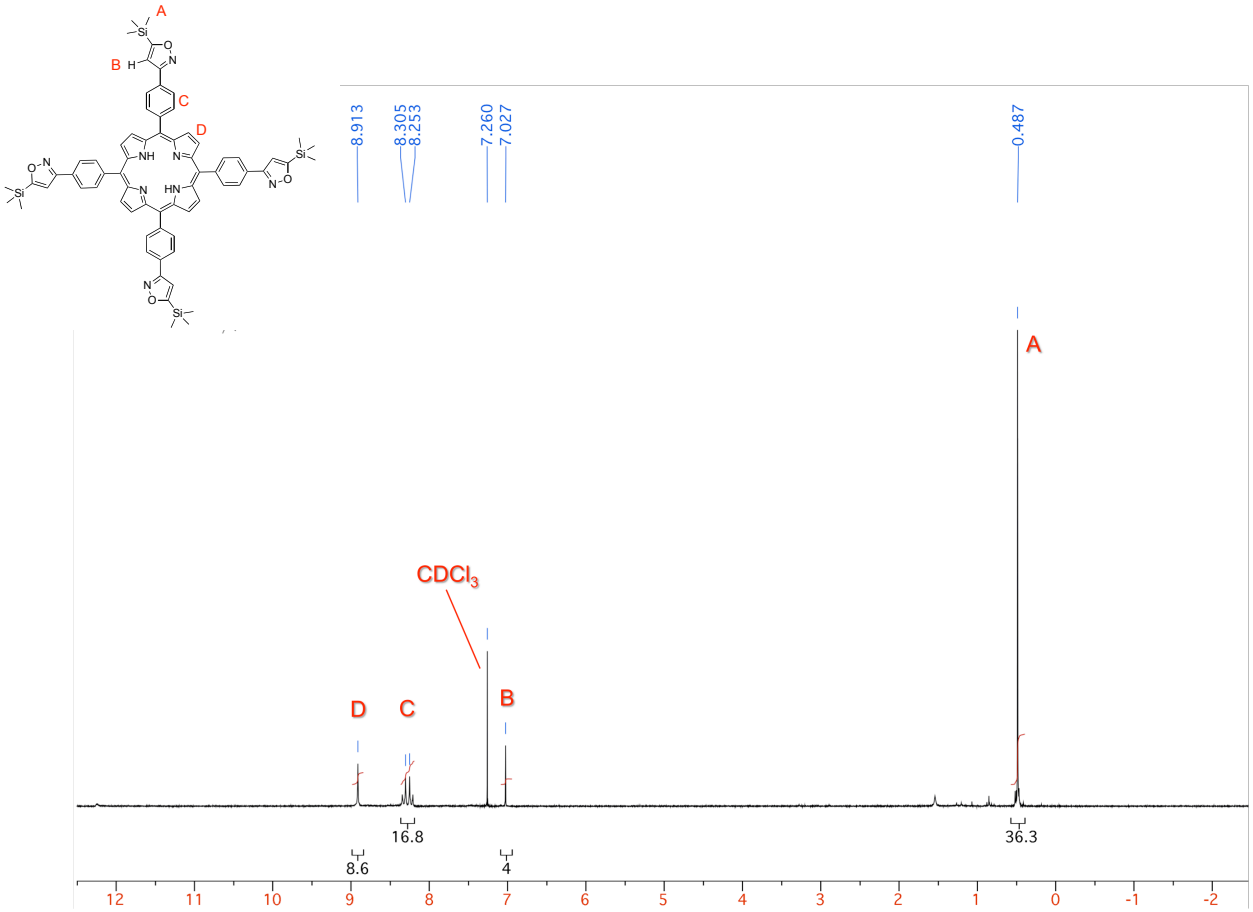

Figure 100. NMR spectrum of tetra-isoxazole porphyrin **169**.

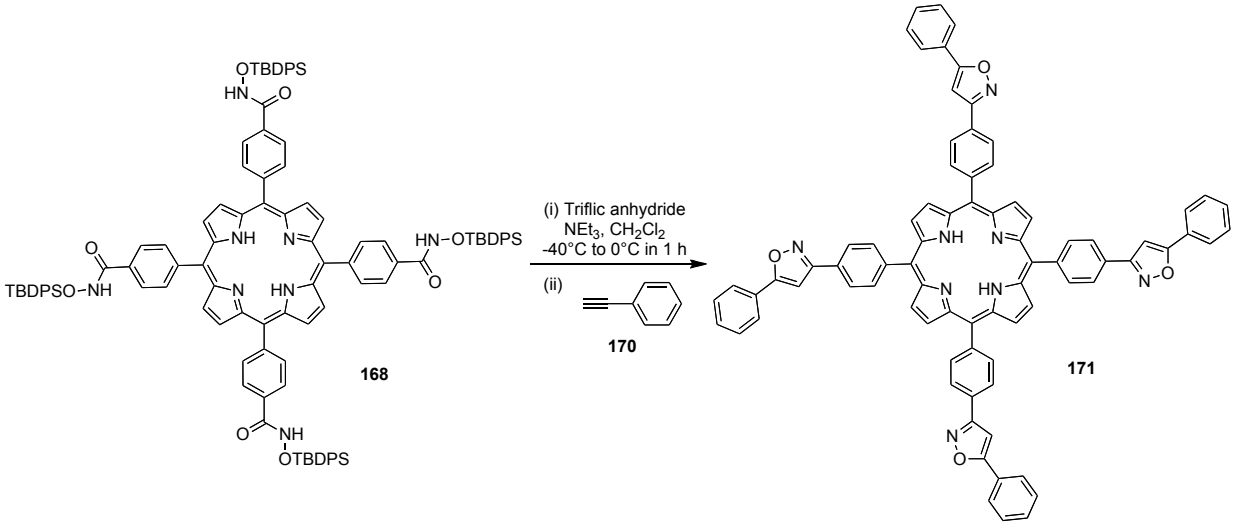

Scheme 31

Entry	Reaction conditions		Eq. of 176	Yield	Yield per cycloaddtion
1	(i) -40°C – 0°C in 1 h	(ii) 16 h at r.t.	200	43%	81%
2	(i) -40°C – 0°C in 1 h	(ii) 16 h at r.t.	50	21%	68%
3	(i) -40°C – 0°C in 1 h	(ii) 16 h at r.t.	20	<10%	<57%
4	(i) -40°C – 0°C in 1 h	(ii) 15 min at 140°C (in microwave)	50	43%	81%
5	(i) -40°C (all reagents added)	(ii) 15 min at 140°C (in microwave)	20	37%	78%
6	(i) -40°C (all reagents added)	(ii) 30 min at 80°C (in microwave)	10	51%	85%
7	(i) -40°C (all reagents added)	(ii) 16 h at r.t.	10	23%	69%

Table 7

of **170** under the same conditions caused a decrease in the yield of product **171**. Next, in entry 4, the first step of the reaction was performed in the same way as before, however, the second step was performed in the microwave. In this case, using 50 equivalents of **171**, the same yield (43%) was achieved as in entry 1, but with a lower number of equivalents. At this point, the effect of adding all the reagents at -40°C, and running the reaction directly in the microwave was examined (entry 5). Using 20 equivalents of **171** in this case, the yield was reduced to 37%, which compared to the 43% obtained in entry 4 with 50 equivalents of **171**, was not a significant reduction considering the lower amount of **171** used. In entry 6, applying the same first step as entry 5, reducing the equivalents of **171** further to 10 equivalents, and using milder microwave conditions, resulted in the best yield of 51% overall for compound **171**, or 85% per cycloaddition. This yield was an improvement over the original conditions in entry 1. For comparison purposes, entry 6 was repeated without microwave irradiation to determine whether the yield increase was due to the addition of all the reagents at -40°C or due to the microwave conditions. Comparing the results of entry 7, entry 2 and entry 3, it can be observed that adding all the reagents at -40°C directly had a beneficial effect on the yield. However, comparing the result to entry 6 shows that the microwave irradiation also had an advantageous effect on the reaction. Therefore, the combination of both changes contributed to the increased yield. These effects are explicable by the fact that as soon as the nitrile oxide is formed, the acetylene is present to react with it, before the nitrile oxide species are able to dimerise to form furoxan species. Also, the increased energy provided by the microwave irradiation enhances the reaction rate, consequently improving the yield since less furoxans have time to form. Following the optimisation of this reaction, it was anticipated that this reaction could be exploited further. Recognizing the importance of the porphyrin scaffold for future nanodevices, the reaction could allow the rapid preparation of a library of tetra-meso-

substituted porphyrins bearing diverse functionalities. Therefore as a perspective to this work, the scope and limitations of this reaction would be tested with a variety of acetylenes (Figure 101).

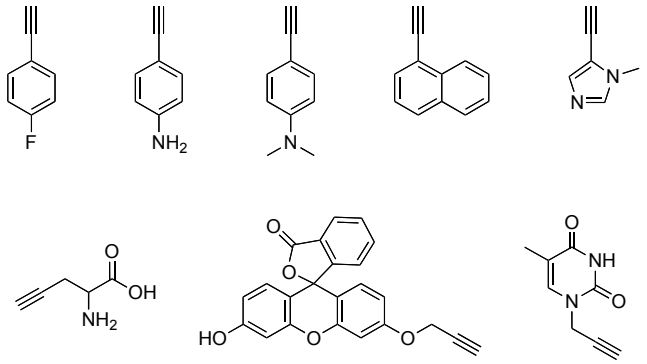

Figure 101. The acetylene library that was planned for testing the scope and limitations of the nitrile oxide-alkyne 1,3-dipolar cycloaddition to prepare a library of tetra-meso-substituted porphyrins.

2.2.3.5 Preparation of PNA-chromophore adducts using via Cu(I)-free nitrile oxide-acetylene 1,3-dipolar cycloaddition reactions

The development of the nitrile oxide-acetylene 1,3-dipolar cycloaddition reaction with PNA and porphyrin respectively, indicated that the method compatible to both classes of molecules was the Carreira approach to preparing the nitrile oxide species. Consequently, we decided to examine the utility of the method to prepare a variety of PNA-chromophore adducts. The chromophores selected were pyrene, porphyrin, phenanthroline and fluorescein.

O-silylated hyrdoxamic acids of pyrene, porphyrin, phenanthroline and fluorescein derivatives were prepared (Scheme 32). The pyrene hydroxamate derivative **173** was prepared from the commercially available 1-pyrenecarboxylic acid **172**, by converting the carboxylic acid moiety into the acid chloride using oxalyl chloride followed by treatment with *O*-silylated hydroxylamine **155** to give pyrene hydroxamate derivative **173** in 45% yield. Using a previously prepared mono-carboxylic acid functionalised porphyrin **133** (Scheme 15), the same conditions applied on the pyrene were used to yield the porphyrin **174** bearing a single *O*-silylated hydroxamic acid moiety.

The hydroxamate of fluorescein was prepared on the end of an extended linker in an attempt to increase it's solubility in apolar media. Furthermore, three 'linkage' points were introduced, a triazole prepared by a copper-catalysed cycloaddition, a thiourea prepared by the reaction between an amine and an isothiocyanate, and the *O*-silylated hydroxamate to prepare the isoxazole. The reason for introducing the three linkage points was so that a comparative study into which linkage is the most efficient in preparing the PNA-fluorescein

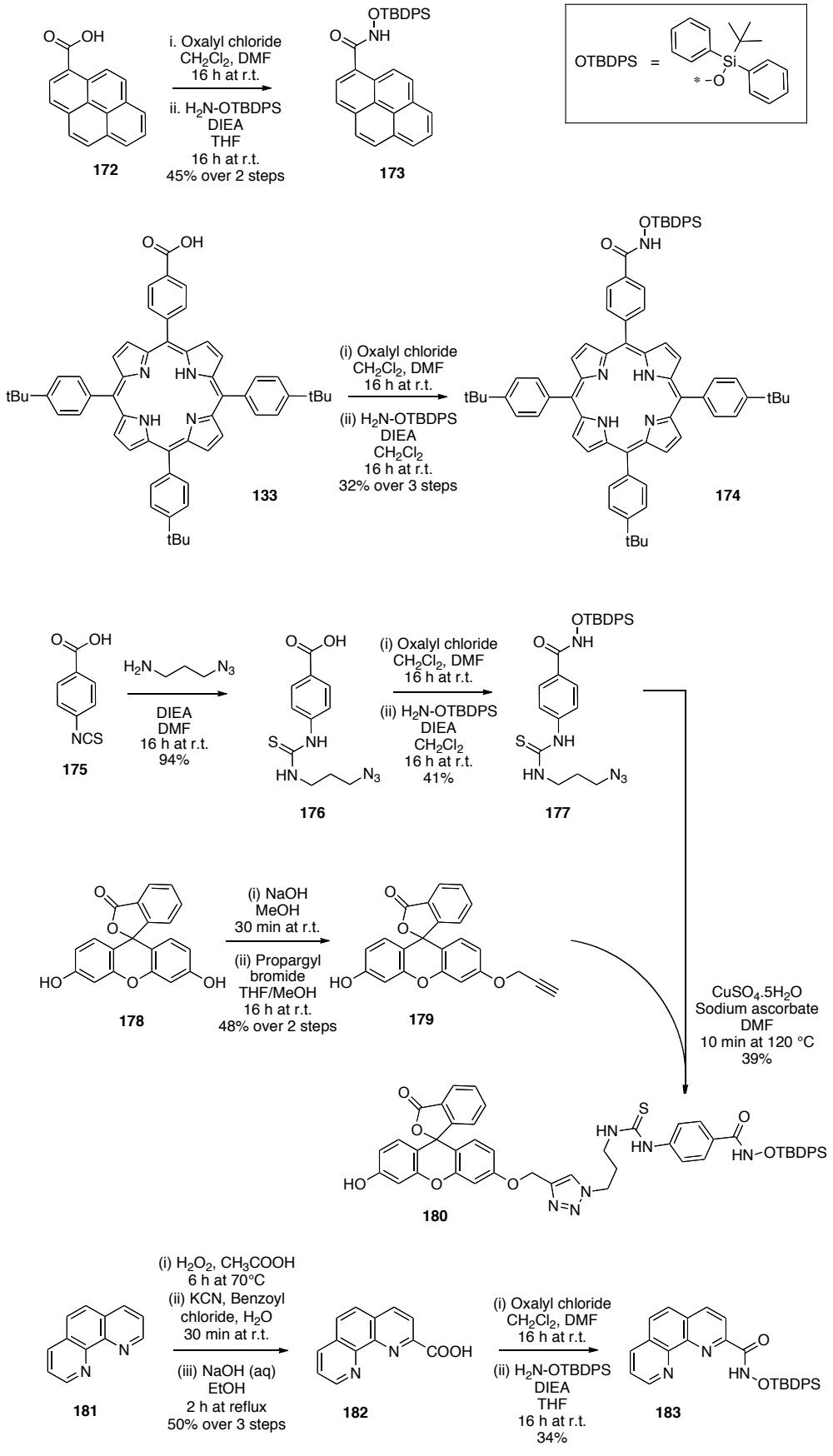
i. Oxalyl chloride
CH2Cl2, DMF
16 h at r.t.
ii. H2N-OTBDPS
DIEA
THF
16 h at r.t.
45% over 2 steps
OTBDPS =
172
173
(i) Oxalyl chloride
CH2Cl2, DMF
16 h at r.t.
(ii) H2N-OTBDPS
DIEA
CH2Cl2
16 h at r.t.
32% over 3 steps
133
174
DIEA
DMF
16 h at r.t.
94%
175
176
(i) Oxalyl chloride
CH2Cl2, DMF
16 h at r.t.
(ii) H2N-OTBDPS
DIEA
CH2Cl2
16 h at r.t.
41%
177
(i) NaOH
MeOH
30 min at r.t.
(ii) Propargyl
bromide
THF/MeOH
16 h at r.t.
48% over 2 steps
178
179
CuSO4.5H2O
Sodium ascorbate
DMF
10 min at 120 °C
39%
180
(i) H2O2, CH3COOH
6 h at 70°C
(ii) KCN, Benzoyl
chloride, H2O
30 min at r.t.
(iii) NaOH (aq)
EtOH
2 h at reflux
50% over 3 steps
181
182
(i) Oxalyl chloride
CH2Cl2, DMF
16 h at r.t.
(ii) H2N-OTBDPS
DIEA
THF
16 h at r.t.
34%
183

Scheme 32

adduct could be carried out. Initially, however, the isoxazole formation was to be investigated, therefore the required fluorescein was prepared as follows. 4-isothiocyanatobenzoic acid **175** was treated with 3-azidopropylamine to prepare the thiourea **176**. Next, **176** was converted to hydroxamate in a manner analogous to that of the pyrene and porphyrin to give **177**, which was ready for attachment to the fluorescein via the azide functional group. Fluorescein **178** was converted to the disodium salt upon treatment with sodium hydroxide, which was then exposed to propargyl bromide yielding **179** in 48% yield over the two steps. Fragments **177** and **179** were then covalently attached via a Cu(I)-catalysed click reaction giving the fluorescein hydroxamate derivative **180**.

Finally, a phenanthroline hydroxamate derivative **183** was also prepared. Using the conditions reported by *Corey et al*.[261], which were later updated by *Sun et al*.[262] a carboxylic acid moiety was introduced in the 2-position of 1,10-phenanthroline to prepare 2-carboxy-1,10-phenanthroline **182**. Briefly, the nitrogen atom in the 1-position was oxidized using hydrogen peroxide in glacial acetic acid, which upon exposure to benzoyl chloride and potassium cyanide yielded 2-cyano-1,10-phenanthroline, which was subsequently hydrolysed under basic conditions to give **182**. As before, treatment of the acid with oxalyl chloride and **155** yielded the hydroxamate derivative of phenanthroline **183** via the acid chloride.

Attempts to synthesize PNA-chromophore adducts using the four *O*-silylated hydroxamic acid derivatives were performed. The general procedure and a summary of the results is described in Scheme 33. The conditions were the same as those used to prepare the PNA-anthracene adduct **160** (Scheme 26), *i.e.*, to prepare the nitrile oxide, 10 equivalents of either **173**, **174**, **180** or **183** were dissolved in CH_2Cl_2, NEt_3 (30 eq.) was added and then following cooling to -40°C, triflic anhydride (11 eq.) was added dropwise. After allowing the temperature of the mixture to reach 0°C in 1 h, the mixture was added to the resin-bound PNA oligomer bearing the acetylenic linker (**158**) suspended in DMF. The suspension was then shaken for 16 h at 50°C. The results obtained following the 1,3 dipolar cycloaddition reactions varied depending on which hydroxamate (**173**, **174**, **180** or **183**) was used.

The reaction with the pyrene derivative **173** yielded a new product **184** as observed by HPLC analysis (Figure 102). It eluted at a retention time (30.16 min) similar to that of the anthracene-PNA adduct **160** (Figure 97), and also it absorbed at the 360 nm wavelength of the HPLC's UV detector, indicating that the target compound **184** had formed. Following purification and deprotection, the compound was sent for MALDI-TOF-MS analysis, which confirmed the presence of the target compound **184** (in its deprotected form). The mass spectrum obtained displayed the presence of impurities indicating that further purification was required (Figure 103). Nonetheless, the peak in the mass spectrum at m/z 3730.5161,

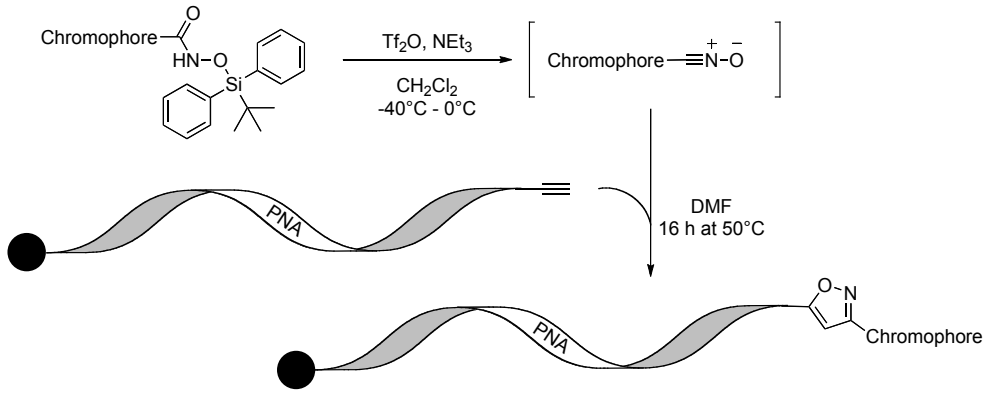

Chromophore	Starting material	Product following resin cleavage	Comment
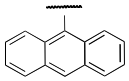	**156**	**160**	Product was isolated.
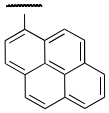	**173**	**184**	Product was isolated.
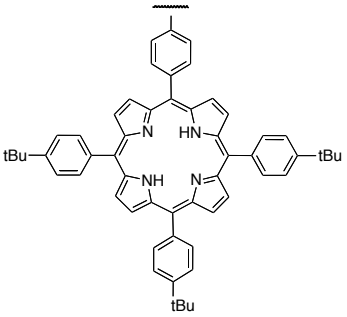	**174**	**185**	Product was not isolated due to the insolubility of the porphyrin nitrile oxide species.
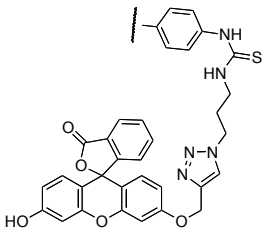	**180**	**186**	Product was not isolated. Nitrile oxide was not formed because the triflic anhydride was reactive towards the nucleophilic functional groups present in fluorescein **180**.
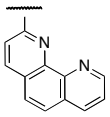	**183**	**187**	New product formed, however, MALDI-TOF-MS analysis indicated that the new product was not **187**.

Scheme 33

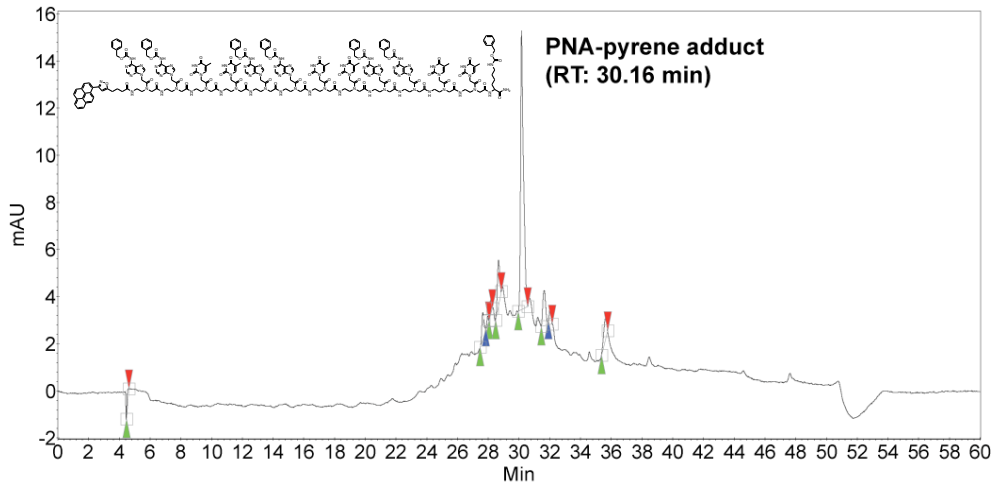

Figure 102. HPLC chromatogram of the crude mixture of **184** isolated from the resin following the nitrile oxide-alkyne 1,3-dipolar cycloaddition performed for 16 h at 50°C. (Varian Pursuit C18, 5 µm, 4.6 x 250 mm, gradient: 0.1% TFA in H_2O to 0.1% TFA in CH_3CN, flow: 1 mL/min, 65°C)

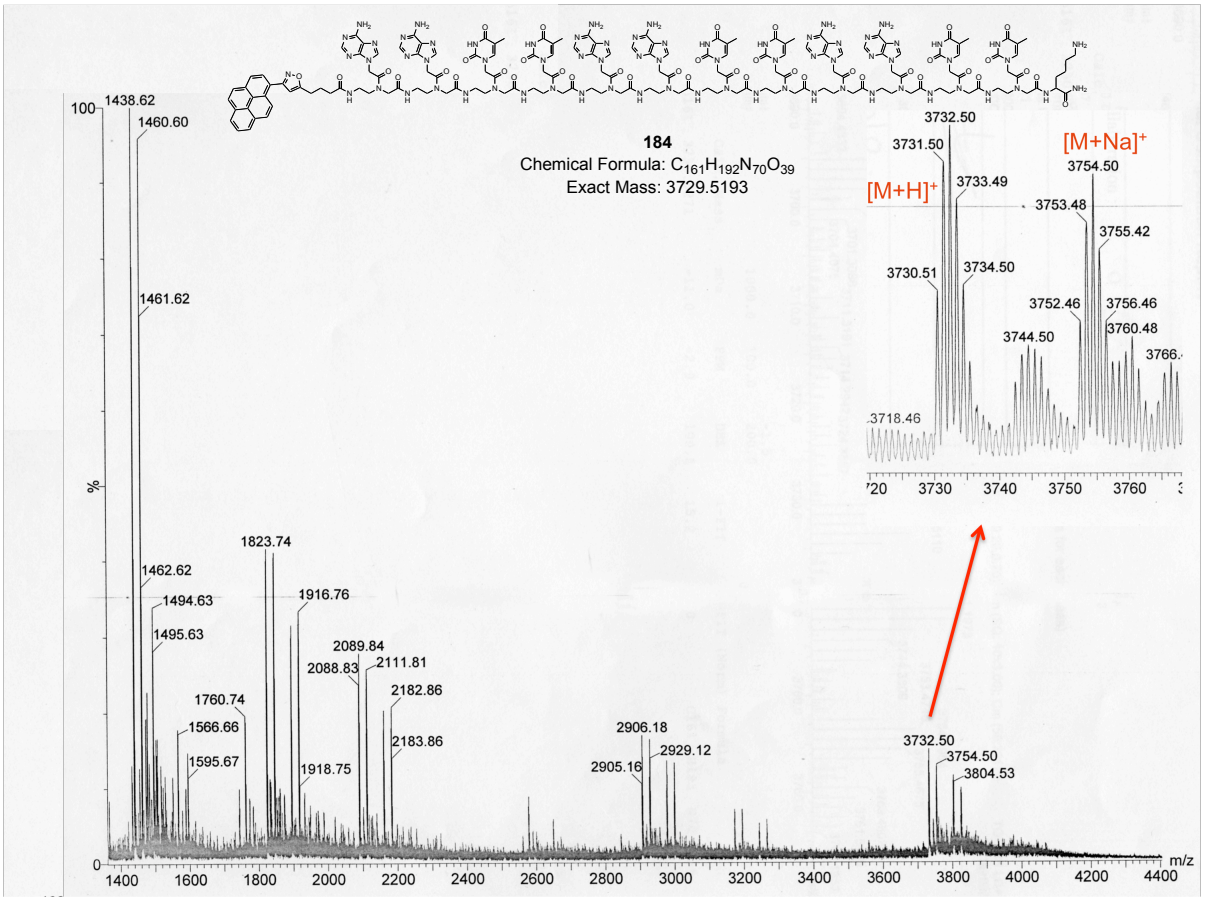

Figure 103. MALDI-TOF-MS of the deprotected PNA-pyrene adduct **184**.

corresponded to the calculated mass for the protonated form, $[M+H]^+$ of **184** ($C_{161}H_{193}N_{70}O_{39}$), m/z 3730.5271.

The attempt to prepare the PNA-porphyrin adduct **185**, using porphyrin hydroxamate **174** did not work. No traces of the isoxazole product were observed in the HPLC chromatogram. The main reason for this failed reaction was due to the solubility of the porphyrin nitrile oxide species. Following the formation of the nitrile oxide species in CH_2Cl_2, the porphyrin was added to the suspension of the PNA derivatised resin, and at this point, the porphyrin was observed to precipitate. The product was not obtained even following repeated trials. It is postulated that if a porphyrin bearing polyglycolic functions in place of the *tert*-butyl groups in porphyrin **174** were used in the reaction, the cycloaddition would proceed as expected.

Unfortunately, the same result was obtained with the fluorescein hydroxamate **180**. The reaction did not yield the target product **186**. In this case, the problem was possibly due to the presence of multiple reactive functional groups in fluorescein derivative **180**. The nucleophilic groups (*e.g.* the alcohol functional group) could react with the triflic anhydride reagent, preventing the formation of the nitrile oxide species, hence preventing the cycloaddition from occurring. Currently, an alternative fluorescein hydroxamate is under preparation to reattempt the cycloaddition reaction.

Finally, the cycloaddition reaction with the phenanthroline derivative **183** was attempted. The HPLC chromatogram obtained following the reaction indicated that the crude mixture contained a new product (Figure 104). The retention time of the new product was 27.81 min, which differed only slightly from the retention time of the PNA-acetylene precursor (27.13 min). The product was purified and deprotected in order to be analysed by MALDI-TOF-MS. The mass spectrometry result obtained indicated that a new product had been obtained having a molecular mass $[M+H]^+$ of m/z 3606.6648, however it was not the target product **187**, since the mass differed by a mass of m/z 102 from the calculated molecular mass of **187** ($C_{157}H_{190}N_{72}O_{39}$), m/z 3707.5098. Also, the mass obtained did not correspond to the PNA-acetylene precursor **159** (m/z 3487.4587). Furthermore, the product did not correspond to any fragmentation that could have occurred during under the ionisation conditions used in the MALDI-TOF-MS analysis, therefore further tests are required to determine the structure of the product obtained.

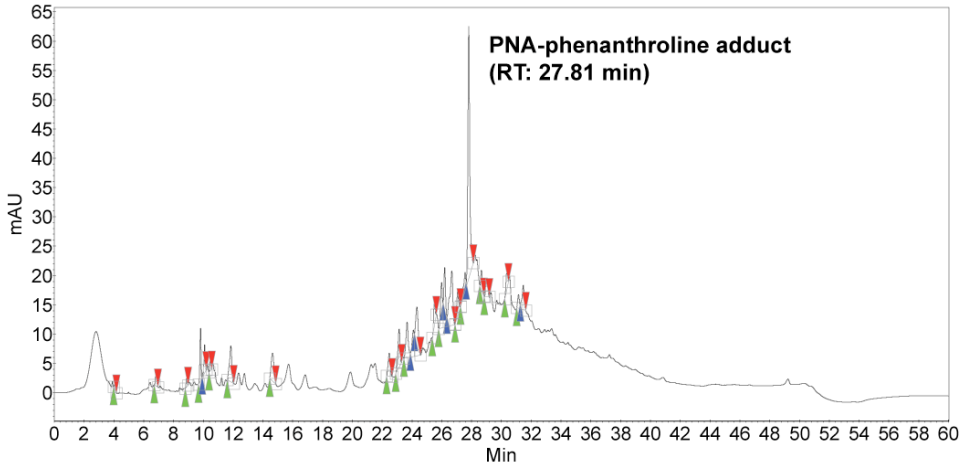

Figure 94. HPLC chromatogram of the crude mixture of **193** isolated from the resin following the nitrile oxide-alkyne 1,3-dipolar cycloaddition performed at 50°C. (Varian Pursuit C18, 5 µm, 4.6 x 250 mm, gradient: 0.1% TFA in H_2O to 0.1% TFA in CH_3CN, flow: 1 mL/min, 65°C)

2.3 PRELIMINARY AFM INVESTIGATION OF THE DEPOSITION OF PNA ONTO MICA SURFACES

As described in the introduction, very few investigations of PNA on surfaces exist, and all of them involve the covalent linkage of PNA strands onto surfaces to prepare self-assembled monolayers (SAMs) mainly for the development of biosensors.[188] Since we are working towards the preparation of porous self-assembled arrays on surface, in our case, the PNA would not be covalently attached to the surface. Therefore, it was necessary to investigate whether the PNA oligomers could be deposited onto surfaces, and whether the single stranded oligomers would be able to form duplexes on the surfaces. To this end, we decided to carry out a preliminary AFM investigation into the deposition of PNA onto mica surfaces using self-complementary PNA dodecamer **127**.

The PNA dodecamer **127** was dissolved in water at a concentration of 0.6 mM and then, one drop of solution was spin coated on a freshly cleaned mica surface (3 minutes at 3000 rpm). AFM imaging in tapping mode was performed on the resultant mica surface (Figure 105 left). Bright irregular spots were observed on the surface, and following height profiling of the protrusions, it was concluded that the spots corresponded to aggregates of PNA, not PNA duplexes, since the height of each spot was in the region of 5-16 nm. The expected height of a PNA duplex is approximately 1 nm (Figure 106). In order to confirm that the observed signals were indeed due to PNA aggregates, rather than surface artefacts, the experiment was repeated with 3 drops of the same solution deposited onto a clean mica surface. As expected, the AFM images obtained (Figure 105 right) displayed larger

aggregates (height profiles: 5-40 nm), confirming that observed signals were likely to be PNA aggregates on the mica surface.

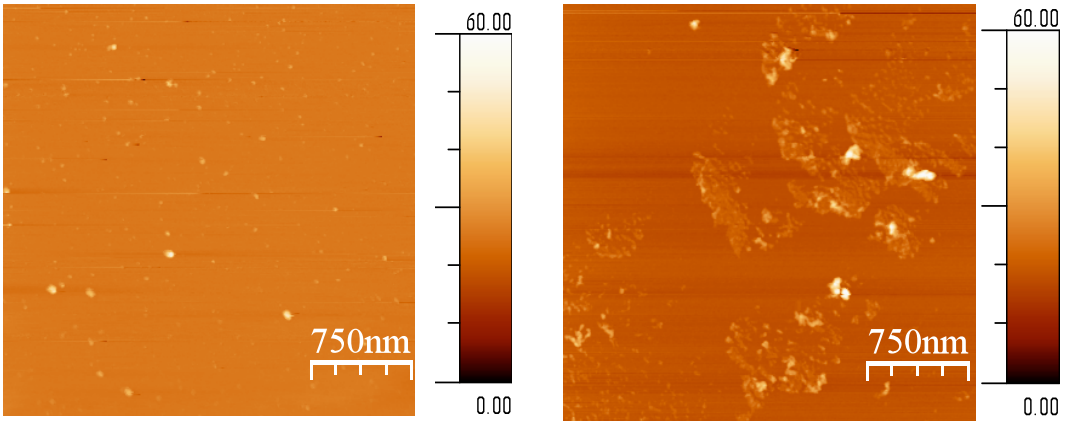

Figure 105. AFM images (height scale: 60 nm) displaying aggregates of PNA formed upon deposition of one drop (left) and three drops (right) of a 0.6 mM solution of dodecamer **127** onto a clean mica surface via spin coating.

It was postulated that annealing the self-complementary PNA strands would allow them to form the thermodynamically stable double helices. In order to anneal the aqueous PNA solution, it was placed in an NMR tube and was loaded into the NMR. Using the temperature control of the instrument, the solution was heated to 80°C for 10 minutes, after which the solution was cooled in a controlled manner from 80 °C to 30 °C at 2°C per minute. The slow rate of cooling was used to ensure that the hydrogen bonds between the nucleobases in PNA were formed in the most thermodynamically favoured manner, thus ensuring duplex formation. Following the completion of the annealing, once again, 1 drop of the solution was

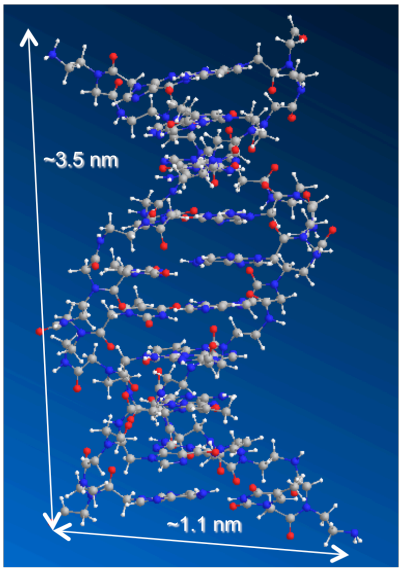

Figure 106. Molecular model of PNA duplex $(\mathbf{127})_2$. The minimized structure was obtained using an Amber2 method. The dimensions of a PNA duplex are displayed.

deposited by spin coating (3 min at 3000 rpm) onto a clean mica surface, and then AFM images were collected. Figure 107 (left) shows the image obtained following the deposition of the annealed PNA solution. Figure 107 (right) shows clean mica as a comparison in order to show that in the image on the left there is the presence of a compound covering the entire surface. Both images are displayed with height profiles of maximum 3 nm, compared with the images in Figures 105, which have height profiles of maximum 60 nm, indicating that the aggregates were no longer present following the annealing.

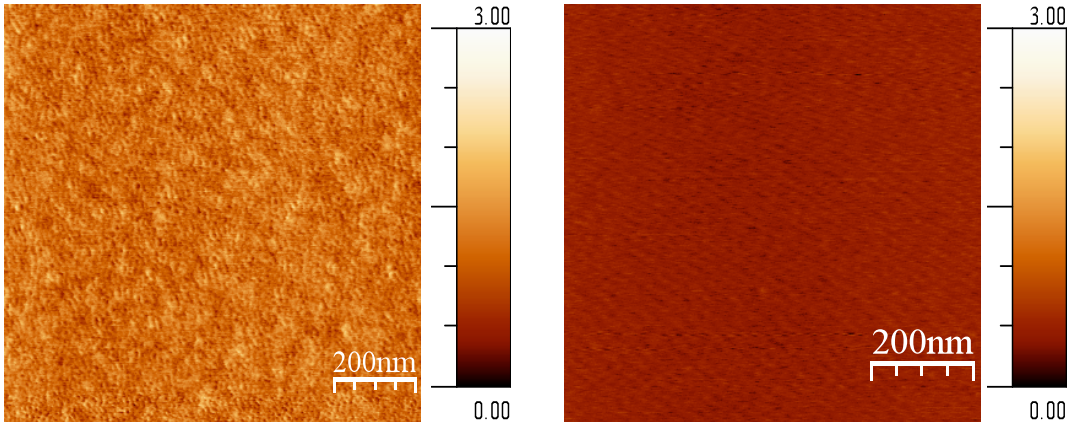

Figure 107. The AFM image (height scale: 3 nm) on the left displays a mica surface saturated with PNA duplexes formed upon deposition of one drop of an annealed solution of dodecamer **127** onto a clean mica surface via spin coating. The AFM image (height scale: 3nm) on the right displays a clean mica surface for comparison.

Since the entire mica surface was thought to be covered by PNA duplexes, the solution was diluted 10-fold and was redeposited onto a clean mica surface in the same manner as described before. The AFM image that resulted from the diluted solution is displayed in Figure 108 (left). The image shows bright spots intermitted by clean mica (dark red regions) indicating that this time the surface was not entirely covered by PNA oligomers. Topographical analysis of the surface (graph in Figure 108) shows that the most frequent height class of the bright protrusions in the image is approximately 1 nm, which closely corresponds to the expected height of the PNA duplexes. These observations confirm that strands of **127** can be successfully annealed into PNA duplexes, which later can be deposited onto mica surfaces through spin coating and imaged by AFM. This preliminary investigation provides evidence that once the target angular units and linear units bearing complementary PNA strands are prepared, the deposition of the self-assembled structures onto surfaces should not impart obstacles to achieving the goal of the project.

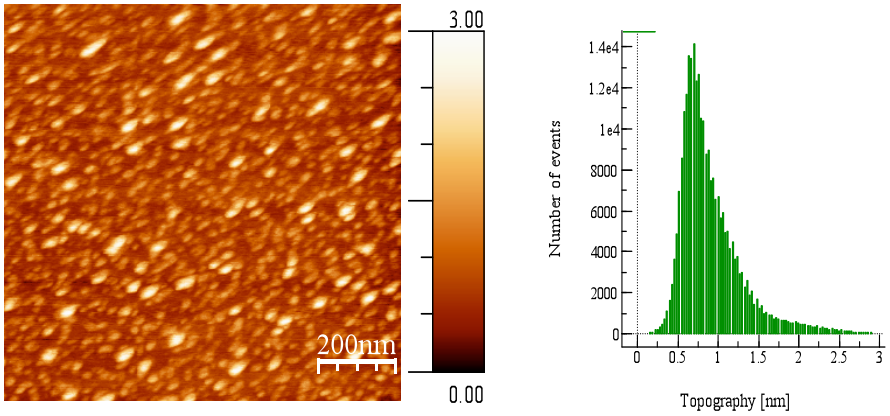

Figure 108. The AFM image (height scale: 3 nm) displays a mica surface coated with PNA duplexes formed upon deposition of one drop of an annealed solution of dodecamer **127** (concentration: 0.06 nM) onto a clean mica surface via spin coating. The graph displays the topographical analysis of the surface. The most frequent height class of the bright protrusions in the image is approximately 1 nm, which corresponds to the expected height of the PNA duplexes.

Conclusions

In conclusion, the work presented in this doctoral dissertation described the synthetic steps taken towards the preparation of nanostructured surfaces using a biomimetic approach where PNA encodes the information necessary for the self-assembly of the molecular components. This objective is summarized schematically in Figure 109.

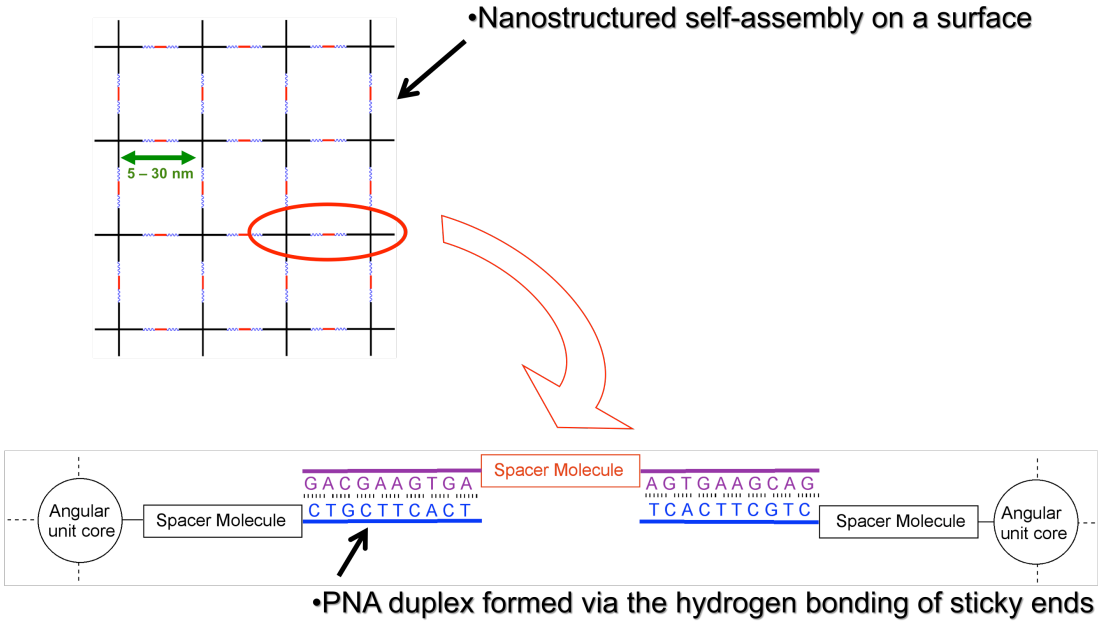

Figure 109

However, prior to synthesizing the angular and linear units bearing complementary PNA oligomers, a proof of principle was required to confirm that the PNA duplexes could be formed on surfaces and that this could also be done in the presence of choromophoric moieties (*e.g.* porphyrin) appending to the PNA oligomer. The molecule designed for the proof of principle consisted of a self-complementary PNA dodecamer bearing a porphyrin adduct (Figure 110).

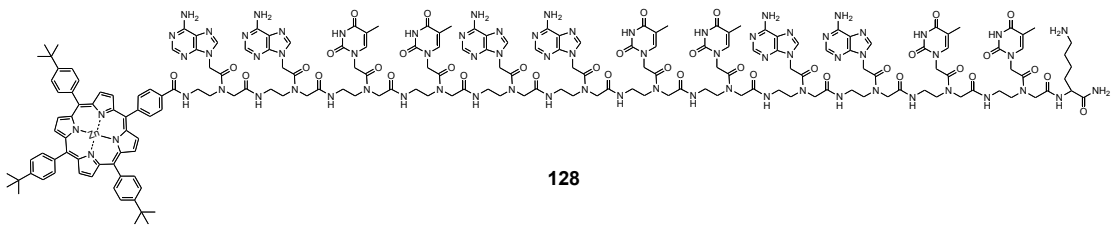

128

Figure 110

The synthesis of the PNA oligomer was tackled first. The general norm in PNA synthesis is to carry out a resin cleavage and nucleobase deprotection simultaneously in the final step following the completion of the PNA oligomerisation cycles, however, since we required a protected PNA strand for subsequent solution phase reactions, an alternative protecting group strategy had to be designed. To this end, an orthogonal protecting group strategy was designed to ensure that protected PNA strands could be cleaved from the solid support resin. In the first design, a Fmoc/Mmt-protecting group strategy was chosen for the PNA synthesis and a Tentagel resin bearing a base-cleavable linker was chosen as the solid support. Following the preparation of the thymine monomer, the oligomerisation conditions were tested. Unfortunately, the hydrolysis of the linker failed under the cleavage conditions, therefore, the PNA synthesis strategy was modified. In the second orthogonal system that was designed, an acid-cleavable Rink linker bound to a polystyrene resin was chosen as the solid support, therefore a more robust nucleobase protecting group strategy was required. A Fmoc/Cbz-protecting group strategy was chosen since it would allow the cleavage of the oligomer from the resin, without the deprotection of the Cbz groups from the nucleobases. The required monomers for the oligomer synthesis (Figure 111) were then prepared using established procedures.[203]

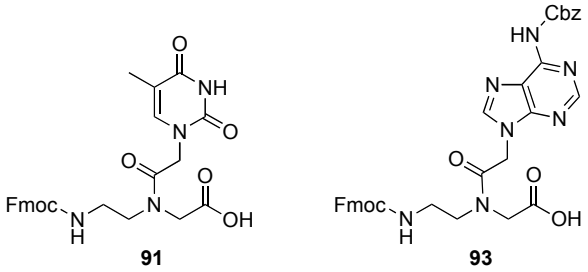

Figure 111

Following reports of the advances in microwave-assisted solid phase peptide synthesis claiming improved purity of oligomeric peptides using short coupling times, the solid phase PNA oligomerisation was attempted using microwave irradiation. Three attempts were performed. The first, using a standard laboratory microwave, resulted in a complex, inseparable mixture of products at the dodecamer stage. An improvement was observed in the results using the CEM discover SPS microwave which was specifically designed for solid phase synthesis, however, the crude dodecamer obtained was still inseparable from the by-products. Similar results were obtained with the CEM liberty microwave, which was an automated solid phase synthesis setup. Finally, utilising manual solid phase synthesis, the target PNA dodecamer was obtained. The oligomerisation process was monitored by cleaving

samples of the growing oligomer at the tetramer, octamer and dodecamer stages and analysing the resultant products. Following purification of the samples, MALDI-TOF-MS analysis was performed. The spectra displayed mainly peaks corresponding ionisation-induced fragmentation products, however, the presence of minor peaks corresponding to the target oligomers gave confidence that the desired products had been isolated. In order to conclusively prove that the desired dodecamer had been obtained, the Cbz-protected nucleobases were deprotected by treatment with TMSI to render the oligomer more easily ionisable. ESI-MS analysis of the deprotected oligomer (Figure 112) subsequently confirmed that the target dodecamer had been obtained.

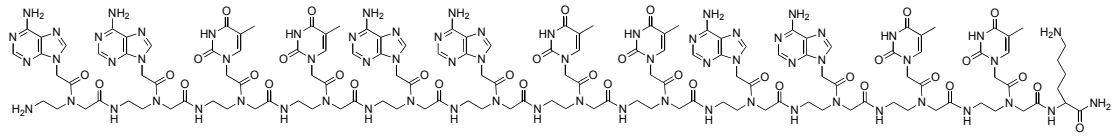

127

Chemical Formula: $C_{138}H_{177}N_{69}O_{37}$
Exact Mass: 3392.4090

Figure 112

Following the isolation of the PNA dodecamer, attempts to covalently attach the porphyrin moiety to the resin-bound oligomer via an amide linkage failed, possibly due to steric hindrance. Subsequently, an azide linker was appended to the oligomer, and attempts to attach an acetylene functionalised porphyrin using a Cu(I)-catalysed 1,3-dipolar cycloaddition were performed. Unfortunately, this approach did not yield the target adduct. These unsuccessful results paved the way to the development of a Cu(I)-free 1,3-dipolar cycloaddition that enabled the attachment of chromophores to the PNA oligomer.

Reports of Cu(I)-free 1,3-dipolar cycloaddition reactions applied on DNA oligomers that were recently published by the groups of Heaney[251, 252] and Carell[253, 254] offered inspiration towards this goal. Their strategies involved the generation of a nitrile oxide species *in situ*, which then reacts with either an alkene or an alkyne to form an isoxazoline or an isoxazole. Two methods of generating the nitrile oxide species were evaluated using anthracene derivatives. The first method involved the base-mediated dehydrochlorination of anthracene hydroximoyl chloride to yield the nitrile oxide, which reacted with a dipolarophile (trimethylsilyl ethylene) that was introduced to the reaction mixture. The second approach to generating a nitrile oxide involved treating an *O*-silylated hydroxamic acid derivative of anthracene with trifluoromethanesulfonic anhydride in the presence of a base (Carreira method). Following successful tests of both methods using trimethylsilyl ethylene as the dipolarophile, the reactions were applied on a resin-bound, acetylene-functionalised PNA

dodecamer. Both methods yielded the target PNA-anthracene adduct. These Cu(I)-free 1,3-dipolar cycloaddition reactions involving TMS acetylene and an acetylene-functionalised PNA dodecamer are summarized in Figure 113.

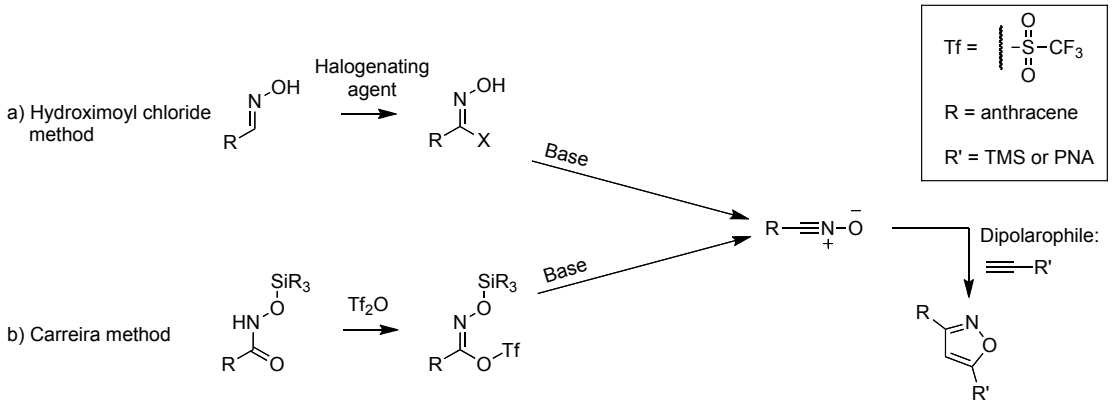

Figure 113

Since the nitrile oxide-acetylene 1,3-dipolar cycloaddition reaction method had never been applied on porphyrins, the two methods were tested. Attempts to prepare a hydroximoyl chloride derivative of a porphyrin resulted in the decomposition of the macrocycle upon treatment with chlorinating agents (NCS, *tert*-BuOCl, and 1-chlorobenzotriazole), therefore, the hydroximoyl chloride method was abandoned in favour of the Carreira method. An *O*-silylated hydroxamic acid derivative of porphyrin was synthesized, and upon exposure to trifluoromethanesulfonic anhydride and Et_3N the nitrile oxide was generated and was trapped with the trimethylsilyl ethylene dipolarophile (Figure 114).

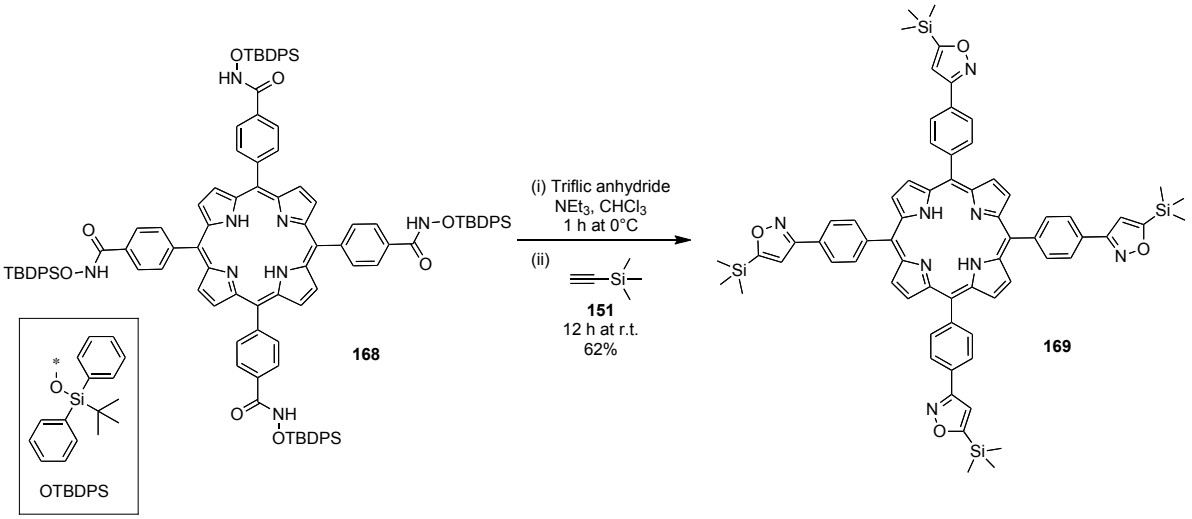

Figure 114

Having developed a protocol that was compatible with both PNA and porphyrin, the utility of the method to prepare a variety of PNA-chromophore adducts was tested. Hydroxamate derivatives of pyrene, porphyrin, phenanthroline and fluorescein chromophores were synthesized. Subsequently, the corresponding nitrile oxide species were generated and were reacted with the resin-bound, acetylene-functionalised PNA dodecamer (Figure 115). The PNA-pyrene adduct was isolated following resin cleavage, however, the other PNA-chromophore products were not isolated. The porphyrin nitrile oxide derivative was insoluble in the reaction medium and since it precipitated, the cycloaddition reaction was unable to proceed. In the case of the fluorescein hydroxamate, the presence of various nucleophilic groups in the starting material could have reacted with the trifluoromethanesulfonic anhydride reagent, preventing the formation of the nitrile oxide species, hence preventing the cycloaddition from occurring. Finally, the reaction with the phenanthroline derivative yielded a new product that did not correspond the target PNA-phenanthroline adduct. These reactions are currently being investigated to ensure that the PNA-chromophore adducts can be prepared successfully (see Chapter 4 - Perspectives).

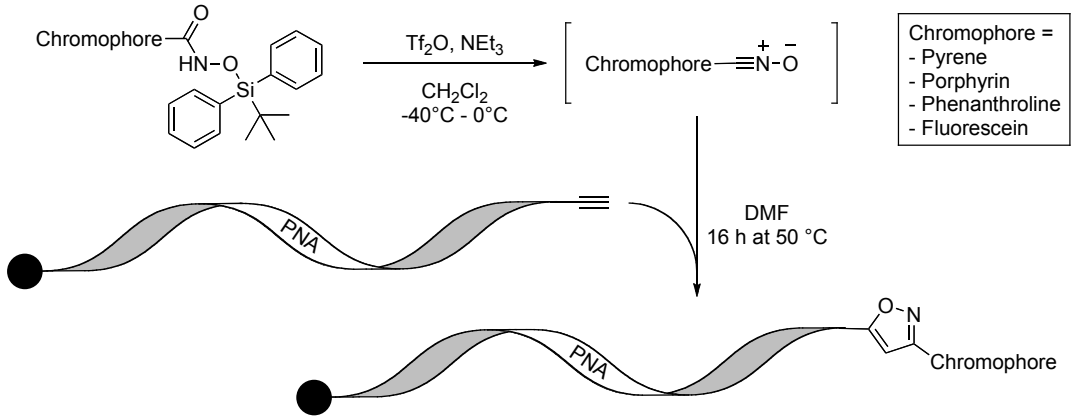

Figure 115

In parallel to the synthetic work, a preliminary study into the deposition of PNA onto mica surfaces was investigated using AFM imaging. Deposition of drops of an aqueous solution of deprotected PNA dodecamer onto clean mica surfaces using spin coating resulted in aggregates of PNA on the surface. Following annealing of the solution, a repeated deposition of a single drop of the solution resulted in a completely different surface assembly. The surface was saturated by what was thought to be PNA duplexes. This was confirmed by the deposition of drop of a solution that was diluted ten-fold which resulted in an AFM image where bright spot were intermitted by clean mica surface. Topographical analysis of the surface indicated that the bright spots were an average in 1 nm in height, which corresponds

to the height of a PNA duplex, thus confirming that PNA duplexes could be deposited onto surfaces. The PNA duplexes imaged by AFM on a mica surface, as well as the topographical analysis are shown in Figure 116.

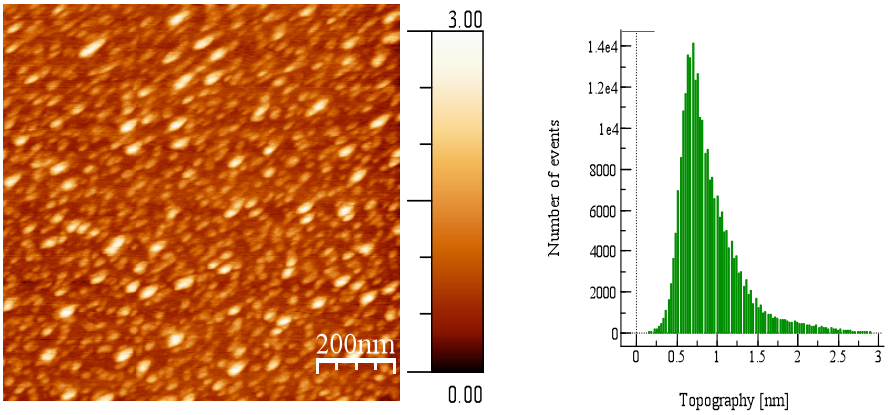

Figure 116

Perspectives

Subsequent work will focus mainly on the synthesis of the chromophores that would be compatible with the Cu(I)-free 1,3-dipolar cycloaddition required for preparing the PNA-chromophore adducts. A porphyrin bearing solubilising polyglycol chains will be prepared **188** (Figure 117), as well as a fluorescein derivative compatible with triflic anhydride will by synthesized **189** (Figure 117). Following their synthesis, the respective PNA-chromophore adducts will be prepared using the developed cycloaddition reaction. Additionally, the reaction with the phenanthroline derivative will be repeated and investigated further. Once all the PNA-chromophore adducts are obtained, their duplex formation will be investigated to determine the effect of the chromophore on the melting temperature of the PNA duplex. Also, using the PNA-phenanthroline adduct **187**, the preparation of molecular wires will be attempted by exploiting the complexation of the phenanthroline with copper and the hydrogen bonding of the PNA to prepare an alternating Cu(I)-complex-PNA duplex supramolecular system.

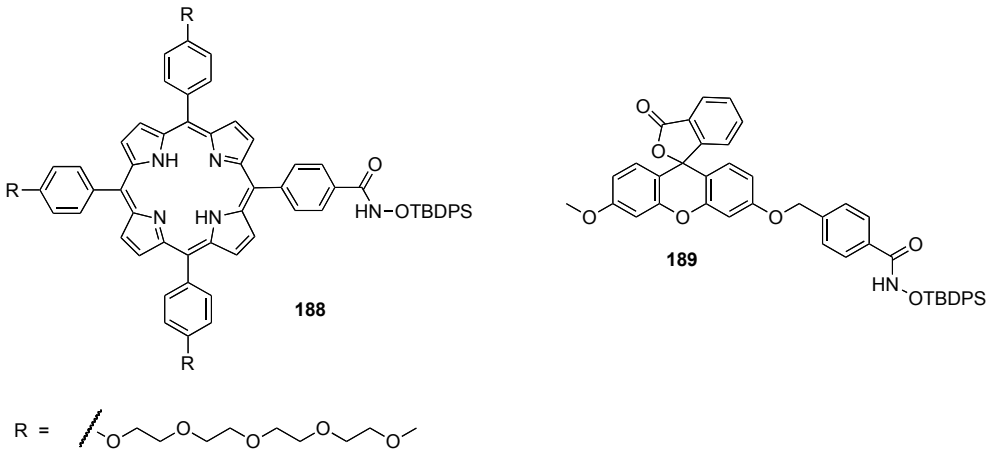

Figure 117

Following the above investigations, future work will move towards the original goals of the project *i.e.* the formation of bi-dimensional architectures on surfaces. To this end, the first task will be the preparation of a tetra-PNA functionalised pyrene bearing the same self-complementary PNA dodecamer introduced in this thesis **190** (Figure 118). Upon completion of its synthesis the evaluation of its self-assembly will be carried out on mica surfaces, and it will be investigated by AFM. Further complexity will ensue, upon the successful self-assembly of the above system, with the preparation of angular and linear units bearing

complementary PNA oligomers, and the examination of the supramolecular self-assembly of the bi-component system *i.e.* the original objective of this project.

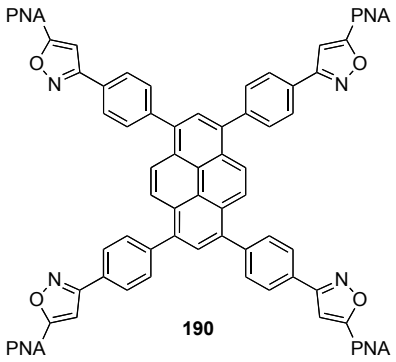

Figure 118

Experimental Part

5.1 INSTRUMENTATION

Thin layer chromatography (TLC) were conducted on pre-coated aluminum sheets with 0.20 mm *Machevery-Nagel* Alugram SIL G/UV_{234} with fluorescent indicator UV_{254}.

Column chromatography was carried out using *Merck Gerduran* silica gel 60 (particle size 40-63 μm). An automatic chromatography system, *Büchi sepacore* was used for the majority of purifications.

Microwave reactions were on an *Biotage AB Initiator microwave instrument* producing controlled irradiation at 2.450 GHz.

HPLC analyses and purifications were performed on the following HPLC systems. Analytical HPLC: (i) *Waters HPLC system* equipped with a *600 controller, 2996 photodiode array detector, 600 pump* and *an in-line degasser AF*. The column used was an *Agilent Zorbax SB-C18, 5 μm, 4.6 x 250 mm column*. (ii) *Varian 940-LC liquid chromatograph system.* . The column used was a *Varian Pursuit C18, 5μm, 4.6 x 250mm column*. Preparative HPLC: (i) *Waters HPLC system* equipped with a *600 controller, 2487 dual absorbance detector, Delta 600 pump* and *an in-line degasser AF*. The column used was an *Agilent Zorbax SB-C18 PrepHT, 7 μm, 21.2 x 250 mm column*. (ii) *Varian 940-LC liquid chromatograph system.* . The column used was a *Varian Pursuit C18, 5μm, 21.2 x 250mm column*. 0.1% TFA in H_2O and 0.1% TFA in CH_3CN were used as eluents in all cases.

Melting points (m.p.) were measured on a *Büchi Melting Point* B-545. All of the melting points have been measured in open capillary tubes and have not been corrected.

Nuclear magnetic resonance (NMR) ^{1}H and ^{13}C spectra were obtained on a 400 MHz NMR *(Jeol JNM EX-400)* or 270 MHz *(Jeol JNM EX-270)* . Chemical shifts were reported in ppm according to tetramethylsilane using the solvent residual signal as an internal reference ($CDCl_3$: δ_H = 7.26 ppm, δ_C = 77.16 ppm, DMSO-d_6: δ_H = 2.50 ppm, δ_C = 39.52 ppm, D_2O: δ_H = 4.79 ppm, Toluene-d_8: δ_H = 2.09 ppm, δ_C = 20.40, THF-d_8: δ_H = 3.58 ppm, δ_C = 67.57). Coupling constants (*J*) were given in Hz. Resonance multiplicity was described as *s* (singulet), *d* (doublet), *t* (triplet), *q* (quartet), *quin* (quintet), *m* (multiplet) and *br* (broad signal). Carbon spectra were acquired with a complete decoupling for the proton.

Infrared spectra (IR) in KBr were recorded on a *Perkin-Elmer spectrum RX I FT-IR System*.

UV spectra were recorded in quartz cuvettes using a Cary-Varian 5000.

Liquid chromatography mass spectrometry (LC-MS) measurements were conducted on an *Agilent 6200 series TOF mass spectrometer* operating in positive mode. The

analyte solutions were delivered to the ESI or APCI source by an *Agilent 1200 series LC system* at a flow rate of 0.25 mL/min. Typical elution gradient start from H_2O (90%) to CH_3CN (100%) for 20 minutes. ESI mode: Typical ESI conditions were, capillary voltage 2.0 kV; cone voltage 65 V; source temperature 150 °C; desolvation temperature 250°C; drying gas 5 L/min, nebuliser 60 psig. APCI: Typical APCI condition were, capillary voltage 2.0 kV; cone voltage 65 V; source temperature 250 °C; desolvation temperature 350°C; drying gas 5L/min; nebuliser 60 psig. Dry nitrogen was used as the ESI and APCI gas.

Mass spectrometry was generally performed by the *Centre de spectrométrie de masse* at the *Université de Mons* were they performed ESI-MS and MALDI-MS on using the following instrumentation. ESI-MS measurements were performed on a *Waters QToF2 mass spectrometer* operating in positive mode. The analyte solutions were delivered to the ESI source by a *Harvard Apparatus* syringe pump at a flow rate of 5 L/min. Typical ESI conditions were, capillary voltage 3.1 kV; cone voltage 20-50 V; source temperature 80 °C; desolvation temperature 120°C. Dry nitrogen was used as the ESI gas. For the recording of the single-stage ESI-MS spectra, the quadrupole (rf-only mode) was set to pass ions from 50 to 1000 Th, and all ions were transmitted into the pusher region of the time-of-flight analyzer where they were mass analyzed with 1 s integration time. MALDI-MS were recorded using a *Waters QToF Premier mass spectrometer* equipped with a nitrogen laser, operating at 337 nm with a maximum output of 500 mW delivered to the sample in 4 ns pulses at 20 Hz repeating rate. Time-of-flight mass analyses were performed in the reflectron mode at a resolution of about 10,000. The matrix solution (1 µl) was applied to a stainless steel target and air dried. Analyte samples were dissolved in a suitable solvent to obtain 1 mg/ml solutions. 1µl aliquots of those solutions were applied onto the target area already bearing the matrix crystals, and air dried. For the recording of the single-stage MS spectra, the quadrupole (rf-only mode) was set to pass ions from 100 to 1000 Th, and all ions were transmitted into the pusher region of the time-of-flight analyzer where they were mass analyzed with 1 s integration time.

AFM imaging was performed using a *Nanoscope IIIa* (Digital Instruments Metrology Group, USA) instrument, model: MMAFMLN. All the data was collected in air at 298 K. The images were collected in tapping-mode AFM, with a single 1-10 Ohm phosphorous-doped silicon cantilever (T: 3.5 – 4.5 µm, L: 115 -135 µm, W: 30 – 40 µm, f_0 ranging from 301.5 to 301.9 kHz and k: 20 -80 $N \cdot m^{-1}$, *VEECO*, USA). The images in the power point have been obtained after the flattening (WsXm software) of the collected data. Roughness analysis and flooding has been performed with the same software.

5.2 MATERIAL AND GENERAL METHODS

Chemicals were purchased from *Sigma Aldrich, Acros Organics, Fluorochem, ABCR, Polypeptide group* and *porphyrin systems* and were used as received. Resins for solid phase synthesis were purchased from *Novabiochem (Merck Chemicals)*. Solvents were purchased from *Sigma Aldrich*, and deuterated solvents from *Eurisotop*.

General solvents were distilled *in vacuo*. Anhydrous solvents as Et_2O, THF and toluene were distilled from Na/benzophenone; CH_2Cl_2 from phosphorus pentoxide; $CHCl_3$ and CH_3CN from CaH_2. Anhydrous DMF was purchased from *Acros Organics*.

Low temperature baths were prepared using different solvent mixtures depending on the desired temperature: -78°C with acetone/liquid N_2 or acetone/dry ice, -40°C with CH_3CN/liquid N_2, -10°C with ice/brine, and 0°C with ice/H_2O.

Anhydrous conditions were achieved by drying *Schlenk* line or 2-neck flasks by flaming with a heat gun under vacuum and then purging with argon. The inert atmosphere was maintained using argon-filled ballons equipped with a syringe and needle that was used to penetrate the silicon stoppers used to close the flasks' necks. The addition of liquid reagents was done by means of dried plastic or crystal syringes.

5.3 EXPERIMENTAL PROCEDURES

5.3.1 PNA MONOMERS

_N_-[2-(_N_-9-Fluorenylmethoxycarbonyl)aminoethyl]-_N_-[(thymin-1-yl)acetyl] glycine (91)

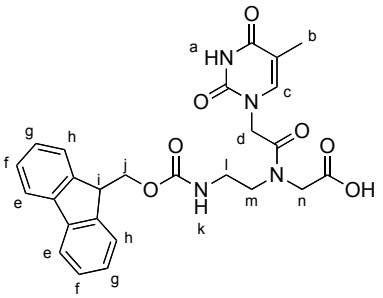

Compound **99** (0.1 g, 0.177 mmol) was suspended in CH_2Cl_2 (1 mL). The mixture was cooled to 0°C before TFA was added portion-wise over 10 minutes. The mixture was then stirred for 2 h at r.t. The solvent was evaporated *in vacuo* and co-evaporated three times using toluene to remove any residual TFA. No further purification was necessary yielding **91** as a white solid (0.09 g, 100%). (Note: If required the product could be recrystallised from CH_2Cl_2 to purify the compound if impurities were present). ^{1}H NMR (400MHz, DMSO): δ 11.27/11.25 (2xs (rotamers), 1H, NH_a), 7.86 (d, J = 7.3, 2H, CH_e), 7.64 (d, J = 7.3, 2H, CH_h), 7.42-7.20 (m, 6H, CH_c, CH_f, CH_g & NH_k), 4.61/4.44 (2 × s, 2H, CH_n), 4.35-4.18 (m, 3H, CH_i & CH_j), 3.95 (s, 2H, CH_d), 3.38-3.00 (m, 4H, CH_l & CH_m), 1.69 (s, 3H, CH_b), (COO*H* proton was not observed); ^{13}C NMR (100MHz, DMSO): δ 171.2, 170.9, 168.1, 167.8, 164.9, 156.8, 151.5, 144.4, 142.6, 141.3, 128.2, 127.6, 125.7, 120.7, 108.6, 66.0, 49.5, 48.2, 47.3, 12.4. Spectral data agrees with previously reported data.[203]

_N_-[2-(_N_-9-fluorenylmethoxycarbonyl)aminoethyl]-_N_-{(6-_N_-(benzoxycarbonyl) adenine-9-yl)acetyl} glycinate (93)

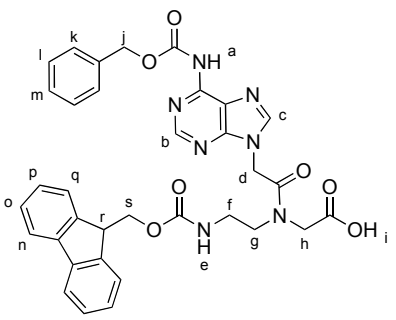

Compound **109** (1.289 g, 1.83 mmol) was dissolved in CH_2Cl_2 (13 mL). The solution was cooled in an ice bath. TFA (13 mL) was added slowly over 10 min at 0°C. The reaction mixture was allowed to warm up to r.t. slowly and then the mixture was stirred for 2 h at r.t. The mixture was evaporated to dryness *in vacuo* and any remaining TFA was removed by co-evaporation with toluene (3 ×). The residue was then triturated with Et_2O and collected by filtration to yield **93** (1.185 g, 100%) as a white solid. m.p. 196-198°C; ^{1}H NMR (400MHz, DMSO-d_6): δ 10.64 (br s, 1H, NH_a), 8.56/8.50 (2 × s (rotamers), 1H, CH_b), 8.31 (s, 1H, CH_c), 7.89 (d, J = 6.4 Hz, 2H, CH_n), 7.68 (t, J = 7.8 Hz, 2H, CH_q), 7.55-7.25 (m, 9H, CH_k, CH_l, CH_m, CH_o & CH_p), 5.34/5.17 (2 × s (rotamers), 2H, CH_d), 5.20 (s, 2H, CH_j), 4.43-4.18 (m, 5H, CH_r, CH_s & CH_h), 3.57 (m (rotamer), 1.4H, CH_g), 3.40-3.27 (m, 1.6H, CH_f & CH_g), 3.15 (m (rotamer), 1H, CH_f), (NH_e and COOH_i protons were not observed); ^{13}C NMR (100MHz, DMSO-d_6): δ (rotamers observed): 170.8, 170.2, 167.0, 166.5, 156.3, 156.1, 152.4, 152.1, 151.4, 149.3, 143.8, 140.7, 136.4, 128.4, 127.9, 127.8, 127.6, 127.0, 125.1, 122.9, 120.1, 68.9, 66.2, 65.5, 63.7, 46.9, 46.7, 43.8 (the presence of rotamers was observed). Spectral data agrees with previously reported data.[203]

Thymin-1-acetic acid (95)

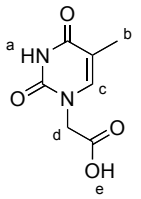

To a suspension of thymine (5.00 g, 39.7 mmol) and K_2CO_3 (5.48 g, 39.7 mmol) in dry DMF (120 mL) was added methyl bromoacetate (3.75 mL, 39.7 mmol), and the mixture was stirred vigorously overnight under argon. The mixture was filtered and evaporated to dryness, *in vacuo*. The solid residue was cooled to 0°C, treated with H_2O (37.5 mL) and 4 M HCl (aqueous, 1.6 mL), and stirred for 30 minutes. The precipitate was collected by filtration and washed with H_2O (3 × 20 mL). The precipitate was then treated H_2O (40 mL) and 2 M NaOH (aqueous, 20 mL) and refluxed for 10 minutes. The mixture was cooled to 0°C, treated with 4 M HCl (aqueous, 13.5 mL), and stirred for 30 min. The precipitate was collected by filtration, washed with H_2O (3 × 20 mL), and dried over P_2O_5 overnight, yielding **95** (4.496 g, 62%) as a white solid. ^{1}H NMR (400MHz, DMSO): δ 11.31 (s, 1H, NH_a), 7.45 (s, 1H, CH_c), 4.33 (s, 2H, CH_d), 1.71 (s, 3H, CH_b), (COOH proton was not observed); ^{13}C NMR (100MHz, DMSO): δ 170.2, 164.9, 151.5, 142.3, 108.9, 40.4, 12.4. Spectral data agrees with previously reported data.[207]

tert-Butyl _N_-(2-aminoethyl) glycinate (97)

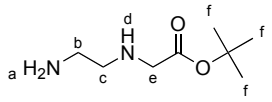

To a vigorously stirred solution of ethylenediamine (60 mL, 900 mmol) in CH_2Cl_2 (400 mL) at 0°C was added *tert*-butyl chloroacetate (14.5 mL, 102 mmol) in CH_2Cl_2 (80 mL) over 5 h. The resulting mixture was allowed to warm slowly to r.t. (approx. 3 h), and then stirred overnight (approx. 18 h). The reaction mixture was washed with H_2O (3 x 100 mL), and the combined aqueous wash was back-extracted with CH_2Cl_2 (100 mL). The combined organics were dried ($MgSO_4$) and filtered. This solution was used directly in the next step to synthesize compound **98**. An analytical sample was obtained by concentration of a 1 mL aliquot to dryness *in vacuo,* yielding 26 mg as a clear oil. The yield was therefore calculated as 0.026 g/mL (0.026 g/mL x 580 mL = 15.1 g, approx. 85% from *tert*-butyl chloroacetate). ^{1}H NMR (400MHz, $CDCl_3$): δ 3.27 (s, 2H, CH_e), 2.77 (m, 2H, CH_b), 2.66 (m, 2H, CH_c), 2.04 (br s, 3H, NH_a & NH_d), 1.44 (s, 9H, CH_f); ^{13}C NMR (100MHz, $CDCl_3$): δ 172.0, 81.3, 51.8, 51.6, 41.6, 28.2. Spectral data agrees with previously reported data.[203]

tert-Butyl _N_-[2-(_N_-9-fluorenylmethoxycarbonyl)aminoethyl] glycinate (98)

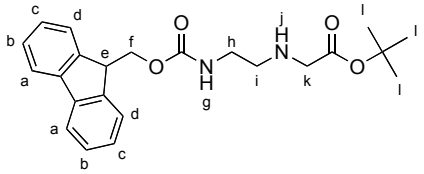

To a solution of **97** (15.1 g, 86.8 mmol) in CH_2Cl_2 (580 mL) was added DIEA (15 mL, 86 mmol) with stirring. A solution of *N*-(9-fluorenylmethoxycarbonyloxy)succinimide (29 g, 86 mmol) in CH_2Cl_2 (160 mL) was added dropwise over 5 hours. The resulting solution was stirred approximately 16 h, and then washed with 1 N aqueous HCl (5 × 100 mL), and brine (100 mL). The organic layer was dried ($MgSO_4$) and partially concentrated *in vacuo* (approx. 200 mL). Cooling (-18°C) overnight resulted in a precipitate which was collected by filtration and washed with CH_2Cl_2 until the filtrate was colorless. The solids were dried *in vacuo* (60°C) to give the HCI salt of **98** (28.498 g, 79%) as a white solid. The yield of the compound was calculated based on the HCl salt of **98**, and also, the compound was characterized and stored in this form since it is reported that it is more stable than the free base form. An analytical sample of the salt was obtained by recrystallisation from acetone. When required, the salt was

converted to the free base form: the HCl salt (1g, 2.3 mmol) was dissolved in $CHCl_3$ (approx. 50 mL), washed with aqueous saturated $NaHCO_3$ (50 mL), dried ($MgSO_4$), and concentrated *in vacuo* to give **98** as a clear oil in the free base form. ^{1}H NMR (400MHz, $CDCl_3$): δ 7.75 (d, J = 7.6 Hz, 2H, CH_a), 7.60 (d, J = 7.3 Hz, 2H, CH_d), 7.39 (t, J = 7.6 Hz, 2H, CH_b), 7.30 (t, J = 7.3 Hz, 2H, CH_c), 5.41 (br s, 1H, NH_g), 4.38 (d, J = 6.8 Hz, 2H, CH_f), 4.21 (t, J = 6.8 Hz, 1H, CH_e), 3.27 (m, 4H, CH_h & CH_k), 2.75 (m, 2H, CH_i), 1.47 (s, 9H, CH_l), (NH_j proton was not observed); ^{13}C NMR (100MHz, $CDCl_3$): δ 171.9, 156.6, 144.1, 141.3, 127.7, 127.1, 125.2, 120.0, 81.5, 66.7, 51.3, 48.7, 47.3, 40.7, 28.2. Spectral data agrees with previously reported data.[203]

***tert*-Butyl *N*-[2-(*N*-9-fluorenylmethoxycarbonyl)aminoethyl]-*N*-[(thymin-1-yl)acetyl] glycinate (99)**

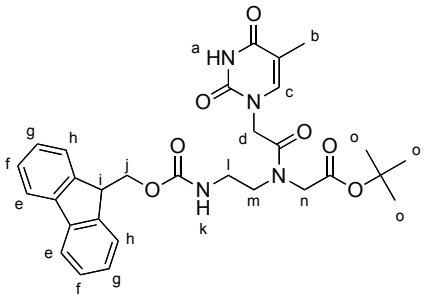

To a solution of **98** (3.66 g, 9.1 mmol) in anhydrous DMF (50 mL) was added thymin-1-ylacetic acid (**95**, 3.60 g, 19.6 mmol), and the mixture was stirred until most of the acid dissolved. EDC (3.60 g, 18.8 mmol) was added in two equal portions over 30 min, and the mixture was stirred overnight. The solution was concentrated *in vacuo*, and to the resulting thick oil, H_2O (100 mL) was added. The mixture was shaken vigorously for several minutes to precipitate a fine white solid. The solids were collected by filtration, and were washed with cold H_2O, and dried *in vacuo*. The crude compound was purified by flash chromatography (CH_2Cl_2/MeOH 95:5) to yield **99** (4.353 g, 85%) as a white solid. An analytically pure sample was obtained by recrystallisation using CH_2Cl_2/EtOAc/Hexane 1:1:1. Several days at 18°C were required for recrystallisation. R_f = 0.45 (CH_2Cl_2/MeOH 95:5). ^{1}H NMR (400MHz, $CDCl_3$): δ 9.13/9.09 (2 × s (rotamers), 1H, NH_a), 7.74 (d, J = 7.5 Hz, 2H, CH_e), 7.60 (t, J = 7.1 Hz, 2H, CH_h), 7.38 (t, J = 7.4 Hz, 2H, CH_f), 7.29 (t, J = 7.6 Hz, 2H, CH_g), 6.97/6.86 (2 × s (rotamers), 1H, CH_c), 6.06/5.51 (2 × br s (rotamers), 1H, NH_k), 4.49-4.32 (m, 4H, CH_j & CH_n), 4.21 (t, J = 6.5 Hz, 1H, CH_i), 4.08/3.94 (2 x s (rotamers), 2H, CH_d), 3.58-3.35 (m, 4H, CH_l & CH_m), 1.88/1.86 (2 × s (rotomers), 3H, CH_b), 1.49/1.46 (2 × s (rotomers), 9H, CH_o); ^{13}C NMR (100MHz, $CDCl_3$): δ 168.7, 164.2, 156.8, 151.1, 143.9, 141.1, 127.8, 127.1, 125.1,

120.0, 110.6, 83.7, 82.7, 66.8, 51.3, 49.9, 48.9, 47.7, 47.3, 39.4, 28.0, 12.3. Spectral data agrees with previously reported data.[203]

Methyl adenin-9-ylacetate (101)

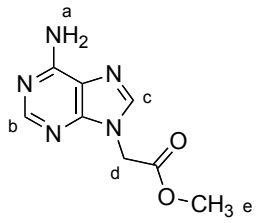

60% NaH in mineral oil (0.83 g) was washed with hexane under argon to give 0.5 g (21.1 mmol) of neat NaH. In the meanwhile, adenine (2.5 g, 18.5 mmol) was suspended in dry DMF (37.5 mL) and the NaH (0.5 g, 21.1 mmol, washed with hexane) was added portionwise with stirring. The reaction mixture was stirred for 2 h at r.t. Subsequently, methyl bromoacetate (3.5 mL, 37.0 mmol) was added dropwise during 3 h at r.t. After an additional 2 h of stirring, the solvent was removed by evaporation *in vacuo*. The remaining oil was shaken with H_2O (25 mL) resulting in precipitation. The mixture was left at 4°C overnight. The precipitate was filtered off and was washed with H_2O. Recrystallisation from EtOH gave **101** (2.069 g, 54%) as white/yellowish solid. ^{1}H NMR (400MHz, DMSO): δ 8.09 (s, 1H, CH_b), 8.07 (s, 1H, CH_c), 7.23 (br s, 2H, NH_a), 5.04 (s, 2H, CH_d), 3.67 (s, 3H, CH_e); ^{13}C NMR (100MHz, DMSO): δ 169.0, 156.5, 153.2, 150.2, 141.7, 118.8, 53.0, 44.3. Spectral data agrees with previously reported data.[207]

[*N*6-(4-Methoxytrityl)-adenin-9-yl] acetic acid (102)

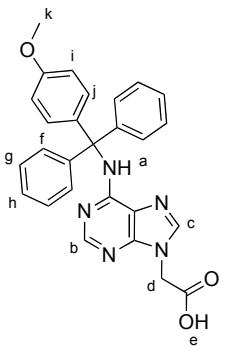

A mixture of ester **101** (0.5 g, 2.39 mmol), NEM (1.23 mL, 2.39 mmol) and 4-monomethoxytrityl chloride (1.1 g, 3.59 mmol) in pyridine (7.4 mL) and CH_2Cl_2 (7.4 mL) was heated at 40°C for 3 h, then at r.t. for 16 h. After evaporation of the solvent *in vacuo*, the residue was redissolved in EtOAc (7.4 mL), washed with 1 N aqueous $KHSO_4$ (7.4 mL), 10% aqueous $NaHCO_3$ (7.4 mL), brine (7.4 mL), dried over $MgSO_4$ and filtered. After evaporation of the solvent *in vacuo*, the residue was dissolved in EtOAc and was filtered through a plug of silica gel using EtOAc as the eluent (R_f = 0.52, eluent: EtOAc). After concentrating the intermediate product was refluxed for 2 h in 1 N aqueous NaOH (15 mL) and stirred at r.t. for 2 h. The solution was then cooled to 0°C. Following addition of 1 N aqueous $KHSO_4$ (18.6 mL), the mixture was stirred at 0°C for 30 min, giving rise to the precipitation of the product. After filtration, the residue was washed with small portions of H_2O until the filtrate was neutral (pH = 7). The product was then dried *in vacuo*. No further purification of was required. **102** (0.412 g, 37% over 2 steps) was collected as a white solid. An analytical sample was recrystallised from CH_2Cl_2. R_f = 0.28 (CH_2Cl_2/MeOH/CH_3COOH 100:10:1); ^{1}H NMR (400MHz, $CDCl_3$): δ 8.06 (s, 1H, CH_b), 7.77 (s, 1H, CH_c), 7.41 – 7.10 (m, 12H, CH_f, CH_g, CH_h & CH_j), 6.78 (d, *J* = 8.7 Hz, 2H, CH_i), 4.84 (s, 2H, CH_d), 3.75 (s, 3H, OCH_k), (NH_a & COOH_e protons were not observed); ^{13}C NMR (100MHz, $CDCl_3$): δ 169.2, 158.4, 154.3, 151.5, 147.6, 144.8, 140.7, 136.8, 130.3, 128.9, 127.9, 126.9, 119.8, 113.2, 71.3, 55.2, 45.1. Spectral data agrees with previously reported data.[232]

Allyl *N*-[2-(*N*-9-fluorenylmethoxycarbonyl)aminoethyl] glycinate (103)

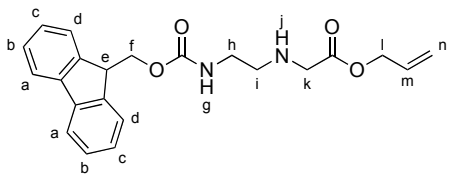

A solution of the hydrochloride salt of **98** (2.0 g, 4.62 mmol) in TFA (13 mL) was stirred for 30 min. The TFA was removed *in vacuo*. The residue was coevaporated with toluene three times. The residue was suspended in allyl alcohol (13 mL) and cooled to 0°C. Thionylchloride (1.16 mL, 15.97 mmol) was added in small portions. The mixture was stirred at 100°C for 1 h. After cooling to room temperature, diethyl ether (33 mL) was added and precipitation was allowed to take place overnight at -18°C. Filtration and washing with Et_2O yielded **103** (1.623 g, 84% over two steps) as a white solid. No further purification was required. ^{1}H NMR (400MHz, $CDCl_3$): δ 7.73 (d, *J* = 7.6 Hz, 2H, CH_a), 7.58 (d, *J* = 7.3 Hz, 2H, CH_d), 7.37 (t, *J* = 7.6 Hz, 2H, CH_b), 7.29 (t, *J* = 7.3 Hz, 2H, CH_c), 5.95-5.82 (m, 1H,

CH_m), 5.64 (br s, 1H, NH_g), 5.33-5.25 (m, 2H, CH_n), 4.59 (d, J = 5.7 Hz, 2H, CH_f), 4.39 (m, 2H, CH_l), 4.19 (t, J = 6.6 Hz, 1H, CH_e), 3.37 (s, 2H, CH_k), 3.24 (m, 2H, CH_h), 2.70 (m, 2H, CH_i), 1.93 (br s, 1H, NH_j); ^{13}C NMR (100MHz, $CDCl_3$): δ 165.7, 144.0, 141.3, 130.6, 127.8, 127.2, 125.5, 120.2, 120.0, 114.4, 67.4, 67.3, 48.9, 47.7, 47.1, 37.8. Spectral data agrees with previously reported data.[233]

Allyl *N*-[2-(*N*-9-fluorenylmethoxycarbonyl)aminoethyl]-*N*-{[6-*N*-(4-methoxytrityl) adenin-9-yl]acetyl}glycinate (104)

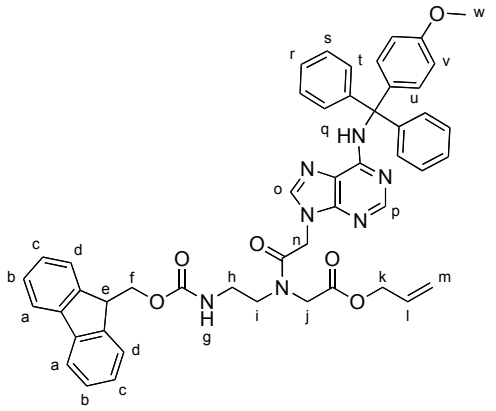

Compound **103** (0.665 g, 1.75 mmol) was dissolved in anhydrous DMF (5 mL). Compound **102** (0.815 g, 1.75 mmol), TOTU (0.57 g, 1.75 mmol) and DIEA (0.595 mL, 3.4 mmol) were added to the solution. The mixture was stirred for 2 h at r.t. The solvent was removed *in vacuo*. The residue was dissolved in EtOAc (25 mL) and was washed with saturated aqueous $NaHCO_3$ (2 × 25 mL), and brine (2 × 25 mL). The combined aqueous phases were back extracted with EtOAc (2 × 25 mL). The combined organic phases were dried ($MgSO_4$) and the solvent was removed *in vacuo*. **104** was obtained following chromatography on silica gel using EtOAc as the eluent (0.900 g, 62%). R_f = 0.74 (EtOAc); ^{1}H NMR (400MHz, $CDCl_3$): δ 7.93 (s, 1H, CH_p), 7.70-7.59 (m, 3H, CH_o & CH_a), 7.46 (d, J = 7.3 Hz, 2H, CH_d), 7.34-7.06 (m, 16H, CH_b, CH_c, CH_r, CH_s, CH_t & CH_u), 6.85 (s, 1H, NH_q), 6.69 (t, J = 7.3 Hz, 2H, CH_v), 6.07 (s, 1H, NH_g), 5.90-5.73 (m, 1H, CH_l), 5.34 – 5.08 (m, 2H, CH_m), 4.86/4.80 (2 × s (rotamers), 2H, CH_n), 4.56 (s, 2H, CH_f), 4.40-3.95 (m, 5H, CH_j, CH_k, & CH_e), 3.69/3.67 (2 × s (rotamers), 3H, OCH_w), 3.55/3.49 (2 × s (rotamers), 2H, CH_h), 3.37/3.29 (2 × s (rotamers), 2H, CH_i); ^{13}C NMR (100MHz, $CDCl_3$): δ 169.4/69.1, 167.7/167.2, 158.5, 156.9, 154.3, 152.5, 149.1, 145.4, 144.0/143.9, 141.5, 141.1/140.9, 137.4, 131.4/131.1, 130.4, 129.1, 128.0, 127.9, 127.2, 127.0, 125.2/125.0, 120.5, 120.2, 119.4, 113.3, 77.4, 71.2, 66.9, 66.4, 55.4, 49.4, 47.4,

43.5, 39.5 (the presence of rotamers was observed). Spectral data incomplete since alternate strategy was pursued.

6-*N*-(Benzyloxycarbonyl)adenine (105)

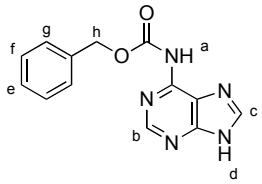

Sodium hydride (12.14 g, 304 mmol, 60% dispersion in oil) was washed with petroleum ether (3 x) under an argon atmosphere. After cooling in an ice bath, anhydrous DMF (300 mL) was added, followed by adenine (10.00 g, 74 mmol) in small portions. The suspension was stirred vigorously for 15 minutes and then benzyl chloroformate (23.2 mL, 163 mmol) was added dropwise over approximately 1 h whilst maintaining the temperature at 0°C using the ice bath. After the addition was complete, the reaction mixture was allowed to reach room temperature slowly and then it was stirred overnight (approximately 12 h). The mixture was poured into ice cold H_2O (600 mL) and the pH adjusted to 7 with 1 N aq. HCl. The resultant precipitate was collected by filtration and washed with H_2O, and ether. It was dried *in vacuo* before being recrystallised from MeOH/$CHCl_3$ 1:1. Two crops were collected yielding **105** (11.800 g, 59%) as a white solid. ^{1}H NMR (400MHz, DMSO): δ 8.60 (s, 1H, C*H*$_b$), 8.45 (s, 1H, C*H*$_c$), 7.56-7.29 (m, 5H, C*H*$_e$, C*H*$_f$ & C*H*$_g$), 5.29 (s, 2H, C*H*$_h$), (N*H*$_a$ & N*H*$_d$ protons were not observed); ^{13}C NMR (100MHz, DMSO + 0.1%DCl): δ 152.8, 152.5, 150.7, 146.5, 144.4, 135.4, 128.5, 128.4, 128.1, 112.8, 67.6. Spectral data agrees with previously reported data.[203]

6-*N*-(Benzyloxycarbonyl)-9-(*tert*-butoxycarbonylmethyl)adenine (106)

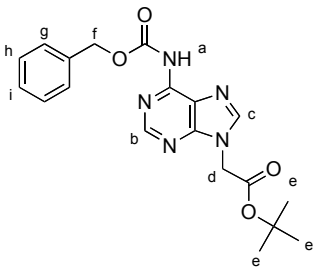

Synthesis according to scheme 5: To a suspension of **105** (7.634 g, 28.4 mmol) in anhydrous DMF (61 mL) was added anhydrous Cs_2CO_3 (0.916 g, 2.8 mmol) and anhydrous K_2CO_3

(3.970 g, 28.4 mmol). After stirring for 5 min, *tert*-butyl chloroacetate (4.57 mL, 32.1 mmol) was added dropwise (approx. 30 min). After stirring for 24 h, the mixture was evaporated to dryness *in vacuo* and the residue partitioned between EtOAc (535 mL) and H_2O (153 mL). The organic phase was washed with H_2O (153 mL) and brine (153 mL), dried ($MgSO_4$), filtered and concentrated *in vacuo*. The residue was recrystallised from EtOAc/hexane 1:1. Two crops of product were collected yielding **106** (6.629 g, 61%) as a white/beige solid.

Synthesis according to scheme 6: Adenine (20.0 g, 148 mmol) in DMF (350 mL) was treated with sodium hydride (60% in mineral oil, 6.88 g, 172 mmol) in two portions at 1 h intervals. After 3 h, all hydrogen gas evolution had stopped and the solution was cooled in an ice bath and *tert*-butylchloroacetate (23.2 mL, 163 mmol) was added drop-wise over 30 min. The reaction was allowed to warm to room temperature while stirring for 12 h after which solvents were removed *in vacuo* and H_2O (160 mL) was added. After brief stirring, the H_2O was decanted and the remaining sticky oil was dissolved in boiling EtOH and stirred overnight to obtain 19.915 g (80 mmol) of *tert*-butyl adenine-9-acetate as a solid (54% yield). This crude material was dissolved in DMF (160 mL), treated with carbonyldiimidazole (19.44 g, 120 mmol), heated slowly until 105 °C and stirred at that temperature for 2 h. The temperature was then decreased to 95 °C before adding benzyl alcohol (12.4 mL, 120mmol) and the reaction was stirred for 12 h without further heating. The reaction was quenched with the addition of H_2O (400 mL) and stirred vigorously for 2 h. The solid was collected and dried under high vacuum yielding **106** (24.802 g, 43% over two steps) as a white/beige solid. ^{1}H NMR (400MHz, $CDCl_3$): δ 8.76 (s, 1H, C*H*$_b$), 8.04 (s, 1H, C*H*$_c$), 7.45-7.28 (m, 5H, C*H*$_g$, C*H*$_h$ & C*H*$_i$), 5.28 (s, 2H, C*H*$_f$), 4.83 (s, 2H, C*H*$_d$), 1.45 (s, 9H, C*H*$_e$), (N*H*$_a$ proton was not observed); ^{13}C NMR (100MHz, $CDCl_3$): δ 165.7, 153.0, 151.6, 151.2, 149.4, 143.5, 135.5, 128.8, 128.7, 128.6, 120.9, 84.0, 67.9, 45.1, 28.1. Spectral data agrees with previously reported data.[203]

6-*N*-(Benzyloxycarbonyl)-9-(carboxymethyl)adenine (107)

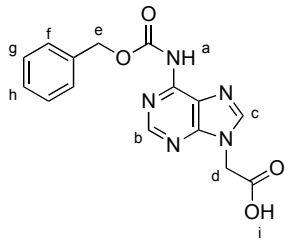

Compound **106** (6.629 g, 17.3 mmol) was dissolved in CH_2Cl_2 (65 mL). The solution was cooled in an ice bath. TFA (65 mL) was added slowly over 20 min at 0°C. The reaction

mixture was stirred for 2 h at r.t. The mixture was evaporated to dryness *in vacuo* and any remaining TFA was removed by co-evaporation with toluene (3 ×). The resultant residue was triturated with Et_2O was used to obtain **107** (5.655 g, 100%) as a white/beige solid. An analytically pure sample of **107** was obtained by recrystallisation from acetone. ^{1}H NMR (300MHz, DMSO): δ 8.64 (s, 1H, C*H*$_b$), 8.50 (s, 1H, C*H*$_c$), 7.50-7.29 (m, 5H, C*H*$_f$, C*H*$_g$ & C*H*$_h$), 5.23 (s, 2H, C*H*$_e$), 5.10 (s, 2H, C*H*$_d$), (N*H*$_a$ & COO*H*$_i$ protons were not observed); ^{13}C NMR (100MHz, DMSO): δ 168.9, 152.2, 152.1, 151.5, 149.2, 144.9, 136.3, 128.4, 128.0, 127.8, 122.4, 66.4, 44.3. Spectral data agrees with previously reported data.[203]

***tert*-Butyl *N*-[2-(*N*-9-fluorenylmethoxycarbonyl)aminoethyl]-*N*-{[6-*N*-(benzoxycarbonyl)adenine-9-yl]acetyl} glycinate (109)**

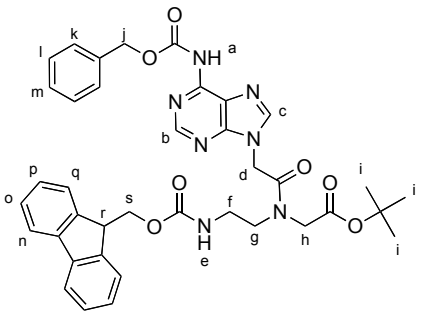

Synthesis according to scheme 7: Compound **98** (1.122 g, 2.833 mmol), compound **107** (0.926 g, 2.833 mmol), HBTU (1.503 g, 3.966 mmol), and HOBT (0.535 g, 3.966 mmol) were mixed in a dry flask under argon. Anhydrous DMF (17.5 mL) was added, followed by DIEA (1.207 mL, 6.941 mmol). The resulting solution was stirred overnight (approx. 12 h), after which the solvent was removed *in vacuo*. The residue was partitioned between EtOAc (34 mL) and half saturated brine (34 mL). The aqueous phase was extracted with EtOAc (4 × 34 mL). The combined organic extract was washed with 1 N aqueous HCl (2 × 17 mL), saturated aqueous $NaHCO_3$ (2 × 17 mL), brine (1 × 17 mL), dried ($MgSO_4$), filtered and concentrated *in vacuo*. The resulting solid was purified by flash chromatography eluting with EtOAc yielding **109** (1.137 g, 57%) as a white crystalline solid.

Synthesis according to scheme 8: Under an argon atmosphere, a suspension of **107** (0.40 g, 1.25 mmol) in anhydrous CH_3CN (3.3 mL) at 0 ºC was treated sequentially with NEM (319 µL, 2.50 mmol) in one portion followed by pivaloyl chloride as a drop-wise addition (185 µL, 1.5 mmol). The mixture was stirred for 20 min at 0 ºC then compound **98** (0.505 g, 1.28 mmol) was added and the reaction was continued for 90 min at room temperature. The reaction was then diluted with CH_2Cl_2 (12 mL) and washed with 20% aq. citric acid (10 mL)

followed by saturated $NaHCO_3$ (10 mL). The organic phase was dried over $MgSO_4$ and was concentrated *in vacuo*. The crude product was purified by silica gel chromatography (eluent: EtOAc), yielding **109** (0.604 g, 69%) as a white crystalline solid. R_f = 0.44 (CH_2Cl_2/MeOH 95:5); ^{1}H NMR (400MHz, DMSO-d_6): δ 10.68 (br s, 1H, NH_a), 8.50 (d, *J* = 12.1 Hz, 1H, CH_b), 8.27 (s, 1H, CH_c), 7.84 (d, *J* = 7.1 Hz, 2H, CH_n), 7.63 (t, *J* = 7.6 Hz, 2H, CH_q), 7.50-7.20 (m, 9H, CH_k, CH_l, CH_m, CH_o & CH_p), 5.29/5.10 (2 × s (rotamers), 2H, CH_d), 5.18 (s, 2H, CH_j), 4.35-4.13 (m, 5H, CH_r, CH_s & CH_h), 3.92 (m (rotamer), 1H, CH_g), 3.49 (m (rotamer), 1H, CH_f), 3.35 (m (rotamer), 1H, CH_g), 3.13 (m (rotamer), 1H, CH_f), 1.46/1.32 (2 × s (rotamers), 9H, CH_i), (NH_e proton was not observed); ^{13}C NMR (100MHz, DMSO-d_6): δ 168.4, 167.9, 167.2, 166.6, 152.4, 152.1, 151.4, 149.3, 145.2, 143.8, 140.7, 136.4, 128.4, 128.0, 127.8, 127.6, 127.0, 125.0, 123.0, 120.1, 82.1, 81.0, 66.2, 65.5, 48.8, 47.1, 46.7, 27.6. Spectral data agrees with previously reported data.[203]

5.3.2 SYNTHESIS OF CHROMOPHORES AND LINKERS

1-Hydroxy-6-[(4-methoxyphenyl)-diphenylmethylamino]-hexane (111)

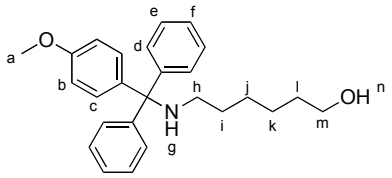

6-Aminohexan-1-ol (1.00 g, 8.55 mmol) was dissolved in anhydrous pyridine (7ml) and triethylamine (0.2 mL). To this solution was added a solution of (4-methoxyphenyl)-diphenylmethyl chloride (2.50 g, 8.12 mmol) in anhydrous pyridine (9 mL) in 3 aliquots at 45 min intervals. The reaction was stirred at room temperature for a further 30 min, and was then quenched by the addition of MeOH (3 mL). The solution was evaporated to a yellow oil, and was co-evaporated 3 times with toluene to remove traces of pyridine. The residue was dissolved in EtOAc and washed with saturated aqueous $NaHCO_3$ solution, H_2O and brine. The organic phase was dried ($MgSO_4$), filtered and evaporated *in vacuo*. The crude product was purified by silica gel chromatography eluting with hexane/EtOAc/NEt_3 (49.5:49.5:1) to give **111** (1.681 g, 53%) as a colourless oil. R_f = 0.44 (hexane/EtOAc 1:1); ^{1}H NMR (400MHz, $CDCl_3$): δ 7.50-7.10 (m, 12H, CH_c, CH_d, CH_e, & CH_f), 6.80 (m, 2H, CH_b), 3.77 (s, 3H, O-CH_a), 3.60 (t, *J* = 6.6 Hz, 2H, CH_m), 2.15 (m, 2H, CH_h), 1.65-1.20 (m, 8H, CH_i, CH_j, CH_k, & CH_l), (NH_g and OH_n protons were not observed); ^{13}C NMR (100MHz, $CDCl_3$): δ

157.8, 146.7, 138.6, 129.9, 128.6, 127.8, 126.1, 113.1, 70.4, 62.9, 55.2, 43.6, 32.8, 30.9, 27.2, 25.8. Spectral data agrees with previously reported data.[215]

6-[(4-Methoxyphenyl)-diphenylmethylamino]-hex-1-yl hemisuccinate (112)

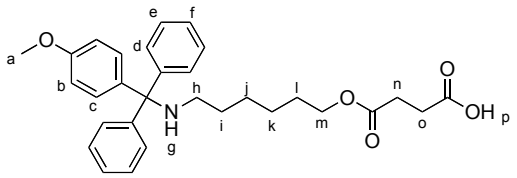

Compound **111** (1.68 g, 4.32 mmol) was dissolved in anhydrous pyridine (16.8 mL). To this solution was added succinic anhydride (0.44 g, 4.32 mmol) and DMAP (52.6 mg, 0.44 mmol). After stirring for 3 h at room temperature further succinic anhydride (43.2 mg, 0.43 mmol) and DMAP (105.2 mg, 0.94 mmol) were added and the solution was warmed to 50°C for 6 h. After a further 16 h at room temperature the solution was evaporated *in vacuo*. The residue was dissolved in EtOAc and washed once with an ice cold 5% aqueous solution of citric acid. The organic phase was dried ($MgSO_4$), filtered and evaporated *in vacuo*. The crude product was purified by silica gel chromatography eluting with CH_2Cl_2/EtOAc/NEt_3 50:49:1 and then with CH_2Cl_2/MeOH/NEt_3 95:5:1 yielding **112** (1.665 g, 79%) as a colourless oil. R_f = 0.30 (CH_2Cl_2/EtOAc 1:1); ^{1}H NMR (400MHz, $CDCl_3$): δ 7.50-7.10 (m, 12H, CH_c, CH_d, CH_e, & CH_f), 6.80 (m, 2H, CH_b), 4.02 (t, J = 6.2 Hz, 2H, CH_m), 3.77 (s, 3H, O-CH_a), 2.55 (m, 4H, CH_n, & CH_o), 2.37 (t, J = 6.9 Hz, 2H, CH_h), 1.65-1.45 (m, 4H, CH_i, & CH_l), 1.35-1.10 (m, 4H, CH_j, & CH_k), (NH_g and COOH_p protons were not observed); ^{13}C NMR (100MHz, $CDCl_3$): δ 176.8, 172.6, 158.4, 144.4, 136.2, 130.2, 128.7, 128.1, 127.8, 126.9, 113.4, 72.2, 64.4, 55.3, 44.4, 29.8, 29.7, 28.3, 26.5, 25.7. Spectral data agrees with previously reported data.[215]

5-(4-Methoxycarbonylphenyl)-10,15,20-tris(4-*tert*-butylphenyl)-porphyrin-Zn(II) (132)

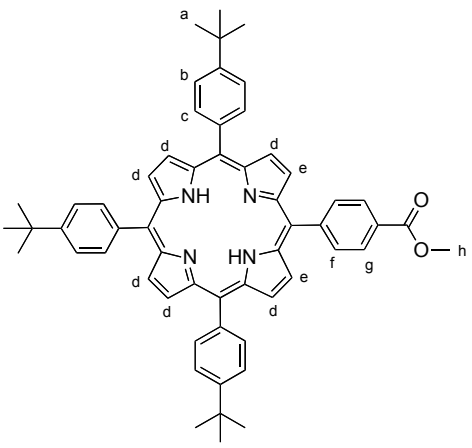

Methyl 4-formylbenzoate (0.33 g, 2.00 mmol) was dissolved in dry and degassed $CHCl_3$ (800 mL) under an inert atmosphere of argon. While stirring at r.t., 4-*tert*-butylbenzaldehyde (1.00 mL, 6.00 mmol), pyrrole (filtered through alumina, 0.56 mL, 8.00 mmol) and borontrifluoride etherate (0.83 mL equivalent to 2.64 mmol of BF_3) were added whilst maintaining the inert atmosphere. The reaction mixture was stirred for 1 h at r.t. in the dark before *p*-chloranil (1.48 g, 6 mmol) was added. The mixture was then refluxed for 1 h. After cooling to r.t., triethylamine (0.37 mL, 2.66 mmol) was added to neutralize the acid catalyst. The solution was then concentrated to about 20 mL and passed through several plugs of silica using CH_2Cl_2 in order to remove the oxidant. Once all the oxidant had been removed (verified by TLC), the crude product was purified by silica gel chromatography (eluent: CH_2Cl_2/cyclohexane 1:1), yielding **132** (263 mg, 16%) as a violet solid. R_f = 0.35 (CH_2Cl_2/cyclohexane 1:1); ^{1}H NMR (400MHz, DMSO): δ 8.80-8.75 (m, 6H; C*H*$_d$), 8.74-9.73 (m, 2H, C*H*$_e$), 8.35 (d, *J* = 8.0 Hz, 2H, C*H*$_g$), 8.32 (d, *J* = 8.0 Hz, 2H, C*H*$_f$), 8.08 (d, *J* = 8.2 Hz, 6H, C*H*$_c$), 7.77 (d, *J* = 8.0 Hz, 6H, C*H*$_b$), 4.03 (s, 3H, C*H*$_h$), 1.56 (s, 27H, C*H*$_a$), (N*H* protons were not observed); ^{13}C NMR (100MHz, DMSO): δ 166.6, 149.7, 149.5, 149.4, 148.6, 147.9, 139.7, 134.6, 134.1, 132.0, 131.8, 131.7, 132.2, 128.7, 127.4, 123.5, 120.8, 120.5, 118.6, 52.4, 34.7, 31.5 (four peaks corresponding to the *tert*-butyl groups were expected, however only two were observed due to overlapping peaks). Spectral data agrees with previously reported data.[263]

5-(4-Carboxyphenyl)-10,15,20-tris(4-*tert*-butylphenyl)-porphyrin-Zn(II) (133)

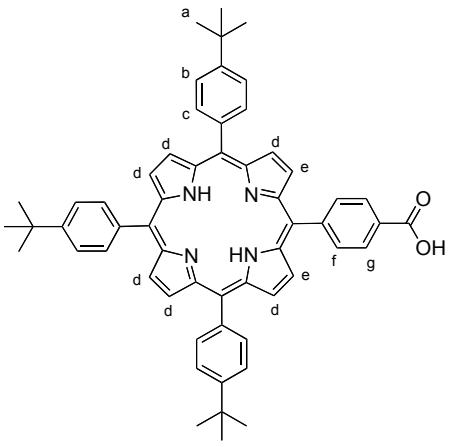

Porphyrin derivative (**132**, 274 mg, 0.30 mmol) was dissolved in THF (15 mL), and 2M aqueous NaOH (15 mL) was added. The mixture was refluxed for 48 h. The solution was then cooled to 0°C, and 1M HCl (60 mL) was added to neutralize the sodium hydroxide. The resulting mixture was extracted with CH_2Cl_2 (3 × 50 mL), dried (Na_2SO_4), and concentrated

in vacuo. The product was purified by silica gel chromatography (eluent: CH_2Cl_2) yielding **133** (254 mg, 95%) as a violet solid. m.p.: decomposed before melting; ^{1}H NMR (400MHz, DMSO): δ 8.78 (m, 8H, C*H*$_{d\&e}$), 8.35 (d, *J* = 6.9 Hz, 2H, C*H*$_g$), 8.29 (d, *J* = 6.9 Hz, 2H, C*H*$_f$), 8.08 (d, *J* = 6.6 Hz, 6H, C*H*$_c$), 7.78 (d, *J* = 6.8 Hz, 6H, C*H*$_b$), 1.56 (s, 27H, C*H*$_a$), (N*H* and COO*H* protons were not observed); ^{13}C NMR (100MHz, DMSO): δ 167.6, 149.6, 149.5, 149.4, 148.7, 147.5, 139.8, 134.4, 134.1, 131.9, 131.7, 131.6, 131.2, 129.7, 127.5, 123.4, 120.7, 120.5, 118.8, 34.6, 31.5 (four peaks corresponding to the *tert*-butyl groups were expected, however only two were observed due to overlapping peaks); IR (cm^{-1}): ν 3436.3, 3399.4, 3315.4, 2960.8, 2902.4, 2867.3, 1604.8, 1473.9, 1384.8, 1268.1, 1967.6, 800.3, 734.5; MS (MALDI-HRMS): Found 826.4256 [M]$^+$, $C_{57}H_{54}N_4O_2$ requires = 826.4247; UV-vis (CH_2Cl_2, r.t.): λ_{max} [nm] (ε [l mol^{-1} cm^{-1}]): 420 (395471), 517 (15254), 552 (8706), 593 (4336), 650 (7023).

5-azidopentanoic acid (138)

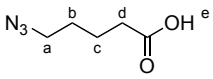

5-Bromovaleric acid (4.0 g, 22 mmol) was dissolved in H_2O (35 mL) and sodium azide (7.2 g, 110 mmol) was added. The mixture was refluxed for 16 h. The solution was cooled to room temperature, and concentrated HCl was added until pH 2 was reached. The solution was then extracted with Et_2O (2 × 130 mL). The combined organic phases were dried ($MgSO_4$) and concentrated *in vacuo*. Distillation of the crude product under high vacuum afforded a **138** (1.207 g, 38%) as a colourless oil. ^{1}H NMR (400 MHz, $CDCl_3$): δ 3.31 (t, *J* = 6.6 Hz, 2H, C*H*$_d$), 2.41 (t, *J* = 6.8 Hz, 2H, C*H*$_a$), 1.77-1.61 (m, 4H, C*H*$_b$ & C*H*$_c$), (COO*H*$_e$ proton was not observed); ^{13}C NMR (100MHz, $CDCl_3$): δ 179.6, 51.1, 33.5, 28.3, 21.9. Spectral data agrees with previously reported data.[264]

5,10,15,20-Tetrakis-(4-ethynylphenyl)-porphyrin-Zn(II) (140)

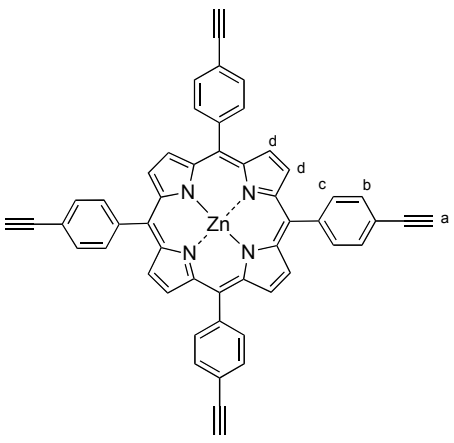

144 (100 mg, 0.094 mmol) was dissolved in anhydrous THF (10 mL) under an argon atmosphere. Tetrabutylammonium fluoride (TBAF, 98 mg, 0.374 mL of 1M TBAF in THF solution, 0.378 mmol) was added and the reaction mixture was stirred for 2 h at r.t. The mixture was filtered through a plug of course silica using CH_2Cl_2 for washing. The mixture was concentrated *in vacuo* and was then purified by silica gel chromatography (eluent: CH_2Cl_2/cyclohexane 15:85 initially, followed by CH_2Cl_2/cyclohexane 1:1), yielding **140** (69 mg, 95%) as a violet solid. m.p.: decomposed before melting; ^{1}H NMR (400 MHz, DMSO): δ 8.79 (s, 8H, CH_d), 8.18 (d, *J* = 8.0 Hz, 8H, CH_c), 7.90 (d, J = 8.0 Hz, 8H, CH_b), 4.46 (s, 4H, CH_a); ^{13}C NMR (100 MHz, DMSO): δ 149.1, 143.3, 134.4, 131.8, 130.0, 121.1, 119.7, 83.6, 81.9. IR (cm^{-1}): ν 3414.3, 3293.3, 2959.0, 2925.1, 2849.4, 2107.2, 1723.4, 1603.7, 1488.8, 1338.4, 1205.3, 1104.3, 1066.2, 995.9, 807.3, 796.0, 655.8, 608.5; MS (MALDI-HRMS): Found 772.1603 $[M]^+$, $C_{52}H_{28}N_4Zn$ requires = 772.1605; UV-vis (CH_2Cl_2, r.t.): λ_{max} [nm] (ε [l mol^{-1} cm^{-1}]): 424 (573824), 516 (6454), 553 (22480), 593 (7107), 646 (512).

5,10,15,20-Tetrakis-{4-[(trimethysilyl)ethynyl]phenyl}-porphyrin-Zn(II) (144)

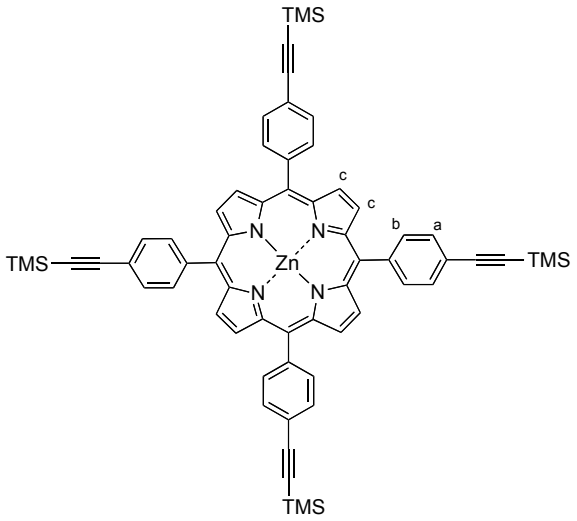

4-(Trimethylsilyl)ethynylbenzaldehyde (1.62 g, 8.00 mmol) was dissolved in dry and degassed $CHCl_3$ (800 mL) under an inert atmosphere of argon. While stirring at r.t., pyrrole (filtered through alumina, 0.56 mL, 8.00 mmol) and borontrifluoride etherate (0.83 mL equivalent to 2.64 mmol of BF_3) were added whilst maintaining the inert atmosphere. The reaction mixture was stirred for 1 h at r.t. in the dark before p-chloranil (1.48 g, 6 mmol) was added. The mixture was then refluxed for 1 h. After cooling to r.t., triethylamine (0.37 mL, 2.66 mmol) was added to neutralize the acid catalyst. The solution was then concentrated to about 20 mL and passed through several plugs of silica using CH_2Cl_2 in order to remove the

oxidant. Once all the oxidant had been removed (verified by TLC), the crude product was dried *in vacuo*. The crude (0.89 g, 0.892 mmol, 45% yield), which was relatively pure after the plugs of silica, was then dissolved in $CHCl_3$ (45 mL). A solution of zinc acetate (1.63 g, 8.9 mmol) in MeOH (45 mL) was added and the mixture was refluxed for 2 h. After cooling the mixture to r.t., the solvent was removed in vacuo, and the crude product was purified by silica gel chromatography (eluent: CH_2Cl_2/cyclohexane 3:7) yielding **144** (884 mg, 42%) as a violet solid. R_f = 0.63 (CH_2Cl_2/cyclohexane 1:1); m.p.: decomposed before melting; ^{1}H NMR (400 MHz, THF-d8): δ 8.76 (s, 8H, CH_c), 7.93 (d, J = 8.0 Hz, 8H, CH_b), 7.73 (d, J = 8.2 Hz, 8H, CH_a), 0.38 (s, 36H, CH_{TMS}); ^{13}C NMR (100 MHz, THF-d8): δ 147.4, 143.2, 134.9, 131.5, 130.8, 123.8, 120.2, 106.3, 95.8, 0.3; IR (cm^{-1}): ν 3292.1, 3268.4, 3031.7, 2959.1, 2159.3, 1809.8, 1603.6, 1490.5, 1395.2, 1338.5, 1249.6, 997.1, 866.0, 855.8, 846.6, 808.6, 796.8, 658.4; MS (MALDI-HRMS): Found 1060.3184 $[M]^+$, $C_{64}H_{60}N_4Si_4Zn$ requires = 1060.3187; UV-vis (CH_2Cl_2, r.t.): λ_{max} [nm] (ε [l mol^{-1} cm^{-1}]): 423 (582190), 516 (6454), 552 (22480), 593 (7107), 648 (512).

5,10,15,20-Tetrakis-{4-[1-(pentanoic acid)-1H-1,2,3-triazole-4]phenyl}-porphyrin-Zn(II) (145)

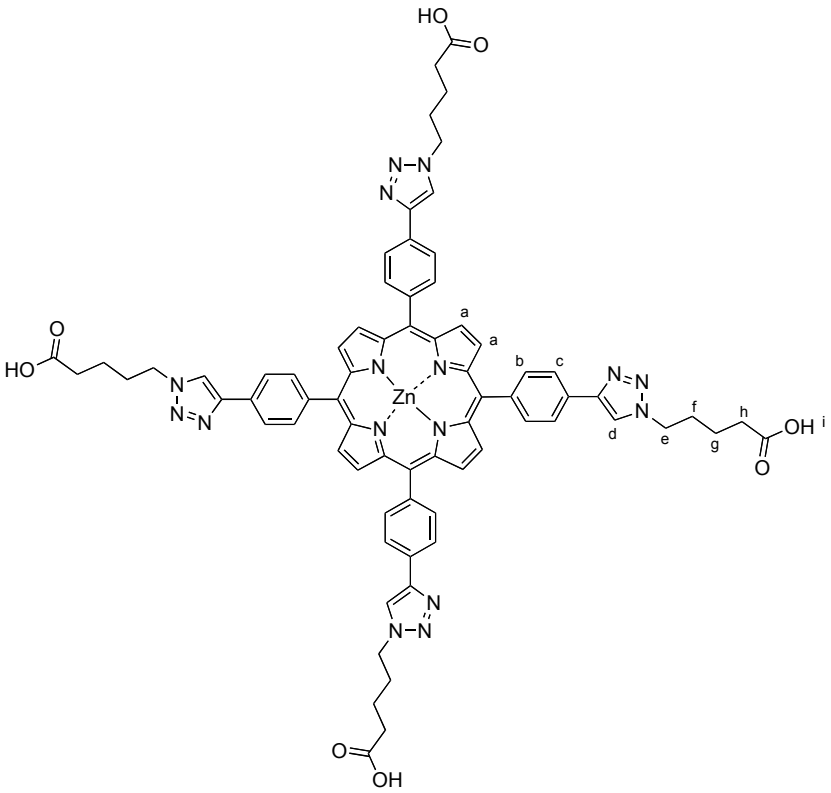

Porphyrin derivative (**140**, 10 mg, 0.013 mmol), 5-azidopentanoic acid (**138**, 7.5 mg, 0.052 mmol), copper sulfate (3.3 mg, 0.013) and sodium ascorbate (10.3 mg, 0.052 mmol) were dissolved in anhydrous DMF (1 mL) under an argon atmosphere. The mixture was stirred for 24 h at 50°C. Excess H_2O (approximately 10 mL) was added to the reaction mixture until the crude product precipitated. The suspension was centrifuged (10 min at 5000 rpm), and after the supernatant was decanted. The crude was resuspended in H_2O (10 mL), and was then centrifugation and decantation was repeated. This was repeated once more. The crude product was then dissolved in excess THF (approximately 25 mL). The solution was then dried (Na_2SO_4) and concentrated *in vacuo*. The product was then dissolved in a minimum quantity of THF and then was precipitated using pentane. The suspension was filtered, and the solid was washed with pentane. After drying under high vacuum, the pure product (**145**) was obtained (15 mg, 86%) as a violet solid. m.p.: decomposed before melting; ^{1}H NMR (400 MHz, THF-d8): δ 10.76 (s, 4H, COO*H*$_i$), 8.94 (s, 8H, C*H*$_a$), 8.45 (s, 4H, C*H*$_d$), 8.30-8.23 (m, 16H, C*H*$_b$ & C*H*$_c$), 4.54 (t, *J* = 6.9 Hz, 8H, C*H*$_e$), 2.52 (m, 8H, C*H*$_f$), 2.38 (t, *J* = 7.2 Hz, 8H, C*H*$_h$), 2.08 (quin, *J* = 7.6 Hz, 8H, C*H*$_g$); ^{13}C NMR (100 MHz, THF-d8): δ 174.4, 151.2, 148.1, 143.9, 135.9, 132.4, 132.0, 124.4, 121.5, 121.2, 50.6, 33.7, 30.9, 23.0; IR (cm^{-1}): ν 3451.1, 2949.8, 2871.1, 1727.9, 1492.3, 1456.8, 1345.2, 1206.0, 1181.6, 1076.4, 1000.2, 800.2, 718.2, 491.0; MS (MALDI-HRMS): Found 1343.4346 $[M]^+$, $C_{72}H_{64}N_{16}O_8Zn$ requires = 1343.4306; UV-vis (THF, r.t.): λ_{max} [nm] (ε [l mol^{-1} cm^{-1}]): 427 (563308), 552 (20567), 593 (10339).

α-Chloro-9-anthraldoxime (148)

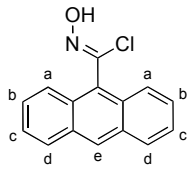

9-Anthraldoxime (0.100 g, 0.45 mmol) was dissolved in anhydrous DMF (1 mL) under an argon atmosphere. The solution was cooled to 0°C and *tert*-butylhypochlorite (63 µL, 0.54 mmol) was added dropwise. The mixture was allowed to reach r.t. slowly and was then stirred for 1 h at r.t. H_2O (10 mL) was then added and the mixture was extracted with Et_2O (2 × 10 mL). The combined organic phases were extracted with H_2O (10 mL), dried ($MgSO_4$) and concentrated *in vacuo,* yielding the pure product (101 mg, 88%) as yellow solid. ^{1}H NMR (400 MHz, $CDCl_3$): δ 8.51 (s, 1H, C*H*$_e$), 8.23 (d, J = 8.7 Hz, 2H, C*H*$_a$), 8.02 (d, J = 8.5 Hz, 2H, C*H*$_d$), 7.65 (t, J = 7.7 Hz, 2H, C*H*$_b$), 7.55 (t, J = 7.6 Hz, 2H, C*H*$_c$), (N-O*H* proton was not

observed); ^{13}C NMR (100 MHz, $CDCl_3$): δ 133.8, 131.1, 130.8, 129.2, 128.8, 128.6, 126.4, 125.9, 125.2. Spectral data agrees with previously reported data.[265]

3-(Anthracen-9-yl)-5-(trimethylsilyl)isoxazole (152)

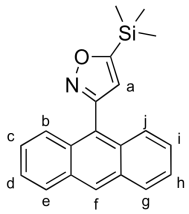

Synthesis according to scheme 22: 9-Anthraldehyde oxime (0.1 g, 0.45 mmol) was dissolved in CH_2Cl_2 (4 mL) under an argon atmosphere and was then cooled to -10°C. *tert*-Butyl hypochlorite (54 µL, 49 mg, 0.45 mmol) was dissolved in CH_2Cl_2 (1 mL) and was added dropwise to the oxime solution. Once the addition was complete, the reaction mixture was allowed to stir for 5 min, after which, trimethylsilyl acetylene (96 µL, 66 mg, 0.68 mmol) was added, followed by NEt_3 (125 µL, 91 mg, 0.90 mmol) dropwise. The resultant mixture was stirred for 16 h at room temperature. The reaction mixture was diluted with CH_2Cl_2 (10 mL) was washed with H_2O (10 mL). The organic layer was dried ($MgSO_4$) and concentrated *in vacuo*. The residue was purified by silica gel chromatography using 2% EtOAc in cyclohexane as the eluent, yielding **152** (64 mg, 45%) as a viscous yellow oil.

Synthesis according to scheme 23: 9-Anthraldehyde oxime (0.1 g, 0.45 mmol) was dissolved in CH_2Cl_2 (4 mL) under an argon atmosphere and was then cooled to -10°C. 1-chlorobenzotriazole (69 mg, 0.45 mmol) was dissolved in CH_2Cl_2 (1 mL) and was added dropwise to the oxime solution. Once the addition was complete, the reaction mixture was allowed to stir for 5 min, after which, trimethylsilyl acetylene (96 µL, 66 mg, 0.68 mmol) was added. The resultant mixture was stirred for 16 h at room temperature. The reaction mixture was diluted with CH_2Cl_2 (10 mL) was washed with H_2O (10 mL). The organic layer was dried ($MgSO_4$) and concentrated *in vacuo*. The residue was purified by silica gel chromatography using 2% EtOAc in cyclohexane as the eluent, yielding **152** (103 mg, 72%) as a viscous yellow oil.

Synthesis according to scheme 24: Compound **156** (62 mg, 0.13 mmol) was dissolved in $CHCl_3$ (2 mL) under an argon atmosphere, NEt_3 (54 µL, 39 mg, 0.39 mmol) was added and the mixture was cooled to -40°C. A 1M solution of trifluoromethanesulfonic anhydride in CH_2Cl_2 (150 µL, 0.15 mmol) was added dropwise. Once the addition was complete, the reaction mixture was allowed to stir for 1 h at 0°C, after which, trimethylsilyl acetylene (90 µL, 64 mg, 0.65 mmol) was added. The resultant mixture was stirred for 16 h at room

temperature. The reaction mixture was diluted with CH_2Cl_2 (10 mL) was washed with H_2O (2 × 10 mL). The organic layer was dried ($MgSO_4$) and concentrated *in vacuo*. The residue was purified by silica gel chromatography using 2% EtOAc in cyclohexane as the eluent, yielding **152** (33 mg, 79%) as a viscous yellow oil. ^{1}H NMR (400MHz, $CDCl_3$): δ 8.56 (s, 1H, C*H*$_f$), 8.05 (d, *J* = 7.8 Hz, 2H, C*H*$_b$ & C*H*$_j$), 7.80 (d, *J* = 8.7 Hz, 2H, C*H*$_e$ & C*H*$_g$), 7.51-7.42 (m, 4H, C*H*$_c$, C*H*$_d$, C*H*$_h$ & C*H*$_i$), 6.69 (s, 1H, C*H*$_a$), 0.48 (s, 9H, C*H*$_{TMS}$); ^{13}C NMR (100MHz, $CDCl_3$): δ 178.6, 159.1, 131.3, 130.8, 128.8, 128.6, 126.4, 125.9, 125.5, 123.8, 116.2, -1.5; IR (cm^{-1}): ν 3554.9, 3476.2, 3411.5, 3050.2, 2959.2, 2922.9, 2850.3, 1637.8, 1617.4, 1381.3, 1307.2, 1252.8, 1073.0, 844.8, 759.4, 734.8, 622.5; MS (APCI-HRMS): Found 318.1313 $[M+H]^+$, $C_{20}H_{20}NOSi$ requires = 318.1314; UV-vis (CH_2Cl_2, r.t.): λ_{max} [nm] (ε [l mol^{-1} cm^{-1}]): 333 (9946), 348 (19591), 366 (29363), 386 (26789).

_O_-tert-Butyldiphenylsilyl hydroxylamine (155)

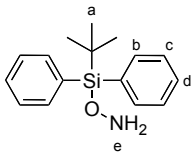

To a stirred suspension of suspension of hydroxylamine hydrochloride (500 mg, 7.19 mmol) in CH_2Cl_2 (100 mL) was added triethylamine (1.602 g, 15.83 mmol). The mixture was allowed to stir for 1 h at room temperature under argon. Neat *tert*-butylchlorodiphenyl silane (2.058 mL, 2.176 g, 7.91 mmol) was added, and the reaction mixture was allowed to stir overnight at room temperature. The mixture was then concentrated to dryness and THF (10 mL) was added to the residue. Triethylamine hydrochloride was removed by filtration. The flask and residue were washed (3 × 5 mL) and the resulting THF solution was concentrated. Pentane (15 mL) was added to the residue, the mixture was briefly sonicated and the compound was allowed to crystallise in the fridge. The solid was collected by filtration and was washed with cold pentane, yielding **155** (1.419 g, 73%) as a colourless crystalline solid. ^{1}H NMR (400MHz, $CDCl_3$): δ 7.74-7.72 (m, 4H, C*H*$_b$), 7.43-7.37 (m, 6H, C*H*$_c$ & C*H*$_d$), 5.27 (s, 2H, N*H*$_e$), 1.08 (s, 9H, C*H*$_a$); ^{13}C NMR (100MHz, $CDCl_3$): δ 135.6, 133.6, 129.8, 127.8, 27.4, 19.3. Spectral data agrees with previously reported data.[266]

_O_-(_tert_-butyldiphenylsilyl)anthracene-9-hydroxamate (156)

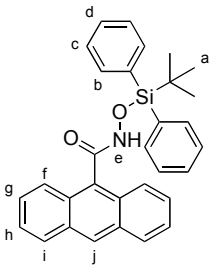

Anthracene-9-carboxylic acid (92 mg, 0.416 mmol) was dissolved in oxalyl chloride (20 mL) under an inert atmosphere of argon. DMF (5 drops) was added and the mixture was refluxed for 16 h. The mixture was cooled to room temperature before the excess oxalyl chloride was removed *in vacuo*. The compound was dried under high vacuum overnight. The residue was dissolved in THF (0.5 mL) maintaining the inert conditions. The solution was cooled to 0°C. A solution of compound **155** (136 mg, 0.5 mmol) and DIEA (145 µL, 107 mg, 0.832 mmol) in THF (0.5 mL) was prepared and was added dropwise to the anthracene solution. The mixture was then stirred for 3 h at room temperature. EtOAc (25 mL) was added and the resultant solution was washed with saturated $NaHCO_3$ (25 mL) and H_2O (25 mL). The organic phase was then dried ($MgSO_4$) and concentrated *in vacuo*. The residue was purified by silica gel chromatography (eluent: 10% EtOAc in cyclohexane), yielding **156** (103 mg, 52%) as a yellow solid. m.p.: 135-136°C; ^{1}H NMR (400MHz, DMSO-d6): δ 11.67 (s, 1H, N*H*$_e$), 8.61 (s, 1H, C*H*$_j$), 8.04 (d, 2H, C*H*$_f$), 7.89 (d, 4H, C*H*$_b$), 7.58 (m, 2H, C*H*$_i$), 7.57-7.46 (m, 6H, C*H*$_c$ & C*H*$_d$), 7.31-7.25 (m, 4H, CH$_g$ & C*H*$_h$) 1.17 (s, 9H, C*H*$_a$). ^{13}C NMR (100MHz, $CDCl_3$): δ 166.7, 136.2, 131.1, 130.9, 130.7, 129.1, 128.4, 128.2, 126.9, 125.6, 125.0, 123.4, 123.0, 27.0, 19.4; IR (cm^{-1}): ν 3200.4, 3052.6, 2955.5, 2929.8, 2856.9, 1648.9, 1498.4, 1471.0, 1427.5, 1116.1, 1060.0, 888.5, 807.9, 737.9, 727.8, 709.2, 698.7, 507.3; MS (APCI-HRMS): Found 476.2043 $[M+H]^+$, $C_{31}H_{29}NO_2Si$ requires = 476.2046; UV-vis (CH_2Cl_2, r.t.): λ_{max} [nm] (ε [l mol^{-1} cm^{-1}]): 348 (18722), 377 (27046), 386 (24683).

5-(4-Benzylalcohol)-10,15,20-tris(4-*tert*-butylphenyl)-porphyrin (162)

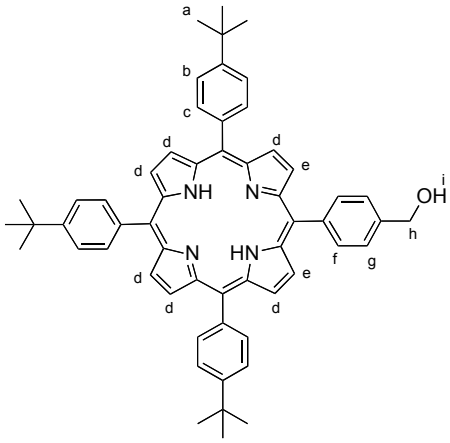

Porphyrin **132** (858 mg, 1.02 mmol) was dissolved in anhydrous THF (75 mL) under an argon atmosphere. The solution was cooled to 0°C and then lithium aluminium hydride (78 mg, 2.04 mmol) was added. The mixture was then refluxed for 2 h. Upon cooling, a TLC indicated a quantitative conversion to the alcohol had occurred. CH_2Cl_2 (250 mL) was added to the mixture, which was then extracted with H_2O (250 mL). The aqueous phase was extracted with CH_2Cl_2 (250 mL) once more. The combined organic phases were dried (Na_2SO_4) and concentrated in vacuo. Anhydrous toluene was added and was evaporated (repeated three times) in order to remove any traces of H_2O. The product obtained was used directly in the next step. An analytical sample was purified by filtration through a plug of silica (eluent: CH_2Cl_2). Removal of the solvent under vacuum and precipitation with MeOH yielded **162** (746 mg, 90%) as a violet solid. m.p.: > 350°C; ^{1}H NMR (400 MHz, $CDCl_3$): δ 8.87 (m, 6H, C*H*$_d$), 8.82 (d, 2H, C*H*$_e$), 8.22 (d, 2H, C*H*$_f$), 8.14 (d, 6H, C*H*$_c$), 7.76 (m, 8H, C*H*$_b$ & C*H*$_g$), 5.07 (d, 2H, C*H*$_h$), 1.97 (t, 1H, O*H*$_i$), 1.61 (s, 27H, C*H*$_a$), (N*H* protons were not observed); ^{13}C NMR (100 MHz, $CDCl_3$): δ 150.5, 141.7, 140.1, 139.1, 134.8, 134.5, 125.3, 123.6, 120.3, 120.2, 119.4, 65.4, 34.9, 31.7; IR (cm^{-1}): ν 3416.3, 3317.9, 3027.2, 2956.4, 2864.2, 2359.9, 1556.2, 1501.9, 1473.5, 1397.3, 1348.9, 1266.4, 1221.7, 1185.9, 1107.5, 1020.6, 981.9, 966.8, 879.9, 848.4, 732.7, 577.5, 456.2, 426.7, 413.9; MS (MALDI-HRMS): Found 812.4451 $[M]^+$, $C_{57}H_{56}N_4$ requires = 812.4454; UV-vis (CH_2Cl_2, r.t.): λ_{max} [nm] (ε [l mol^{-1} cm^{-1}]): 419 (360808), 517 (8775), 552 (3377), 592 (486).

5-(4-Benzaldehyde)-10,15,20-tris(4-*tert*-butylphenyl)-porphyrin (163)

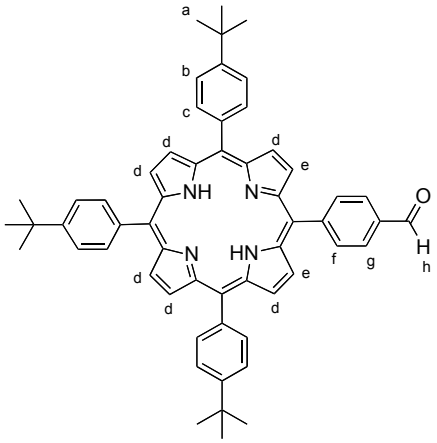

162 (175 mg, 0.215 mmol) was dissolved in anhydrous CH_2Cl_2 (20 mL) and triethylamine (90 µL, 0.645 mmol) was added (to neutralize the acidity of the pyridinium chlorochromate oxidant). In a separate flask, pyridinium chlorochromate (70 mg, 0.323 mmol) was suspended in anhydrous CH_2Cl_2 (4 mL). A spatula tip of celite was added (in order to adsorb the used up oxidant and facilitate the purification following the reaction). The porphyrin solution was then cannulated into the flask containing the oxidant. Anhydrous CH_2Cl_2 (4 mL) was used to rinse the porphyrin flask, and was also cannulated into the reaction mixture. The reaction solution was observed to turn dark green and was stirred for 1.5 h at r.t. The mixture was then filtered through course silica. The silica was washed with CH_2Cl_2 until no more violet solution eluted. The solution was concentrated in vacuo. The residue was dissolved in a minimum volume of THF, and then pentane was added to precipitate the product. The product was collected by filtration and was washed with pentane. **163** (157 mg, 90%) was isolated as a violet solid, and no further purification was required. m.p.: > 350°C; ^{1}H NMR (400 MHz, $CDCl_3$): δ 10.39 (s, 1H, C*H*$_h$), 8.91-8.88 (m, 6H, C*H*$_d$), 8.76 (m, 2H, C*H*$_e$), 8.40 (d, *J* = 8.0 Hz, 2H, C*H*$_g$), 8.29 (d, *J* = 8.0 Hz, 2H, C*H*$_f$), 8.15-8.13 (m, *J* = 8.0 Hz, 6H, C*H*$_c$), 7.76 (d, *J* = 8.0 Hz, 6H, C*H*$_b$), 1.61 (s, 27H, C*H*$_a$), (N*H* protons were not observed); ^{13}C NMR (100 MHz, $CDCl_3$): δ 192.5, 150.6, 148.9, 139.0, 135.5, 135.2, 134.5, 128.0, 123.7, 120.9, 120.6, 119.9, 34.9, 31.7; IR (cm^{-1}): ν 3943.3, 3733.9, 3441.6, 2961.4, 1702.6, 2359.9, 1600.7, 1546.0, 1501.5, 1471.8, 1397.7, 1361.7, 1266.7, 1203.6, 1107.3, 1020.7, 981.5, 966.3, 847.2, 734.1, 577.5, 411.7; MS (MALDI-HRMS): Found 810.4313 $[M]^+$, $C_{57}H_{54}N_4$ requires = 810.4298; UV-vis (CH_2Cl_2, r.t.): λ_{max} [nm] (ε [l mol^{-1} cm^{-1}]): 419 (371321), 517 (8785), 552 (5926), 592 (1692).

5-(4-benzaldehyde oxime)-10,15,20-tris(4-*tert*-butylphenyl)-porphyrin (164)

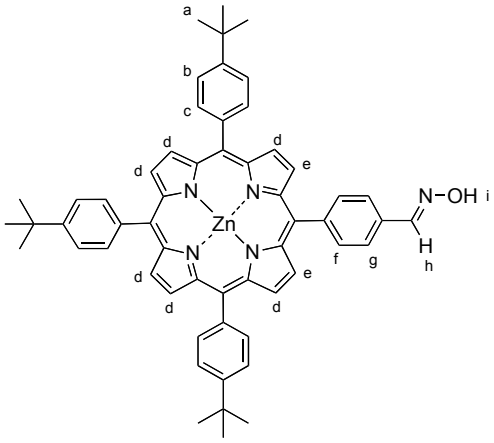

Porphyrin **163** (150 mg, 0.185 mmol) was dissolved in anhydrous THF (12 mL) under an argon atmosphere. Anhydrous MeOH (12 mL) was added, followed by hydroxylamine hydrochloride (19 mg, 0.278 mmol) and sodium acetate (23 mg, 0.278 mmol). The mixture was stirred for 2 h at r.t. CH_2Cl_2 (100 mL) was added to the mixture, which was then extracted with H_2O (100 mL). The aqueous phase was extracted with CH_2Cl_2 (100 mL) once more. The combined organic phases were dried (Na_2SO_4), filtered and concentrated in vacuo. Anhydrous toluene was added and was evaporated (repeated three times) in order to remove any traces of H_2O. The porphyrin was then dissolved in THF (10 mL), and a solution of zinc acetate (0.340 g, 1.85 mmol) in MeOH (10 mL) was added and the mixture was refluxed for 2 h. After cooling the mixture to r.t., the solvent was removed in vacuo, and the crude product was purified by silica gel chromatography (eluent: CH_2Cl_2). The residue was dissolved in a minimum volume of THF, and then pentane was added to precipitate the product. The product was collected by filtration and was washed with pentane yielding **164** (141 mg, 86%) as a violet solid. m.p.: > 350°C; ^{1}H NMR (400 MHz, THF-d8): δ 10.84/10.47 (2 x s (rotamers), 1H, O*H*$_i$), 8.87-8.84 (m, 8H, C*H*$_d$ & C*H*$_e$), 8.38 (s, 1H, C*H*$_h$), 8.21 (d, *J* = 8.0 Hz, 2H, C*H*$_g$), 8.13 (d, *J* = 8.2 Hz, 6H, C*H*$_c$), 7.98 (d, *J* = 8.0 Hz, 2H, C*H*$_f$), 7.80 (d, *J* = 8.2 Hz, 6H, C*H*$_b$), 1.61 (s, 27H, C*H*$_a$); ^{13}C NMR (100 MHz, THF-d8): δ 151.3, 151.2, 151.0, 150.9, 149.1, 149.0, 145.6, 141.8, 135.8, 135.5, 133.9, 132.6, 132.4, 132.0, 125.6, 124.3, 121.8, 121.7, 120.8, 35.7, 32.2 (four peaks corresponding to the *tert*-butyl groups were expected, however only two were observed due to overlapping peaks); IR (cm^{-1}): ν 3552.2, 3479.7, 3412.3, 3235.1, 2960.3, 2923.9, 2856.3, 1638.3, 1616.1, 1492.3, 1461.5, 1338.0, 1264.0, 1205.3, 1108.5, 1067.4, 998.3, 809.1, 800.3; MS (MALDI-HRMS): Found 887.3524 [M]$^+$,

$C_{57}H_{53}N_5OZn$ requires = 887.3542; UV-vis (CH_2Cl_2, r.t.): λ_{max} [nm] (ε [l mol^{-1} cm^{-1}]): 423 (377838), 552 (14510), 593 (4924).

5,10,15,20-Tetrakis-{[*O*-(*tert*-butyldiphenylsilyl)]phenyl-4-hydroxamate}-21,23H-porphyrin (168)

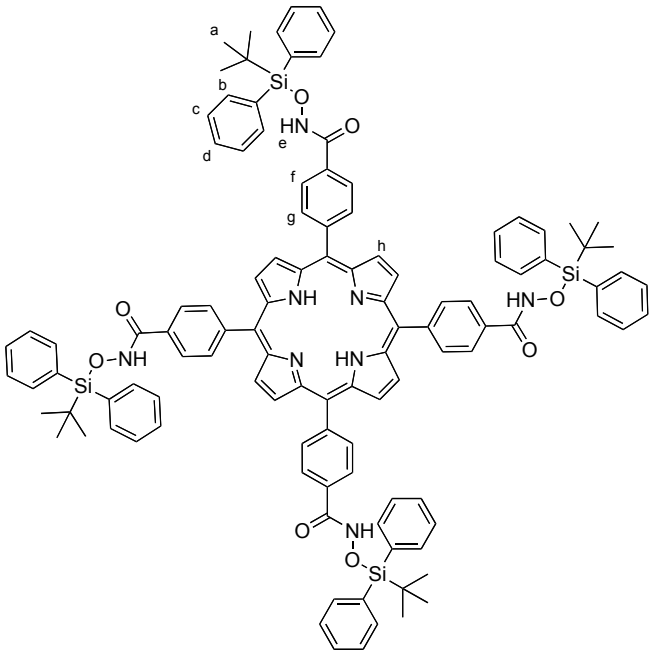

Meso-tetrakis-(4-carboxyphenyl) porphyrin (160 mg, 0.20 mmol) was suspended in anhydrous CH_2Cl_2 (16 mL) under an inert atmosphere of argon. Oxalyl chloride (419 µL, 616 mg, 4.848 mmol) was added followed by a catalytic amount of DMF (2 drops). The mixture was stirred for 16 h at room temperature. After concentrating the solution *in vacuo*, traces of oxalyl chloride were removed under high vacuum. The crude acid chloride was then redissolved in anhydrous CH_2Cl_2 (10 mL), and was added dropwise to a pre-cooled solution (0°C) of compound **155** (438 mg, 1.616 mmol) and DIEA (842 µL, 4.848 mmol) in anhydrous CH_2Cl_2 (5 mL). The resultant mixture was stirred under an inert atmosphere overnight. The mixture was then concentrated *in vacuo*, and the residue was purified by silica gel chromatography (eluent: 1% EtOAc in CH_2Cl_2). The product from the column was dissolved in a minimal quantity of CH_2Cl_2 and was precipitated using pentane. The precipitate was collected by filtration and was washed with pentane, yielding **168** (80 mg, 22%) was obtained as a violet solid. m.p.: >350°C; ^{1}H NMR (400MHz, $CDCl_3$): δ 8.83-8.79 (m (rotamer), 4H, CH_h), 8.71-8.68 (m (rotamer), 4H, CH_h), 8.55/8.26 (2 × s (rotamers), 4H, NH_e), 8.22-8.11 (m, 12H, CH_f [8H] & rotamer of CH_b [4H]), 7.95-7.93 (m, 8H, CH_g), 7.85-

7.83 (m (rotamer), 12H, C*H*$_b$), 7.55-7.43 (m, 24H, C*H*$_c$ & C*H*$_d$), 1.29 (s, 36H, C*H*$_a$), (N*H* protons of the porphyrin core were not observed); ^{13}C NMR (100MHz, $CDCl_3$/THF-d8 1:1): δ 167.2, 135.7, 135.1, 133.9, 131.7, 131.4, 129.7, 129.4, 127.8, 127.3, 125.3, 124.0, 26.5, 19.0; IR (cm^{-1}): ν 3391.8, 3317.9, 3071.5, 3047.6, 2931.6, 2892.2, 2857.7, 1680.0, 1624.5, 1607.8, 1472.2, 1428.0, 1392.6, 1115.1, 967.1, 935.6, 909.3, 801.2, 739.6, 700.6, 520.5; MS (MALDI-HRMS): Found 1802.7223 $[M]^+$, $C_{112}H_{106}N_8O_8Si_4$ requires = 1802.7211; UV-vis (CH_2Cl_2, r.t.): λ_{max} [nm] (ε [l mol^{-1} cm^{-1}]): 421 (608164), 516 (25735), 551 (13329), 591 (8336), 646 (6501).

5,10,15,20-Tetrakis-{4-[5-(trimethylsilyl)isoxazol-3-yl]phenyl}-21,23H-porphyrin (169)

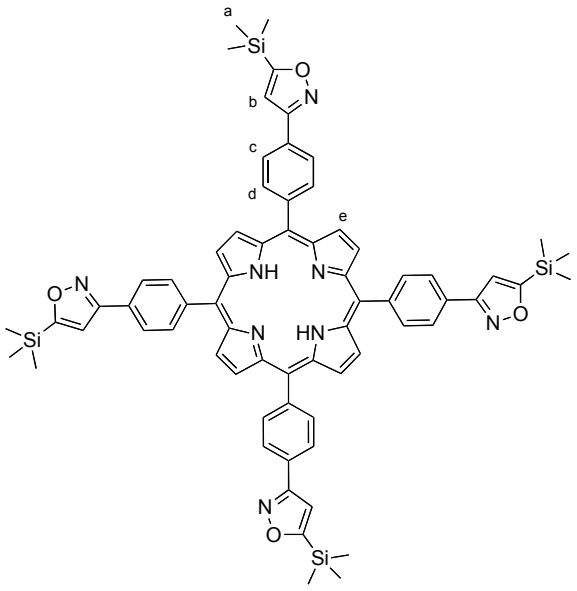

Compound **168** (25 mg, 0.014 mmol) was dissolved in $CHCl_3$ (2 mL) under an argon atmosphere. Triethylamine (23 µL, 17 mg, 0.168 mmol) was added and the solution was cooled to -40°C. A 1M solution of trifluoromethanesulfonic anhydride in CH_2Cl_2 (62 µL, 0.616 mmol) was added dropwise. Once the addition was complete, the reaction mixture was allowed to stir for 1 h at 0°C, after which, trimethylsilyl acetylene (390 µL, 270 mg, 2.8 mmol) was added. The resultant mixture was stirred for 16 h at room temperature. The reaction mixture was diluted with CH_2Cl_2 (10 mL) was washed with H_2O (2 × 10 mL). The organic layer was dried (Na_2SO_4) and concentrated *in vacuo*. The residue was purified by silica gel chromatography (eluent: CH_2Cl_2), yielding **169** (10 mg, 62%) as a violet solid. m.p.: >350°C; ^{1}H NMR (400MHz, $CDCl_3$): δ 8.91 (s, 8H, C*H*$_e$), 8.33 (d, *J* = 8.5, 8H, C*H*$_c$), 8.22 (d, *J* = 8.2, 8H, C*H*$_d$), 7.03 (s, 4H, C*H*$_b$), 0.49 (s, 36H, C*H*$_a$), (N*H* protons of the porphyrin core were not observed); ^{13}C NMR (100MHz, $CDCl_3$): δ 179.4, 161.0, 143.7, 135.2, 131.2, 129.1,

125.7, 123.0, 119.8, 111.1, -1.6; IR (cm^{-1}): ν 3550.2, 3476.0, 3414.0, 3320.7, 2956.8, 2899.1, 2854.8, 1615.6, 1416.4, 1252.8, 1098.4, 967.9, 949.9, 847.0, 801.6, 761.0; MS (MALDI-HRMS): Found 1170.4254 $[M]^+$, $C_{68}H_{66}N_8O_4Si_4$ requires = 1170.4284; UV-vis (CH_2Cl_2, r.t.): λ_{max} [nm] (ε [l mol^{-1} cm^{-1}]): 421 (650436), 516 (24374), 551 (12190), 591 (6224), 648 (4893).

5,10,15,20-Tetrakis-{4-[5-(phenyl)isoxazol-3-yl]phenyl}-21,23H-porphyrin (171)

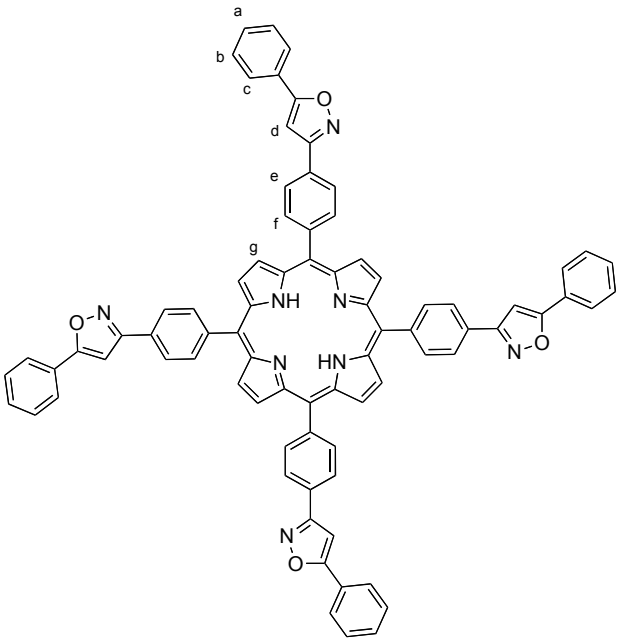

Compound **168** (25 mg, 0.0138 mmol) was dissolved in $CHCl_3$ (2 mL) under an argon atmosphere. Triethylamine (23 µL, 17 mg, 0.168 mmol) was added and the mixture was cooled to -40°C. A 1M solution of trifluoromethanesulfonic anhydride in CH_2Cl_2 (62 µL, 0.616 mmol) was added dropwise. Once the addition was complete, ethynylbenzene (16 µL, 14.3 mg, 0.138 mmol) was added in one portion, and the reaction mixture was irradiated in the microwave at 80°C for 0.5 h. The reaction mixture was diluted with CH_2Cl_2 (10 mL) was washed with H_2O (2 × 10 mL). The organic layer was dried (Na_2SO_4) and concentrated *in vacuo*. The residue was purified by silica gel chromatography (eluent: CH_2Cl_2), yielding **171** (8.3 mg, 51% or 85% per cycloaddition) as a violet solid. m.p.: >350°C; ^{1}H NMR (400MHz, $CDCl_3$): δ 8.94 (s, 8H, CH_g), 8.36 (d, J = 8.0, 8H, CH_e), 8.29 (d, J = 8.0, 8H, CH_f), 8.29 (d, J = 6.9, 8H, CH_c), 7.60-7.50 (m, 12H, CH_a & CH_b), 7.12 (s, 4H, CH_d), (N*H* protons of the porphyrin core were not observed); ^{13}C NMR (100MHz, $CDCl_3$): δ 171.0, 163.1, 144.0, 135.2, 130.6, 129.3, 128.9, 127.7, 126.1, 125.4, 119.8, 97.9 (two signals corresponding to quaternary carbons were not observed); IR (cm^{-1}): ν 3547.3, 3413.3, 3318.5, 3126.2, 3056.8, 3037.0, 2929.7, 2855.2, 1810.9, 1614.1, 1560.8, 1492.6, 1446.6, 1425.9, 1384.3, 966.9, 949.2,

798.9, 762.9, 688.7; MS (MALDI-HRMS): Found 1186.3967 $[M]^+$, $C_{80}H_{50}N_8O_4$ requires = 1186.3955; UV-vis (CH_2Cl_2, r.t.): λ_{max} [nm] (ε [l mol^{-1} cm^{-1}]): 421 (668758), 516 (26334), 552 (14290), 591 (7696), 647 (6232).

_O_-(_tert_-butyldiphenylsilyl)pyrene-1-hydroxamate (173)

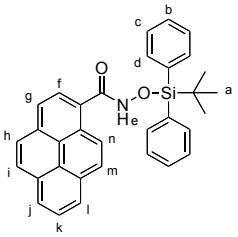

1-Pyrenecarboxylic acid (123 mg, 0.5 mmol) was dissolved in anhydrous CH_2Cl_2 (5 mL) under an inert atmosphere of argon. A catalytic amount of DMF (2 drops) and the mixture was cooled to 0°C. Oxalyl chloride (262 µL, 3.0 mmol) was added dropwise, after which the mixture was stirred for 16 h at room temperature. After concentrating the solution *in vacuo*, traces of oxalyl chloride were removed under high vacuum. The crude acid chloride was then redissolved in anhydrous CH_2Cl_2 (3 mL), and was added dropwise to a pre-cooled solution (0°C) of compound **155** (271 mg, 1.0 mmol) and DIEA (521 µL, 3.0 mmol) in anhydrous CH_2Cl_2 (2 mL). The resultant mixture was stirred under an inert atmosphere overnight, after which the mixture was concentrated *in vacuo*. The residue was dissolved in EtOAc (20 mL) and was washed with H_2O (20 mL) and brine (20 mL). The organic phase was dried ($MgSO_4$), filtered and concentrated *in vacuo*. The residue was purified by silica gel chromatography (eluent: cyclohexane initially, followed by 10% EtOAc in cyclohexane), yielding **173** (100 mg, 40%) as a pale yellow solid. m.p.: 175-176°C; ^{1}H NMR (400MHz, $CDCl_3$): δ 8.89 (s (rotamer), 0.2H, NH_e), 8.73 (d (rotamer), J = 9.4 Hz, 0.2H, CH_f), 8.37 (d (rotamer), J = 8.0 Hz, 0.2H, CH_g), 8.21-7.87 (m, 11.4H, CH_f [0.8H], CH_g [0.8H], CH_h [1H], CH_i [1H], CH_k [1H], CH_m [1H], CH_n [1H], CH_d [4H] & NH_e [0.8H]), 7.85-7.82 (m, 1H, CH_j), 7.73 (d, J = 7.8 Hz, 1H, CH_l), 7.53-7.43 (m, 6H, CH_b & CH_c), 1.26 (s, 9H, CH_a); ^{13}C NMR (100MHz, $CDCl_3$): δ 167.7, 136.0, 135.7, 133.3, 132.9, 131.4, 131.2, 130.8, 130.7, 130.1, 129.3, 129.1, 128.9, 128.5, 128.2, 127.9, 127.5, 127.4, 127.1, 126.6, 126.5, 126.3, 126.0, 125.9, 125.8, 125.7, 125.6, 125.0, 124.7, 124.5, 124.4, 124.3, 124.2, 27.5, 27.0, 19.7, 19.5 (the presence of rotamers was observed); IR (cm^{-1}): ν 3201.0, 3073.1, 3045.3, 2959.6, 2948.2, 2929.8, 2892.2, 2856.1, 1674.8, 1638.3, 1602.1, 1510.4, 1489.6, 1471.3, 1428.2, 1116.0, 1061.9, 919.6, 844.2, 823.9, 712.5, 707.2, 700.5, 503.8; MS (APCI-HRMS): Found 500.2048 $[M+H]^+$,

$C_{33}H_{30}NO_2Si$ requires = 500.2046; UV-vis (CH_2Cl_2, r.t.): λ_{max} [nm] (ε [l mol^{-1} cm^{-1}]): 332 (21912), 345 (30865).

5-{[*O*-(*tert*-butyldiphenylsilyl)]phenyl-4-hydroxamate}-10,15,20-tris(4-*tert*-butylphenyl)-21,23H-porphyrin (174)

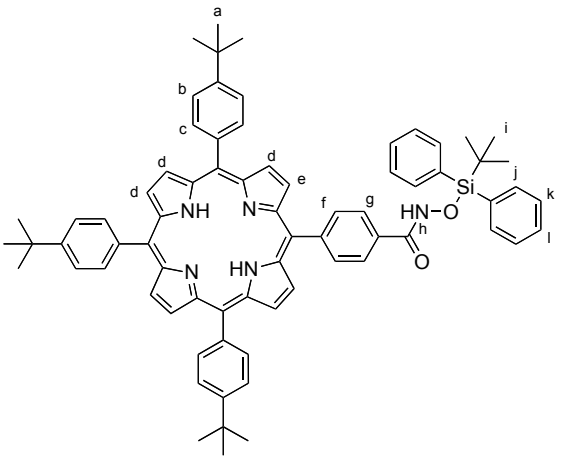

Porphyrin **133** (50 mg, 0.057 mmol) was suspended in anhydrous CH_2Cl_2 (4 mL) under an inert atmosphere of argon. Oxalyl chloride (29 µL, 43 mg, 0.34 mmol) was added followed by a catalytic amount of DMF (2 drops). The mixture was stirred for 16 h at room temperature. After concentrating the solution *in vacuo*, traces of oxalyl chloride were removed under high vacuum. The crude acid chloride was then redissolved in anhydrous CH_2Cl_2 (4 mL), and was added dropwise to a pre-cooled solution (0°C) of compound **155** (31 mg, 0.114 mmol) and DIEA (59 µL, 0.34 mmol) in anhydrous CH_2Cl_2 (2 mL). The resultant mixture was stirred under an inert atmosphere overnight. The mixture was then concentrated *in vacuo*, and the residue was purified by silica gel chromatography (eluent: CH_2Cl_2). The product from the column was dissolved in a minimal quantity of CH_2Cl_2 and was precipitated using pentane. The precipitate was collected by filtration and was washed with pentane, yielding **174** (20 mg, 32%) as a violet solid. m.p.: >350°C; ^{1}H NMR (400MHz, $CDCl_3$): δ 8.87 (s, 6H, CH_d), 8.81/8.68 (2 × d (rotamers), J = 4.8 Hz, 2H, CH_e), 8.56/8.23 (2 × s (rotamers), 1H, NH_h), 8.22-8.11 (m, 9H, CH_g [2H], CH_c [6H] & rotamer of CH_j [1H]), 7.96-7.93 (m, 2H, CH_f), 7.87-7.84 (m (rotamer), 3H, CH_j), 7.78-7.75 (m, 6H, CH_b), 7.55-7.43 (m, 6H, CH_k & CH_l), 1.61 (s, 27H, CH_a), 1.29 (s, 9H, CH_i), (N*H* protons of the porphyrin core were not observed); ^{13}C NMR (100MHz, $CDCl_3$): δ 159.3, 150.7, 139.2, 136.0, 135.7, 134.9, 134.6, 133.4, 131.7, 131.5, 130.7, 130.1, 128.3, 128.0, 125.5, 124.4, 123.8, 120.6, 120.5, 118.8, 118.0, 35.0, 31.8, 27.6, 27.0, 19.9, 19.5 (the presence of rotamers was observed); IR (cm^{-1}): ν 3314.3, 2951.5, 2922.4, 2902.3, 2853.8, 1809.4, 1722.3, 1606.5, 1472.6, 1462.4,

1397.5, 1348.9, 1270.2, 1108.0, 994.4, 966.4, 802.8; MS (MALDI-HRMS): Found 1079.5576 $[M]^+$, $C_{73}H_{73}N_5O_2Si$ requires = 1079.5534; UV-vis (CH_2Cl_2, r.t.): λ_{max} [nm] (ε [l mol^{-1} cm^{-1}]): 420 (592748), 516 (19667), 552 (15347), 593 (7059), 650 (8553).

4-[3-(3-Azidopropyl)thioureido]benzoic acid (176)

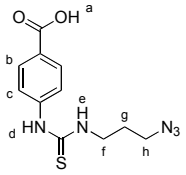

4-Carboxyphenyl isothiocyanate (179 mg, 1.0 mmol) was dissolved in DMF (1.0 mL). 3-Bromopropylamine hydrobromide (200 mg, 2.0 mmol) was added followed by DIEA (142 mg, 1.1 mmol). The mixture was stirred for 16 h at r.t. before 1M HCl (10 mL) was added to give a white precipitate. The solid was collected, washed with H_2O and dried yielding **176** (263, 94%) as a white solid. m.p.: 178-179°C; ^{1}H NMR (400MHz, DMSO-d6): δ 12.74 (s, 1H, COOH_a), 9.85 (s, 1H, NH_d), 8.12 (s, 1H, NH_e), 7.86 (d, J = 8.7 Hz, 2H, CH_b), 7.86 (d, J = 9.0 Hz, 2H, CH_c), 3.57-3.55 (m, 2H, CH_f), 3.42 (t, J = 6.7 Hz, 2H, CH_h), 1.83 (quin, J = 6.7 Hz, 2H, CH_g); ^{13}C NMR (100MHz, DMSO-d6): δ 180.3, 167.0, 143.7, 130.1, 125.1, 121.0, 48.5, 41.4, 27.7; IR (cm^{-1}): ν 3569.6, 3342.1, 3260.6, 3180.6, 3062.1, 2973.3, 2937.1, 2881.7, 2544.7, 2108.3, 2090.5, 1689.4, 1671.0, 1606.5, 1671.0, 1428.0, 1335.7, 1315.2, 1296.7, 1264.3, 1181.1, 1017.3, 990.8, 714.5, 647.9, 548.4, 480.0; MS (APCI-HRMS): Found 280.0865 $[M+H]^+$, $C_{11}H_{14}N_5O_2S$ requires = 280.0868.

***O*-(*tert*-Butyldiphenylsilyl)-4-[3-(3-azidopropyl)thioureido]phenyl hydroxamate (177)**

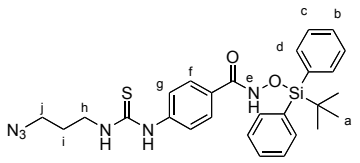

176 (400 mg, 1.43 mmol) was suspended in anhydrous CH_2Cl_2 (15 mL) under an inert atmosphere of argon. A catalytic amount of DMF (4 drops) and the mixture was cooled to 0°C. Oxalyl chloride (146 µL, 1.72 mmol) was added dropwise, after which the mixture was stirred for 3 h at room temperature. The solution was then cooled to 0°C and was added dropwise to a solution of compound **155** (466 mg, 1.72 mmol) and DIEA (897 µL, 5.16

mmol) in anhydrous CH_2Cl_2 (5 mL). The resultant mixture was stirred under an inert atmosphere overnight. The reaction mixture was then diluted with CH_2Cl_2 (30 mL) and was washed with H_2O (50 mL) and brine (50 mL). The organic phase was dried ($MgSO_4$), filtered and concentrated *in vacuo*. The residue was purified by silica gel chromatography (eluent: 25% EtOAc in cyclohexane), yielding **177** (312 mg, 41%) as a yellow solid. m.p.: 71-72°C; ^{1}H NMR (400MHz, $CDCl_3$): δ 8.31 (s, 1H, NH_e), 7.98 (d (rotamer), J = 8.7 Hz, 1.5H, CH_f), 7.81/7.71 (2 × d (rotamers), J = 6.7 Hz, 4H, CH_d), 7.60 (d (rotamer), J = 8.2 Hz, 0.5H, CH_f), 7.50-7.27 (m, 8H, CH_b, CH_c & CH_g), 4.18-4.14 (m, 2H, CH_h), 3.47-3.44 (m, 2H, CH_j), 2.07-2.01 (m, 2H, CH_i), 1.19 (s, 9H, CH_a); ^{13}C NMR (100MHz, $CDCl_3$): δ 179.5, 157.9, 135.8, 135.5, 133.2, 133.1, 131.1, 130.7, 130.1, 128.3, 128.0, 127.1, 118.9, 49.1, 40.2, 27.4, 27.2, 26.9, 19.7, 18.7 (the presence of rotamers was observed); IR (cm^{-1}): ν 3595.0, 3531.7, 3355.3, 2955.9, 2932.3, 2857.8, 2099.5, 1777.5, 1653.6, 1427.8, 1399.1, 1364.1, 1283.5, 1172.0, 1115.1, 1016.7, 910.6, 822.8, 741.1, 701.8, 614.1, 504.6; MS (ESI-MS): $[M+H]^+$ was not observed ($C_{27}H_{33}N_6O_2SSi$ requires = 533.2155). Fragmentation observed: Found 398.2 $[M-C_{10}H_{14}]^+$, 298.1 $[M-C_{10}H_{12}N_5S]^+$.

_O_-Propargylfluorescein (179)

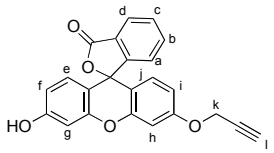

Propargyl bromide (7.8 g, 9.75 mL of an 80% solution in toluene, 65.6 mmol) was added to a solution of fluorescein sodium salt (120 mg, 3.125 mmol) in a mixture of anhydrous THF/MeOH (1:1). The resultant solution was stirred for 16 h at r.t. The crude mixture was concentrated *in vacuo*, diluted in H_2O (150 mL) and extracted with EtOAc (2 × 150 mL). The combined organic layers were dried ($MgSO_4$), filtered and concentrated *in vacuo*. The residue was then purified by silica gel chromatography (eluent: 1% MeOH in CH_2Cl_2) yielding **179** (552 mg, 48%) as a yellow solid. R_f = 0.6 (10% MeOH in CH_2Cl_2); ^{1}H NMR (400MHz, $CDCl_3$): δ 8.02 (d, J = 7.3 Hz, 1H, CH_d), 7.70-7.60 (m, 2H, CH_b & CH_c), 7.16 (d, J = 7.6 Hz, 1H, CH_a), 6.87 (d, J = 2.3 Hz, 1H, CH_j), 6.74 (d, J = 2.5 Hz, 1H, CH_e), 6.70-6.62 (m, 3H, CH_g, CH_h & CH_i), 6.55-6.52 (m, 1H, CH_f), 4.72 (s, 2H, CH_k), 2.56 (s, 1H, CH_l); ^{13}C NMR (100MHz, $CDCl_3$): δ 169.7, 159.3, 157.6, 153.2, 152.6, 152.5, 135.2, 129.9, 129.6, 129.4, 126.9, 125.2, 124.1, 112.3, 112.2, 111.7, 110.7, 103.3, 102.2, 84.4, 77.8, 76.3, 56.2; MS (APCI-HRMS): Found 371.0920 $[M+H]^+$, $C_{23}H_{15}O_5$ requires = 371.0919. Spectral data agrees with previously reported data.[267]

_O_-(_tert_-Butyldiphenylsilyl)-4-(3-{3-[4-(fluorescein-_O_-methyl)-1_H_-1,2,3-triazol-1-yl]propyl}thioureido)phenyl hydroxamate (180)

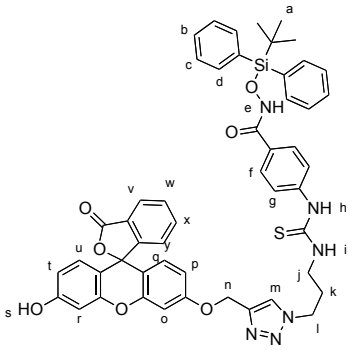

179 (37.0 mg, 0.1 mmol) and **177** (53.2 mg, 0.1 mmol) were dissolved in DMF (1 mL) in a microwave reaction vessel. Copper sulfate pentahydrate (2.5 mg, 0.01 mmol) and sodium ascorbate (7.9 mg, 0.04 mmol) were added and the resultant mixture was irradiated in the microwave at 120°C for 10 min. The reaction mixture was then diluted with EtOAc (20 mL) and was washed with 1M $HCl_{(aq)}$ (2 × 20 mL) and brine (20 mL). The organic phase was dried ($MgSO_4$), filtered and concentrated *in vacuo*. The residue was purified by silica gel chromatography (eluent: 1% MeOH in CH_2Cl_2). The solid residue obtained was dissolved in a minimal quantity of CH_2Cl_2 and was added dropwise to an excess of pentane. The resultant precipitate was collected by filtration and was washed with pentane, yielding **180** (35 mg, 39%) as a yellow solid. m.p.: 170-172°C; ^{1}H NMR (400MHz, DMSO-d6): δ 11.33 (s, 1H, OH_s), 11.14/10.88 (2 × s (rotamers), 1H, NH_e), 9.91 (s, 1H, NH_h), 8.19 (s, 1H, NH_i), 7.98 (d, J = 7.3 Hz, 1H, CH_v), 7.90-7.62 (m, 9H, CH_d, CH_f, CH_m, CH_w & CH_x), 7.48-7.37 (m, 8H, CH_b, CH_c & CH_g), 7.24 (d, *J* = 7.1 Hz, 1H, CH_y), 7.06 (s, 1H, CH_p), 6.80-6.63 (m, 3H, CH_q, CH_t & CH_u), 6.58 (s, 2H, CH_o & CH_r), 5.25 (s, 2H, CH_n), 4.52 (m, 2H, CH_l), 3.99 (m, 2H, CH_j), 2.31 (m, 2H, CH_k), 1.15/0.99 (2 × s (rotamers), 9H, CH_a); ^{13}C NMR (100MHz, DMSO-d6): δ 181.7, 168.7, 163.6, 159.7, 159.6, 155.5, 155.3, 152.5, 151.8, 142.2, 136.4, 135.7, 134.8, 134.5, 133.8, 130.2, 129.2, 129.0, 128.5, 127.8, 127.6, 126.1, 124.9, 124.7, 124.1, 112.8, 112.5, 111.3, 109.5, 102.2, 101.7, 82.7, 61.5, 47.1, 27.8, 26.6, 18.7 (two peaks overlapping); IR (cm^{-1}): ν 3527.3, 2954.6, 2933.1, 2858.1, 2348.5, 2336.4, 1776.8, 1632.5, 1609.1, 1503.3, 1464.2, 1428.5, 1399.1, 1363.2, 1285.0, 1249.4, 1177.9, 1114.7, 1010.4, 998.3, 702.4, 503.1; MS (APCI-HRMS): $[M+H]^+$ was not observed ($C_{50}H_{47}N_6O_7SSi$ requires = 903.2996). MALDI-TOF was not attempted; UV-vis (CH_2Cl_2, r.t.): λ_{max} [nm] (ε [l mol^{-1} cm^{-1}]): 425 (1565).

2-Carboxy-1,10-phenanthroline (182)

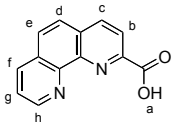

A solution of 1,10-phenanthroline (2.5 g, 13.9 mmol) in glacial acetic acid (3 mL) was prepared. 30% hydrogen peroxide (1.5 mL) was added to the solution and the reaction mixture was maintained at 70-75°C for 3 h, after which further 30% hydrogen peroxide (1.5 mL) was added and the heating was continued for another 3 h. After cooling to r.t., the pH of the mixture was adjusted to pH ~10 with saturated aqueous potassium hydroxide and then was extracted repeatedly (5 times) with $CHCl_3$. The combined organic extracts were dried ($MgSO_4$), filtered and concentrated *in vacuo* to give a yellow solid (2.1 g). The crude solid was dissolved in H_2O (35 mL). KCN (2.5 g) was added, followed by a dropwise addition of benzoyl chloride (3 mL). The resultant mixture was stirred at r.t. for 30 min. After cooling to 0°C, a tan coloured sticky solid was observed. By careful decantation the supernatant solvent was removed. All the residual H_2O was removed by co-evaporation with anhydrous toluene (3 times). The resultant solid, the crude 2-cyano-1,10-phenanthroline was dissolved in EtOH (20 mL) and a solution of NaOH (1.6 g) in H_2O (10 mL) was added. The mixture was refluxed for 2 h. The solution was then cooled to r.t. and was acidified to pH 5-6 using concentrated HCl. The solution was then dried *in vacuo*. H_2O (10 mL) was added to the residue. The suspension was heated to the boiling point and was filtered whilst hot. The isolated solid was dried yielding **182** (1.57 g, 50% over 3 steps) as a light tan coloured solid. No further purification was required. m.p.: 210-211°C; ^{1}H NMR (400MHz, DMSO-d6): δ 12.97 (br s, 1H, COOH_a), 7.97-7.91 (m, 3H, CH_c, CH_f & CH_h), 7.66-7.58 (m, 1H, CH_b), 7.53-7.45 (m, 3H, CH_d, CH_e & CH_g); ^{13}C NMR (100MHz, DMSO-d6): δ 167.4, 132.9, 130.8, 129.3, 128.6 (quaternary carbon signals were not observed). Spectral data agrees with previously reported data.[261, 262]

***O*-(*tert*-butyldiphenylsilyl)-1,10-phenanthroline-2-hydroxamate (183)**

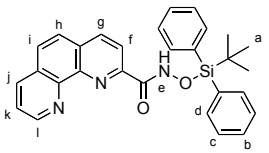

2-Carboxy-1,10-phenanthrolinem, **182** (224 mg, 1.0 mmol) was dissolved in thionyl chloride (10 mL) under an inert atmosphere of argon, and the mixture was refluxed for 4 h. The mixture was cooled to room temperature before the excess thionyl chloride was removed *in vacuo*. The compound was also dried under high vacuum to remove any residual thionyl chloride. The crude acid chloride was then dissolved in anhydrous CH_2Cl_2 (3 mL), and was added dropwise to a pre-cooled solution (0°C) of compound **155** (542 mg, 2.0 mmol) and DIEA (1043 µL, 6.0 mmol) in anhydrous CH_2Cl_2 (2 mL). The resultant mixture was stirred under an inert atmosphere overnight, after which the mixture was concentrated *in vacuo*. The residue was dissolved in EtOAc (20 mL) and was washed with H_2O (20 mL) and brine (20 mL). The organic phase was dried ($MgSO_4$), filtered and concentrated *in vacuo*. The residue was purified by chromatography on basic alumina (eluent: EtOAc), yielding **183** (164 mg, 34%) as a colourless crystalline solid. m.p.: 115-117°C; ^{1}H NMR (400MHz, $CDCl_3$): δ 8.31/7.93 (2 × s (rotamers), 1H, NH_e), 7.83-7.80 (m, 3H, CH_g, CH_j & CH_l), 7.74-7.71 (m (rotamer), 2H, CH_d), 7.51-7.27 (m, 12H, rotamer of CH_d [2H], CH_b [2H], CH_c [4H], CH_f [1H], CH_h [1H], CH_i [1H] & CH_k [1H]), 1.18 (s, 9H, CH_a); ^{1}H NMR (100MHz, $CDCl_3$): δ 167.1, 159.0, 135.9, 135.5, 133.3, 132.4, 131.9, 131.4, 130.7, 130.6, 130.0, 129.1, 128.8, 128.4, 128.2, 127.8, 127.1, 126.1, 27.4, 26.9, 19.8, 19.4 (the presence of rotamers was observed); IR (cm^{-1}): ν 3439.9, 3206.0, 3074.2, 3047.9, 2957.5, 2857.7, 2892.3, 2857.7, 1653.7, 1514.9, 1485.5, 1470.2, 1428.0, 1313.6, 1163.4, 1116.7, 902.9, 822.5, 764.3, 738.1, 712.6, 702.1, 693.3, 614.8, 505.2; MS (ESI-MS): $[M+H]^+$ was not observed ($C_{29}H_{28}N_3O_2Si$ requires = 478.1951). Fragmentation observed: Found 398.2 $[M-C_6H_5]^+$, 264.1 $[M-C_{16}H_{19}]^+$.

5.3.3 SOLID PHASE PNA SYNTHESIS

5.3.3.1 Initial trials utilising Tentagel resin

6-((4-Methoxyphenyl)-diphenylmethylamino)-hex-1-yl succinylamido-Tentagel (113)

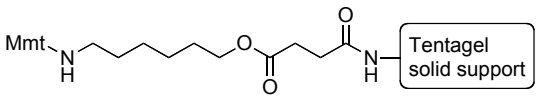

Amino-Tentagel (0.25 g) was swollen for 10 min with a solution of NEM (0.05 mL) and DMF (2.5 mL), then filtered. A solution of **112** (48.7 mg, 0.082 mmol), NEM (8.7µL, 0.069 mmol) and TBTU (26.5 mg, 0.082 mmol) in DMF (1.5 mL) was prepared and immediately

added to the Tentagel-NH_2. The resulting suspension was shaken for 16 h at room temperature. The derivatised Tentagel was filtered off and washed with DMF (3 × 3 mL), CH_2Cl_2 (3 × 1 mL) and Et_2O (3 × 1 mL), then dried *in vacuo*. A qualitative Kaiser test was applied to a sample of the resin at this stage and it indicated that there was an absence of free amines. The resin was then capped by treatment with a solution of 0.5 M acetic anhydride, 0.5 M lutidine and 0.5 M 1-methyl imidazole in THF (1 mL) for 1 h. The derivatised and capped Tentagel was filtered off and washed with CH_2Cl_2 (3 × 1 mL), followed by Et_2O (3 × 1 mL), and was then dried *in vacuo*. Another Kaiser test was applied. No free amines were detected.

6-aminohex-1-yl succinylamido-Tentagel (114)

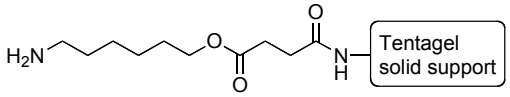

113 (250mg, 0.0625 mmol of active sites) was suspended in a 3% solution of TFA in CH_2Cl_2 (2 mL). The mixture was shaken for 5 min at r.t. after which the resin was filtered. This was repeated a further two times. After the third treatment, the resin was washed with DMF (3 × 2 mL), CH_2Cl_2 (3 × 2 mL) and Et_2O (3 × 2 mL). Each wash was shaken for 5s before draining. A qualitative Kaiser test was then applied to a sample of the resin to determine if the deprotection had been successful. If a positive test was observed, then the procedure to synthesize **40** was performed. If a negative or partial positive test was observed, the whole deprotection procedure was repeated.
Result: The Kaiser test was positive (the resin beads changed from colourless to blue) indicating free amine groups were present, therefore the deprotection was successful.

6-(*N*-(2-(*N*-9-Fluorenylmethoxycarbonyl)aminoethyl)-*N*-((thymin-1-yl)acetyl)glycine amido)-hex-1-yl succinylamido-Tentagel (115)

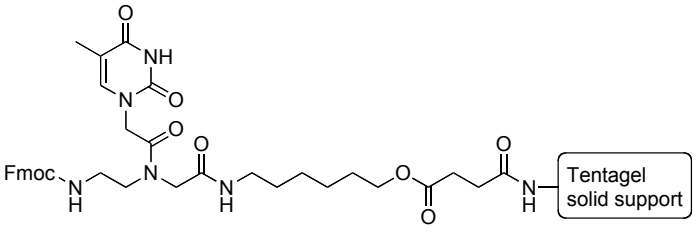

Refer to the monomer coupling procedure in the general solid phase synthesis procedures (section 5.3.3.5).

Result: The Kaiser test was negative (the resin beads remained colourless) indicating free amine groups were absent, therefore the coupling was successful.

6-(*N*-(2-(*N*-9-Acetyl)aminoethyl)-*N*-((thymin-1-yl)acetyl)glycine amido)-hex-1-yl succinylamido-Tentagel (116)

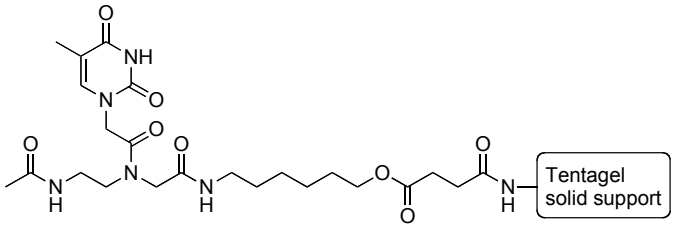

Refer to the FMOC deprotection and capping procedures in the general solid phase synthesis procedures (section 5.3.3.5). Both procedures were carried out starting from the deprotection and followed by the capping.

Result: The Kaiser test following the deprotection was positive (the resin beads changed from colourless to blue) indicating free amine groups were present, therefore the deprotection was successful. The Kaiser test following the capping was negative (the resin beads remained colourless) indicating free amine groups were absent, therefore the capping was successful.

5.3.3.2 Microwave solid phase PNA synthesis procedures (Biotage microwave)

Swelling – The resin (200 mg) was placed in a MacroKan™ vessel (obtained from IRORI, a subsidiary of Discovery Partners International Inc.) and was immersed in CH_2Cl_2. After allowing the suspension to stand at r.t. for 1 h, the resin was filtered and washed with DMF (5 × 4 mL).

Deprotection of the N-terminal FMOC protecting group – 20% piperidine in DMF (4 mL for 200 mg resin) was added to the resin. The mixture was irradiated in the microwave for 30s at 60°C (pre-stirring: 15s, stirring rate: 900rpm, heating mode: very high, FHT: on). The resin was filtered *in vacuo* and washed with DMF (2 × 4 mL). Another 4 mL of 20% piperidine in DMF was added to the resin. The mixture was irradiated for 150s at 60°C (pre-stirring: 15s,

stirring rate: 900rpm, heating mode: very high, FHT: on). The resin was filtered *in vacuo* and washed with DMF (5 × 4 mL). A qualitative Kaiser test was then applied to a small sample of the resin to determine if the deprotection had been successful. If a positive test was observed, then the monomer coupling procedure was performed. If a negative or partial positive test was observed, the second irradiation was repeated.

Monomer coupling – The rink amide resin had a loading of 0.64 mmol/g. 200 mg were used *i.e.* 0.128 mmol. 4 equivalents of the appropriate monomer (0.512 mmol, lysine: 257 mg, thymine: 259 mg, adenine: 332 mg) and 4 equivalents of HBTU (0.512 mmol, 194 mg) were dissolved in 270 equivalents of anhydrous DMF (35 mol, 2.7 mL) and 8 equivalents of NEM (1.024 mmol, 130 µL). The mixture was stirred for 2 min at r.t. before the resin in the macrokan was added to the solution. The mixture was then irradiated for 5 min at 60°C (pre-stirring: 15s, stirring rate: 900rpm, heating mode: very high, FHT: on). The resin was filtered *in vacuo* and washed with DMF (5 × 4 mL). A qualitative Kaiser test was then applied to a sample of the resin to determine if the coupling had been successful. If a negative test was observed, then the next deprotection was performed. If a positive or partial positive test was observed, the whole coupling procedure was repeated.

Storage – Following any coupling reaction, *i.e.* when the N-terminal of the growing oligomer was protected, the process could be stopped for a brief period e.g. overnight. The derivatised resin was stored suspended in 1:1 CH_2Cl_2/DMF at 4°C.

Resin cleavage – The derivatised resin was shaken in TFA/*m*-cresol 4:1 (2 mL) for 1 h. The colour of the resin was observed to change from its original clear/yellowish colour to red. The resin was filtered and the filtrate was collected. An excess of ice-cold Et_2O (5-fold or more) was added to the filtrate yielding a precipitate. The suspension was centrifuged to give a white pellet. The supernatant solution was decanted carefully. To the pellet was added further ice-cold Et_2O, and after vortexing to resuspend the pellet, the centrifugation and decantation was repeated. This was repeated once more (3 centrifugations in total) to give the crude PNA.

PNA analysis – Refer to the procedures described in section 5.3.3.5.

5.3.3.3 Microwave solid phase PNA synthesis procedures (CEM Discover microwave)

Swelling – The resin (200 mg) was placed in a CEM reaction vessel and was immersed in CH_2Cl_2. After allowing the suspension to stand at r.t. for 1 h, the resin was filtered and washed with DMF (5 × 4 mL).

Deprotection of the N-terminal FMOC protecting group – 20% piperidine in DMF (4 mL for 200 mg resin) was added to the resin. The mixture was irradiated in the microwave for 2min at 60°C (power: 20W, ΔT: 3°C). The resin was filtered *in vacuo* and washed with DMF (2 × 4 mL). Another 4 mL of 20% piperidine in DMF was added to the resin. The mixture was irradiated for 4min at 60°C (power: 20W, ΔT: 3°C). The resin was filtered *in vacuo* and washed with DMF (5 × 4 mL). During all the reactions, nitrogen was bubbled through the mixture for agitation purposes. A qualitative Kaiser test was then applied to a small sample of the resin to determine if the deprotection had been successful. If a positive test was observed, then the monomer coupling procedure was performed. If a negative or partial positive test was observed, the second irradiation was repeated.

Monomer coupling – The rink amide resin had a loading of 0.64 mmol/g. 200 mg were used *i.e.* 0.128 mmol. 4 equivalents of the appropriate monomer (0.512 mmol, lysine: 257 mg, thymine: 259 mg, adenine: 332 mg) and 4 equivalents of HBTU (0.512 mmol, 194 mg) were dissolved in 270 equivalents of anhydrous DMF (35 mol, 2.7 mL) and 8 equivalents of NEM (1.024 mmol, 130 μL). The mixture was then irradiated for 12min at 60°C (power: 10W, ΔT: 3°C). During all the reactions, nitrogen was bubbled through the mixture for agitation purposes. The resin was filtered *in vacuo* and washed with DMF (5 × 4 mL). A qualitative Kaiser test was then applied to a sample of the resin to determine if the coupling had been successful. If a negative test was observed, then the next deprotection was performed. If a positive or partial positive test was observed, the whole coupling procedure was repeated.

Storage – Following any coupling reaction, *i.e.* when the N-terminal of the growing oligomer is protected, the process can be stopped for a brief period e.g. overnight. The derivatised resin is stored suspended in 1:1 CH_2Cl_2/DMF at 4°C.

Resin cleavage – The derivatised resin was shaken in TFA/*m*-cresol 4:1 (2 mL) for 1 h. The colour of the resin was observed to change from its original clear/yellowish colour to red. The resin was filtered and the filtrate was collected. An excess of ice-cold Et_2O (5-fold or more)

was added to the filtrate yielding a precipitate. The suspension was centrifuged to give a white pellet. The supernatant solution was decanted carefully. To the pellet was added further ice-cold Et_2O, and after vortexing to resuspend the pellet, the centrifugation and decantation was repeated. This was repeated once more (3 centrifugations in total) to give the crude PNA.

PNA analysis – Refer to the procedures described in section 5.3.3.5.

5.3.3.4 Microwave solid phase PNA synthesis procedures (CEM Liberty microwave)

Swelling – The resin (156 mg) was placed in a CEM reaction vessel and was immersed in CH_2Cl_2. After allowing the suspension to stand at r.t. for 1 h, the resin was filtered and washed with DMF (5 × 4 mL).

The following solutions were prepared and set up on the liberty machine:

- Deprotection solution: 20% piperidine in DMF
- 0.2M of Fmoc-Lys-Z-OH in DMF
- 0.2M of thymine monomer in DMF
- 0.2M of adenine monomer in DMF
- 0.5M of HBTU in DMF
- 2.0M of NEM in DMF
- Capping solution: 20% acetic anhydride in DMF
- Washing solvent: DMF

Deprotection of the N-terminal FMOC protecting group – During each cycle, the resin (156 mg) was irradiated twice in the presence of 20% piperidine in DMF in the microwave as follows:

i) 30 s at 75°C (power: 35W).
ii) 3 min at 75°C (power: 44W).

The resin was then subjected to the washing sequence (see below).

Monomer coupling – The rink amide resin had a loading of 0.64 mmol/g. 156 mg were used *i.e.* 0.1 mmol. During each cycle the following quantities of solutions were added:

a) 2.5 mL of the appropriate 0.2M amino acid solution
b) 1.0 mL of the HBTU solution

c) 0.5 mL of the NEM solution

The mixture was then irradiated for 7 min at 75°C (power: 25W). The resin was then subjected to the washing sequence (see below).

Capping – The resin was capped following every coupling reaction. 2.5 mL of the capping solution was added to the resin and following microwave irradiation sequence was applied maintaining the same solution:

i) 30 s at 65°C (power: 40W).
ii) 30 s at 65°C (power: 0W).
iii) 30 s at 65°C (power: 40W).
iv) 30 s at 65°C (power: 0W).

Once the sequence was complete, the resin was then subjected to the washing sequence (see below).

Washing – The resin was filtered and washed 6 times with DMF (4 mL) alternating the between top and bottom washes i.e. the washing solvent was either sprayed into the reaction vessel from the top or bottom.

Resin cleavage – The derivatised resin was shaken in TFA/*m*-cresol 4:1 (2 mL) for 1 h. The colour of the resin was observed to change from its original clear/yellowish colour to red. The resin was filtered and the filtrate was collected. An excess of ice-cold Et_2O (5-fold or more) was added to the filtrate yielding a precipitate. The suspension was centrifuged to give a white pellet. The supernatant solution was decanted carefully. To the pellet was added further ice-cold Et_2O, and after vortexing to resuspend the pellet, the centrifugation and decantation was repeated. This was repeated once more (3 centrifugations in total) to give the crude PNA.

PNA analysis – Refer to the procedures described in section 5.3.3.5.

5.3.3.5 Manual solid phase PNA synthesis procedures

RESIN PREPARATION

Resin – Rink amide resin (250 mg, 0.52 mmol/g loading).

Swelling – The resin was immersed in CH_2Cl_2, and after allowing the suspension to stand at r.t. for 16 h, the resin was filtered.

Deprotection of the N-terminal FMOC protecting group – 20% piperidine in DMF (4 mL) was added to the resin. After 5 min of shaking, the resin was filtered. Once again, 20% piperidine in DMF (4 mL) was added to the resin. After 10 min of shaking, the resin was filtered. The resin was then washed (2 × DMF, 2 × CH_2Cl_2, 1 × DMF). Each wash was agitated for 5s before draining. A qualitative Kaiser test was then applied to a sample of the resin to determine if the deprotection had been successful. If a positive test was observed, then the monomer coupling procedure was performed. If a negative or partial positive test was observed, the whole deprotection procedure was repeated.

Lysine coupling and control of the resin loading – The desired loading of the resin in this oligomerisation was 0.4 mmol/g. In order to achieve this loading the following reagent quantities were used in this first coupling.

Reagent/solvent	**Equivalents**	**Molecular weight ($gmol^{-1}$)**	**Moles (mmol)**	**Mass (mg)**	**Volume (µL)**
Rink amide resin	1.00	0.52 mmol/g	0.13	250	-
Fmoc-Lys(Z)-OH	0.92	503	0.12	60	-
HBTU	0.77	379	0.10	38	-
DIEA	9.20	129	1.20	155	198
NMP	-	-	-	-	1704

Fmoc-Lys(Z)-OH and HBTU were dissolved in NMP. DIEA was added and the mixture was stirred at 45°C for 5 min before being added to the deprotected resin. The resultant resin suspension was agitated using argon bubbling for 1 h at r.t. The solution was then filtered and the resin was washed (5 × DMF). Each wash was agitated for 5s before draining.

The remaining unreacted terminal amino groups on the resin were then capped by exposing the resin to 10% acetic anhydride in NMP (2.5 mL) for 30 min at r.t. The solution was then filtered and the resin was washed (5 × DMF). At this point the resin was assumed to have a loading of 0.4 mmol/g. Therefore, since 250 mg of resin were used, the scale of the PNA oligomerisation was 0.1 mmol.
At this point, a qualitative Kaiser test was then applied to a sample of the resin to determine if the coupling and capping procedures had been successful. If a positive test was observed, then the capping procedure was performed once again. If a negative test was observed, the PNA oligomerisation could be started.

PNA OLIGOMERISATION CYCLES

Weighing – Before starting the oligomerisation, the solids (PNA monomer and HBTU) were pre-weighed and mixed into vials labeled according to their position in the sequence *i.e.* in this case 1-12. The vials were closed and stored in the fridge until approximately 1 h before their use.

Deprotection of the N-terminal FMOC protecting group – 20% piperidine in DMF (4 mL) was added to the resin. After 2 min of shaking, the resin was filtered. Once again, 20% piperidine in DMF (4 mL) was added to the resin. After 10 min of shaking, the resin was filtered. (Note: the coupling solution was prepared during these 10 minutes!) The resin was then washed (2 × DMF, 1 × CH_2Cl_2, 1 × DMF). Each wash was agitated for 5s before draining. A qualitative Kaiser test was then applied to a sample of the resin to determine if the deprotection had been successful. If a positive test was observed, then the monomer coupling procedure was performed. If a negative or partial positive test was observed, the whole deprotection procedure was repeated.

Monomer coupling – The monomer coupling were performed with the following reagent quantities.

Reagent/solvent	Equivalents	Molecular weight ($gmol^{-1}$)	Moles (mmol)	Mass (mg)	Volume (µL)
Rink amide resin bearing lysine	1.0	0.4 mmol/g	0.10	250	-
PNA monomer:					
Thymine	5.0	506	0.50	253	-
Adenine	5.0	650	0.50	325	-
HBTU	4.5	379	0.45	171	-
DIEA	12.0	129	1.20	155	198
NMP	-	-	-	-	1800

When 5 min were remaining in the final deprotection with 20% piperidine, the coupling solution was prepared. The pre-weighed mixture of PNA monomer and HBTU was dissolved in NMP. DIEA was added and the resultant solution was stirred at 45°C for 5 min before being added to the deprotected resin. (Note: the addition to the resin should be done as soon as the resin deprotection is complete to prevent side reactions from occurring). The resultant resin suspension was agitated using argon bubbling for 30 min at r.t. The solution was then filtered and the resin was washed (5 × DMF). Each wash was agitated for 5s before draining.
A qualitative Kaiser test was then applied to a sample of the resin to determine if the coupling had been successful. If a negative test was observed, then the capping procedure was performed. If a positive or partially positive test was observed, the whole coupling procedure was repeated with a fresh coupling solution.

Capping – The resin was exposed to 10% acetic anhydride in NMP (2.5 mL). The resultant resin suspension was agitated using argon bubbling for 5 min at r.t. The solution was then filtered and the resin was washed (5 × DMF). Each wash was agitated for 5s before draining.

The deprotection, coupling, capping cycle was repeated until the desired oligomer sequence was complete. If the process was not continuous, or upon completing the sequence, then the resin was stored as follows:

Storage – Derivatised resins were always stored suspended in 1:1 CH_2Cl_2/DMF at 4°C.

PNA ISOLATION

Resin cleavage – The derivatised resin (25 mg) was stirred in TFA/*m*-cresol 4:1 (250 μL) for 1 h. The colour of the resin was observed to change from its original clear/yellowish colour to red. The resin was filtered and the filtrate was collected. The flask and resin were washed with TFA. The washing were added to the filtrate. The filtrate was concentrated using a stream of nitrogen until all volatiles were removed. Then, an excess of ice-cold Et_2O (5-fold or more) was added to the filtrate yielding a precipitate. The suspension was centrifuged to give a white pellet. The supernatant solution was decanted carefully. To the pellet was added further ice-cold Et_2O, and after vortexing to resuspend the pellet, the centrifugation and decantation was repeated. This was repeated once more (3 centrifugations in total) to give the crude PNA, which was dried under vacuo.

PNA HPLC analysis – The crude PNA oligomers that were isolated, as well as purified PNA oligomers were analysed by analytical reverse phase HPLC using 0.1% TFA in H_2O (A) and 0.1% TFA in CH_3CN (B) as eluents. The flow rate was 1 mL per min. The gradient of the eluents is described in the table below.

Time (min)	Gradient	
	From	To
0-5	100% A	65% A : 35% B
5-15	65% A : 35% B	65% A : 35% B
15-40	65% A : 35% B	15% A : 85% B
40-41	15% A : 85% B	100% B
41-46	100% B	100% B
46-48	100% B	100% A

PNA purification – The crude PNA oligomers that were isolated were purified by semi-preparative reverse phase HPLC using 0.1% TFA in H_2O (A) and 0.1% TFA in CH_3CN (B) as eluents. The flow rate was 18 mL per min. The gradient of the eluents is described in the table below.

Time (min)	Gradient	
	From	To
0-5	100% A	65% A : 35% B
5-15	65% A : 35% B	65% A : 35% B
15-50	65% A : 35% B	15% A : 85% B
50-51	15% A : 85% B	100% B
51-56	100% B	100% B
56-60	100% B	100% A

PNA identification – Analysis of the purified PNA oligomers was carried out by MALDI-TOF MS or ESI MS.

PNA DEPROTECTION IN SOLUTION

Fmoc deprotection – 20% piperidine in DMF (1 mL) was added to PNA oligomer (2.5 mg) and was stirred for 20 min at r.t. Et_2O (45 mL) was added to precipitate the PNA. The suspension was centrifuged (5 min at 5000 rpm) and then the supernatant was decanted. The whole procedure was repeated once more on the residue that was obtained, however the precipitation and decantation was performed three times instead of once. The residue that was obtained was dried *in vacuo*.

Cbz deprotection – The dried residue was dissolved in anhydrous DMF (30 µL) and was cannulated into a 1 mL flask (microwave tube). Trimethylsilyl iodide (TMSI, 12 µL, 0.084 mmol) was added using a dry microliter syringe. The mixture was stirred for 16 h at 50°C, after which anhydrous MeOH (14 µL, 0.336 mmol) was added. The resultant mixture was stirred for 30 min at r.t. The volatile components were then removed under high vacuum leaving an oily residue, which was then precipitated with Et_2O (45 mL). The suspension was centrifuged (5 min at 5000 rpm) and then the supernatant was decanted. The precipitation, centrifugation and decantation was repeated twice more. The residue was then dried *in vacuo*, and was analysed and purified by HPLC.

Deprotected PNA HPLC analysis – The crude PNA oligomers that were isolated, as well as purified PNA oligomers were analysed by analytical reverse phase HPLC using 0.1% TFA in H_2O (A) and 0.1% TFA in CH_3CN (B) as eluents. The flow rate was 1 mL per min. The gradient of the eluents is described in the table below.

Time (min)	Gradient	
	From	To
0-25	100% A	40% A : 60% B
25-35	40% A : 60% B	100% B
35-45	100% B	100% B
45-47	100% B	100% A
47-50	100% A	100% A

Deprotected PNA purification – The crude PNA oligomers that were isolated were purified by semi-preparative reverse phase HPLC using 0.1% TFA in H_2O (A) and 0.1% TFA in CH_3CN (B) as eluents. The flow rate was 15 mL per min. The gradient of the eluents is described in the table below.

Time (min)	Gradient	
	From	
0-30	100% A	0-25
30-40	40% A : 60% B	25-35
40-50	100% B	35-45
50-55	100% B	45-47
55-60	100% A	47-50

PNA identification – Analysis of the purified PNA oligomers was carried out by MALDI-TOF MS or ESI MS.

5.3.4 ISOLATED PNA OLIGOMERS

PNA dimer – sequence: lys-TT (122)

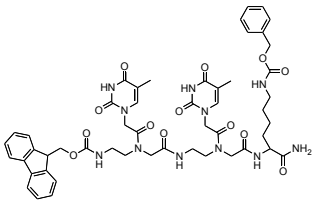

122 was synthesized according to the procedures described in section 5.3.3.5. HPLC retention time: 26.6 min. MS (MALDI-HRMS): Found 1056.3824 $[M+Na]^+$, $C_{51}H_{59}N_{11}O_{13}Na$ requires = 1056.4192.

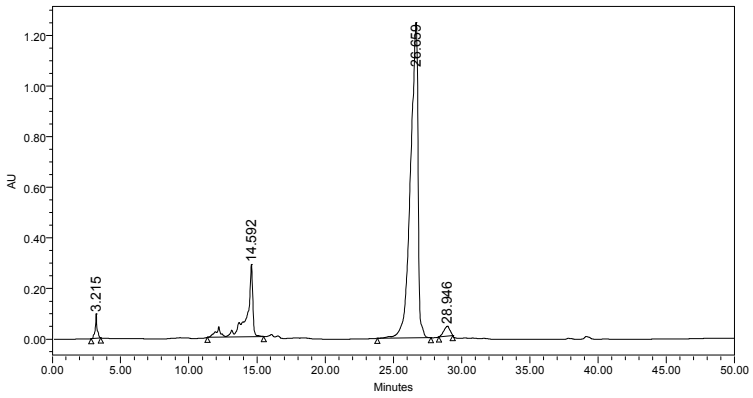

HPLC chromatogram of **122** (crude product). Agilent Zorbax SB-C18, 5 µm, 4.6 x 250 mm, gradient: 0.1% TFA in H_2O to 0.1% TFA in CH_3CN, flow: 1 mL/min, r.t.

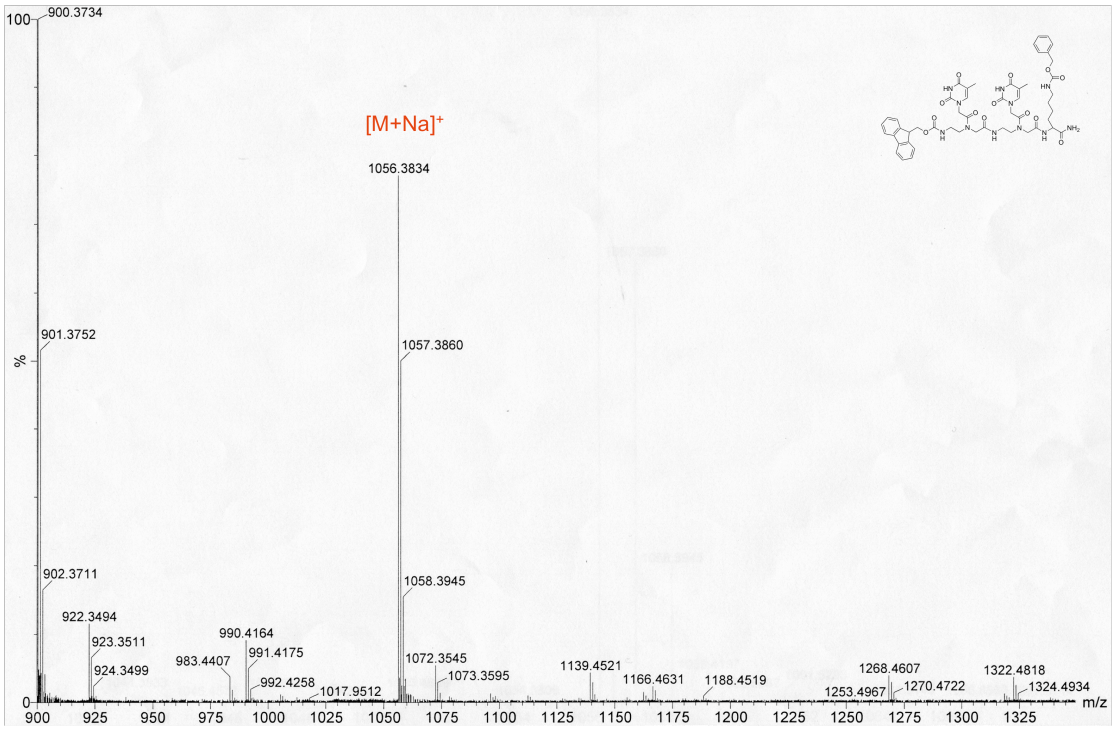

MALDI-TOF MS of **122**

PNA tetramer – sequence: lys-TTAA (123)

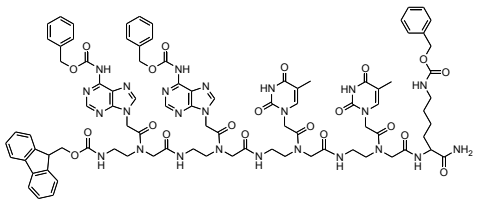

123 was synthesized according to the procedures described in section 5.3.3.5. HPLC retention time: 30.3 min. MS (MALDI-HRMS): Found 1852.81 $[M+H]^+$, $C_{89}H_{98}N_{25}O_{21}$ requires = 1852.73, Found 1744.75 $[M-F1]^+$, $C_{82}H_{90}N_{25}O_{20}$ requires = 1744.68; Found 1656.65 $[M-F2]^+$, $C_{75}H_{86}N_{25}O_{20}$ requires = 1656.64. Refer to Figure 81 (Page 104) for structures of F1 and F2.

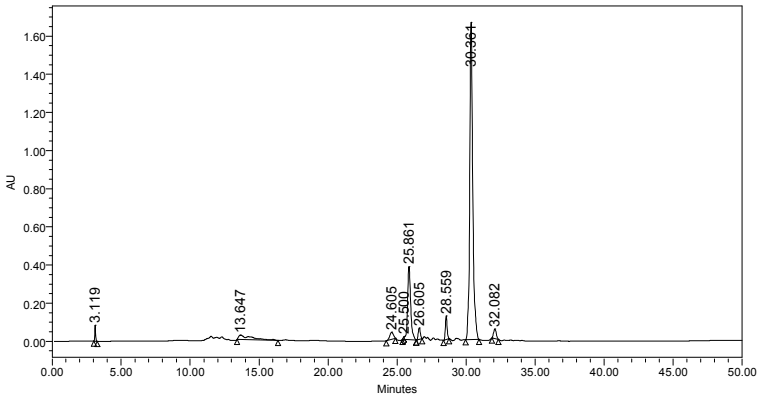

HPLC chromatogram of **123** (crude product). Agilent Zorbax SB-C18, 5 µm, 4.6 x 250 mm, gradient: 0.1% TFA in H_2O to 0.1% TFA in CH_3CN, flow: 1 mL/min, r.t.

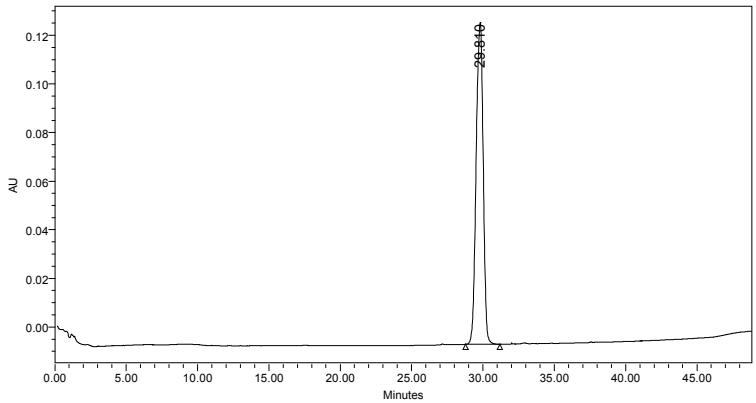

HPLC chromatogram of **123** (purified product). Agilent Zorbax SB-C18, 5 µm, 4.6 x 250 mm, gradient: 0.1% TFA in H_2O to 0.1% TFA in CH_3CN, flow: 1 mL/min, r.t.

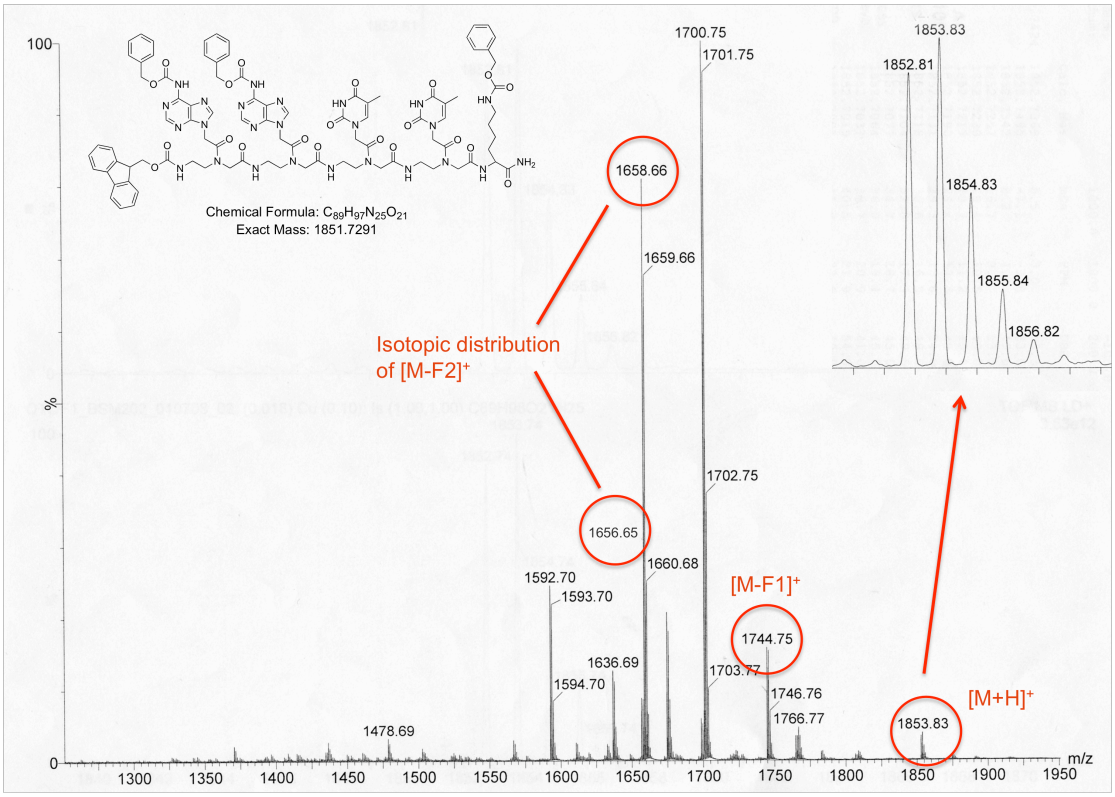

MALDI-TOF MS of **123**

PNA octamer – sequence: lys-TTAATTAA (125)

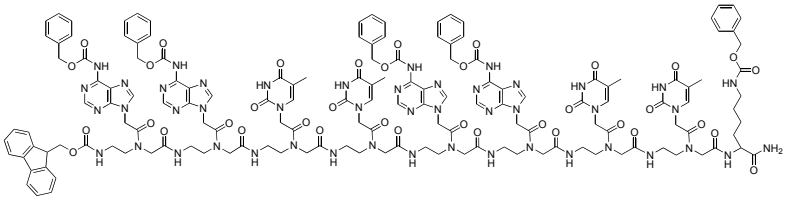

125 was synthesized according to the procedures described in section 5.3.3.5. HPLC retention time: 30.3 min. MS (MALDI-HRMS): Found 3203.32 $[M+H]^+$, $C_{149}H_{164}N_{47}O_{37}$ requires = 3203.24, Found 2793.09 $[M-2F1-F2]^+$, $C_{82}H_{90}N_{25}O_{20}$ requires = 2793.05. Refer to Figure 81 (Page 104) for structures of F1 and F2.

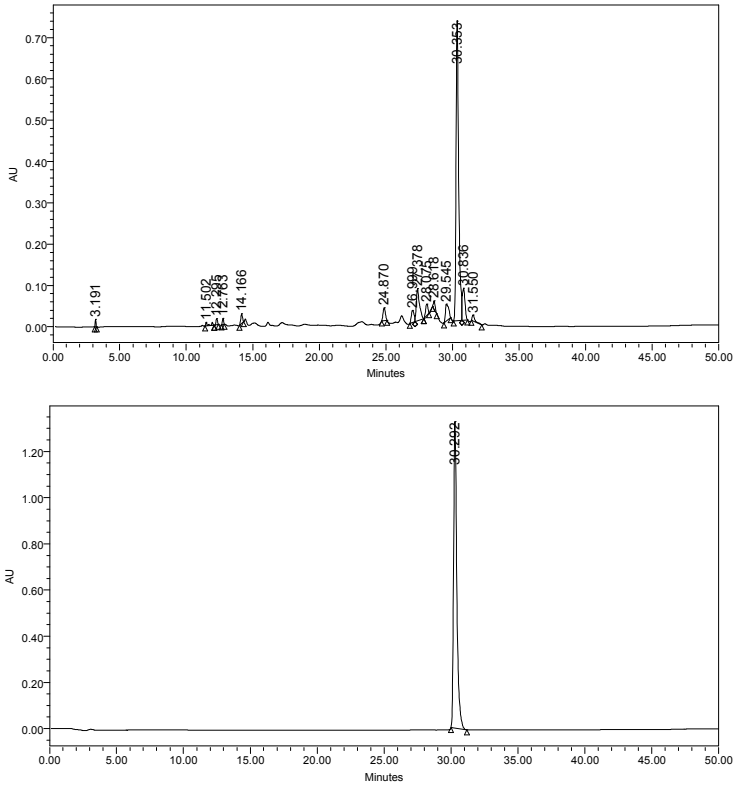

HPLC chromatograms of **125** (crude and purified product). Agilent Zorbax SB-C18, 5 µm, 4.6 x 250 mm, gradient: 0.1% TFA in H_2O to 0.1% TFA in CH_3CN, flow: 1 mL/min, r.t.

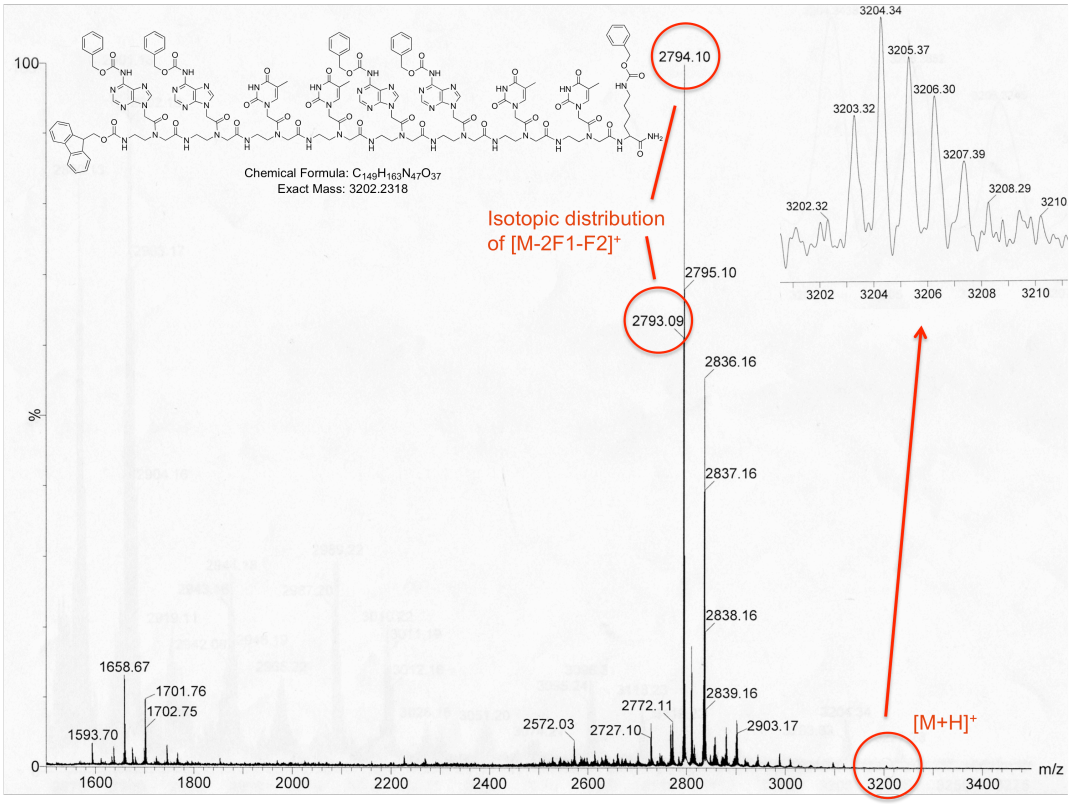

MALDI-TOF MS of **125**

PNA dodecamer – sequence: lys-TTAATTAATTAA (126)

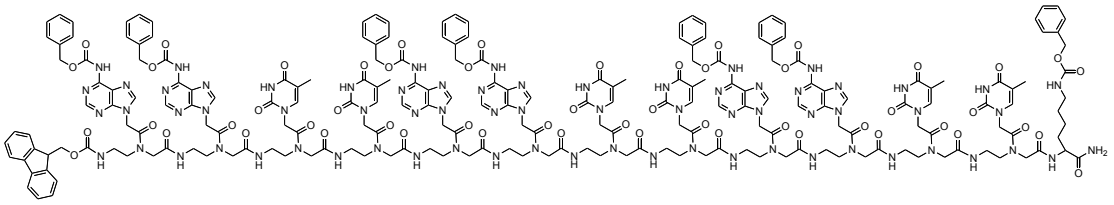

126 was synthesized according to the procedures described in section 5.3.3.5. HPLC retention time: 30.5 min. MS (MALDI-HRMS): Found 4143.63 $[M -2F1 -F2]^+$, $C_{181}H_{204}N_{69}O_{50}$ requires = 4143.55, Found 4036.53 $[M -3F1 -F2]^+$, $C_{174}H_{197}N_{69}O_{49}$ requires = 4036.50; Found 3927.46 $[M -4F1 -F2]^+$, $C_{167}H_{190}N_{69}O_{48}$ requires = 3929.45. Refer to Figure 81 (Page 104) for structures of F1 and F2.

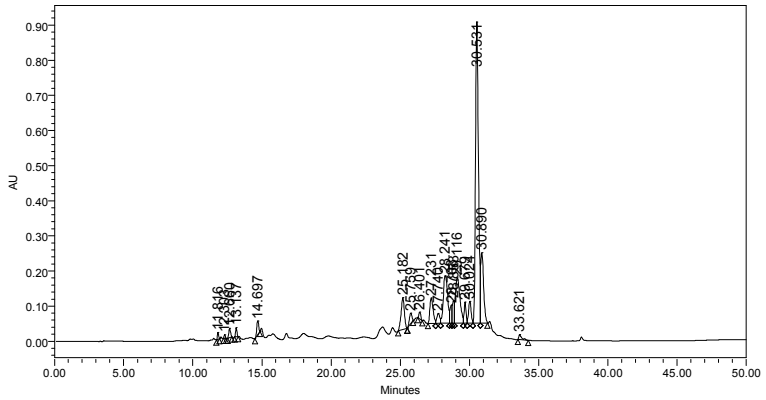

HPLC chromatogram of **126** (crude product). Agilent Zorbax SB-C18, 5 µm, 4.6 x 250 mm, gradient: 0.1% TFA in H_2O to 0.1% TFA in CH_3CN, flow: 1 mL/min, r.t.

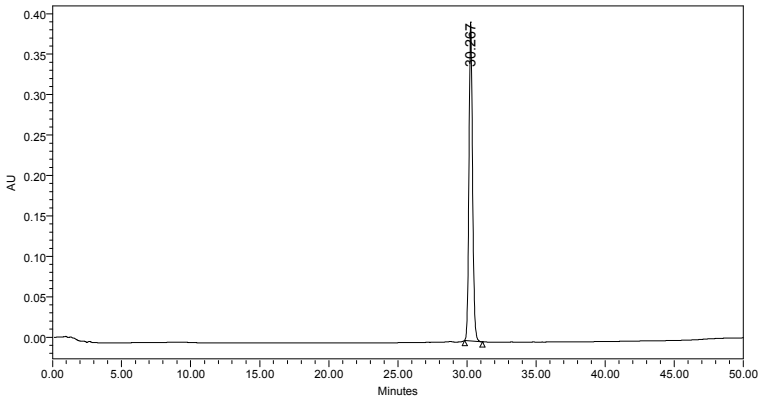

HPLC chromatogram of **126** (purified product). Agilent Zorbax SB-C18, 5 µm, 4.6 x 250 mm, gradient: 0.1% TFA in H_2O to 0.1% TFA in CH_3CN, flow: 1 mL/min, r.t.

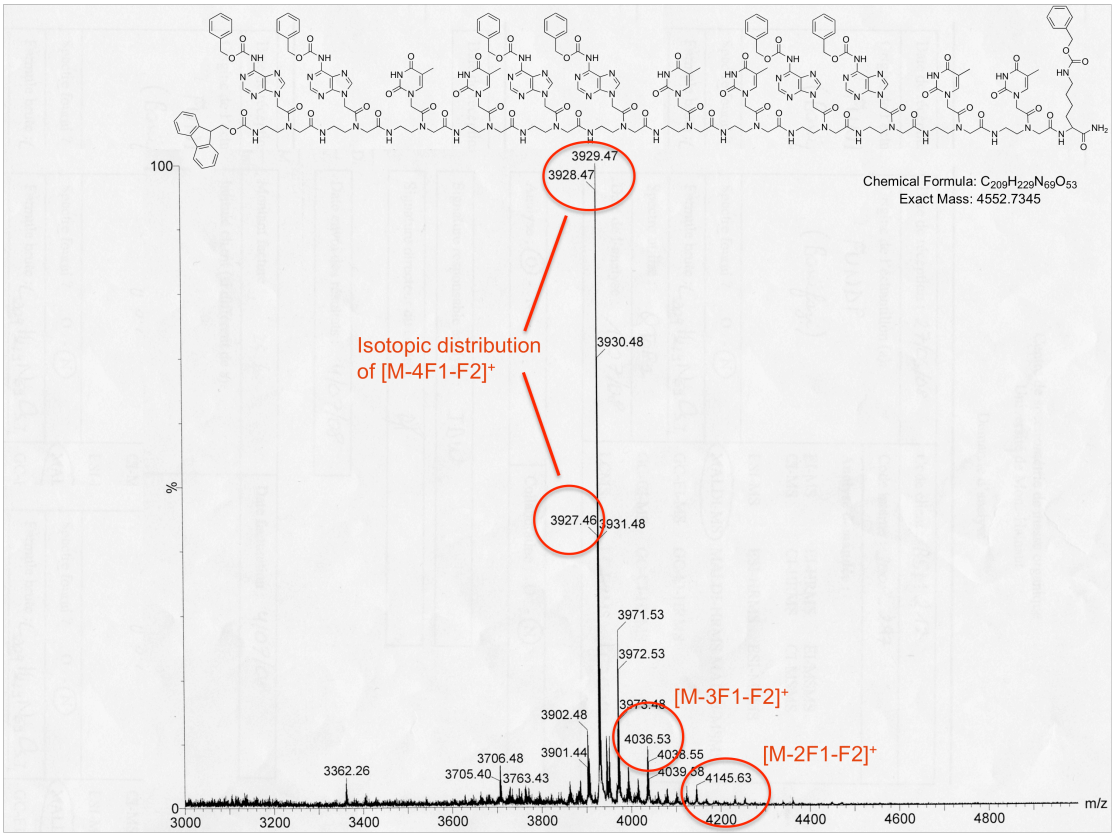

MALDI-TOF MS of **126**

Deprotected PNA dodecamer – sequence: lys-TTAATTAATTAA (127)

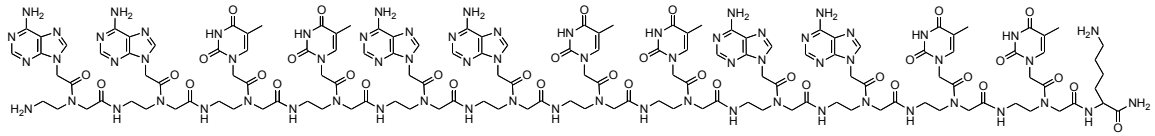

20% piperidine in DMF (1 mL) was added to **126** (2.5 mg, 0.55 µmol) and was stirred for 20 min at r.t. Et_2O (45 mL) was added to precipitate the PNA. The suspension was centrifuged (5 min at 5000 rpm) and then the supernatant was decanted. The whole procedure was repeated once more on the residue that was obtained, however the precipitation and decantation was performed three times instead of once. The residue that was obtained was dried *in vacuo*. The dried residue was dissolved in anhydrous DMF (30 µL) and was cannulated into a 1 mL flask (microwave tube). Trimethylsilyl iodide (TMSI, 12 µL, 0.084 mmol) was added using a dry microliter syringe. The mixture was stirred for 16 h at 50°C, after which anhydrous MeOH (14 µL, 0.336 mmol) was added. The resultant mixture was stirred for 30 min at r.t. The volatile components were then removed under high vacuum leaving an oily residue, which was then precipitated with Et_2O (45 mL). The suspension was centrifuged (5 min at 5000 rpm) and then the supernatant was decanted. The precipitation, centrifugation and decantation

was repeated twice more. The residue was then dried *in vacuo*, and was analysed and purified by HPLC according to the procedures described in section 5.3.3.5. Following lyophilisation of the HPLC fractions, **127** was isolated as a white solid, which was soluble in H_2O. HPLC retention time: 15.1 min. MS (ESI-MS), multiple ionization observed: Found 1697.3651 $[M+2H]^{2+}$, 1131.6075 $[M+3H]^{3+}$, 848.9363 $[M+4H]^{4+}$, 679.3599 $[M+5H]^{5+}$,which resolved to 3392.73 ± 0.03 $[M]^{+}$, $C_{138}H_{177}N_{69}O_{37}$ requires = 3392.4090.

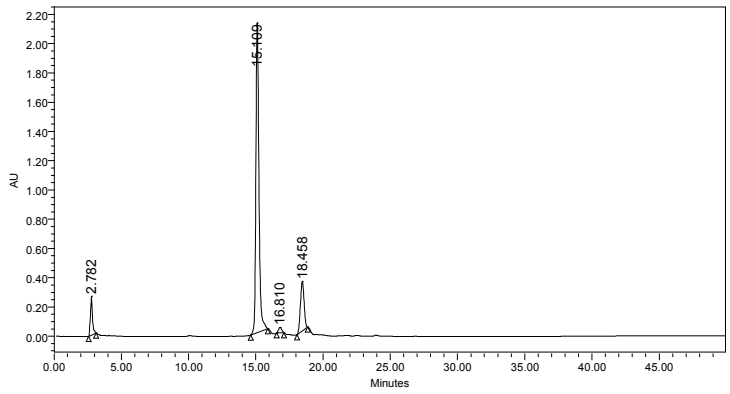

HPLC chromatogram of **127** (crude product). Agilent Zorbax SB-C18, 5 µm, 4.6 x 250 mm, gradient: 0.1% TFA in H_2O to 0.1% TFA in CH_3CN, flow: 1 mL/min, r.t.

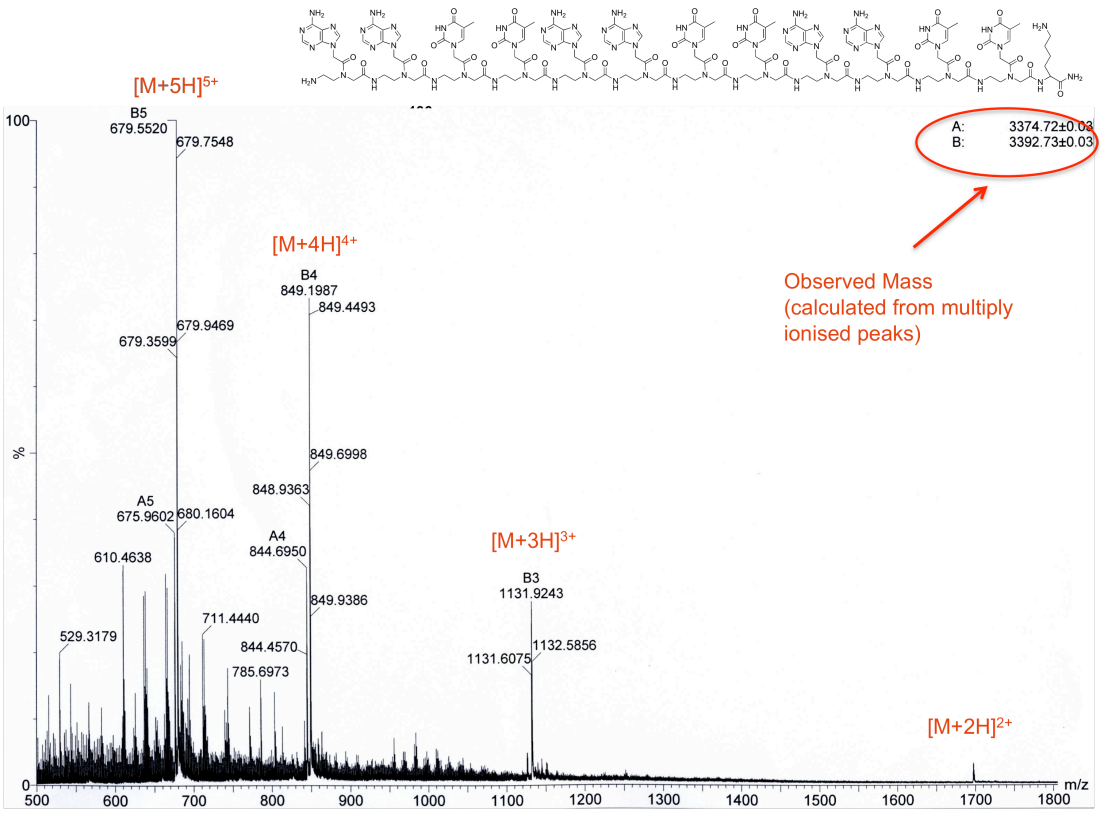

ESI-MS of **127**

PNA dodecamer (sequence: lys-TTAATTAATTAA) with azide linker (146)

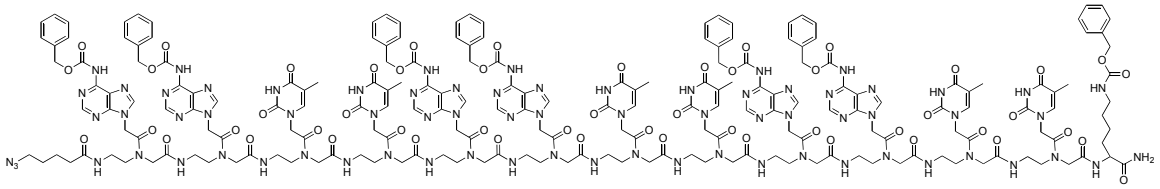

Compound **146** was synthesized using the protocols described in section 5.3.3.5. The attachment of the azide linker was performed on 40 mg of resin bearing the dodecamer using the following steps: (i) *Deprotection of the FMOC protecting group* – the same procedure as described (section 5.3.3.5) was used. (ii) *Coupling of the azide linker (**138**)* – the same procedure as described (section 5.3.3.5) was used, however in place of the PNA monomer, 5 equivalents of **138** was used. The reaction mixture was shaken for 4 h instead of 2 h. (iii) *Cleavage from the resin* – a small sample (5 mg) was subjected to the described cleavage procedure (section 5.3.3.5). (iv) *HPLC analysis of the crude* – the crude product was analysed by HPLC using the conditions described in section 5.3.3.5. The retention time of the product was 28.3 minutes. (v) *Purification* – the product was purified by semi-preparative scale HPLC using the conditions described in section 5.3.3.5. (vi) *Mass analysis* – both MALDI and ESI-MS were attempted, however, a mass spectrum of the product was not obtained due to the lack of ionisable functional groups in the compound.

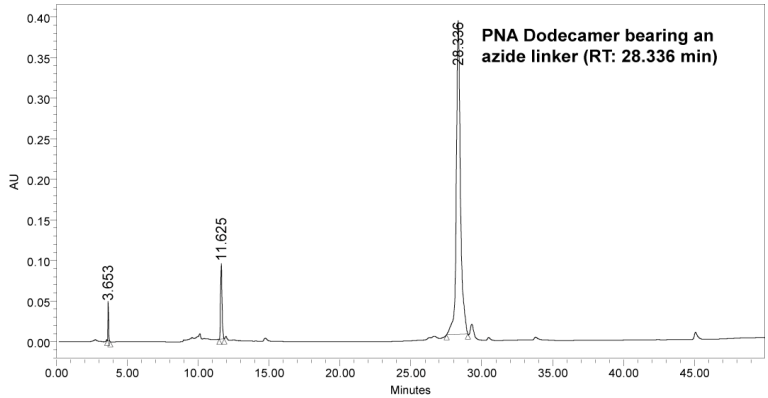

HPLC chromatogram of **146** (purified product). Agilent Zorbax SB-C18, 5 µm, 4.6 x 250 mm, gradient: 0.1% TFA in H_2O to 0.1% TFA in CH_3CN, flow: 1 mL/min, r.t.

PNA dodecamer (sequence: lys-TTAATTAATTAA) with acetylene linker (158)

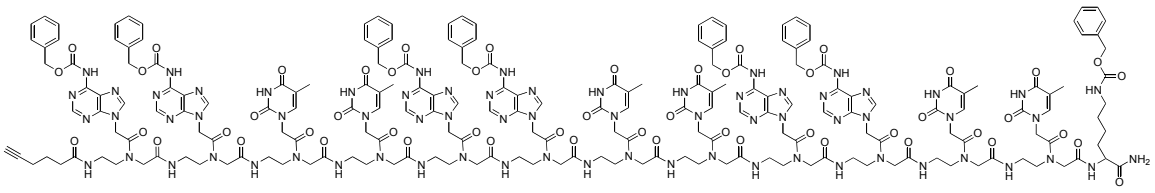

Compound **158** was synthesized using the protocols described in section 5.3.3.5. The attachment of the acetylene linker was performed on 50 mg of resin bearing the dodecamer using the following steps: (i) *Deprotection of the FMOC protecting group* – the same procedure as described (section 5.3.3.5) was used. (ii) *Coupling of the acetylene linker* – the same procedure as described (section 5.3.3.5) was used, however in place of the PNA monomer, 5 equivalents of 5-hexynoic acid (14.3 mg, 0.128 mmol) was used. (iii) *Cleavage from the resin* – a small sample (5 mg) was subjected to the described cleavage procedure (section 5.3.3.5). (iv) *HPLC analysis of the crude* – the crude product was analysed by HPLC using the conditions described in section 5.3.3.5. The retention time of the product was 28.1 minutes. (v) *Purification* – the product was purified by semi-preparative scale HPLC using the conditions described in section 5.3.3.5. (vi) *Mass analysis* – both MALDI and ESI-MS were attempted, however, a mass spectrum of the product was not obtained due to the lack of ionisable functional groups in the compound.

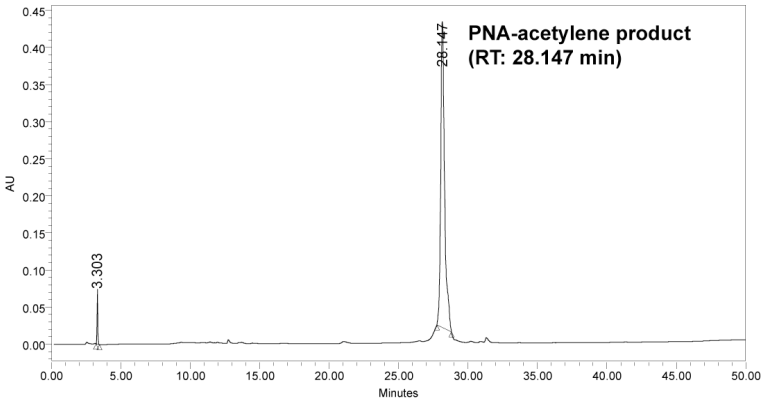

HPLC chromatogram of **158** (purified product). Agilent Zorbax SB-C18, 5 µm, 4.6 x 250 mm, gradient: 0.1% TFA in H_2O to 0.1% TFA in CH_3CN, flow: 1 mL/min, r.t.

PNA dodecamer (sequence: lys-TTAATTAATTAA) with acetylene linker (159)

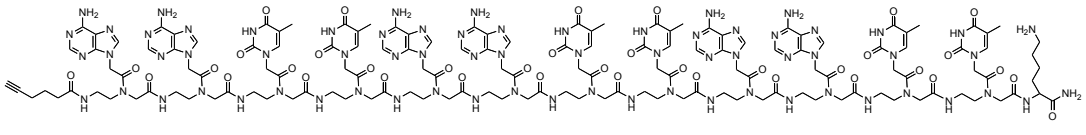

The nucleobases of **158** were deprotected from the Cbz-protecting groups using the procedures described in section 5.3.3.5. Following HPLC analysis, purification and lyophilisation, **159** was obtained as a white solid. MS (MALDI-MS): Found 3487.5 $[M+H]^+$, $C_{144}H_{184}N_{69}O_{38}$ requires = 3487.46, Found 3509.5 $[M+Na]^+$, $C_{144}H_{183}N_{69}NaO_{38}$ requires = 3509.44.

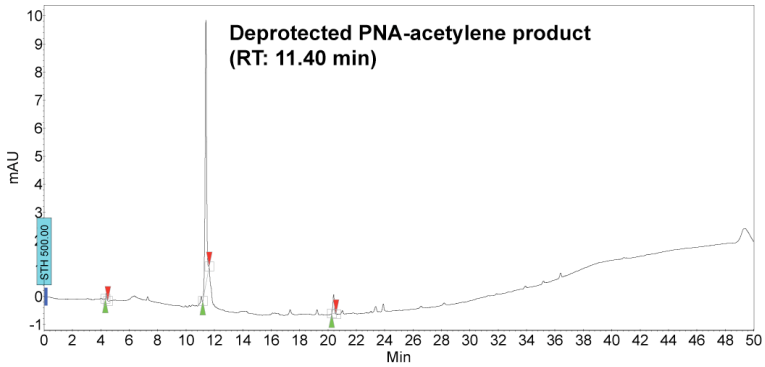

HPLC chromatogram of **159** (purified product). Varian Pursuit C18, 5 µm, 4.6 x 250 mm, gradient: 0.1% TFA in H_2O to 0.1% TFA in CH_3CN, flow: 1 mL/min, 65°C

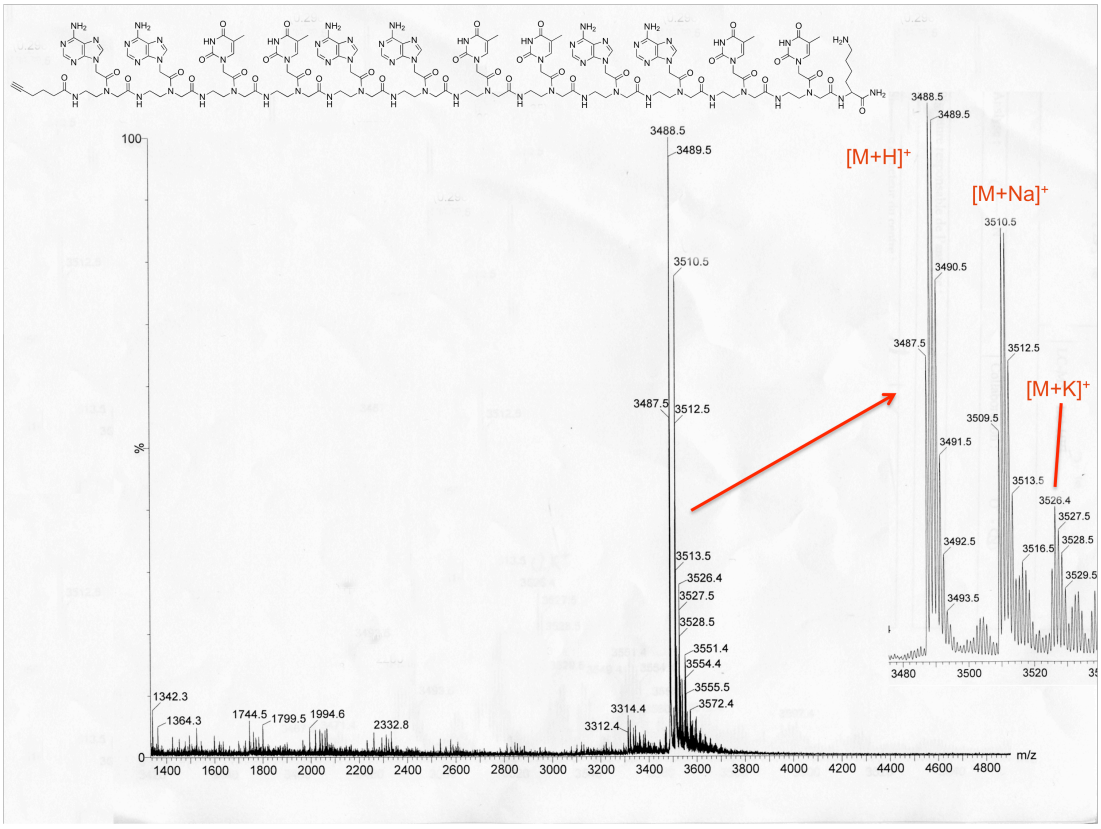

MALDI-TOF MS of **159**

PNA dodecamer (sequence: lys-TTAATTAATTAA) with anthracene adduct (160)

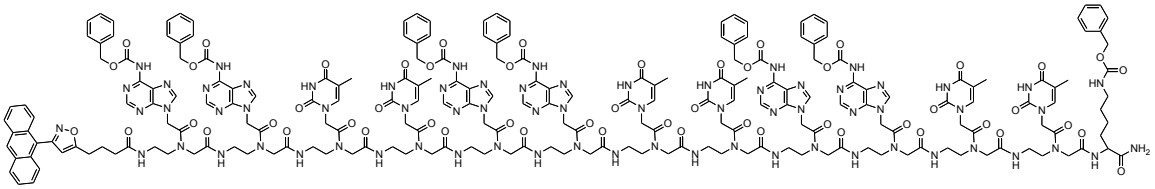

Synthesis according to scheme 25: The resin-attached acetylene bearing dodecamer (resin attached **158**, 10mg, equivalent to 0.0064 mmol) was suspended in DMF (250 µL). **148** (6.5 mg, 0.0256 mmol) was added, followed by triethylamine (3.6 µL, 0.0256 mmol). The mixture was shaken for 16 h at 50°C. The resin was then filtered and washed with DMF (5 × 2 mL) and CH_2Cl_2 (3 × 2 mL). The resin was then subjected to the cleavage, HPLC analysis and purification procedures as described in section 5.3.3.5. The HPLC retention time was 30.4 minutes. A mass spectrum could not be obtained for this compound due to the lack of ionisable groups in the molecule.

Synthesis according to scheme 26: Under an argon atmosphere, **156** (30.4 mg, 0.064 mmol) was dissolved in anhydrous CH_2Cl_2 (50 µL). Triethylamine (28 µL, 0.192 mmol) was added and the mixture was cooled to -40°C. A 1M solution of trifluoromethanesulfonic anhydride in CH_2Cl_2 (68 µL, 0.068 mmol) was added dropwise. Once the addition was complete, the reaction mixture was allowed to stir for 1 h at 0°C, after which, it was added to a suspension of the resin-attached acetylene bearing dodecamer (resin attached **158**, 10mg, equivalent to 0.0064 mmol) in DMF (200 µL). The resultant mixture was shaken for 16 h at 50°C. The resin was then filtered and washed with DMF (5 × 2 mL) and CH_2Cl_2 (3 × 2 mL). The resin was then subjected to the cleavage procedure. The isolated crude product was subjected to HPLC analysis and purification as described in section 5.3.3.5. The HPLC retention time was 30.2 minutes. A mass spectrum could not be obtained for this compound due to the lack of ionisable groups in the molecule.

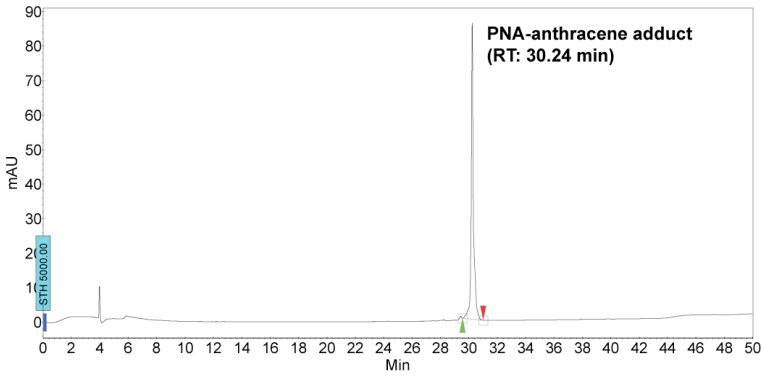

HPLC chromatogram of **160** (purified product). Varian Pursuit C18, 5 µm, 4.6 x 250 mm, gradient: 0.1% TFA in H_2O to 0.1% TFA in CH_3CN, flow: 1 mL/min, 65°C

Deprotected PNA-anthracene adduct (sequence: lys-TTAATTAATTAA) (161)

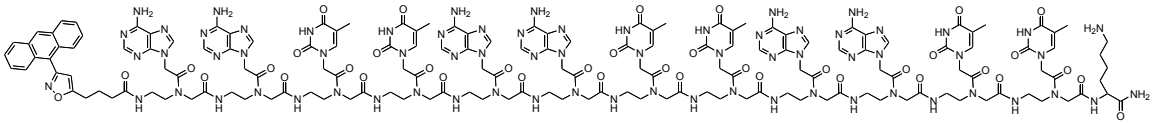

The nucleobases of **160** were deprotected from the Cbz-protecting groups using the procedures described in section 5.3.3.5. Following HPLC analysis (retention time: 17.2 min), purification and lyophilisation, **161** was obtained as a white solid which was H_2O soluble. MS (MALDI-HRMS): Found 3706.5244 $[M+H]^+$, $C_{159}H_{193}N_{70}O_{39}$ requires = 3706.5271, Found 3728.7 $[M+Na]^+$, $C_{159}H_{192}N_{70}NaO_{39}$ requires = 3728.5.

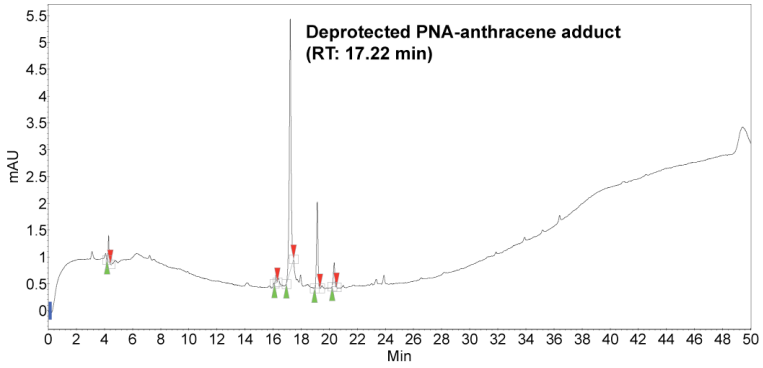

HPLC chromatogram of **161** (crude product). Varian Pursuit C18, 5 µm, 4.6 x 250 mm, gradient: 0.1% TFA in H_2O to 0.1% TFA in CH_3CN, flow: 1 mL/min, 65°C

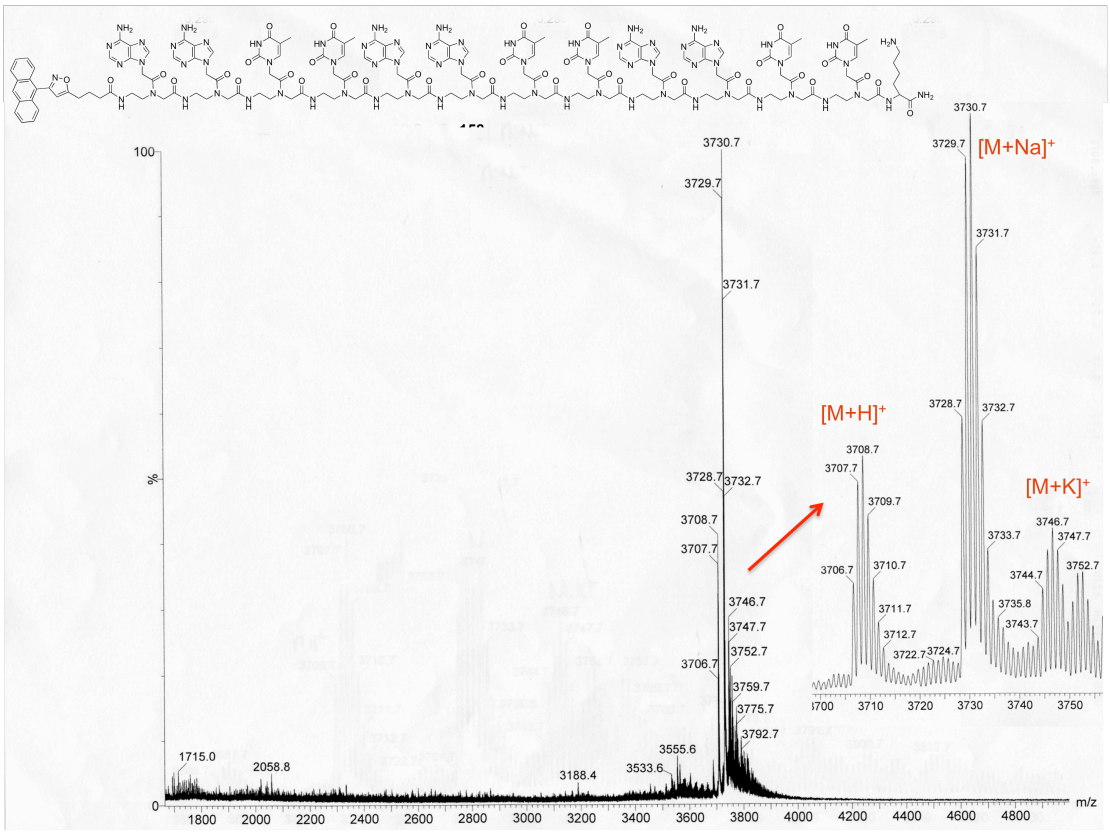

MALDI-TOF MS of **161**

PNA dodecamer (sequence: lys-TTAATTAATTAA) with pyrene adduct (184)

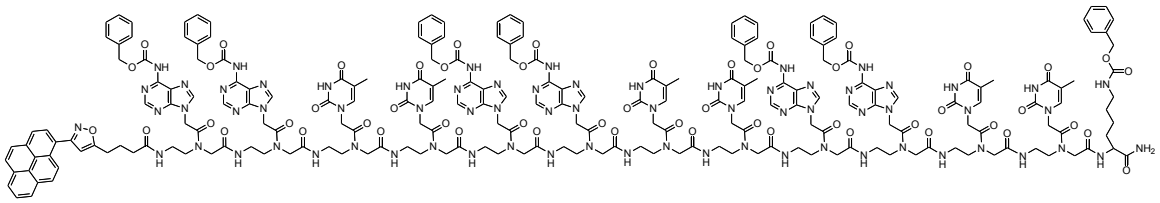

Under an argon atmosphere, **173** (20 mg, 0.04 mmol) was dissolved in anhydrous CH_2Cl_2 (50 µL). Triethylamine (16.6 µL, 0.12 mmol) was added and the mixture was cooled to -40°C. A 1M solution of trifluoromethanesulfonic anhydride in CH_2Cl_2 (44 µL, 0.044 mmol) was added dropwise. Once the addition was complete, the reaction mixture was allowed to stir for 1 h at 0°C, after which, it was added to a suspension of the resin-attached acetylene bearing dodecamer (resin attached **158**, 10mg, equivalent to 0.004 mmol) in DMF (200 µL). The resultant mixture was shaken for 16 h at 50°C. The resin was then filtered and washed with DMF (5 × 2 mL) and CH_2Cl_2 (3 × 2 mL). The resin was then subjected to the cleavage procedure. The isolated crude product was subjected to HPLC analysis and purification as described in section 5.3.3.5. The HPLC retention time was 30.1 minutes. A mass spectrum could not be obtained for this compound due to the lack of ionisable groups in the molecule.

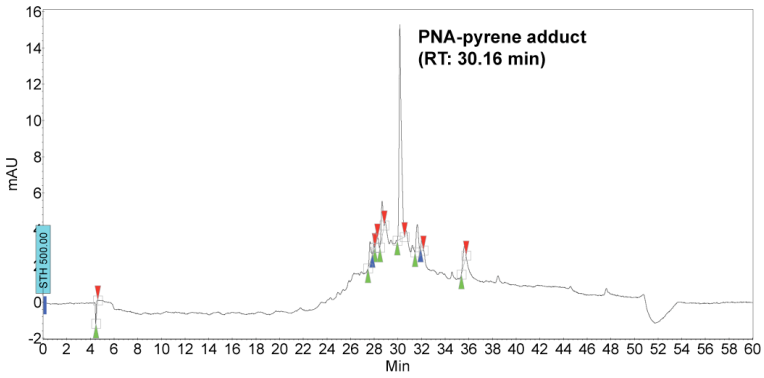

HPLC chromatogram of **184** (crude product). Varian Pursuit C18, 5 µm, 4.6 x 250 mm, gradient: 0.1% TFA in H_2O to 0.1% TFA in CH_3CN, flow: 1 mL/min, 65°C

Deprotected PNA-pyrene adduct (sequence: lys-TTAATTAATTAA) (191)

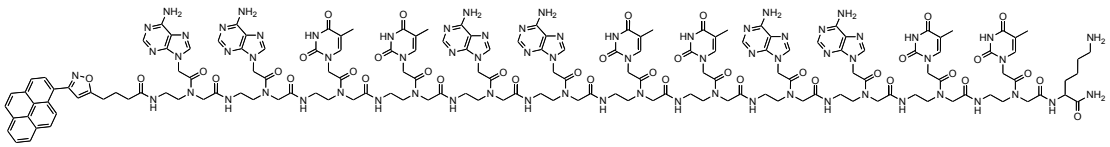

The nucleobases of **184** were deprotected from the Cbz-protecting groups using the procedures described in section 5.3.3.5. Following HPLC analysis, purification and

lyophilisation, **191** was obtained as a white solid, which was H_2O soluble. MS (MALDI-HRMS): Found 3730.5161 $[M+H]^+$, $C_{161}H_{193}N_{70}O_{39}$ requires = 3730.5271.

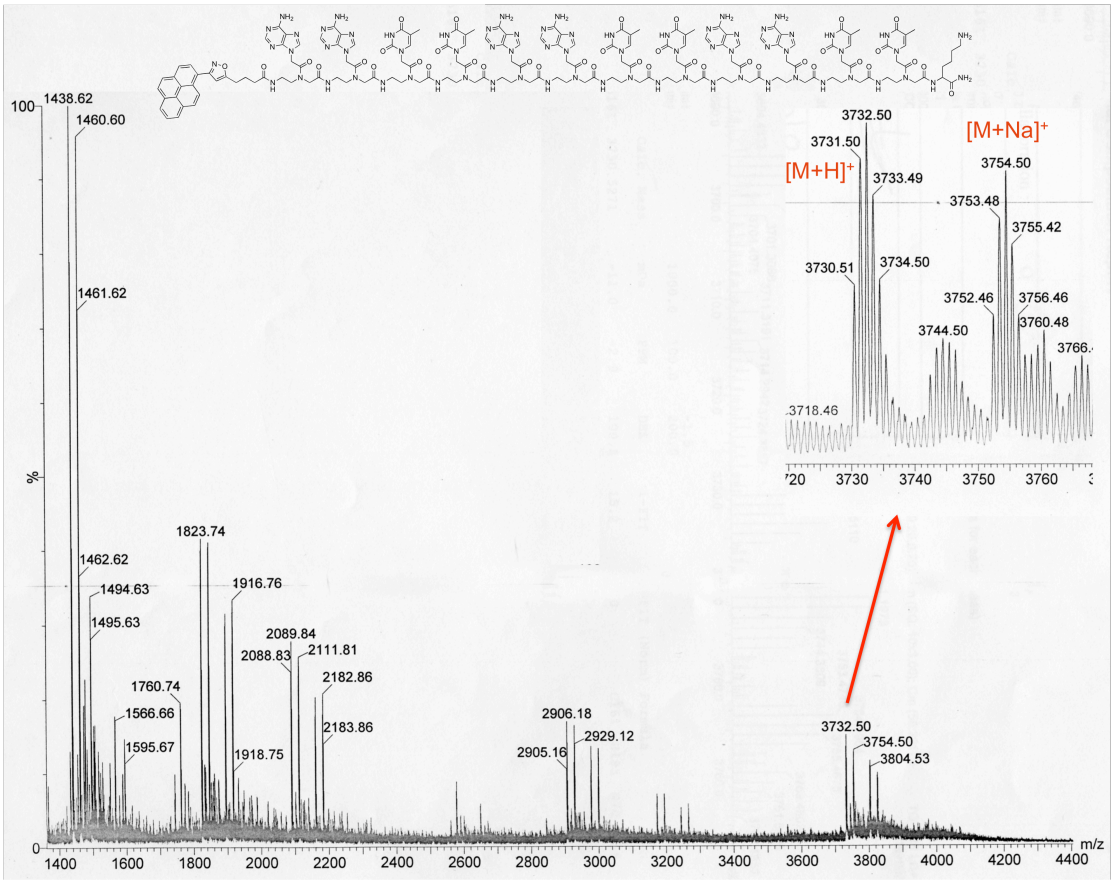

MALDI-TOF MS of **191**

5.3.5 PROCEDURES FOR AFM EXPERIMENTS

A solution (0.6 mM) of deprotected dodecamer PNA (**127**, 1 mg) in H_2O (0.5 mL) was prepared and used in the following experiments.

Preparation of the mica surface – The mica surface (Bayville chemical supply company Inc.) was cleaned by attaching a piece a sticky tape and gently removing it along with a layer of mica. This process was repeated three times in total.

Spin coating – One or more drops (depending on the experiment) of the solution of **127** were added to the clean mica surface using spin coating (3000 rpm for 3 min).

AFM imaging - All the data was collected in air at 298 K, using a *Nanoscope IIIa* (Digital Instruments Metrology Group, USA) instrument, model: MMAFMLN. The images were collected in tapping-mode AFM, with a single 1-10 Ohm phosphorous-doped silicon cantilever (T: 3.5 – 4.5 μm, L: 115 -135 μm, W: 30 – 40 μm, f_0 ranging from 301.5 to 301.9 kHz and k: 20 -80 $N \cdot m^{-1}$, *VEECO*, USA). The images in the power point have been obtained after the flattening (WsXm software) of the collected data. Roughness analysis and flooding has been performed with the same software.

Annealing – The solution was placed in an NMR tube, and using the NMR's temperature control, the solution was heated to 80°C for 10 minutes, after which the solution was cooled in a controlled manner as follows: 80°C to 70°C at 2°C per minute; 70°C to 60°C at 1°C per minute; and 60°C to 30°C at 2°C per minute.

Deposition and imaging experiments performed (Figures 95-97):

i) One drop of solution (pre-annealing) – aggregates of PNA observed

ii) Three drops of solution (pre-annealing) – larger aggregates observed

iii) Clean mica – as a control for comparison purposes

iv) One drop of solution (post-annealing) – mica surface was completely covered in fibres.

v) One drop of a 10-fold diluted solution (post-annealing) – PNA duplexes observed with an average height corresponding to approximately 1 nm.

Bibliography

[1] L. J. Prins, D. N. Reinhoudt, P. Timmerman, *Angew. Chem. Int. Ed.* **2001**, *40*, 2382-2426.

[2] Special Issue: Supramolecular Chemistry and Self-Assembly, in *Science* **2002**, *295*, 2396-2396.

[3] Special Issue: Supramolecular Chemistry Anniversary, in *Chem. Soc. Rev.* **2007**, *36*, 127-140.

[4] F. J. M. Hoeben, P. Jonkheijm, E. W. Meijer, A. P. H. J. Schenning, *Chem. Rev.* **2005**, *105*, 1491-1546.

[5] D. M. Guldi, G. M. A. Rahman, F. Zerbetto, M. Prato, *Acc. Chem. Res.* **2005**, *38*, 871-878.

[6] K. Yoosaf, A. Belbakra, N. Armaroli, A. Llanes-Pallas, D. Bonifazi, *Chem. Commun.* **2009**, 2830-2832.

[7] P. Samori, *J. Mater. Chem.* **2004**, *14*, 1353-1366.

[8] P. Samori, *Chem. Soc. Rev.* **2005**, *34*, 551-561.

[9] S. De Feyter, F. C. De Schryver, *Chem. Soc. Rev.* **2003**, *32*, 139-150.

[10] S. De Feyter, A. Gesquière, M. M. Abdel-Mottaleb, P. C. M. Grim, F. C. De Schryver, C. Meiners, M. Sieffert, S. Valiyaveettil, K. Müllen, *Acc. Chem. Res.* **2000**, *33*, 520-531.

[11] D. Bonifazi, H. Spillmann, A. Kiebele, M. de Wild, P. Seiler, F. Cheng, H.-J. Güntherodt, T. Jung, F. Diederich, *Angew. Chem. Int. Ed.* **2004**, *43*, 4759-4763.

[12] J. V. Barth, G. Costantini, K. Kern, *Nature* **2005**, *437*, 671-679.

[13] S. De Feyter, H. Uji-i, W. Mamdouh, A. Miura, J. Zhang, P. Jonkheijm, A. P. H. J. Schenning, E. W. Meijer, Z. Chen, F. Wurthner, N. Schuurmans, J. V. Esch, B. L. Feringa, A. E. Dulcey, V. Percec, F. C. D. S, *Int. J. Nanotechnol.* **2006**, *3*, 462-479.

[14] L.-J. Wan, *Acc. Chem. Res.* **2006**, *39*, 334-342.

[15] J. V. Barth, *Annu. Rev. Phys. Chem.* **2007**, *58*, 375-407.

[16] N. Miyashita, D. G. Kurth, *J. Mater. Chem.* **2008**, *18*, 2636-2649.

[17] E. Gomar-Nadal, J. Puigmarti-Luis, D. B. Amabilino, *Chem. Soc. Rev.* **2008**, *37*, 490-504.

[18] A. Kuhnle, *Curr. Opin. Colloid Interface Sci.* **2009**, *14*, 157-168.

[19] X. Ma, Y. Yang, K. Deng, Q. Zeng, K. Zhao, C. Wang, C. Bai, *J. Mater. Chem.* **2008**, *18*, 2074-2081.

[20] F. Cicoira, C. Santato, F. Rosei, *Top. Curr. Chem.* **2008**, *285*, 203-267.

[21] D. Bonifazi, O. Enger, F. Diederich, *Chem. Soc. Rev.* **2007**, *36*, 390-414.

[22] A. Llanes-Pallas, M. Matena, T. Jung, M. Prato, M. Stöhr, D. Bonifazi, *Angew. Chem. Int. Ed.* **2008**, *47*, 7726-7730.

[23] T. Kudernac, S. Lei, J. A. A. W. Elemans, S. De Feyter, *Chem. Soc. Rev.* **2009**, *38*, 402-421.

[24] P. Alivisatos, P. F. Barbara, A. W. Castleman, J. Chang, D. A. Dixon, M. L. Klein, G. L. McLendon, J. S. Miller, M. A. Ratner, P. J. Rossky, S. I. Stupp, M. E. Thompson, *Adv. Mater.* **1998**, *10*, 1297-1336.

[25] C. B. Gorman, R. L. Caroll, *Angew. Chem. Int. Ed.,* **2002**, *41*, 4378.

[26] C. Joachim, M. A. Ratner, *Proc. Natl. Acad. Sci. U. S. A.* **2005**, *102*, 8801-8808.

[27] A. P. H. J. Schenning, E. W. Meijer, *Chem. Commun.* **2005**, 3245-3258.

[28] H. Yang, T. J. Shin, L. Yang, K. Cho, C. Y. Ryu, Z. Bao, *Adv. Funct. Mater.* **2005**, *15*, 671-676.

[29] Special Issue: Supramolecular Approaches to Organic Electronics and Nanotechnology, in *Adv. Mater.* **2006**, *18*, 1227-1227.

[30] J. E. Green, J. Wook Choi, A. Boukai, Y. Bunimovich, E. Johnston-Halperin, E. DeIonno, Y. Luo, B. A. Sheriff, K. Xu, Y. Shik Shin, H.-R. Tseng, J. F. Stoddart, J. R. Heath, *Nature* **2007**, *445*, 414-417.

[31] J. Wu, W. Pisula, K. Müllen, *Chem. Rev.* **2007**, *107*, 718-747.

[32] A. R. Murphy, J. M. J. Fréchet, *Chem. Rev.* **2007**, *107*, 1066-1096.

[33] H. Haick, D. Cahen, *Acc. Chem. Res.* **2008**, *41*, 359-366.

[34] R. H. Friend, R. W. Gymer, A. B. Holmes, J. H. Burroughes, R. N. Marks, C. Taliani, D. D. C. Bradley, D. A. D. Santos, J. L. Bredas, M. Logdlund, W. R. Salaneck, *Nature* **1999**, *397*, 121-128.

[35] F. Cacialli, J. S. Wilson, J. J. Michels, C. Daniel, C. Silva, R. H. Friend, N. Severin, P. Samori, J. P. Rabe, M. J. O'Connell, P. N. Taylor, H. L. Anderson, *Nature Mater.* **2002**, *1*, 160-164.

[36] S. R. Forrest, *Nature* **2004**, *428*, 911-918.

[37] Y. Yamamoto, T. Fukushima, Y. Suna, N. Ishii, A. Saeki, S. Seki, S. Tagawa, M. Taniguchi, T. Kawai, T. Aida, *Science* **2006**, *314*, 1761-1764.

[38] D. L. Taylor, E. S. Woo, K. A. Giuliano, *Curr. Opin. Biotechnol.* **2001**, *12*, 75-81.

[39] M. Sarikaya, C. Tamerler, A. K. Y. Jen, K. Schulten, F. Baneyx, *Nat Mater* **2003**, *2*, 577-585.

[40] L. Piot, D. Bonifazi, P. Samorì, *Adv. Funct. Mater.* **2007**, *17*, 3689-3693.

[41] S. Griessl, M. Lackinger, M. Edelwirth, M. Hietschold, W. M. Heckl, *Single Mol.* **2002**, *3*, 25-31.

[42] A. Dmitriev, N. Lin, J. Weckesser, J. V. Barth, K. Kern, *J. Phys. Chem. B* **2002**, *106*, 6907-6912.

[43] J. Lu, Q.-d. Zeng, C. Wang, Q.-y. Zheng, L. Wan, C. Bai, *J. Mater. Chem.* **2002**, *12*, 2856-2858.

[44] D. Payer, A. Comisso, A. Dmitriev, T. Strunskus, N. Lin, C. Wöll, A. DeVita, J. V. Barth, K. Kern, *Chem. Eur. J.* **2007**, *13*, 3900-3906.

[45] M. Lackinger, S. Griessl, T. Markert, F. Jamitzky, W. M. Heckl, *J. Phys. Chem. B* **2004**, *108*, 13652-13655.

[46] L. Kampschulte, M. Lackinger, A.-K. Maier, R. S. K. Kishore, S. Griessl, M. Schmittel, W. M. Heckl, *J. Phys. Chem. B* **2006**, *110*, 10829-10836.

[47] L. Kampschulte, S. Griessl, W. M. Heckl, M. Lackinger, *J. Phys. Chem. B* **2005**, *109*, 14074-14078.

[48] J. A. Theobald, N. S. Oxtoby, M. A. Phillips, N. R. Champness, P. H. Beton, *Nature* **2003**, *424*, 1029-1031.

[49] L. M. A. Perdigao, N. R. Champness, P. H. Beton, *Chem. Commun.* **2006**, 538-540.

[50] W. Xu, M. Dong, H. Gersen, E. Rauls, S. Vázquez-Campos, M. Crego-Calama, D. N. Reinhoudt, I. Stensgaard, E. Laegsgaard, T. R. Linderoth, F. Besenbacher, *Small* **2007**, *3*, 854-858.

[51] M. Stöhr, M. Wahl, C. H. Galka, T. Riehm, T. A. Jung, L. H. Gade, *Angew. Chem. Int. Ed.* **2005**, *44*, 7394-7398.

[52] M. Stöhr, M. Wahl, H. Spillmann, L. H. Gade, T. A. Jung, *Small* **2007**, *3*, 1336-1340.

[53] C.-A. Palma, M. Bonini, A. Llanes-Pallas, T. Breiner, M. Prato, D. Bonifazi, P. Samori, *Chem. Commun.* **2008**, 5289-5291.

[54] C.-A. Palma, J. Bjork, M. Bonini, M. S. Dyer, A. Llanes-Pallas, D. Bonifazi, M. Persson, P. Samorì, *J. Am. Chem. Soc.* **2009**, *131*, 13062-13071.

[55] M. Bonini, L. Zalewski, T. Breiner, F. Dötz, M. Kastler, V. Schädler, M. Surin, R. Lazzaroni, P. Samorì, *Small* **2009**, *5*, 1521-1526.

[56] X.-H. Kong, K. Deng, Y.-L. Yang, Q.-D. Zeng, C. Wang, *J. Phys. Chem. C* **2007**, *111*, 17382-17387.

[57] S. Lei, M. Surin, K. Tahara, J. Adisoejoso, R. Lazzaroni, Y. Tobe, S. D. Feyter, *Nano Lett.* **2008**, *8*, 2541-2546.

[58] M. Li, K. Deng, S.-B. Lei, Y.-L. Yang, T.-S. Wang, Y.-T. Shen, C.-R. Wang, Q.-D. Zeng, C. Wang, *Angew. Chem. Int. Ed.* **2008**, *47*, 6717-6721.

[59] J. Adisoejoso, K. Tahara, S. Okuhata, S. Lei, Y. Tobe, S. De Feyter, *Angew. Chem. Int. Ed.* **2009**, *48*, 7353-7357.

[60] A. Llanes-Pallas, C.-A. Palma, L. Piot, A. Belbakra, A. Listorti, M. Prato, P. Samorì, N. Armaroli, D. Bonifazi, *J. Am. Chem. Soc.* **2009**, *131*, 509-520.

[61] M. Matena, A. Llanes-Pallas, M. Enache, T. Jung, J. Wouters, B. Champagne, M. StAhr, D. Bonifazi, *Chem. Commun.* **2009**, 3525-3527.

[62] G. M. Whitesides, J. P. Mathias, C. T. Seto, *Science* **1991**, *254*, 1312-1319.

[63] H. Spillmann, A. Kiebele, M. Stöhr, T. A. Jung, D. Bonifazi, F. Cheng, F. Diederich, *Adv. Mater.* **2006**, *18*, 275-279.

[64] D. Bonifazi, A. Kiebele, M. Stöhr, F. Cheng, T. Jung, F. Diederich, H. Spillmann, *Adv. Funct. Mater.* **2007**, *17*, 1051-1062.

[65] T. Yokoyama, S. Yokoyama, T. Kamikado, Y. Okuno, S. Mashiko, *Nature* **2001**, *413*, 619-621.

[66] N. Wintjes, J. Hornung, J. Lobo-Checa, T. Voigt, T. Samuely, C. Thilgen, M. Stöhr, F. Diederich, T. A. Jung, *Chem. Eur. J.* **2008**, *14*, 5794-5802.

[67] S. Furukawa, H. Uji-i, K. Tahara, T. Ichikawa, M. Sonoda, F. C. De Schryver, Y. Tobe, S. De Feyter, *J. Am. Chem. Soc.* **2006**, *128*, 3502-3503.

[68] K. Tahara, S. Furukawa, H. Uji-i, T. Uchino, T. Ichikawa, J. Zhang, W. Mamdouh, M. Sonoda, F. C. De Schryver, S. De Feyter, Y. Tobe, *J. Am. Chem. Soc.* **2006**, *128*, 16613-16625.

[69] S. Lei, K. Tahara, X. Feng, S. Furukawa, F. C. De Schryver, K. Müllen, Y. Tobe, S. De Feyter, *J. Am. Chem. Soc.* **2008**, *130*, 7119-7129.

[70] S. Lei, K. Tahara, F. C. De Schryver, M. Van der Auweraer, Y. Tobe, S. De Feyter, *Angew. Chem. Int. Ed.* **2008**, *47*, 2964-2968.

[71] G. Schull, L. Douillard, C. Fiorini-Debuisschert, F. Charra, F. Mathevet, D. Kreher, A.-J. Attias, *Nano Lett.* **2006**, *6*, 1360-1363.

[72] K. Tahara, S. Lei, D. Mossinger, H. Kozuma, K. Inukai, M. Van der Auweraer, F. C. De Schryver, S. Hoger, Y. Tobe, S. De Feyter, *Chem. Commun.* **2008**, 3897-3899.

[73] H. Spillmann, A. Dmitriev, N. Lin, P. Messina, J. V. Barth, K. Kern, *J. Am. Chem. Soc.* **2003**, *125*, 10725-10728.

[74] A. Dmitriev, H. Spillmann, N. Lin, J. V. Barth, K. Kern, *Angew. Chem. Int. Ed.* **2003**, *42*, 2670-2673.

[75] S. Stepanow, M. Lingenfelder, A. Dmitriev, H. Spillmann, E. Delvigne, N. Lin, X. Deng, C. Cai, J. V. Barth, K. Kern, *Nature Mater.* **2004**, *3*, 229-233.

[76] N. Lin, S. Stepanow, F. Vidal, J. V. Barth, K. Kern, *Chem. Commun.* **2005**, 1681-1683.

[77] S. Stepanow, N. Lin, J. V. Barth, K. Kern, *J. Phys. Chem. B* **2006**, *110*, 23472-23477.

[78] U. Schlickum, R. Decker, F. Klappenberger, G. Zoppellaro, S. Klyatskaya, M. Ruben, I. Silanes, A. Arnau, K. Kern, H. Brune, J. V. Barth, *Nano Lett.* **2007**, *7*, 3813-3817.

[79] J. A. A. W. Elemans, S. De Feyter, *Soft Matter* **2009**, *5*, 721-735.

[80] M. Surin, P. Samorì, A. Jouaiti, N. Kyritsakas, M. W. Hosseini, *Angew. Chem. Int. Ed.* **2007**, *46*, 245-249.

[81] U. Schlickum, R. Decker, F. Klappenberger, G. Zoppellaro, S. Klyatskaya, M. Ruben, I. Silanes, A. Arnau, K. Kern, H. Brune, J. V. Barth, *Nano Lett.,* **2007**, *7*, 3813-3817.

[82] S. H. Joo, S. J. Choi, I. Oh, J. Kwak, Z. Liu, O. Terasaki, R. Ryoo, *Nature* **2001**, *412*, 169-172.

[83] L. Grill, M. Dyer, L. Lafferentz, M. Persson, M. V. Peters, S. Hecht, *Nature Nanotechnol.* **2007**, *2*, 687-691.

[84] N. A. A. Zwaneveld, R. m. Pawlak, M. Abel, D. Catalin, D. Gigmes, D. Bertin, L. Porte, *J. Am. Chem. Soc.* **2008**, *130*, 6678-6679.

[85] S. Weigelt, C. Bombis, C. Busse, M. M. Knudsen, K. V. Gothelf, E. Lægsgaard, F. Besenbacher, T. R. Linderoth, *ACS Nano* **2008**, *2*, 651-660.

[86] S. Weigelt, C. Busse, C. Bombis, M. M. Knudsen, K. V. Gothelf, T. Strunskus, C. Wöll, M. Dahlbom, B. Hammer, E. Lægsgaard, F. Besenbacher, T. R. Linderoth, *Angew. Chem. Int. Ed.* **2007**, *46*, 9227-9230.

[87] S. Weigelt, C. Busse, C. Bombis, M. M. Knudsen, K. V. Gothelf, E. Lægsgaard, F. Besenbacher, T. R. Linderoth, *Angew. Chem. Int. Ed.* **2008**, *47*, 4406-4410.

[88] G.-B. Pan, J.-M. Liu, H.-M. Zhang, L.-J. Wan, Q.-Y. Zheng, C.-L. Bai, *Angew. Chem. Int. Ed.* **2003**, *42*, 2747-2751.

[89] G.-B. Pan, X.-H. Cheng, S. Höger, W. Freyland, *J. Am. Chem. Soc.* **2006**, *128*, 4218-4219.

[90] B. Schmaltz, A. Rouhanipour, H. J. Räder, W. Pisula, K. Müllen, *Angew. Chem. Int. Ed.* **2009**, *48*, 720-724.

[91] J. Krömer, I. Rios-Carreras, G. Fuhrmann, C. Musch, M. Wunderlin, T. Debaerdemaeker, E. Mena-Osteritz, P. Bäuerle, *Angew. Chem. Int. Ed.* **2000**, *39*, 3481-3486.

[92] E. Mena-Osteritz, *Adv. Mater.* **2002**, *14*, 609-616.

[93] E. Mena-Osteritz, P. Bäuerle, *Adv. Mater.* **2006**, *18*, 447-451.

[94] S. Leininger, B. Olenyuk, P. J. Stang, *Chem. Rev.* **2000**, *100*, 853-908.

[95] E. Zangrando, M. Casanova, E. Alessio, *Chem. Rev.* **2008**, *108*, 4979-5013.

[96] A. Semenov, J. P. Spatz, M. Möller, J.-M. Lehn, B. Sell, D. Schubert, C. H. Weidl, U. S. Schubert, *Angew. Chem. Int. Ed.* **1999**, *38*, 2547-2550.

[97] M. S. Alam, S. Strömsdörfer, V. Dremov, P. Müller, J. Kortus, M. Ruben, J.-M. Lehn, *Angew. Chem. Int. Ed.* **2005**, *44*, 7896-7900.

[98] A. Mourran, U. Ziener, M. Möller, E. Breuning, M. Ohkita, J.-M. Lehn, *Eur. J. Inorg. Chem.* **2005**, *2005*, 2641-2647.

[99] C. Safarowsky, L. Merz, A. Rang, P. Broekmann, B. A. Hermann, C. A. Schalley, *Angew. Chem. Int. Ed.* **2004**, *43*, 1291-1294.

[100] Q.-H. Yuan, L.-J. Wan, H. Jude, P. J. Stang, *J. Am. Chem. Soc.* **2005**, *127*, 16279-16286.

[101] L.-A. Fendt, M. Stöhr, N. Wintjes, M. Enache, T. A. Jung, F. Diederich, *Chem. Eur. J.* **2009**, *15*, 11139-11150.

[102] D. Heim, K. Seufert, W. Auwä rter, C. Aurisicchio, C. Fabbro, D. Bonifazi, J. V. Barth, *Nano Lett.* **2010**, *10*, 122-128.

[103] W. Auwärter, F. Klappenberger, A. Weber-Bargioni, A. Schiffrin, T. Strunskus, C. Wöll, Y. Pennec, A. Riemann, J. V. Barth, *J. Am. Chem. Soc.* **2007**, *129*, 11279-11285.

[104] H. L. Zhang, W. Chen, H. Huang, L. Chen, A. T. S. Wee, *J. Am. Chem. Soc.* **2008**, *130*, 2720-2721.

[105] N. Wintjes, D. Bonifazi, F. Cheng, A. Kiebele, M. Stöhr, T. Jung, H. Spillmann, F. Diederich, *Angew. Chem. Int. Ed.* **2007**, *46*, 4089-4092.

[106] G. Schull, L. Douillard, C. Fiorini-Debuisschert, F. Charra, F. Mathevet, D. Kreher, A. J. Attias, *Adv. Mater.* **2006**, *18*, 2954-2957.

[107] K. Tahara, S. Lei, W. Mamdouh, Y. Yamaguchi, T. Ichikawa, H. Uji-i, M. Sonoda, K. Hirose, F. C. De Schryver, S. De Feyter, Y. Tobe, *J. Am. Chem. Soc.* **2008**, *130*, 6666-6667.

[108] Y. Tobe, A. Nagano, K. Kawabata, M. Sonoda, K. Naemura, *Org. Lett.* **2000**, *2*, 3265-3268.

[109] S. Furukawa, K. Tahara, F. C. De Schryver, M. Van der Auweraer, Y. Tobe, S. De Feyter, *Angew. Chem. Int. Ed.* **2007**, *46*, 2831-2834.

[110] D. Bléger, D. Kreher, F. Mathevet, A.-J. Attias, G. Schull, A. Huard, L. Douillard, C. Fiorini-Debuischert, F. Charra, *Angew. Chem. Int. Ed.* **2007**, *46*, 7404-7407.

[111] F. Nishiyama, T. Yokoyama, T. Kamikado, S. Yokoyama, S. Mashiko, K. Sakaguchi, K. Kikuchi, *Adv. Mater.* **2007**, *19*, 117-120.

[112] B. Calmettes, S. Nagarajan, A. Gourdon, M. Abel, L. Porte, R. Coratger, *Angew. Chem. Int. Ed.* **2008**, *47*, 6994-6998.

[113] S. Stepanow, N. Lin, J. V. Barth, K. Kern, *Chem. Commun.* **2006**, 2153-2155.

[114] J.-R. Gong, H.-J. Yan, Q.-H. Yuan, L.-P. Xu, Z.-S. Bo, L.-J. Wan, *J. Am. Chem. Soc.* **2006**, *128*, 12384-12385.

[115] L. M. A. Perdigão, A. Saywell, G. N. Fontes, P. A. Staniec, G. Goretzki, A. G. Phillips, N. R. Champness, P. H. Beton, *Chem. Eur. J.* **2008**, *14*, 7600-7607.

[116] R. Madueno, M. T. Raisanen, C. Silien, M. Buck, *Nature* **2008**, *454*, 618-621.

[117] R. Friedlein, X. Crispin, W. Osikowicz, S. Braun, M. P. de Jong, C. D. Simpson, M. D. Watson, F. von Kieseritzky, P. Samori, S. K. M. Jonsson, M. Fahlman, F. Jackel, J. P. Rabe, J. Hellberg, K. Mullen, W. R. Salaneck, *Synth. Met.* **2004**, *147*, 79-83.

[118] J. Otsuki, S. Kawaguchi, T. Yamakawa, M. Asakawa, K. Miyake, *Langmuir* **2006**, *22*, 5708-5715.

[119] T. Ikeda, M. Asakawa, M. Goto, K. Miyake, T. Ishida, T. Shimizu, *Langmuir* **2004**, *20*, 5454-5459.

[120] F. J. Williams, O. P. H. Vaughan, K. J. Knox, N. Bampos, R. M. Lambert, *Chem. Commun.* **2004**, 1688-1689.

[121] O. P. H. Vaughan, F. J. Williams, N. Bampos, R. M. Lambert, *Angew. Chem. Int. Ed.* **2006**, *45*, 3779-3781.

[122] S. Yoshimoto, A. Tada, K. Suto, R. Narita, K. Itaya, *Langmuir* **2003**, *19*, 672-677.

[123] S. Yoshimoto, K. Sato, S. Sugawara, Y. Chen, O. Ito, T. Sawaguchi, O. Niwa, K. Itaya, *Langmuir* **2007**, *23*, 809-816.

[124] J. P. Collman, R. R. Gagne, T. R. Halbert, J. C. Marchon, C. A. Reed, *J. Am. Chem. Soc.* **1973**, *95*, 7868-7870.

[125] J. P. Collman, R. R. Gagne, C. Reed, T. R. Halbert, G. Lang, W. T. Robinson, *J. Am. Chem. Soc.* **1975**, *97*, 1427-1439.

[126] B. Hulsken, R. Van Hameren, J. W. Gerritsen, T. Khoury, P. Thordarson, M. J. Crossley, A. E. Rowan, R. J. M. Nolte, J. A. A. W. Elemans, S. Speller, *Nat Nano* **2007**, *2*, 285-289.

[127] B. Meunier, *Chem. Rev.* **1992**, *92*, 1411-1456.

[128] K. V. Gothelf, T. H. LaBean, *Org. Biomol. Chem.* **2005**, *3*, 4023-4037.

[129] S. Pitchiaya, Y. Krishnan, *Chem. Soc. Rev.* **2006**, *35*, 1111-1121.

[130] E. Winfree, F. Liu, L. A. Wenzler, N. C. Seeman, *Nature* **1998**, *394*, 539-544.

[131] R. Otero, W. Xu, M. Lukas, R. E. A. Kelly, E. Lægsgaard, I. Stensgaard, J. Kjems, L. N. Kantorovich, F. Besenbacher, *Angew. Chem. Int. Ed.* **2008**, *47*, 9673-9676.

[132] P. W. K. Rothemund, *Nature* **2006**, *440*, 297-302.

[133] Y. Liu, Y. Ke, H. Yan, *J. Am. Chem. Soc.* **2005**, *127*, 17140-17141.

[134] S. H. Park, C. Pistol, S. J. Ahn, J. H. Reif, A. R. Lebeck, C. Dwyer, T. H. LaBean, *Angew. Chem. Int. Ed.* **2006**, *45*, 735-739.

[135] Y. He, Y. Chen, H. Liu, A. E. Ribbe, C. Mao, *J. Am. Chem. Soc.* **2005**, *127*, 12202-12203.

[136] X. Sun, S. Hyeon Ko, C. Zhang, A. E. Ribbe, C. Mao, *J. Am. Chem. Soc.* **2009**, *131*, 13248-13249.

[137] H. Yan, S. H. Park, G. Finkelstein, J. H. Reif, T. H. LaBean, *Science* **2003**, *301*, 1882-1884.

[138] C. Zhang, M. Su, Y. He, X. Zhao, P.-a. Fang, A. E. Ribbe, W. Jiang, C. Mao, *Proc. Natl. Acad. Sci. U. S. A.* **2008**, *105*, 10665-10669.

[139] Y. He, Y. Tian, A. E. Ribbe, C. Mao, *J. Am. Chem. Soc.* **2006**, *128*, 15978-15979.

[140] W. Liu, H. Zhong, R. Wang, N. C. Seeman, *Angew. Chem. Int. Ed.* **2011**, *50*, 264-267.

[141] S. Hamada, S. Murata, *Angew. Chem. Int. Ed.* **2009**, *48*, 6820-6823.

[142] J. D. Le, Y. Pinto, N. C. Seeman, K. Musier-Forsyth, T. A. Taton, R. A. Kiehl, *Nano Lett.* **2004**, *4*, 2343-2347.

[143] J. Zhang, Y. Liu, Y. Ke, H. Yan, *Nano Lett.* **2006**, *6*, 248-251.

[144] J. Sharma, R. Chhabra, A. Cheng, J. Brownell, Y. Liu, H. Yan, *Science* **2009**, *323*, 112-116.

[145] H. Yang, C. K. McLaughlin, F. A. Aldaye, G. D. Hamblin, A. Z. Rys, I. Rouiller, H. F. Sleiman, *Nature Chem.* **2009**, *1*, 390-396.

[146] E. S. Andersen, M. Dong, M. M. Nielsen, K. Jahn, R. Subramani, W. Mamdouh, M. M. Golas, B. Sander, H. Stark, C. L. P. Oliveira, J. S. Pedersen, V. Birkedal, F. Besenbacher, K. V. Gothelf, J. Kjems, *Nature* **2009**, *459*, 73-76.

[147] P. E. Nielsen, M. Egholm, R. H. Berg, O. Buchardt, *Science* **1991**, *254*, 1497-1500.

[148] B. Hyrup, P. E. Nielsen, *Biorg. Med. Chem.* **1996**, *4*, 5-23.

[149] P. Wittung, P. E. Nielsen, O. Buchardt, M. Egholm, B. Norden, *Nature* **1994**, *368*, 561-563.

[150] V. V. Demidov, V. N. Potaman, M. D. Frank-Kamenetskil, M. Egholm, O. Buchard, S. H. Sonnichsen, P. E. Nlelsen, *Biochem. Pharmacol.* **1994**, *48*, 1310-1313.

[151] E. Uhlmann, A. Peyman, G. Breipohl, D. W. Will, *Angew. Chem. Int. Ed.* **1998**, *37*, 2796-2823.

[152] P. Nielsen, *Mol. Biotechnol.* **2004**, *26*, 233-248.

[153] J. C. Hanvey, N. J. Peffer, J. E. Bisi, S. A. Thomson, R. Cadilla, J. A. Josey, D. J. Ricca, C. F. Hassman, M. A. Bonham, K. G. Au, S. G. Carter, D. A. Bruckenstein, A. L. Boyd, S. A. Noble, L. E. Babiss, *Science* **1992**, *258*, 1481-1485.

[154] H. Knudsen, P. E. Nielsen, *Nucleic Acids Res.* **1996**, *24*, 494-500.

[155] M. A. Bonham, S. Brown, A. L. Boyd, P. H. Brown, D. A. Bruckenstein, J. C. Hanvey, S. A. Thomson, A. Pipe, F. Hassman, J. E. Bisi, B. C. Froehler, M. D. Matteucci, R. W. Wagner, S. A. Noble, L. E. Babiss, *Nucleic Acids Res.* **1995**, *23*, 1197-1203.

[156] P. E. Nielsen, M. Egholm, O. Buchardt, *Gene* **1994**, *149*, 139-145.

[157] J. C. Norton, M. A. Piatyszek, W. E. Wright, J. W. Shay, D. R. Corey, *Nat. Biotechnol.* **1996**, *14*, 615-619.

[158] P. E. Nielsen, G. Haaima, *Chem. Soc. Rev.* **1997**, *26*, 73-78.

[159] T. Hirano, K. Kuroda, M. Kataoka, Y. Hayakawa, *Org. Biomol. Chem.* **2009**, *7*, 2905-2911.

[160] P. Wittung, J. Kajanus, K. Edwards, P. Nielsen, B. Norden, B. G. Malmstrom, *FEBS Lett.* **1995**, *365*, 27-29.

[161] C. Chen, B. Wu, T. Wei, M. Egholm, W. M. Strauss, *Mamm. genome* **2000**, *11*, 384-391.

[162] F. A. Drobniewski, P. G. More, G. S. Harris, *J. Clin. Microbiol.* **2000**, *38*, 444-447.

[163] P. Hongmanee, H. Stender, O. F. Rasmussen, *J. Clin. Microbiol.* **2001**, *39*, 1032-1035.

[164] H. Keefe, H. Stender, A. Broomer, K. Oliveira, J. Coull, J. J. Hyldig-Nielsen, P. N. A. Filter-based, *J. Appl. Microbiol.* **2001**, *90*, 180-189.

[165] P. M. Lansdorp, N. P. Verwoerd, F. M. van de Rijke, V. Dragowska, M. T. Little, R. W. Dirks, A. K. Raap, H. J. Tanke, *Hum. Mol. Genet.* **1996**, *5*, 685-691.

[166] G. Mathioudakis, R. Storb, P. A. McSweeney, B. Torok-Storb, P. M. Lansdorp, T. H. Brümmendorf, M. J. Gass, E. M. Bryant, J. Storek, M. E. Flowers, T. Gooley, R. A. Nash, *Blood* **2000**, *96*, 3991-3994.

[167] H. Stender, C. Kurtzman, J. J. Hyldig-Nielsen, D. Sørensen, A. Broomer, K. Oliveira, H. Perry-O'Keefe, A. Sage, B. Young, J. Coull, *Appl. Environ. Microbiol.* **2001**, *67*, 938-941.

[168] H. Stender, T. A. Mollerup, K. Lund, K. H. Petersen, P. Hongmanee, S. E. Godtfredsen, *Int. J. Tuberc. Lung Dis.* **1999**, *3*, 830-837.

[169] H. Stender, K. Oliveira, S. Rigby, F. Bargoot, J. Coull, *J. Microbiol. Methods* **2001**, *45*, 31-39.

[170] H. Stender, A. Sage, K. Oliveira, A. J. Broomer, B. Young, J. Coull, *J. Microbiol. Methods* **2001**, *46*, 69-75.

[171] A. Z. Worden, S. W. Chisholm, B. J. Binder, *Appl. Environ. Microbiol.* **2000**, *66*, 284-289.

[172] J. M. Zijlmans, U. M. Martens, S. S. Poon, A. K. Raap, H. J. Tanke, R. K. Ward, P. M. Lansdorp, *Proc. Natl. Acad. Sci. U. S. A.* **1997**, *94*, 7423-7428.

[173] M. Behn, M. Schuermann, *Nucleic Acids Res.* **1998**, *26*, 1356-1358.

[174] M. Behn, C. Thiede, A. Neubauer, W. Pankow, M. Schuermann, *J. Pathol.* **2000**, *190*, 69-75.

[175] D. G. Murdock, N. C. Christacos, D. C. Wallace, *Nucleic Acids Res.* **2000**, *28*, 4350-4355.

[176] Y. Myal, A. Blanchard, P. Watson, M. Corrin, R. Shiu, B. Iwasiow, *Anal. Biochem.* **2000**, *285*, 169-172.

[177] H. Orum, P. E. Nielsen, M. Egholm, R. H. Berg, O. Buchardt, C. Stanley, *Nucleic Acids Res.* **1993**, *21*, 5332.

[178] F. Von Wintzingerode, O. Landt, A. Ehrlich, U. B. Gobel, *Appl Environ Microbiol* **2000**, *66*, 549-557.

[179] P. E. Nielsen, M. Egholm, R. H. Berg, O. Buchardt, *Nucleic Acids Res.* **1993**, *21*, 197-200.

[180] V. V. Demidov, M. D. Frank-Kamenetskii, M. Egholm, O. Buchardt, P. E. Nielsen, *Nucleic Acids Res.* **1993**, *21*, 2103-2107.

[181] A. G. Veselkov, V. V. Demidov, M. D. Frank-Kamenetskii, P. E. Nielsen, *Nature* **1996**, *379*, 214.

[182] A. G. Veselkov, V. V. Demidov, P. E. Nielson, M. D. Frank-Kamenetskii, *Nucleic Acids Res.* **1996**, *24*, 2483-2487.

[183] D. P. Chandler, J. R. Stults, K. K. Anderson, S. Cebula, B. L. Schuck, F. J. Brockman, *Anal. Biochem.* **2000**, *283*, 241-249.

[184] D. P. Chandler, J. R. Stults, S. Cebula, B. L. Schuck, D. W. Weaver, K. K. Anderson, M. Egholm, F. J. Brockman, *Appl. Environ. Microbiol.* **2000**, *66*, 3438-3445.

[185] H. Orum, P. E. Nielsen, M. Jorgensen, C. Larsson, C. Stanley, T. Koch, *BioTechniques* **1995**, *19*, 472-480.

[186] C. Seeger, H. G. Batz, H. Orum, *BioTechniques* **1997**, *23*, 512-517.

[187] P. G. A. Janssen, N. Meeuwenoord, G. van der Marel, S. Jabbari-Farouji, P. van der Schoot, M. Surin, Z. Tomovic, E. W. Meijer, A. Schenning, *Chem. Commun.* **2010**, *46*, 109-111.

[188] C. Briones, E. Mateo-Martí, C. Gomez-Navarro, V. Parro, E. Román, J. A. Martín-Gago, *J. Mol. Catal. A: Chem.* **2005**, *228*, 131-136.

[189] Z.-C. Liu, D.-S. Shin, M. Shokouhimehr, K.-N. Lee, B.-W. Yoo, Y.-K. Kim, Y.-S. Lee, *Biosens. Bioelectron.* **2007**, *22*, 2891-2897.

[190] E. Mateo-Martí, C. Briones, C. M. Pradier, J. A. Martín-Gago, *Biosens. Bioelectron.* **2007**, *22*, 1926-1932.

[191] E. Mateo-Martí, C. Briones, E. Román, E. Briand, C. M. Pradier, J. A. Martín-Gago, *Langmuir* **2005**, *21*, 9510-9517.

[192] E. Mateo-Martí, C. Rogero, C. Briones, J. A. Martín-Gago, *Surf. Sci.* **2007**, *601*, 4195-4199.

[193] R. P. Singh, B.-K. Oh, J.-W. Choi, *Bioelectrochemistry* **2010**, *79*, 153-161.

[194] A. Calabretta, D. Wasserberg, G. A. Posthuma-Trumpie, V. Subramaniam, A. van Amerongen, R. Corradini, T. Tedeschi, S. Sforza, D. N. Reinhoudt, R. Marchelli, J. Huskens, P. Jonkheijm, *Langmuir* **2010**, doi: 10.1021/la102756k.

[195] J. C. Wang, *Proc. Natl. Acad. Sci. U. S. A.* **1979**, *76*, 200-203.

[196] M. Eriksson, P. E. Nielsen, *Nat. Struct. Mol. Biol.* **1996**, *3*, 410-413.

[197] H. Rasmussen, J. S. Kastrup, J. N. Nielsen, J. M. Nielsen, P. E. Nielsen, *Nat. Struct. Mol. Biol.* **1997**, *4*, 98-101.

[198] A. Sen, P. E. Nielsen, *Biophys. J.* **2006**, *90*, 1329-1337.

[199] B. Bacsa, C. O. Kappe, *Nat. Protocols* **2007**, *2*, 2222-2227.

[200] G. Breipohl, D. W. Will, A. Peyman, E. Uhlmann, *Tetrahedron* **1997**, *53*, 14671-14686.

[201] E. P. Heimer, H. E. Gallo-Torres, A. M. Felix, M. Ahmad, T. J. LamBros, F. Scheidl, J. Meienhofer, *Int. J. Pept. Protein Res.* **1984**, *23*, 203-211.

[202] D. A. Stetsenko, E. N. Lubyako, V. K. Potapov, T. L. Azhikima, E. D. Sverdlov, *Tetrahedron Lett.* **1996**, *37*, 3571-3574.

[203] S. A. Thomson, J. A. Josey, R. Cadilla, M. D. Gaul, C. F. Hassman, M. J. Luzzio, A. J. Pipe, K. L. Reed, D. J. Ricca, R. W. Wiethe, S. A. Noble, *Tetrahedron* **1995**, *51*, 6179-6194.

[204] P. J. Finn, N. J. Gibson, R. Fallon, A. Hamilton, T. Brown, *Nucleic Acids Res.* **1996**, *24*, 3357-3363.

[205] K. L. Dueholm, M. Egholm, O. Buchardt, *Org. Prep. Proced. Int* **1993**, *25*, 457 - 461.

[206] L. Christensen, R. Fitzpatrick, B. Gildea, K. H. Petersen, H. F. Hansen, T. Koch, M. Egholm, O. Buchardt, P. E. Nielsen, J. Coull, R. H. Berg, *J. Pept. Sci.* **1995**, *1*, 175-183.

[207] K. L. Dueholm, M. Egholm, C. Behrens, L. Christensen, H. F. Hansen, T. Vulpius, K. H. Petersen, R. H. Berg, P. E. Nielsen, O. Buchardt, *J. Org. Chem.* **1994**, *59*, 5767-5773.

[208] M. Egholm, O. Buchardt, P. E. Nielsen, R. H. Berg, *J. Am. Chem. Soc.* **1992**, *114*, 1895-1897.

[209] O. Buchardt, M. Egholm, R. H. Berg, P. E. Nielsen, *Trends Biotechnol.* **1993**, *11*, 384-386.

[210] G. Breipohl, J. Knolle, D. Langner, G. O'Malley, E. Uhlmann, *Bioorg. Med. Chem. Lett.* **1996**, *6*, 665-670.

[211] M. Kuwahara, M. Arimitsu, M. Sisido, *J. Am. Chem. Soc.* **1999**, *121*, 256-257.

[212] Z. Timar, L. Kovacs, G. Kovacs, Z. Schmel, *J. Chem. Soc., Perkin Trans. 1* **2000**, 19-26.

[213] R. Casale, I. S. Jensen, M. Egholm, in *Peptide Nucleic Acids: Protocols and Applications* (Eds.: P. E. Nielsen, M. Egholm), Horizon Scientific Press, **1999**, p. 39.

[214] F. Bergmann, W. Bannwarth, S. Tam, *Tetrahedron Lett.* **1995**, *36*, 6823-6826.

[215] D. W. Will, G. Breipohl, D. Langner, J. Knolle, E. Uhlmann, *Tetrahedron* **1995**, *51*, 12069-12082.

[216] E. Uhlmann, D. W. Will, G. Breipohl, D. Langner, A. Ryte, *Angew. Chem. Int. Ed.* **1996**, *35*, 2632-2635.

[217] A. C. van der Laan, R. Brill, R. G. Kuimelis, E. Kuyl-Yeheskiely, J. H. van Boom, A. Andrus, R. Vinayak, *Tetrahedron Lett.* **1997**, *38*, 2249-2252.

[218] M. Planas, E. Bardaji, K. J. Jensen, G. Barany, *J. Org. Chem.* **1999**, *64*, 7281-7289.

[219] R. D. Viirre, R. H. E. Hudson, *Org. Lett.* **2001**, *3*, 3931-3934.

[220] F. Debaene, N. Winssinger, *Org. Lett.* **2003**, *5*, 4445-4447.

[221] F. Debaene, L. Mejias, J. L. Harris, N. Winssinger, *Tetrahedron* **2004**, *60*, 8677-8690.

[222] J. J. Diaz-Mochon, L. Bialy, M. Bradley, *Org. Lett.* **2004**, *6*, 1127-1129.

[223] Z.-C. Liu, D.-S. Shin, K.-T. Lee, B.-H. Jun, Y.-K. Kim, Y.-S. Lee, *Tetrahedron* **2005**, *61*, 7967-7973.

[224] H. Lee, J. H. Jeon, J. C. Lim, H. Choi, Y. Yoon, S. K. Kim, *Org. Lett.* **2007**, *9*, 3291-3293.

[225] S. Pothukanuri, Z. Pianowski, N. Winssinger, *Eur. J. Org. Chem.* **2008**, *2008*, 3141-3148.

[226] F. Guillier, D. Orain, M. Bradley, *Chem. Rev.* **2000**, *100*, 2091-2158.

[227] R. Sheppard, *J. Pept. Sci.* **2003**, *9*, 545-552.

[228] G. M. Dubowchik, S. Radia, *Tetrahedron Lett.* **1997**, *38*, 5257-5260.

[229] S. Caldarelli, G. Depecker, N. Patino, A. Di Giorgio, T. Barouillet, A. Doglio, R. Condom, *Bioorg. Med. Chem. Lett.* **2004**, *14*, 4435-4438.

[230] P. G. M. Wuts, T. W. Greene, *Greene's Protective Groups in Organic Synthesis*, 4 ed., John Wiley & Sons, Inc., New Jersey, **2006**.

[231] L. Kosynkina, W. Wang, T. C. Liang, *Tetrahedron Lett.* **1994**, *35*, 5173-5176.

[232] L. Bialy, J. J. Díaz-Mochón, E. Specker, L. Keinicke, M. Bradley, *Tetrahedron* **2005**, *61*, 8295-8305.

[233] O. Seitz, O. Köhler, *Chem. Eur. J.* **2001**, *7*, 3911-3925.

[234] R. Deziel, *Tetrahedron Lett.* **1987**, *28*, 4371-4372.

[235] R. Quarrell, T. Claridge, G. Weaver, G. Lowe, *Mol. Divers.* **1996**, *1*, 223-232.

[236] G. Kovacs, Z. Timar, Z. Kupihar, Z. Kele, L. Kovacs, *J. Chem. Soc., Perkin Trans. 1* **2002**, 1266-1270.

[237] T. Tedeschi, S. Sforza, R. Corradini, R. Marchelli, *Tetrahedron Lett.* **2005**, *46*, 8395-8399.

[238] M. M. Fabani, C. Abreu-Goodger, D. Williams, P. A. Lyons, A. G. Torres, K. G. C. Smith, A. J. Enright, M. J. Gait, E. Vigorito, *Nucleic Acids Res.*, *38*, 4466-4475.

[239] S. Bregant, F. Burlina, J. Vaissermann, G. Chassaing, *Eur. J. Org. Chem.* **2001**, *2001*, 3285-3294.

[240] V. V. Rostovtsev, L. G. Green, V. V. Fokin, K. B. Sharpless, *Angew. Chem. Int. Ed.* **2002**, *41*, 2596-2599.

[241] S. Y. Lim, W. Y. Chung, H. K. Lee, M. S. Park, H. G. Park, *Biochem. Biophys. Res. Commun.* **2008**, *376*, 633-636.

[242] K. Gogoi, M. V. Mane, S. S. Kunte, V. A. Kumar, *Nucleic Acids Res.* **2007**, *35*, e139.

[243] X. Peng, H. Li, M. Seidman, *Eur. J. Org. Chem.* **2010**, *22*, 4194-4197.

[244] J. Alguacil, S. Defaus, A. Claudio, A. Trapote, M. Masides, J. Robles, *Eur. J. Org. Chem.* **2010**, *16*, 3102-3109.

[245] G. Gasser, N. Husken, S. D. Koster, N. Metzler-Nolte, *Chem. Commun.* **2008**, 3675-3677.

[246] N. Husken, G. Gasser, S. D. Koster, N. Metzler-Nolte, *Bioconjugate Chem.* **2009**, *20*, 1578-1586.

[247] A. M. Sosniak, G. Gasser, N. Metzler-Nolte, *Org. Biomol. Chem.* **2009**, *7*, 4992-5000.

[248] D. Chouikhi, S. Barluenga, N. Winssinger, *Chem. Commun.* **2010**, *46*, 5476-5478.

[249] M. W. Kanan, M. M. Rozenman, K. Sakurai, T. M. Snyder, D. R. Liu, *Nature* **2004**, *431*, 545-549.

[250] R. Kumar, A. El-Sagheer, J. Tumpane, P. Lincoln, L. M. Wilhelmsson, T. Brown, *J. Am. Chem. Soc.* **2007**, *129*, 6859-6864.

[251] I. Singh, J. S. Vyle, F. Heaney, *Chem. Commun.* **2009**, 3276-3278.

[252] I. Singh, F. Heaney, *Org. Biomol. Chem.* **2010**, *8*, 451-456.

[253] K. Gutsmiedl, D. Fazio, T. Carell, *Chem. Eur. J.* **2010**, *16*, 6877-6883.

[254] K. Gutsmiedl, C. T. Wirges, V. Ehmke, T. Carell, *Org. Lett.* **2009**, *11*, 2405-2408.

[255] H. Feuer, *Nitrile Oxides, Nitrones and Nitronates in Organic Synthesis: Novel Strategies in Synthesis*, 2 ed., Wiley, New Jersey, **2008**.

[256] F. Himo, T. Lovell, R. Hilgraf, V. V. Rostovtsev, L. Noodleman, K. B. Sharpless, V. V. Fokin, *J. Am. Chem. Soc.* **2005**, *127*, 210-216.

[257] E. Coutouli-Argyropoulou, P. Lianis, M. Mitakou, A. Giannoulis, J. Nowak, *Tetrahedron* **2006**, *62*, 1494-1501.

[258] D. Muri, J. W. Bode, E. M. Carreira, *Org. Lett.* **2000**, *2*, 539-541.

[259] T. Mukaiyama, T. Hoshino, *J. Am. Chem. Soc.* **1960**, *82*, 5339-5342.

[260] M. Christl, R. Huisgen, *Chem. Ber.* **1973**, *106*, 3345-3367.

[261] E. J. Corey, A. L. Borror, T. Foglia, *J. Org. Chem.* **1965**, *30*, 288-290.

[262] W.-H. Sun, S. Jie, S. Zhang, W. Zhang, Y. Song, H. Ma, J. Chen, K. Wedeking, R. Fröhlich, *Organometallics* **2006**, *25*, 666-677.

[263] F. Wessendorf, J.-F. Gnichwitz, G. H. Sarova, K. Hager, U. Hartnagel, D. M. Guldi, A. Hirsch, *J. Am. Chem. Soc.* **2007**, *129*, 16057-16071.

[264] P. Antoni, D. Nystrom, C. J. Hawker, A. Hult, M. Malkoch, *Chem. Commun.* **2007**, 2249-2251.

[265] C. Grundmann, J. M. Dean, *J. Org. Chem.* **1965**, *30*, 2809-2812.

[266] K. Tadano, J. Ishihara, H. Yamada, S. Ogawa, *J. Org. Chem.* **1989**, *54*, 1223-1227.

[267] S. Derbré, G. Roué, E. Poupon, S. A. Susin, R. Hocquemiller, *ChemBioChem* **2005**, *6*, 979-982.

Curriculum Vitae

1981 Born on September 16, in Saarijarvi, Finland, but was brought up in Malta

1986 – 1999 Primary, secondary and post-secondary school at St. Edward's College, Malta

1999 – 2004 University of Malta
First class BSc (Honours) in Chemistry and Biology
Dissertation project under the supervision of *Prof. Robert Borg*
"Further investigation into the trapping of the photo-NOCAS intermediate – A novel photo-NOCAS reaction" (awarded grade: A)

2004 – 2005 Loughborough University
MSc in Pharmaceutical Science & Medicinal Chemistry (Distinction)
Industrial training project undertaken at AstraZeneca's Medicinal Chemistry Department, Charnwood
"Microwave synthesis of privileged structure building blocks and their use in combinatorial chemistry"

2005 – 2006 Medichem Manufacturing (Malta) Ltd.
Production shift leader
Job which involved the supervision of production of active pharmaceutical ingredients (API) on an industrial scale in a good manufacturing practice (GMP) factory

2006 – 2011 FUNDP, Namur & University of Trieste
Cotutelle PhD in organic chemistry under the supervision of *Prof. Davide Bonifazi*
"Synthetic approaches towards modified peptide nucleic acids (PNAs) for biomimetical nanostructured surfaces"

2011 onwards Medichem Manufacturing (Malta) Ltd.
Head of Research and Development

Publications

- Bonifazi, D.; Mohnani, S.; Llanes-Pallas, A. *Chemistry - A European Journal* **2009**, *15*, 7004-7025.
  "Supramolecular chemistry at interfaces: molecular recognition on nanopatterned porous surfaces."
  URL: http://dx.doi.org/10.1002/chem.200900900

- Mohnani, S.; Llanes-Pallas, A.; Bonifazi D. *Pure and Applied Chemistry* **2010**, *82*, 917- 929.
  "Mastering nanostructured materials through H‐bonding recognitions at interfaces."
  URL: http://dx.doi.org/10.1351/PAC-CON-10-01-06

- Mohnani, S.; Bonifazi, D. *Coordination Chemistry Review* **2010**, *254,* 2342-2362.
  "Supramolecular architectures of porphyrins on surfaces: the structural evolution from 1D to 2D to 3D to devices."
  URL: http://dx.doi.org/10.1016/j.ccr.2010.05.006

- Mohnani, S.; Bonifazi, D. *Organic Letters* **2010,** *Manuscript in preparation*.
  A copper-free 1,3-dipolar cycloaddition strategy to functionalize peptide nucleic acids with chromophoric tags.